The Dicke Effect in Electronic Systems

Habilitationsschrift

Tobias Brandes

The Dicke Effect in Electronic Systems
Habilitationsschrift

The Dicke Effect in Electronic Systems

Habilitationsschrift

Tobias Brandes

Hamburg, January 2000

Universität Hamburg, 1. Institut für Theoretische Physik

PREFACE

Two decades after the discovery of the quantum Hall effect [1], quantum coherent electronic transport can be considered as one of the central subjects of modern solid state physics [2–10]. Phase coherence of quantum states leads to effects such as, e.g., localization [11,12] of electron wave functions, the quantization of the Hall resistance in two–dimensional electron gases [5,13,14] or steps in the conductance of quasi one–dimensional quantum wires or quantum point contacts [15–18]. Quantum mechanical effects appear as Aharonov–Bohm like interference oscillations of the conductance of metallic rings or cylinders [19]. It has become possible to observe quantum mechanical coherence on its smallest scale in artificial semiconductor structures like single [20–26] or coupled quantum dots [27–31], where single charging effects [32] like the Coulomb blockade occurs.

It was the experimental progress in the last few years which has opened the test–ground of a number of fundamental physical concepts related to the motion of electrons in lower dimensions. The quantum Hall effect was only one of the first highlights of the new physics that by now has established itself as the area of 'mesoscopic phenomena'. The theoretical understanding of the related physical effects like electron–electron interactions in low dimensions [33–38] and even the concept of phase coherence in mesoscopic systems itself [39–48] is still on a very rudimentary level. This is due to the fact that in low–dimensional structures, the interactions of electrons with one another and with other degrees of freedoms such as lattice vibrations or light give rise to new phenomena that are very different from those familiar in the bulk material [49]. At the same time, in order to describe fast transport processes in small nanostructures [6,50,51], not only the interaction but also the non–equilibrium aspect of quantum transport becomes of fundamental importance. This means that theories are required which comprise both the non–equilibrium and the interaction aspect.

Although the development of such theories is a demanding task for a

theorist, in this thesis I will take a more modest attitude and look at only one of the central issues that is common in many of the above mentioned effects: in the widest sence, it is *interference* which is the key issue towards the understanding of many of the experiments.

The present thesis is devoted to the study of the *Dicke effect* in electronic systems. This effect was predicted by Dicke in 1954 [52] and is originally known in quantum optics as the collective spontaneous decay of a coherent ensemble of a large number of radiating atoms. Dicke also predicted another, but related effect in 1953 [53] as a narrowing of spectral line shapes of radiating atoms due to collisions. The Dicke effect [1] has been extensively studied both theoretically and experimentally in quantum optics, and only recently the interest in its analogon and in similar coherent coupling effects in electronic systems has started to increase.

Here, we will not try to give a complete review over this still emerging field, but rather concentrate on the appearance of the effect in a number of physical interesting situations which mainly summarize, not surprisingly, our own contributions during the last few years. We therefore discuss the Dicke effect in the spontaneous emission of phonons in double quantum dots and its relation to the emission of light from laser–trapped ions, furthermore a superradiance model for the effect in quantum dot arrays and in the coherent optical properties of two–dimensional magnetoplasmas. Finally, we shortly review the Dicke spectral line narrowing effect and its recent re–discovery in resonant tunneling, as well as a new prediction for its appearance in the AC electronic transport properties of disordered quantum wires in magnetic fields.

We close this preface with the remark that mesoscopic physics nowadays is a field situated not only at the junction between large and small size scales, but also between two at first glance largely independent disciplines: modern optics and electronic transport. Our believe is that more and more concepts in particular from quantum optics will enter (and have already entered) the field of coherent electronic transport. The inclusion of optics as a new direction for mesoscopic physics has come about as a natural consequence of the trend toward smaller optical devices exploiting coherent and intense laser light. From a more idealistic point of view, one could even argue that bring-

---

[1] In this thesis, we will use the singular form 'Dicke effect' throughout. The (1954) Dicke superradiance effect is a generalization (as will become clear in the following chapters) of the splitting of coupled modes into one sub– and one superradiant mode. This splitting, on the other hand, is the reason for the spectral line narrowing (Dicke 1953 effect).

ing together electronics and optics at the mesoscopic scale is the continuation of a historic endeavor which originated at the very beginning of quantum mechanics itself [54–56]. The present thesis tries to contribute to the transfer of ideas between both disciplines. In the end, both of them are based on and formulated in the framework of a physical language that was born exactly one century ago: quantum mechanics.

Hamburg, January 2000   *Tobias Brandes*

CONTENTS

1. PHONONS IN DOUBLE QUANTUM DOTS

Abstract

We present the theory of interference effects in the spontaneous emission properties of coupled real and artificial atoms. Electron–phonon interactions can dominate the nonlinear transport properties of coupled semiconductor quantum dots even for temperatures close to zero. The intradot electron tunnel process leads to a 'shake up' of the phonon system and is dominated by a double–slit–like interference effect of spontaneously emitted phonons. The effect is closely related to subradiance of photons in a laser–trapped two–ion system and explains the experimentally observed oscillations in the nonlinear current–voltage characteristics of coupled dots.

1.1 Quantum Dots

1.1.1 Quantum dots and Coulomb blockade

Quantum dots are artificial atoms in semiconductor nano-structures fabricated with typical sizes in the sub-micrometer range [21–24,57]. Many properties of such systems can be investigated by transport, i.e. current-voltage measurements, if the dots are fabricated between contacts acting as source and drain for electrons which can enter or leave the dot. In contrast to real atoms, quantum dots are *open* systems where the number of electrons N can vary depending on external parameters. By changing the size and the shape of the dot with external gate voltages, one can conduct atomic physics experiments with large artificial atoms that can be 'scanned through the periodic table'. In fact, quantum effects such as discrete energy levels (atomic shell structure) and quantum chaos (as in atom nuclei) are observable in a controlled manner in quantum dots [24]. Moreover, the experiments can be

conducted in a regime which usually is not accessible to experiments with real atoms. For example, a singlet-triplet transition should occur in real helium atoms for magnetic fields such large as of the order of 10^5T, as the they occur only in the vicinity of white dwarfs and pulsars [58]. In artificial atoms, which have a much larger size than real atoms, much smaller magnetic fields are sufficient to observe such effects [59, 60].

Many properties of quantum dots are studied by transport experiments which are very sensitive to energy scales down to a few micro electron volts. Transport through quantum dots is basically determined by two effects: 1. The tunnel effect, which is a quantum mechanical phenomenon in which electrons can penetrate tunnel barriers. 2. A classical charging effect which is due to the discreteness of the electron charge and which leads to the so-called Coulomb blockade effect. This last effect becomes important if the charging energy $U = e^2/2C$ of one additional electron becomes a relevant energy scale. Here, e is the electron charge and C an estimated effective 'capacitance' of the dot. The geometric smallness of the dots can then lead to very small capacitances such that U becomes a relevant energy scale.

1.1.2   Coulomb blockade in single dots: a simple model

The main essence of the Coulomb blockade effect in single quantum dots, connected to equilibrium electron reservoirs (source and drain) at chemical potentials μ_L and $\mu_R < \mu_L$, can be understood in a simple model that we shortly discuss in the following [62, 63]. We assume that the confinement area of the dot is coupled to the reservoirs via high tunnel barriers, and that the confinement leads to discrete one-particle levels, the lowest of which we denote by $E_1 = \varepsilon_1 + eV_g$ and $E_1' = \varepsilon_2 + eV_g$ ($\varepsilon_1 < \varepsilon_2$), where the gate voltage V_g is an external parameter that can shift the levels up or down. We restrict ourselves to these two single-particle levels and introduce the energy for *two* electrons in the dot $E_2 = \varepsilon_1 + \varepsilon_2 + 2eV_g + U$, where U is a Hubbard interaction energy that mimics the Coulomb repulsion between electrons. The dot then has the four possible states 'empty', 'one electron in the lower level/upper level', and 'two electrons'.

The tunneling of electrons in or out of the dot can lead to a finite stationary *current* at an applied bias $V_{SD} = \mu_L - \mu_R$ between left and right reservoir (Fig.(1.1)). Energy conservation requires that a current can only flow through the system if the ground state energy difference $E_{N+1} - E_N$ for a transition from N to $N+1$ electrons is within the window $[\mu_L, \mu_R]$. For small
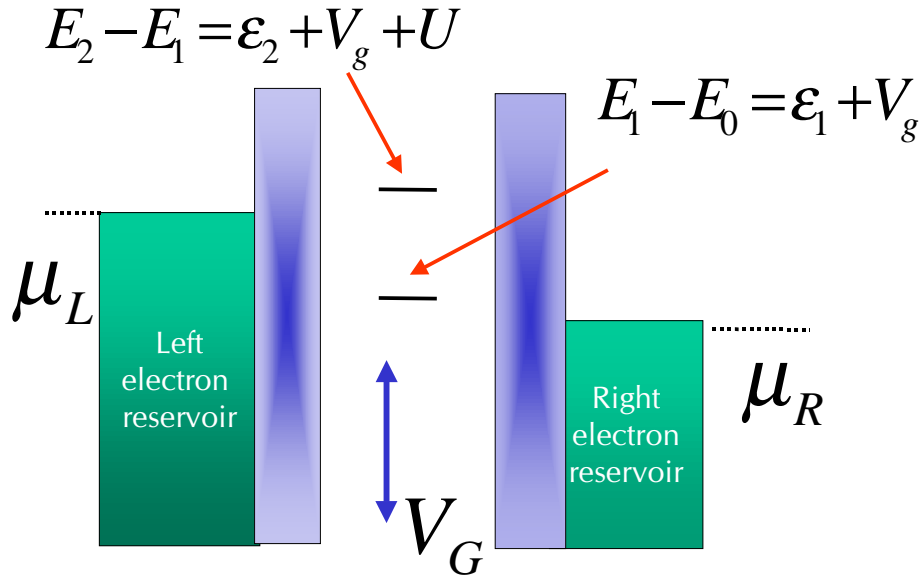
Fig. 1.1: Scheme of a single quantum dot coupled via tunnel barriers (shaded) to electron reservoirs. Levels within the dot indicate the position of the chemical potentials for adding the first and the second electron to the dot. The chemical potentials can be moved up or down with a gate voltage V_G so that one can tune the system from a current carrying state to a state where current flow is energetically forbidden (Coulomb blockade). Continuous tuning of the gate voltage in systems with more levels involved leads to the Coulomb blockade oscillations, i.e. a sequence of peaks in the current–gate voltage curve, see Fig. (1.2). E_i ($i = 0, 1, 2$) is the energy for i electrons in the dot (see text).

source drain voltage $\mu_L \approx \mu_R$, this condition means either $\mu_L = \varepsilon_1 + eV_g$ or $\mu_L = \varepsilon_2 + U + eV_g$. For fixed ε_i and fixed source drain voltage, the condition for current flow can be fulfilled by varying the gate voltage V_g. As a function of V_g, the current therefore shows peaks where the chemical potential μ_L of the reservoir hits the chemical potential of the dot, i.e. the energy required to add one additional electron to the dot.

This simple model demonstrates that this addition energy is a combination of the charging energy and the single particle energies. Thus, transport
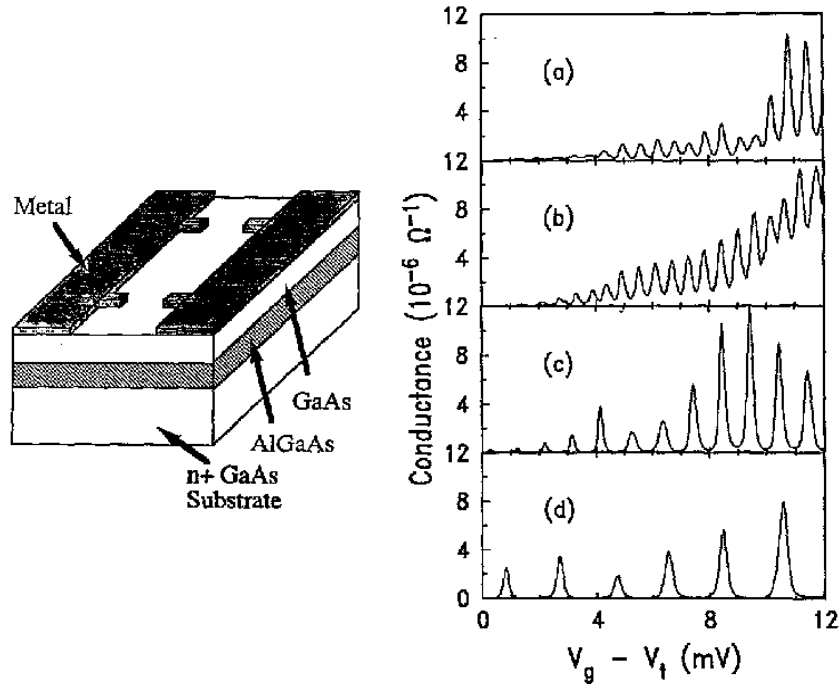
Fig. 1.2: Coulomb blockade oscillations as observed by Meirav, Kastner and Wind [61]. Left: view of the sample, right: conductance versus gate voltage for different samples. Each oscillation corresponds to the addition of a single electron. Temperature $T = 50$ mK.

spectroscopy is sensitive to both the effect of quantum confinement and the electron correlations within the dot.

1.2   Coupled atoms and spontaneous emission

1.2.1   Spontaneous emission of photons and phonons

Spontaneous emission is one of the fundamental concepts of quantum mechanics that can be traced back to such early works as that of Albert Einstein [55]. An excited state of a single atom decays exponentially at a rate Γ due to the coupling to photons. In frequency space, this leads to the Wigner–Weisskopf form of spectral lines [64–66] that have a Lorentzian lineshape with half width $\Gamma/2$ [67].
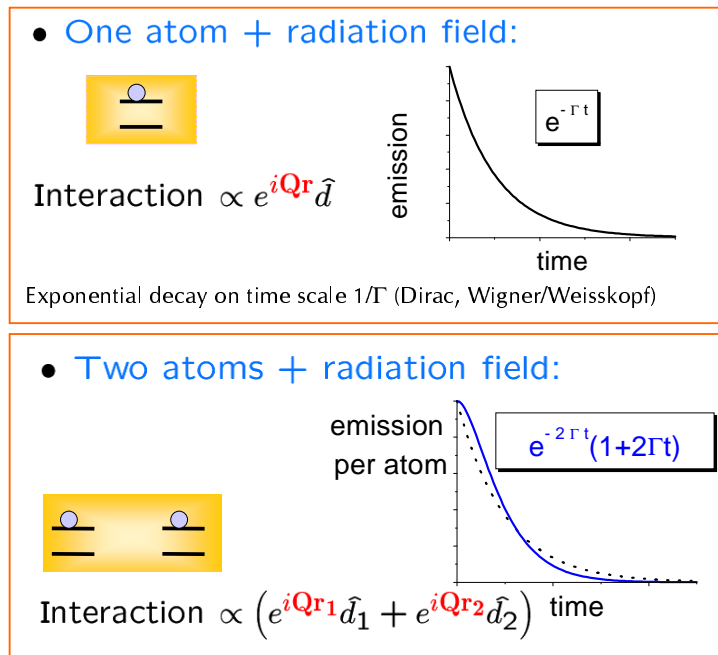
Fig. 1.3: Comparison between spontaneous decay behavior of a single atom and a two–atom system. For the latter case, the dashed curve indicates the emission of light from two independent atoms, cp. Fig.(1.6).

In a system of *two* atoms interacting via the common photon field, the decay splits into a (slow) sub- and a (fast) superradiant channel. The details of this splitting are described in section 1.2.2. In Fig.(1.3), the comparison between the time–dependence of the decay of a single atom and a two atom 'molecule' is indicated. This effect is a precursor of the famous *Dicke superradiance phenomenon* [52] which will be the central subject of section 2. For the case of two radiators, it was verified experimentally by DeVoe and Brewer in the spontaneous emission of photons from two trapped ions in 1996 [68], see below. Recently, in a completely different physical system, the emission of *phonons* from two artificial atoms has been observed [30]. Here, the coupling to the *phonon* degrees of freedom turned out to dominate the non–linear electron transport through semiconductor double quantum dots even at mK temperatures.

Double quantum dots are well-defined artificial systems for the study of

Fig. 1.4: Image of a two–ion 'molecule' from the experiment of DeVoe and Brewer [68]

interaction [31, 69] and coherent time-dependent [27–30, 70] effects. Here, we propose a theory for a new non–linear transport effect in double quantum dots which corresponds to the *Dicke effect*, i.e. the collective decay of initially excited real atoms. In our theory, the tunneling of single electrons through coupled artificial atoms is renormalized by the interaction with piezoelectric acoustic phonons and leads to an orthogonality catastrophe of the phonon bath if an electron tunnels between the dots. This 'boson shake up' effect [71, 72] is determined by an effective density of states $\rho(\omega)$ of the phonon modes $\mathbf{Q}$ that couple to the tunnel process. These interfere like in a double slit experiment when interacting with the electron densities in the two dots. As a result, $\rho(\omega)$ shows oscillations on a scale $\omega_d := c_s/d$, where c_s is the speed of sound and d the distance between the centers of the two dots. It turns out that the non–linear current peak as a function of the difference ε between the two relevant many-particle energies is determined by the shape of $\rho(\omega = \varepsilon/\hbar)$.

Furthermore, this quantity is analogous to the rate for emission of sub-radiant *photons* from two laser–trapped ions [68], when c_s is replaced by the speed of light and d by the distance of the ions. Thus, both phenomena are physically closely related. This provides the microscopic mechanism for the oscillations observed recently in a double dot current spectrum [30].

Finally, we predict that future experiments with artificial atoms can exploit this analogy to real atoms in more detail. In particular, our results in chapter 2 and 4 imply that coherent effects such as superradiance [73] can be manipulated by gate–voltages and external leads.

1.2.2 Sub– and superradiance of two ions: theory

As mentioned above, the spontaneous emission of phonons from double dots is closely analogous to the subradiant spontaneous decay by emissions of *photons* from a laser–trapped two–ion system , as observed by DeVoe and Brewer [68] .

In a two–ion system, the interaction of the atomic dipoles $\hat{\mathbf{d}}_i$ at positions $\mathbf{r}_i$ $(i = 1, 2)$ with a transverse quantized electromagnetic field within a volume V is of the form [74]

$$H_{eph} = \sum_{\mathbf{Q}s} \tilde{\mathbf{g}}_{\mathbf{Q}s} \left(a_{-\mathbf{Q}s} + a_{\mathbf{Q}s}^+ \right) \left[\hat{\mathbf{d}}_1 \exp i(\mathbf{Q}\mathbf{r}_1) + \hat{\mathbf{d}}_2 \exp i(\mathbf{Q}\mathbf{r}_2) \right], \qquad (1.1)$$

with the coupling matrix element

$$\tilde{\mathbf{g}}_{\mathbf{Q}s} = -i \left(\frac{2\pi c Q}{V} \right)^{1/2} \vec{\varepsilon}_{\mathbf{Q}s}. \qquad (1.2)$$

Here, c is the speed of light, $\mathbf{Q}$ the photon wave vector, and the light polarization vectors are $\vec{\varepsilon}_{\mathbf{Q},s}$ for polarization direction s. The spontaneous emission rate Γ of photons is proportional to the square of the interaction (Fermi's Golden Rule). The contribution $\Gamma_{\mathbf{Q}}$ of a mode with wave vector $\mathbf{Q}$ to Γ is

$$\begin{aligned} \Gamma_{\mathbf{Q}} &\propto |\hat{\mathbf{d}}_1 \exp i(\mathbf{Q}\mathbf{r}_1) + \hat{\mathbf{d}}_2 \exp i(\mathbf{Q}\mathbf{r}_2)|^2 \\ &= |\exp i(\mathbf{Q}\mathbf{r}_1) \pm \exp i(\mathbf{Q}\mathbf{r}_2)|^2, \end{aligned} \qquad (1.3)$$

where the two signs $\pm$ correspond to the two different relative orientations of the dipole moments of the two ions. In fact, a more detailed calculation leads to

$$\Gamma(Q)_{\pm} = \Gamma_0(Q) \left[1 \pm \alpha \frac{\sin(Qd)}{(Qd)} \right], \quad Q = \omega_0/c \qquad (1.4)$$

with $\alpha = 1$ ($\alpha = 3/2$) if the vector character of the light is (not) neglected, $Q = \omega_0/c$, and $\Gamma_0(Q) \propto Q^3$. Here, $d = |\mathbf{r}_2 - \mathbf{r}_1|$ is the distance between the two ions and ω_0 the transition frequency, i.e. the energy difference of the upper and the lower level in both atoms ($\hbar = 1$). The assumption of identical transition frequencies ω_0 for *both* atoms is of importance for the Dicke effect to occur in its pure form as discussed below.

Eq. (1.4) can be easily derived from second order perturbation theory (Fermi's Golden Rule): The Hamiltonian for two atoms interacting with the electromagnetic field reads

$$
\begin{aligned}
H &= H_0 + H_{eph} + H_{ph} \\
H_0 &:= \frac{1}{2}\omega_0 \left(\sigma_z^1 + \sigma_z^2\right) \\
H_{eph} &:= \sum_{\mathbf{Q}s} g_{Qs} \left(a_{-\mathbf{Q}s} + a_{\mathbf{Q}s}^+\right) \left[e^{i\mathbf{Q}\mathbf{r}_1}\sigma_x^1 + e^{i\mathbf{Q}\mathbf{r}_2}\sigma_x^2\right] \\
H_{ph} &:= \sum_{\mathbf{Q}s} \omega_Q a_{\mathbf{Q}s}^+ a_{\mathbf{Q}s}, \quad g_{Qs} = \tilde{\mathbf{g}}_{Qs}\mathbf{d},
\end{aligned}
\tag{1.5}
$$

where the dipole operators are $\hat{\mathbf{d}}_i = \mathbf{d}\sigma_x^i$, and σ_z^i and σ_x^i are the Pauli matrices in the 2×2 space of the upper/lower level $|\uparrow\rangle^i, |\downarrow\rangle^i$ of atom i. Furthermore, $\omega_Q = c|\mathbf{Q}|$, and $a_{\mathbf{Q}s}^+$ creates a photon with wave vector $\mathbf{Q}$ and polarization s.

One defines the basis of so–called *Dicke states* (which are the usual singlet and triplet combinations in this case of two atoms here),

$$
\begin{aligned}
|S_0\rangle &:= \frac{1}{\sqrt{2}}\left(|\uparrow\downarrow\rangle - |\downarrow\uparrow\rangle\right) \\
|T_1\rangle &:= |\uparrow\uparrow\rangle \\
|T_0\rangle &:= \frac{1}{\sqrt{2}}\left(|\uparrow\downarrow\rangle + |\downarrow\uparrow\rangle\right) \\
|T_{-1}\rangle &:= |\downarrow\downarrow\rangle.
\end{aligned}
\tag{1.6}
$$
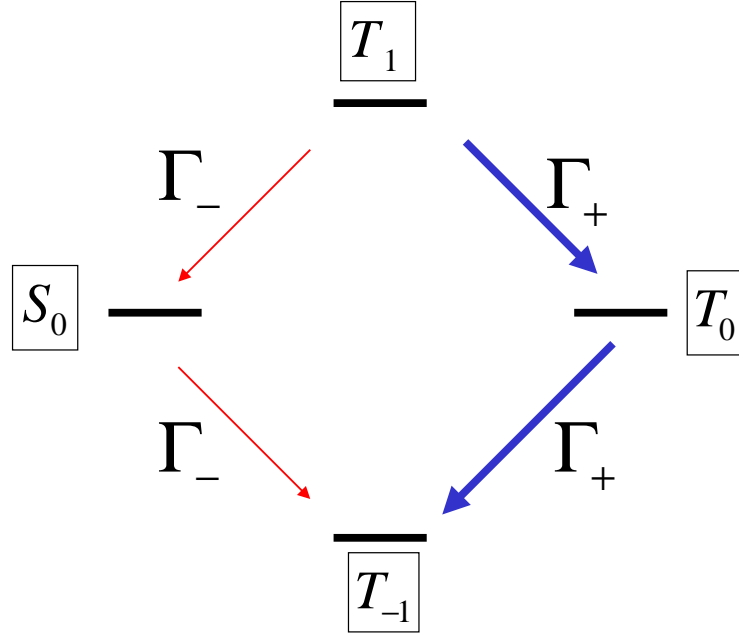
Fig. 1.5: Decay scheme for two–ion system. Indicated are the four states, Eq. (1.6), and the subradiant (Γ_-) and superradiant (Γ_+) decay channels.

Using this basis, one can easily calculate the matrix elements

$$
\begin{aligned}
\langle T_1 | \sigma_x^i | T_1 \rangle &= \langle T_1 | \sigma_x^i | T_{-1} \rangle = 0, \quad i = 1, 2 \\
\langle T_1 | \sigma_x^i | T_0 \rangle &= \langle T_0 | \sigma_x^i | T_{-1} \rangle = \frac{1}{\sqrt{2}}, \quad i = 1, 2 \\
\langle T_0 | \sigma_x^i | S_0 \rangle &= 0, \quad i = 1, 2 \\
\langle T_1 | \sigma_x^1 | S_0 \rangle &= -\frac{1}{\sqrt{2}}, \quad \langle T_1 | \sigma_x^2 | S_0 \rangle = \frac{1}{\sqrt{2}} \\
\langle S_0 | \sigma_x^1 | T_{-1} \rangle &= \frac{1}{\sqrt{2}}, \quad \langle S_0 | \sigma_x^2 | T_{-1} \rangle = -\frac{1}{\sqrt{2}}.
\end{aligned}
\tag{1.7}
$$

This means that there are only two transition rates $\Gamma_\pm$ (see Fig.(1.5)) for spontaneous emission of photons into a photon vacuum,

$$
\Gamma_\pm(Q) = 2\pi \sum_{\mathbf{Q}s} \frac{|\alpha_{\mathbf{Q}s} \pm \beta_{\mathbf{Q}s}|^2}{2} \delta(\omega_0 - \omega_Q), \quad Q = \omega_0/c,
\tag{1.8}
$$
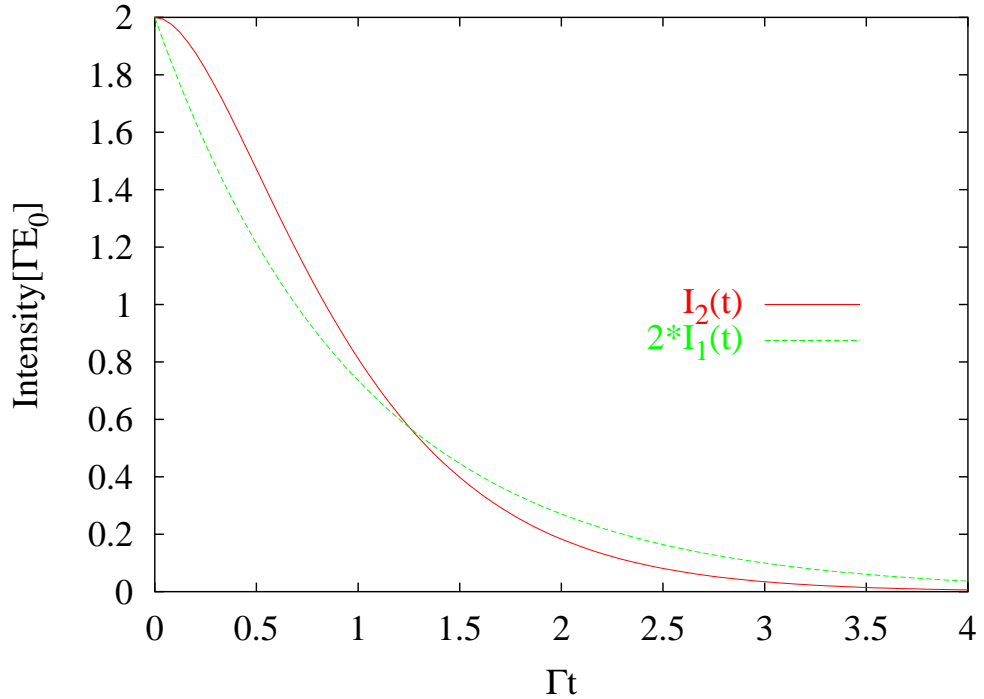
Fig. 1.6: Emission rate intensity of radiation from the coherent ($I_2(t)$) and incoherent ($2I_1(t)$) decay of a system consisting of two radiators. The radiation rate of one individual radiator is Γ.

where we defined the coupling constants $\alpha_{\mathbf{Q}s} = g_{Qs}e^{i\mathbf{Q}\mathbf{r}_1}$ and $\beta_{\mathbf{Q}s} = g_{Qs}e^{i\mathbf{Q}\mathbf{r}_2}$. Evaluation of this expression with Eq. (1.2) yields the expression Eq. (1.4), cp. [73].

The appearance of two decay channels, that is the super- and subradiant decay channels $\pm$ in the emission rate, has been discovered by Dicke [52]. This effect is the precursor of the more general case of N radiators (ions, atoms,...), where the phenomenon is known as *Dicke superradiance* and will be discussed in detail in chapter 2. Here, we show how the time-dependence of the *collective* decay of two radiators differs from the decay of two single radiators.

We denote the occupation probabilities of the four levels, Eq.(1.6), by $T_1(t)$, $T_0(t)$, $T_{-1}(t)$, and $S_0(t)$, respectively. The time dependence of the

occupations is then govered by the two decay rates Γ_+ and Γ_-:

$$
\begin{aligned}
\dot{T}_1 &= -(\Gamma_- + \Gamma_+)T_1 \\
\dot{S}_0 &= \Gamma_-(T_1 - S_0) \\
\dot{T}_0 &= \Gamma_+(T_1 - T_0) \\
\dot{T}_{-1} &= \Gamma_- S_0 + \Gamma_+ T_0.
\end{aligned}
\tag{1.9}
$$

For simplicity, we consider the case where the subradiant channel is completely suppressed, i.e. a situation where $\Gamma_- = 0$ and $\Gamma_+ = 2\Gamma$. This would correspond to the case $\alpha = 1$ and $Qd \to 0$ in Eq. (1.4), i.e. the so–called *small–sample limit* where the wave length of the emitted light is much larger than the distance between the two radiators. Furthermore, in this case $\Gamma = \Gamma_0(Q)$ is the emission rate of one individual radiator.

The above equations can be easily solved [75],

$$
\begin{aligned}
T_1(t) &= e^{-\Gamma_+ t} \\
T_0(t) &= \Gamma_+ t e^{-\Gamma_+ t} \\
T_{-1}(t) &= 1 - e^{-\Gamma_+ t}(1 + \Gamma_+ t),
\end{aligned}
\tag{1.10}
$$

where initial conditions $T_1(0) = 1$, $T_0(0) = S_0(0) = T_{-1}(0) = 0$ have been assumed. The total *coherent emission rate* $I_2(t)$ at time t is the sum of the emission rates from T_1 and T_0 (the lowest level T_{-1} does not radiate):

$$
I_2(t) = E_0 \Gamma_+ e^{-\Gamma_+ t}(1 + \Gamma_+ t), \quad \Gamma_+ = 2\Gamma,
\tag{1.11}
$$

where E_0 is a constant with dimension energy. This has to be compared with the *incoherent sum* $2I_1(t)$ of the emission rates $I_1(t)$ from two independent radiators, which would give

$$
2I_1(t) = 2E_0 \Gamma e^{-\Gamma t}.
\tag{1.12}
$$

We conclude this short discussion, which followed the one by Gross and Haroche [75], by comparing the time-dependence of the coherent and the incoherent rate in Fig.(1.6). The effect is not very drastic in the time domain (in the frequency domain it is, cp. chapter 5). Still, one clearly reckognizes that the coherent emission rate is larger than its coherent counterpart for time $t > 0$ up to larger times, where it becomes smaller again: energy conservation requires that the total emitted energies are the same in both the coherent and the incoherent case, i.e.

$$
\int_0^\infty dt I_2(t) = \int_0^\infty dt 2 I_1(t) \quad (= 2E_0).
\tag{1.13}
$$

1.2.3 Sub– and superradiance of two ions: experiments

DeVoe and Brewer [68] measured the spontaneous emission rate of two ions [1] as a function of the ion–ion distance in a trap of planar geometry which was strong enough to bring the ions (Ba_{138}^+) to a distance of the order of 1μm of each other. The idea of their experiment was to determine $\Gamma_\pm(Q)$, Eq. (1.4), and to compare it to the spontaneous emission rate $\Gamma_0(Q)$ of a *single* ion within the same setup. This was done in a transient technique by exciting the ion molecule by a short laser pulse and recording the subsequent signal, i.e. the time of arrival of spontaneously emitted photons.
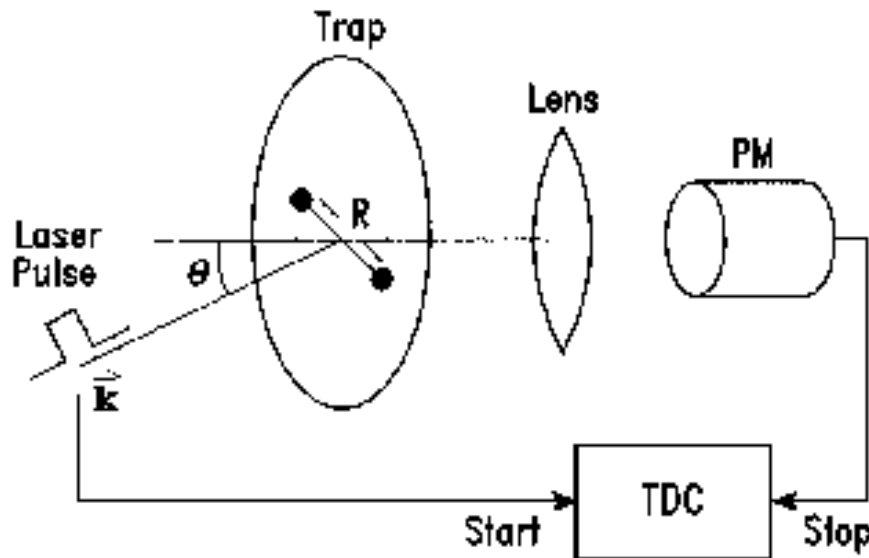
Fig. 1.7: Setup of the 'double ion' trap experiment by DeVoe and Brewer [68]. The two–ion molecule is confined within a 80μm radius planar trap and excited with a laser pulse. The time–to–digital converter (TDC) records the time of arrival of spontaneously emitted photons.

---

[1] DeVoe and Brewer [68] called their system a 'two–ion–crystal'. Since the term 'crystal' is usually used for a periodic structure of a large number of masses (like in solid state physics), we find the term 'two–ion–molecule' more appropriate.
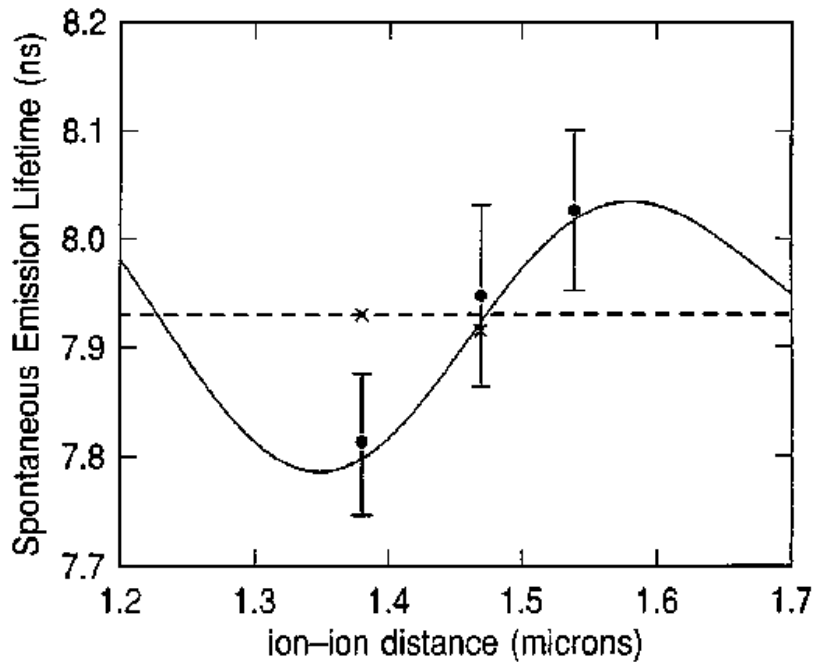
Fig. 1.8: Comparison of theory, see Eq. (1.4), and measured data in the experiment of deVoe and Brewer [68] for the identification of sub– and super–radiance (Dicke effect) in a two–ion molecule. A laser beam excites the system at $t = 0$; the start of the exciting pulse and the arrival of the spontaneous photons are recorded on a time to digital converter, which is fit to an exponential decay. The dashed line indicates the lifetime of a single ion in the same trap. Full circles with error bars are data for laser polarization perpendicular to the axis connecting the two ions, crosses are for parallel polarization. The points below the dashed line belong to the superradiant decay channel, whereas the points above the dashed line indicate belong to the subradiant channel.

It turned out that the best way to distinguish between the sub– and the superradiant decay channel, cp. Fig.(1.5), was to choose the initial states of the system as the two states S_0 (singlet) and T_0 (triplet), which yield the subradiant and the superradiant emission rate, respectively. This was achieved by coherent excitation of the two–ion molecule, exciting dipole moments in the two ions with a phase difference of 0 or π. Due to level degeneracy of the relevant $6^2P_{1/2}$ to $6^2S_{1/2}$ transition and due to loss of coherence because

of micromotion Doppler shifts, the theoretical value for an effective factor α in Eq.(1.4) turned out to be $\alpha = 0.33$. Diffraction limited images of the molecule, viewed through a window with a microscope, give the information on the distance between the ions [68], see Fig.(1.4).

Measurements of the spontaneous rate Γ at three different ion distances turned out to be in good agreement with the (parameter free) theoretical prediction [76], Eq.(1.4). The data (statistical and systematic tests were performed) were averaged over a large number of runs.

1.3   Phonons in double quantum dots: Experiments

We now turn from experiments with reals atoms (ions) to a description of a recent experiment in coupled *artificial* atoms, that is coupled quantum dots. Here, we describe the main results of the experiment by Fujisawa and co–workers (TU Delft, [30]).

The double quantum dot is realized in a 2DEG AlGaAs–GaAs semiconductor heterostructure [29], see Fig.(1.9). Focused ion beam implanted in–plane gates define a narrow channel of tunable width which connects source and drain (left and right electron reservoir). On top of it, three Schottky gates define tunable tunnel barriers for electrons moving through the channel. By applying negative voltages to the left, central, and right Schottky gate, two quantum dots (left L and right R) are defined which are coupled to each other and to the source and to the drain. The tunneling of electrons through the structure is large enough to detect current but small enough to have a well–defined number of electrons (~ 15 and ~ 25) on the left and the right dot, respectively. The Coulomb charging energy (~ 4 meV and ~ 1 meV) for putting an additional electron onto the dots is the largest energy scale, see Fig.(1.10). By tuning simultaneously the gate voltages of the left and the right gate while keeping the central gate voltage constant, the double dot switches between the three states $|0\rangle = |N_L, N_R\rangle$, $|L\rangle = |N_L + 1, N_R\rangle$, and $|R\rangle = |N_L, N_R + 1\rangle$ with only *one additional electron* either in the left or in the right dot (see the following section, where the model is explained in detail).

The main experimental trick is to keep the system within these states and to change only the energy difference $\varepsilon = \varepsilon_L - \varepsilon_R$ of the dots without changing too much, e.g., the barrier transmissions. The measured average spacing between single–particle states (~ 0.5 and ~ 0.25 meV) is still a large
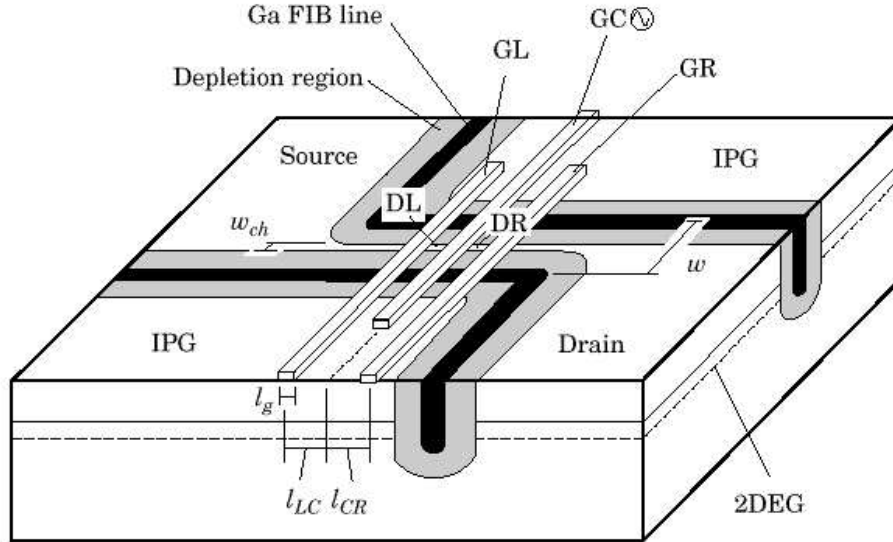
Fig. 1.9: Schematic diagram of a 'double gate single electron transistor' by Fujisawa and Tarucha [29]. The 2DEG is located 100 nm below the surface of an AlGaAs/GaAs modulation–doped heterostructure with mobility $8 \cdot 10^5$ cm^2 (Vs)$^{-1}$ and carrier concentration $3 \cdot 10^{11}$ cm^{-2} at 1.6 K in the dark and ungated. Ga focused ion beam implanted in–plane gates and Schottky gates define the dot system. A double dot is formed by applying negative gate voltages to the gates GL, GC, and GR. The structure can also be used for single–dot experiments, where negative voltages are applied to GL and GC only.

energy scale compared to the scale on which ε is varied. The largest value of ε is determined by the source–drain voltage which is around 0.14 meV.

The main findings are the following:

1. At a low temperature of 23 mK, the stationary tunnel current I as a function of ε shows a peak at $\varepsilon = 0$ with a broad shoulder for $\varepsilon > 0$ that oscillates on a scale of $\approx 20 - 30 \mu$eV, see Fig.(1.11).

2. For larger temperatures T, the current increases stronger on the absorption side $\varepsilon < 0$ than on the emission side. The data for larger T can be
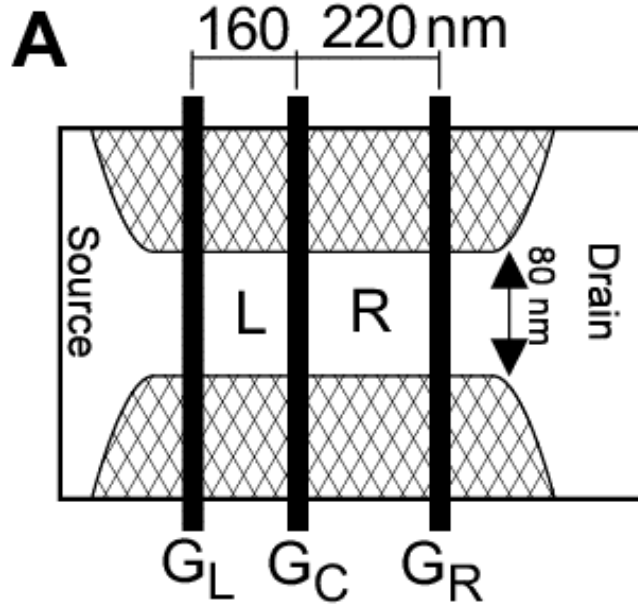
Fig. 1.10: Double quantum dots as used in the experiment by Fujisawa *et al.* [30] (top view). Transport of electrons is through the narrow channel that connects source and drain. The gates themselves have widths of 40 nm. The two quantum dots contain approximately 15 (Left, L) and 25 (Right, R) electrons. The charging energies are 4 meV (L) and 1 meV (R), the energy spacing for single particle states in both dots is approximately 0.5 meV (L) and 0.25 meV (R).

reconstructed from the 23 mK data by multiplication with the Einstein–Bose factors $n(T)$ and $1 + n(T)$ for emission and absorption, see section 1.8.2.

3. The energy dependence of the current on the emission side is between $1/\varepsilon$ and $1/\varepsilon^2$. For larger distance of the left and right barrier (600 nm on a surface gate sample instead of 380 nm for a focused ion beam sample), the period of the oscillations on the emission side appears to become shorter, see Fig.(1.13).

From these experimental findings, Fujisawa *et al.* concluded that the *coupling to a bosonic environment* is of key importance in this experiment. To identify the microscopic mechanism of the spontaneous emission, they placed
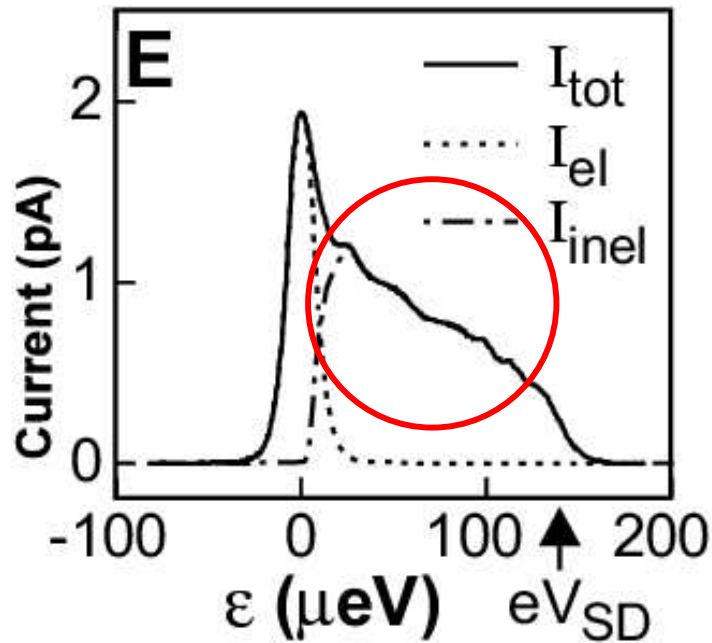
Fig. 1.11: Current at temperature $T = 23$mK as a function of the energy difference ε in the experiment by Fujisawa *et al.* [30]. The total measured current is decomposed into an elastic and an inelastic component. If the difference ε between left and right dot energies E_L and E_R is larger than the source–drain–voltage, tunneling is no longer possible and the current drops to zero. The red circle marks the region of spontaneous emission, characterized by the large 'shoulder' for $\varepsilon > 0$ with an oscillation–like structure on top of it.

the double dot in different electromagnetic environments in order to test if a coupling to photons was responsible for these effects. Typical wavelengths in the regime of relevant energies ε are in the cm range for both photons and 2DEG plasmons. Placing the sample in microwave cavities of different sizes showed no effect on the spontaneous emission spectrum. Neither was there an effect by measuring different types of devices with different dimensions, which should change the coupling to plasmon.

From this, Fujisawa *et al.* concluded that it is the coupling to *acoustic phonons* (optical phonons have too large energies in order to be relevant here) which is the microscopic mechanism responsible for the emission spectrum.
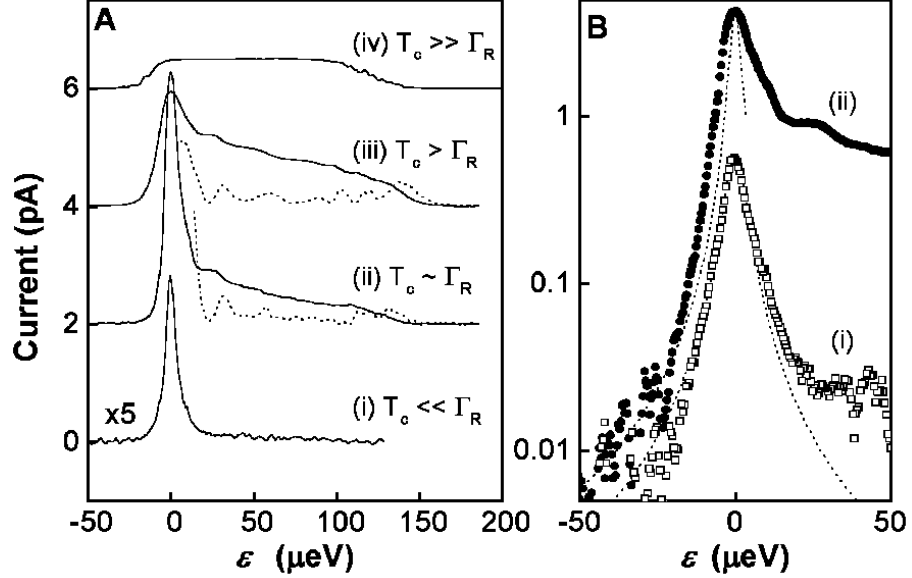
Fig. 1.12: Current at $T = 23$mK as a function of the energy difference ε in the experiment by Fujisawa *et al.* [30]. The curves in **A** have an offset and are for different values of the coupling T_c between the dots and the rate Γ_R for tunneling out into the drain region. The dotted curves are the negative derivatives of the currents with respect to energy ε to enhance the structure on the emission side of the current. **B** shows curves (i) and (ii) from A in a double–logarithmic plot, where the dashed lines are Lorentzian fits.

In fact, phonon energies in the relevant ε regime correspond to wavelengths that roughly fit with the typical dimensions (a few 100 nm) of the double dot device used in the experiments.

In the following, we will try to understand the experimental findings in the framework of a theoretical model for transport through double dots in presence of inelastic degrees of freedom (phonons).
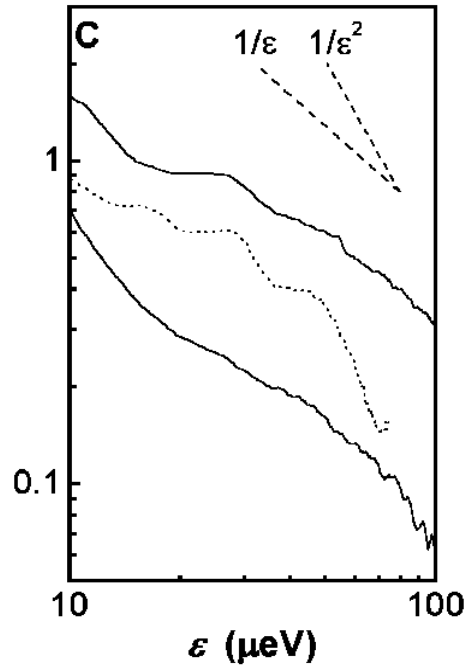
Fig. 1.13: Current on the emission side $\varepsilon > 0$ in the experiment by Fujisawa *et al.* [30]. The solid lines correspond to data from the sample Fig.(1.10) for different coupling parameters. The dotted line represents data from a *surface gate sample* where the distance between left and right barriers is larger, that is 600 nm.

1.4   Model

We consider a double quantum dot composed of a small left and a small right dot (L and R) which are connected through a tunnel barrier. The left dot is connected to a reservoir of free two–dimensional electrons (source) and the right dot is connected to another reservoir of electrons (drain). Both reservoirs are assumed to be in thermal equilibrium with chemical potentials μ_L (left reservoir) and μ_R (right reservoir). In the following, we always consider the case $\mu_L > \mu_R$, i.e. we have tunneling of electrons from the left to the right.
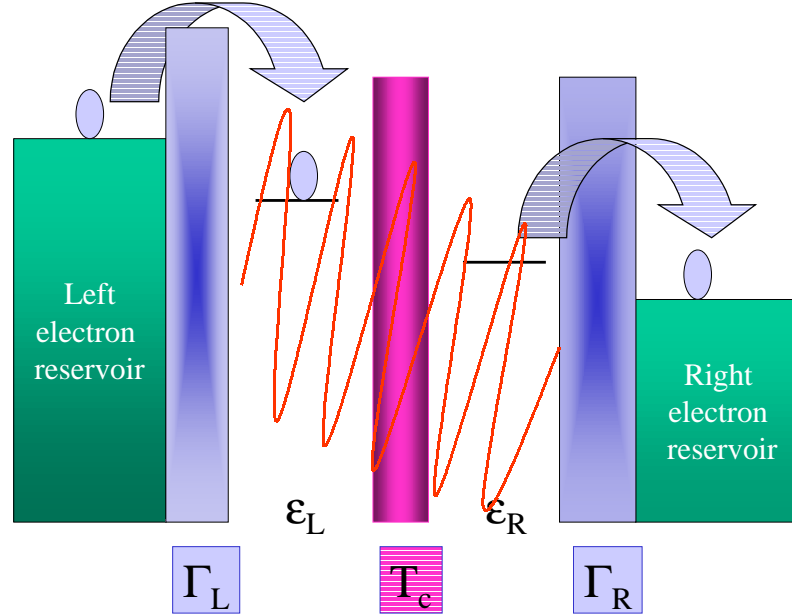
Fig. 1.14: The model: double dot consisting of left and right dot, coupled by
a tunnel matrix element T_c. Left and right electron reservoirs act as source
and drain for electrons tunneling from left to right. The energies ε_L and ε_R
have to be understood as chemical potentials for the addition of one additional
electron to the left and the right dots, respectively. The system is in the strong
Coulomb blockade regime with only one additional electron allowed to enter
the double dot. Phonons couple to the electronic density in both dots.

1.4.1   Three–state basis

We assume that for the physical phenomena we are interested in, a basis of
only three dot states is sufficient [77]. That is, the Hilbert space of the dot
is spanned by the three states

$$
\begin{aligned}
|0\rangle &= |N_L, N_R\rangle \\
|L\rangle &= |N_L + 1, N_R\rangle \\
|R\rangle &= |N_L, N_R + 1\rangle
\end{aligned}
\tag{1.14}
$$

which correspond to three different many–particle ground states with N_L electrons in the left and N_R electrons in the right dot. We assume that the corresponding ground state energies ε_L of $|L\rangle$ and ε_R of $|R\rangle$ are in the window between source and drain energy, i.e. $\mu_L > \varepsilon_L, \varepsilon_R > \mu_R$. Physically, this restriction means the following:

1. The source–drain voltage $V_{SD} := \mu_L - \mu_R$ is much smaller than the energy U_c to put an additional electron onto the dot if the dot is in the state $|L\rangle$ or $|R\rangle$. Then, the Coulomb charging energy of the double dot is the largest energy scale in the problem and it is not possible to charge the double dot with more than one additional electron.

2. The many–body excited states over the ground states eq. (1.14) can be disregarded, i.e. only ground–state to ground–state transitions determine the transport properties.

In [30], no enhanced tunnel current was observed for $\varepsilon := \varepsilon_L - \varepsilon_R < 0$ at low temperatures so that excited many–body states play no role. In particular, $U_c \sim 1$ meV was one order of magnitude larger than the external source drain voltage V_{SD}. This situation has to be contrasted with the regime $V_{SD} \gtrsim U_c$, where the blockade becomes lifted. The crossover from small to large source–drain voltages (with respect to U_c) has been studied by Raikh and Asenov [78]. They considered tunneling through a system of two localized states, coupled to metallic reservoirs. The crossover to the regime $V_{SD} \gtrsim U_c$ showed up in the I–V characteristic as a *step*, the height of which could be determined by considering the different time scales for charging and de–charging of the system. We make the distinction between the case of large bias–voltage V_{SD} and the case of small bias voltage to point out that our model does not cover the crossover from the Coulomb blockade to the unblocked regime as investigated by Raikh and Asenov.

We now define dot–operators

$$
\begin{aligned}
n_L &:= |L\rangle\langle L|, \quad n_R := |R\rangle\langle R| \\
p &:= |L\rangle\langle R|, \quad p^\dagger := |R\rangle\langle L| \\
s_L &= |0\rangle\langle L|, \quad s_R := |0\rangle\langle R|.
\end{aligned}
\tag{1.15}
$$

These operators fulfill

$$
\begin{aligned}
n_L^2 &= n_L, \quad n_L p = p, \quad n_L p^\dagger = 0 \\
p^\dagger n_R &= 0, \quad p p^\dagger = n_L, \quad p^\dagger p = n_R \\
n_R^2 &= n_R, \quad n_R p = 0, \quad n_R p^\dagger = p^\dagger \\
p n_L &= 0, \quad p n_R = p, \quad p^\dagger n_L = p^\dagger
\end{aligned}
\tag{1.16}
$$

The total system Hamiltonian H consists of three parts: the double dot Hamiltonian, the phonon bath, and the two electron reservoirs. Furthermore, there is the interaction between the phonon system and the double dot. The interaction between phonons and the reservoirs is not considered explicitely here. The Hamiltonian of the dot is

$$
H_d = \varepsilon_L n_L + \varepsilon_R n_R + T_c(p + p^\dagger),
\tag{1.17}
$$

where the tunneling between left and right dot is described by a single tunnel matrix element T_c.

It is useful to split H into a sum in the following manner

$$
\begin{aligned}
H &= H_0' + H_T + H_V + H_{ep} + H_{\alpha\beta} \\
H_0' &= \varepsilon_L n_L + \varepsilon_R n_R + H_p + H_{res} \\
H_T &= T_c(p + p^\dagger) \\
H_{ep} &= \sum_{\mathbf{Q}} \left(\gamma_{\mathbf{Q}} p + \gamma_{-\mathbf{Q}}^* p^\dagger \right) \left(a_{-\mathbf{Q}} + a_{\mathbf{Q}}^\dagger \right) \\
H_{\alpha\beta} &= \sum_{\mathbf{Q}} \left(\alpha_{\mathbf{Q}} n_L + \beta_{\mathbf{Q}} n_R \right) \left(a_{-\mathbf{Q}} + a_{\mathbf{Q}}^\dagger \right) \\
H_p &= \sum_{\mathbf{Q}} \omega_{\mathbf{Q}} a_{\mathbf{Q}}^\dagger a_{\mathbf{Q}} \\
H_V &= \sum_{\mathbf{k}} \left(V_{\mathbf{k}} c_{\mathbf{k}}^\dagger s_L + W_{\mathbf{k}} d_{\mathbf{k}}^\dagger s_R + c.c. \right) \\
H_{res} &= \sum_{\mathbf{k}} \varepsilon_{\mathbf{k}}^L c_{\mathbf{k}}^\dagger c_{\mathbf{k}} + \sum_{\mathbf{k}} \varepsilon_{\mathbf{k}}^R d_{\mathbf{k}}^\dagger d_{\mathbf{k}}.
\end{aligned}
\tag{1.18}
$$

Here, H_p describes the lattice vibrations in harmonic approximation; the creation operator for a phonon of mode $\mathbf{Q}$ is denoted as $a_{\mathbf{Q}}^\dagger$. We have already split the electron–phonon interaction into the diagonal part $H_{\alpha\beta}$ and

the non-diagonal part H_{ep}. The matrix elements $\alpha_{\mathbf{Q}}$, $\beta_{\mathbf{Q}}$, $\gamma_{\mathbf{Q}}$ are defined by

$$
\begin{aligned}
\alpha_{\mathbf{Q}} &:= \lambda_{\mathbf{Q}}\langle L|e^{i\mathbf{Q}\mathbf{r}}|L\rangle, \quad \beta_{\mathbf{Q}} := \lambda_{\mathbf{Q}}\langle R|e^{i\mathbf{Q}\mathbf{r}}|R\rangle \\
\gamma_{\mathbf{Q}} &:= \lambda_{\mathbf{Q}}\langle L|e^{i\mathbf{Q}\mathbf{r}}|R\rangle,
\end{aligned}
\tag{1.19}
$$

where $\lambda_{\mathbf{Q}}$ is the matrix element for the interaction of 2DEG electrons and phonons. The form of $\lambda_{\mathbf{Q}}$ depends on the specific coupling mechanism to the phonons and will be discussed below.

The coupling to the electron reservoirs is given by the standard tunnel Hamiltonian H_V, where $V_{\mathbf{k}}$ and $W_{\mathbf{k}}$ couple to a continuum of channels $\mathbf{k}$ of the left and right electron reservoir H_{res}. The latter are assumed to be in thermal equilibrium as described by Fermi distribution functions. We note that the splitting of the whole electron system into reservoir and dot regions bears some fundamental problems that are inherent in all descriptions that use the tunnel Hamiltonian formalism. This relatively old problem of how to describe tunnel junctions in a quantum mechanical model has been pointed out first by Prange [79–81]. We do not discuss this point here but only note that the tunnel Hamiltonian formalism has turned out to be a successful tool for a variety of problems in electronic transport in mesoscopic systems [5, 6, 50].

The spin of the electron plays no role here and is suppressed in all notations. In the experiment [30], a magnetic field between 1.6 and 2.4 T was applied perpendicular to the dots in order to maximize the single–particle spacing. In particular, we therefore assume spin polarization of the electrons.

We note that in the case $\gamma_{\mathbf{Q}} = 0$, our Hamiltonian Eq. (1.18) is equivalent to a model by Glazman and Matveev [82], who considered inelastic tunneling across thin amorphous films via pairs of impurities. They showed that phonon terms $\sim \gamma_{\mathbf{Q}}$ can be neglected. We checked in a seperate master equation calculation that such terms indeed modify the tunnel current only weakly, and therefore neglect them in the following. In particular, they do not lead to the oscillatory phenomena observed in [30], which is due to the non–perturbative shake–up process that we describe in the following.

1.4.2 Boson shake–up effect

Suppose an electron tunnels between two regions of space (L and R) and interacts with a boson field. Suppose the interaction is of the form $H_{\alpha\beta}$, eq.(1.18), i.e. a coupling that locally changes the energy of the electron, depending if it is in L or in R. When the electron tunnels, its wave function

will experience a phase shift $e^{i\phi}$ due to this coupling. This phase shift is zero if the coupling is identical in both regions, i.e. if $\alpha_{\mathbf{Q}} = \beta_{\mathbf{Q}}$. If $\alpha_{\mathbf{Q}} \neq \beta_{\mathbf{Q}}$, however, the phase shift depends on the coordinates of the boson field, i.e. ϕ is an operator depending on the boson field operators $a_{\mathbf{Q}}$ and $a_{\mathbf{Q}}^{\dagger}$. This operator acts on the boson field and 'shakes it up' when the electron tunnels. From the point of view of the electron, its phase is renormalized through the tunnel process. Since this phase is environment dependent, the effective tunnel amplitude changes in a non–trivial way; in particular it becomes time–dependent. From the point of view of the boson system, its initial (before the tunneling) and final (after tunneling) state are no longer the same and there is an 'orthogonality catastrophe' which changes the tunneling amplitude, cp. the discussion in section 1.8.1. Strictly speaking, an explanation in terms of electron states and states of the boson system is not correct because electrons and bosons are coupled and one has to speak of the eigenstates of the coupled system. In the following, we will formalize this by introducing a unitary transformation of the Hamiltonian that naturally leads to the phase factors mentioned above.

1.4.3   Canonical Transformation

One can introduce a unitary polaron transformation [83] of the Hamiltonian that naturally leads to the phase factors mentioned above. The latter are well–known from problems where bosonic degrees of freedom couple to a single localized state [50, 84, 85].

We define for any operator O a unitary transformation by

$$
\begin{aligned}
\overline{O} &:= e^{S} O e^{-S}, \quad S := n_L A + n_R B \\
A &:= \sum_{\mathbf{Q}} (\lambda_{\mathbf{Q}} a_{\mathbf{Q}}^{\dagger} - \lambda_{-\mathbf{Q}} a_{\mathbf{Q}}) \\
B &:= \sum_{\mathbf{Q}} (\mu_{\mathbf{Q}} a_{\mathbf{Q}}^{\dagger} - \mu_{-\mathbf{Q}} a_{\mathbf{Q}}) \\
\lambda_{\mathbf{Q}} &:= \frac{1}{\omega_{\mathbf{Q}}} \alpha_{\mathbf{Q}}, \quad \mu_{\mathbf{Q}} := \frac{1}{\omega_{\mathbf{Q}}} \beta_{\mathbf{Q}}.
\end{aligned}
\tag{1.20}
$$

Using the relation

$$
\overline{O} = O + [S, O] + \frac{1}{2!}[S, [S, O]] + ...,
\tag{1.21}
$$

one obtains

$$
\begin{aligned}
\overline{n_L} &= n_L, \quad \overline{n_R} = n_R \\
\overline{a}_{\mathbf{Q}} &= a_{\mathbf{Q}} + \sum_{\mathbf{Q}}(\lambda_{\mathbf{Q}}n_L + \mu_{\mathbf{Q}}n_R)[a_{\mathbf{Q}}^\dagger - a_{-\mathbf{Q}}, a_{\mathbf{Q}}] = \\
&= a_{\mathbf{Q}} - \lambda_{\mathbf{Q}}n_L - \mu_{\mathbf{Q}}n_R,
\end{aligned}
\tag{1.22}
$$

where we used $[a_{\mathbf{Q}}^\dagger, a_{\mathbf{Q}}] = -1$, $[n_L, S] = [n_R, S] = 0$, and the fact that in the sum $\sum_{\mathbf{Q}}$ we can change from $\mathbf{Q}$ to $-\mathbf{Q}$. The commutator

$$
\begin{aligned}
[A, B] &= \sum_{\mathbf{Q}}[\lambda_{\mathbf{Q}}a_{\mathbf{Q}}^\dagger - \lambda_{-\mathbf{Q}}a_{\mathbf{Q}}, \mu_{\mathbf{Q}}a_{\mathbf{Q}}^\dagger - \mu_{-\mathbf{Q}}a_{\mathbf{Q}}] = \\
&= \sum_{\mathbf{Q}}(\lambda_{\mathbf{Q}}\mu_{-\mathbf{Q}} - \lambda_{-\mathbf{Q}}\mu_{\mathbf{Q}}) = 0,
\end{aligned}
\tag{1.23}
$$

and consequently $[n_L A, n_R B] = 0$. We now use the commutators

$$
[n_L, p] = p, \quad [n_R, p] = -p
\tag{1.24}
$$

to calculate

$$
\begin{aligned}
\overline{p} &= e^{n_R B}e^{n_L A}pe^{-n_L A}e^{-n_R B} \\
&= e^{n_R B}\left(p + [n_L A, p] + \frac{1}{2!}[n_L A, Ap] + ...\right)e^{-n_R B} = \\
&= e^{n_R B}\left(p + Ap + \frac{1}{2!}A^2 p + ...\right)e^{-n_R B} \\
&= e^{n_R B}pe^A e^{-n_R B} = \\
&= \left(p + [n_R B, p] + \frac{1}{2!}[n_R B, -Bp] + ...\right)e^A \\
&= \left(p - Bp + \frac{1}{2!}B^2 p + ...\right)e^A = pe^{-B}e^A = pe^{A-B}.
\end{aligned}
\tag{1.25}
$$

It follows

$$
\overline{p} = pX, \quad X = \prod_{\mathbf{Q}} D_{\mathbf{Q}}\left(\frac{\alpha_{\mathbf{Q}} - \beta_{\mathbf{Q}}}{\omega_{\mathbf{Q}}}\right)
$$

$$
D_{\mathbf{Q}}(z) := e^{za_{\mathbf{Q}}^\dagger - z^* a_{\mathbf{Q}}}.
\tag{1.26}
$$

The operator

$$D(z) := \exp(za^\dagger - z^* a \ ) \tag{1.27}$$

is called *unitary displacement operator* in quantum optics [67]. The operation of $D(z)$ on the vacuum of a boson field mode with creation operator $a^\dagger$ and ground state $|0\rangle$ creates a coherent state $|z\rangle = D(z)|0\rangle$ of the boson field.

The operators s_L and s_R, Eq.(1.15) are transformed in a similar way. One has to use

$$
\begin{aligned}
{} [n_L, s_L] &= -s_L, \quad [n_R, s_R] = -s_R \\
[n_R, s_L] &= [n_L, s_R] = 0.
\end{aligned}
\tag{1.28}
$$

The result is

$$\overline{s}_L = s_L e^{-A}, \quad \overline{s}_R = s_R e^{-B}. \tag{1.29}$$

1.4.4   The transformed Hamiltonian

The transformed Hamiltonian $\overline{H}$ is obtained by transforming each term in Eq.(1.18) according to Eq.(1.20). The main effect of the transformation is that in $\overline{H}$ the term $H_{\alpha\beta}$ does no longer appear:

$$
\begin{aligned}
\overline{H} &= H_0 + \overline{H_T} + \overline{H_V} + \overline{H_{ep}} \\
H_0 &= \overline{\varepsilon_L} n_L + \overline{\varepsilon_R} n_R + H_p + H_{res} \\
\overline{H_T} &= T_c(pX + p^\dagger X^\dagger) \\
\overline{\varepsilon_L} &= \varepsilon_L - \sum_{\mathbf{Q}} \frac{|\alpha_{\mathbf{Q}}|^2}{\omega_{\mathbf{Q}}}, \quad \overline{\varepsilon_R} = \varepsilon_R - \sum_{\mathbf{Q}} \frac{|\beta_{\mathbf{Q}}|^2}{\omega_{\mathbf{Q}}}.
\end{aligned}
\tag{1.30}
$$

The energies ε_L and ε_R are renormalized to smaller values. The main effect, however, is the appearance of the factors X and $X^\dagger$ in the tunnel Hamiltonian $\overline{H}_T$. As we will see below, these factors will drastically change the transport properties of the double dot.

1.5   Master equation

No exact solution is possible for the expectation values of the dot variables. Our strategy will be to derive a master equation from the exact

time–evolution of the system. We will assume that the coupling to the left and right electron reservoirs is weak and a standard Born and Markov approximation with respect to this coupling is reasonable. On the other hand, the renormalization of the *intra*dot tunneling T by the phase factors X is non–perturbative in the electron–phonon coupling and one has to go beyond the standard Born and Markov approximation with respect to the electron–phonon interaction .

The assumption of weak reservoir coupling means that we neglect effects from higher order tunneling such as co–tunneling processes [86] throughout. In particular, we are outside the regime of strong coupling to the leads where signatures of the *Kondo effect* start to play a role [87–90]. We only mention that the study of the Kondo physics in coupled dots [69, 91–94] and in presence of additional inelastic processes such as microwaves [95–98] is another, extremely interesting field of recent research activities in mesoscopic transport.

1.5.1   Interaction picture

We define an interaction picture for arbitrary operators O and by the X operators by

$$\tilde{O} := e^{iH_0 t}\overline{O}e^{-iH_0 t}, \quad X_t := e^{iH_0 t}Xe^{-iH_0 t}. \tag{1.31}$$

Furthermore, for the total density matrix $\chi(t)$ which obeys the Liouville equation

$$\chi(t) = e^{-iHt}\chi_{t=0}e^{iHt}, \tag{1.32}$$

we define

$$\tilde{\chi}(t) := e^{iH_0 t}\overline{\chi(t)}e^{-iH_0 t}, \quad \overline{\chi(t)} := e^{-i\overline{H}t}\overline{\chi}_{t=0}e^{i\overline{H}t}. \tag{1.33}$$

The expectation value of any operator O is given by

$$\begin{aligned}
\langle O \rangle_t &:= \operatorname{Tr}(\chi(t)O) = \langle e^S \chi(t)e^{-S}e^S O e^{-S}\rangle \tag{1.34}\\
&= \langle \overline{\chi(t)O}\rangle = \langle e^{iH_0 t}\overline{\chi(t)}e^{-iH_0 t}e^{iH_0 t}\overline{O}e^{-iH_0 t}\rangle = \operatorname{Tr}\left(\tilde{\chi}(t)\tilde{O}(t)\right).
\end{aligned}$$

We therefore have

$$\begin{aligned}
\tilde{n}_L(t) &= n_L, \quad \tilde{n}_R(t) = n_R\\
\tilde{p}(t) &= pe^{i\varepsilon t}X_t, \quad \tilde{p^\dagger}(t) = p^\dagger e^{-i\varepsilon t}X_t^\dagger\\
\varepsilon &:= \overline{\varepsilon_L} - \overline{\varepsilon_R}. \tag{1.35}
\end{aligned}$$

The equation of motion for $\tilde{\chi}$ becomes

$$i\frac{d}{dt}\tilde{\chi}(t) = [\tilde{H}_T(t) + \tilde{H}_V(t) + \tilde{H}_{ep}(t), \tilde{\chi}(t)]. \tag{1.36}$$

This can be written as

$$
\begin{aligned}
\frac{d}{dt}\tilde{\chi}(t) &= -i[\tilde{H}_T(t), \tilde{\chi}(t)] - i[\tilde{H}_V(t) + \tilde{H}_{ep}(t), \tilde{\chi}(t)] = \\
&= -i[\tilde{H}_T(t), \tilde{\chi}(t)] - i[\tilde{H}_V(t) + \tilde{H}_{ep}(t), \chi_0] + \\
&\quad - \int_0^t dt'[\tilde{H}_V(t) + \tilde{H}_{ep}(t), [\tilde{H}_T(t') + \tilde{H}_V(t') + \tilde{H}_{ep}(t'), \tilde{\chi}(t')]].
\end{aligned}
\tag{1.37}
$$

As mentioned above, we completely concentrate on the boson shake up effect which originates from the diagonal part $H_{\alpha\beta}$ of the electron–phonon interaction. The off–diagonal terms will neglected in the following.

1.5.2 Perturbation theory in the coupling to the electron reservoirs

We define the effective density operator of the system dot+phonons,

$$\tilde{\rho}(t) = \mathrm{Tr}_{\mathrm{res}}\tilde{\chi}(t) \tag{1.38}$$

as the trace over the electron reservoirs (res). The trace $\mathrm{Tr}_{\mathrm{res}}$ over terms linear in $\overline{H}_V$ vanishes, and it remains

$$\frac{d}{dt}\tilde{\rho}(t) = -i[\tilde{H}_T(t), \tilde{\rho}(t)] - \mathrm{Tr}_{\mathrm{res}}\int_0^t dt'[\tilde{H}_V(t), [\tilde{H}_V(t'), \tilde{\chi}(t')]]. \tag{1.39}$$

Since the last term in Eq.(1.39) is already second order in $\overline{H}_V$, we can approximate

$$\tilde{\chi}(t') \approx R_0\tilde{\rho}(t') \tag{1.40}$$

under the integral, where R_0 is the equilibrium density matrix for the two electron reservoirs (left and right). Performing the commutators and using the free time evolution of the electron reservoir operators

$$\tilde{c}_{\mathbf{k}}(t) = c_{\mathbf{k}}(t) = e^{-i\varepsilon_{\mathbf{k}}^L t}c_k, \quad d_{\mathbf{k}}(t) = e^{-i\varepsilon_{\mathbf{k}}^R t}d_k, \tag{1.41}$$

one finds

$$
\begin{aligned}
\frac{d}{dt}\tilde{\rho}(t) \;=\; & -i[\tilde{H}_T(t), \tilde{\rho}(t)] \\
& - \sum_{\mathbf{k}} \int_0^t dt' g_{\mathbf{k}}(t-t') \left\{ \tilde{s}_L(t)\tilde{s}_L^\dagger(t')\tilde{\rho}(t') - \tilde{s}_L(t')^\dagger \tilde{\rho}(t')\tilde{s}_L(t) \right\} \\
& - \sum_{\mathbf{k}} \int_0^t dt' \bar{g}_{\mathbf{k}}(t'-t) \left\{ \tilde{s}_L^\dagger(t)\tilde{s}_L(t')\tilde{\rho}(t') - \tilde{s}_L(t')\tilde{\rho}(t')\tilde{s}_L^\dagger(t) \right\} \\
& - \sum_{\mathbf{k}} \int_0^t dt' g_{\mathbf{k}}(t'-t) \left\{ \tilde{\rho}(t')\tilde{s}_L(t')\tilde{s}_L^\dagger(t) - \tilde{s}_L^\dagger(t)\tilde{\rho}(t')\tilde{s}_L(t') \right\} \\
& - \sum_{\mathbf{k}} \int_0^t dt' \bar{g}_{\mathbf{k}}(t-t') \left\{ \tilde{\rho}(t')\tilde{s}_L^\dagger(t')\tilde{s}_L(t) - \tilde{s}_L(t)\tilde{\rho}(t')\tilde{s}_L^\dagger(t') \right\} \\
& - (V_{\mathbf{k}} \to W_{\mathbf{k}} \, and \, L \to R), \quad \overline{f}_{\mathbf{k}}^L := 1 - f_{\mathbf{k}}^L \\
& g_{\mathbf{k}}(\tau) := V_{\mathbf{k}}^2 f_{\mathbf{k}}^L e^{i\varepsilon_{\mathbf{k}}^L \tau}, \quad \bar{g}_{\mathbf{k}}(\tau) := V_{\mathbf{k}}^2 \bar{f}_{\mathbf{k}}^L e^{i\varepsilon_{\mathbf{k}}^L \tau}. \tag{1.42}
\end{aligned}
$$

Here, we introduced the Fermi distributions

$$
\begin{aligned}
f_{\mathbf{k}}^L &\equiv f^L(\varepsilon_{\mathbf{k}}) := \mathrm{Tr}_{res}(R_0 c_{\mathbf{k}}^\dagger c_{\mathbf{k}}) \\
f_{\mathbf{k}}^R &:= \mathrm{Tr}_{res}(R_0 d_{\mathbf{k}}^\dagger d_{\mathbf{k}}). \tag{1.43}
\end{aligned}
$$

We now write

$$
\sum_{\mathbf{k}} V_{\mathbf{k}}^2 f_{\mathbf{k}}^L e^{i\varepsilon_{\mathbf{k}}^L(t-t')} = \int_{-\infty}^{\infty} d\varepsilon \, \nu(\varepsilon) f^L(\varepsilon) e^{i\varepsilon(t-t')} \tag{1.44}
$$

and assume that the tunneling density of states

$$
\nu(\varepsilon) := \sum_{\mathbf{k}} V_{\mathbf{k}}^2 \delta(\varepsilon - \varepsilon_{\mathbf{k}}) \approx \nu(\overline{\varepsilon}_L) \tag{1.45}
$$

can be considered as a constant around $\overline{\varepsilon}_L$ and its energy dependence can be neglected. Furthermore, the chemical potential μ_L of the left electron reservoir is assumed be so large that no electrons can tunnel back from the left dot to the left reservoir. In the limit $\mu_L \to +\infty$, the Fermi distribution $f_L(\varepsilon)$ equals unity, and one obtains

$$
\begin{aligned}
\sum_{\mathbf{k}} V_{\mathbf{k}}^2 f_{\mathbf{k}}^L e^{i\varepsilon_{\mathbf{k}}^L(t-t')} &\approx \Gamma_L \delta(t-t') \\
\Gamma_L &:= 2\pi \sum_{\mathbf{k}} V_{\mathbf{k}}^2 \delta(\overline{\varepsilon}_L - \varepsilon_{\mathbf{k}}^L). \tag{1.46}
\end{aligned}
$$

In the same way, we assume the chemical potential μ_R of the *right* electron reservoir to be deep below the energy $\overline{\varepsilon}_R$ so that no electrons can tunnel from the right reservoir to the right dot. In this limit $\mu_R \to -\infty$,

$$\sum_{\mathbf{k}} W_{\mathbf{k}}^2 (1 - f_{\mathbf{k}}^R) e^{i\varepsilon_{\mathbf{k}}^R (t-t')} \approx \Gamma_R \delta(t - t')$$

$$\Gamma_R := 2\pi \sum_{\mathbf{k}} W_{\mathbf{k}}^2 \delta(\overline{\varepsilon}_R - \varepsilon_{\mathbf{k}}^R). \tag{1.47}$$

With these approximations, the master equation Eq.(1.42) becomes

$$\begin{aligned}
\tilde{\rho}(t) &= \bar{\rho}_0 - i \int_0^t dt' [\tilde{H}_T(t), \tilde{\rho}(t)] \tag{1.48} \\
&- \Gamma_L \int_0^t dt' \left\{ \tilde{s}_L(t') \tilde{s}_L^\dagger(t') \tilde{\rho}(t') - 2\tilde{s}_L(t')^\dagger \tilde{\rho}(t') \tilde{s}_L(t') \right\} \\
&- \Gamma_L \int_0^t dt' \left\{ \tilde{\rho}(t') \tilde{s}_L(t') \tilde{s}_L^\dagger(t') \right\} \\
&- \Gamma_R \int_0^t dt' \left\{ \tilde{s}_R^\dagger(t') \tilde{s}_R(t') \tilde{\rho}(t') \right\} \\
&- \Gamma_R \int_0^t dt' \left\{ -2\tilde{s}_R(t') \tilde{\rho}(t') \tilde{s}_R^\dagger(t') + \tilde{\rho}(t') \tilde{s}_R^\dagger(t') \tilde{s}_R(t') \right\},
\end{aligned}$$

where we performed one integration from 0 to t.

1.5.3   Equations of motions

It is convenient to derive the equations of motions for the expectation values of the dot variables directly from the master equation Eq.(1.48). One first calculates the commutators

$$\begin{aligned}
[\tilde{n}_L(t), \tilde{H}_T(t')] &= -[\tilde{n}_R(t), \tilde{H}_T(t')] = T_c \left(\tilde{p}(t') - \tilde{p}^\dagger(t') \right) \\
\left[\tilde{p}(t), \tilde{H}_T(t') \right] &= T_c e^{i\varepsilon(t-t')} \left\{ n_L X_t X_{t'}^\dagger - n_R X_{t'}^\dagger X_t \right\} \\
\left[\tilde{p}^\dagger(t), \tilde{H}_T(t') \right] &= T_c e^{-i\varepsilon(t-t')} \left\{ n_R X_t^\dagger X_{t'} - n_L X_{t'} X_t^\dagger \right\}. \tag{1.49}
\end{aligned}$$

One has to use the completeness relation

$$1 = |0\rangle\langle 0| + n_R + n_L \tag{1.50}$$

in the three–dimensional Hilbertspace of the double dot to express $\tilde{s}_L(t')\tilde{s}_L^\dagger(t') = |0\rangle\langle 0| = 1 - n_R - n_L$. Multiplying Eq.(1.48) with n_L, n_R, p, and $p^\dagger$ and performing the trace with the three dot states Eq.(1.14), one obtains

$$
\begin{aligned}
\langle n_L\rangle_t - \langle n_L\rangle_0 &= -iT_c \int_0^t dt' \left\{ \langle p\rangle_{t'} - \langle p^\dagger\rangle_{t'} \right\} + 2\Gamma_L \int_0^t dt' (1 - \langle n_L\rangle_{t'} - \langle n_R\rangle_{t'}) \\
\langle n_R\rangle_t - \langle n_R\rangle_0 &= iT_c \int_0^t dt' \left\{ \langle p\rangle_{t'} - \langle p^\dagger\rangle_{t'} \right\} - 2\Gamma_R \int_0^t dt' \langle n_R\rangle_{t'} \\
\langle p\rangle_t - \langle p\rangle_t^0 &= -\Gamma_R \int_0^t dt' e^{i\varepsilon(t-t')} \langle X_t X_{t'}^\dagger \tilde{p}(t')\rangle_{t'} \\
&\quad - iT_c \int_0^t dt' e^{i\varepsilon(t-t')} \left\{ \langle n_L X_t X_{t'}^\dagger\rangle_{t'} - \langle n_R X_{t'}^\dagger X_t\rangle_{t'} \right\} \\
\langle p^\dagger\rangle_t - \langle p^\dagger\rangle_t^0 &= -\Gamma_R \int_0^t dt' e^{-i\varepsilon(t-t')} \langle \tilde{p}^\dagger(t') X_{t'} X_t^\dagger\rangle_{t'} \\
&\quad + iT_c \int_0^t dt' e^{-i\varepsilon(t-t')} \left\{ \langle n_L X_{t'} X_t^\dagger\rangle_{t'} - \langle n_R X_t^\dagger X_{t'}\rangle_{t'} \right\}.
\end{aligned}
\tag{1.51}
$$

Here, the expectation value

$$
\langle A\rangle_{t'} := \mathrm{Tr}_{d,ph}\left(\tilde{\rho}(t') \tilde{A}(t') \right) \tag{1.52}
$$

is defined as the trace over the dot and the phonon system. Furthermore, we defined

$$
\langle p^{(\dagger)}\rangle_t^0 := \mathrm{Tr}_{d,ph}\left(\bar{\rho}_0 (p e^{i\varepsilon t} X_t)^{(\dagger)} \right). \tag{1.53}
$$

In the following, we assume a factorization of the initial density matrix at time $t = 0$ into phonon and dot variables according to

$$
\bar{\rho}_0 = \rho_{ph}^0 \mathrm{Tr}_{ph}\rho_0. \tag{1.54}
$$

Such a factorized form of the density operator is given, e.g., when at time $t = 0$ the density matrix ρ_0 has the form $\rho_0 \propto \exp(-\beta(H - H_V))$, i.e. the system is isolated from the electron reservoirs for times $t \leq 0$. In general, such a factorization condition is a (plausible) assumption; in general, initial density matrices for interacting systems have to be constructed from, e.g., thermodynamical principles.

The time evolution of the expectation values $\langle p^{(\dagger)}\rangle_t^0$ describes the decay of an initial polarization of the system and can be calculated exactly [99, 100].

This decay, however, plays no role for the stationary current, and we assume that the inital expectation values of $p^{(\dagger)}$ vanish at time $t = 0$, whence they vanish for all times $t > 0$.

1.5.4 Decoupling and Laplace transformation

As can be reckognized from Eq.(1.51), the system of equations for the dot expectation values is not closed. There are terms like $\langle n_L X_t X_{t'}^{\dagger} \rangle_{t'}$ which contain products of dot operators and phonon operators. At this point, one can use a physical argument to decouple the equations: if one is not interested in the backaction of the electron system onto the phonon system, the latter can be assumed to be in thermal equilibrium all the time. Since the operators X correspond to a continuum of phonon modes $\mathbf{Q}$, it makes sence to treat them as an equilibrium bath. We use a *decoupling* of the reduced density matrix $\tilde{\rho}(t')$ according to

$$\tilde{\rho}(t') \approx \rho_{ph}^0 \mathrm{Tr}_{ph}\tilde{\rho}(t'). \tag{1.55}$$

This is an approximation by which the results following from it become no longer exact. The comparison to the spin–boson problem (appendix A.2) shows that the decoupling approximation corresponds to the so–called non–interacting–blib–approximation [101,102], which is a standard approximation in the dissipative spin–boson problem. Corrections to this approximations in principle can be obtained by setting up equations of motions for terms like $\langle n_L X_t X_{t'}^{\dagger} \rangle_{t'}$ which leads to higher order correlation functions. The latter can then be decoupled at any higher level. Since we are interested in small coupling parameters here, we do not further pursue this method [103] and stay within the lowest level of the decoupling hierarchy.

Using Eq.(1.55), one immediately obtains

$$\mathrm{Tr}(\tilde{\rho}(t') n_L X_t X_{t'}^{\dagger}) \quad \approx \quad \langle n_L \rangle_{t'} \langle X_t X_{t'}^{\dagger} \rangle_0 \tag{1.56}$$

and corresponding for the other products of operators.

For an equilibrium bath, the expectation value

$$\begin{aligned}
\langle X_t X_{t'}^{\dagger} \rangle_0 &=: \quad C(t - t') \\
C(t - t') &= \quad C^*(t' - t)
\end{aligned} \tag{1.57}$$

is a function of the time difference only. We therefore can define the Laplace transformation for real z,

$$
\begin{aligned}
C_\varepsilon(z) &:= \int_0^\infty dt e^{-zt} e^{i\varepsilon t} C(t) \\
n_L(z) &:= \int_0^\infty dt e^{-zt} \langle n_L \rangle_t \quad etc., \quad z > 0
\end{aligned}
\tag{1.58}
$$

and transform the whole equations of motion into z-space,

$$
\begin{aligned}
n_L(z) &= -i\frac{T_c}{z}\left(p(z) - p^*(z)\right) + 2\frac{\Gamma_L}{z}(1/z - n_L(z) - n_R(z)) \\
n_R(z) &= i\frac{T_c}{z}\left(p(z) - p^*(z)\right) - 2\frac{\Gamma_R}{z}n_R(z) \\
p(z) &= -iT_c\left\{n_L(z)C_\varepsilon(z) - n_R(z)C_{-\varepsilon}^*(z)\right\} - \Gamma_R p(z)C_\varepsilon(z) \\
p^*(z) &= iT_c\left\{n_L(z)C_\varepsilon^*(z) - n_R(z)C_{-\varepsilon}(z)\right\} - \Gamma_R p^*(z)C_\varepsilon^*(z).
\end{aligned}
\tag{1.59}
$$

These equations can now be solved algebraically.

1.5.5   The stationary tunnel current

The operator for the tunnel current, $\hat{I}$, can be defined in the following way: we consider the change of the occupation of the left dot n_L due to tunneling from/to the right dot as a function of time. This change is given by

$$
\begin{aligned}
\dot{n}_L|_{LR} &= iT(p^\dagger - p) \\
&+ \sum_{\mathbf{Q}}\left(-\gamma_{\mathbf{Q}}p + \gamma_{\mathbf{Q}}^*p^\dagger\right)\left(a_{-\mathbf{Q}} + a_{\mathbf{Q}}^\dagger\right).
\end{aligned}
\tag{1.60}
$$

The last term is proportional to the off–diagonal electron–phonon matrix element and involves combinations of electron and phonon operators. It corresponds to the tunneling of an electron with simultaneous emission/absorption of a phonon. Since we assumed $\gamma_{\mathbf{Q}} = 0$ here, this term does not contribute here. We set the electron charge $e = 1$ for convenience and therefore have for the current operator

$$
\hat{I} := iT_c(p - p^\dagger).
\tag{1.61}
$$

The full time-dependence of the expectation value $\langle I \rangle_t$ can be obtained from algebraically solving Eq.(1.59) and performing the Laplace back–transformation.

This is a formidable task; fortunately the physically most relevant quantity is the *stationary* current which is expected to flow in the stationary state of the system for time $t \to \infty$. One then obtains the expectation value $\langle I \rangle_{t \to \infty}$ from the $1/z$–coefficient of the $I(z)$–expansion into a Laurent series for $z \to 0$ [104]. The result is

$$
\begin{aligned}
\langle I \rangle_{t \to \infty} &= T_c^2 \frac{2\Re\mathrm{e}(C_\varepsilon) + 2\Gamma_R |C_\varepsilon|^2}{|1 + \Gamma_R C_\varepsilon|^2 + 2T^2 B_\varepsilon} \\
B_\varepsilon &:= \Re\mathrm{e}\left\{ (1 + \Gamma_R C_\varepsilon) \left[\frac{C_{-\varepsilon}}{2\Gamma_R} + \frac{C_\varepsilon^*}{2\Gamma_L} \left(1 + \frac{\Gamma_L}{\Gamma_R}\right)\right]\right\}.
\end{aligned}
\tag{1.62}
$$

Here, we defined

$$
C_\varepsilon = \lim_{\delta \to 0} \int_0^\infty dt\, e^{-\delta t} e^{i\varepsilon t} C(t).
\tag{1.63}
$$

As a first check we verify that in the elastic limit, i.e. in the case when no phonon coupling is present, one reproduces the results of Stoof and Nazarov [77] . That is, in the elastic case, one has $C_\varepsilon = i/\varepsilon$, and

$$
\langle I \rangle_{t \to \infty} = T^2 \frac{2\Gamma_R}{\Gamma_R^2 + \varepsilon^2 + 2T^2(1 + \Gamma_R/2\Gamma_L)}
\tag{1.64}
$$

which is a Lorentzian curve for the stationary tunnel current as a function of the energy difference ε. Note that we use a definition of $\Gamma_{R/L} = (1/2)\Gamma_{R/L}(\text{Stoof/Nazarov})$.

The appearance of the intradot tunneling matrix element T_c in the denominator of Eq.(1.64) indicates that this result is non–perturbative, i.e. valid to all orders in T_c. The modification of this curve by the electron–phonon interaction is completely described by the form of the function C_ε which we will discuss now.

1.6   Interference and electron–phonon interaction

We recall the form of the electron–phonon coupling in our model,

$$
H_{\alpha\beta} = \sum_{\mathbf{Q}} (\alpha_{\mathbf{Q}} n_L + \beta_{\mathbf{Q}} n_R) \left(a_{-\mathbf{Q}} + a_{\mathbf{Q}}^\dagger \right),
\tag{1.65}
$$

that couples only to the occupation number operators n_L and n_R. For a harmonic phonon system in thermal equilibrium at inverse temperature $\beta = 1/k_B T$, one finds for the correlation function $C(t - t')$,

$$
\begin{aligned}
C(t - t') &\equiv \langle X_t X_{t'}^\dagger \rangle_0 = e^{-\Phi(t - t')} \\
\Phi(t) &:= \int_0^\infty d\omega \rho(\omega) \left\{ (1 - \cos \omega t) \coth(\beta \omega / 2) + i \sin \omega t \right\} \\
\rho(\omega) &= \sum_{\mathbf{Q}} \frac{|\alpha_{\mathbf{Q}} - \beta_{\mathbf{Q}}|^2}{\omega^2} \delta(\omega - \omega_{\mathbf{Q}}).
\end{aligned}
\tag{1.66}
$$

The derivation of these relations is quite straightforward. One has to use the definition Eq. (1.26),

$$
X = \prod_{\mathbf{Q}} D_{\mathbf{Q}} \left(\frac{\alpha_{\mathbf{Q}} - \beta_{\mathbf{Q}}}{\omega_{\mathbf{Q}}} \right), \quad D_{\mathbf{Q}}(z) := e^{z a_{\mathbf{Q}}^\dagger - z^* a_{\mathbf{Q}}},
\tag{1.67}
$$

and the relations for the unitary displacement operator for the harmonic oscillator mode with creation operator $a^\dagger$ and frequency ω,

$$
\begin{aligned}
D(\alpha) &:= \exp(\alpha a^\dagger - \alpha^* a) \\
D(\alpha)^\dagger &= D(-\alpha), \quad D(\alpha)D(\beta) = D(\alpha + \beta) e^{i\Im m(\alpha \beta^*)},
\end{aligned}
\tag{1.68}
$$

as is explained, e.g., in [67]. Furthermore, one requires the thermal equilibrium expectation value of $D(\alpha)$

$$
\langle D(\alpha) \rangle_0 := \frac{\mathrm{Tr}(e^{-\beta \omega a^\dagger a} D(\alpha))}{\mathrm{Tr}(e^{-\beta \omega a^\dagger a})} = \exp \left\{ -\frac{1}{2} |\alpha|^2 \coth(\beta \omega / 2) \right\}.
\tag{1.69}
$$

1.6.1 Electron-Phonon coupling

For the following we always assume a coupling to (bulk) three dimensional phonons. This assumption is a matter of convenience because our intention here is to concentrate on the main physics of the interference effects for phonon coupling in double quantum dots. In section 1.9.2 we comment on other, probably more realistic choices that take into account the effect of surface acoustic phonons.

The electron–phonon interaction potential in real space in first quantization is given by

$$V_{ep}(\mathbf{x}) = \sum_{\mathbf{Q}} \lambda_{\mathbf{Q}} e^{i\mathbf{Q}\mathbf{x}} \left(a_{-\mathbf{Q}} + a^{\dagger}_{-\mathbf{Q}} \right), \quad \lambda_{\mathbf{Q}} = \lambda^{*}_{-\mathbf{Q}}. \tag{1.70}$$

In second quantization with respect to the dot system, this interaction becomes

$$V_{ep} = \int d^3\mathbf{x}\Psi^{\dagger}(\mathbf{x})V_{ep}(\mathbf{x})\Psi(\mathbf{x}), \tag{1.71}$$

where $\Psi(\mathbf{x})$ is the electron field operator. Then, the matrix elements $\alpha_{\mathbf{Q}}$ and $\beta_{\mathbf{Q}}$ become

$$\alpha_{\mathbf{Q}} = \lambda_{\mathbf{Q}} \int d^3\mathbf{x} e^{i\mathbf{Q}\mathbf{x}} \rho_L(\mathbf{x}) \quad \beta_{\mathbf{Q}} = \lambda_{\mathbf{Q}} \int d^3\mathbf{x} e^{i\mathbf{Q}\mathbf{x}} \rho_R(\mathbf{x})$$

$$\rho_L(\mathbf{x}) := \langle L|\Psi^{\dagger}(\mathbf{x})\Psi(\mathbf{x})|L\rangle \quad \rho_R(\mathbf{x}) := \langle R|\Psi^{\dagger}(\mathbf{x})\Psi(\mathbf{x})|R\rangle, \tag{1.72}$$

where we introduced the local electron densities $\rho_L(\mathbf{x})$ and $\rho_R(\mathbf{x})$ in the left and the right dot, respectively. The exact form of both $\rho_L(\mathbf{x})$ and $\rho_R(\mathbf{x})$ depends on the shape of the left and the right quantum dots and on the number of electrons N_L and N_R in both dots. In general, it will be impossible to calculate both densities exactly. It is, however, reasonable to assume that in the stationary state for $t \to \infty$ both densities are smooth functions of $\mathbf{x}$ centered around the center of the left ($\rho_L(\mathbf{x})$) and the right ($\rho_L(\mathbf{x})$) dot, i.e.

$$\rho_L(\mathbf{x}) \approx \rho_e(\mathbf{x} - \mathbf{x}_L), \quad \rho_R(\mathbf{x}) \approx \rho_e(\mathbf{x} - \mathbf{x}_R), \tag{1.73}$$

where for simplicity we assumed that both left and right electron densities are described by the same profile. Here, the function $\rho_e(\mathbf{x})$ is relatively sharply peaked around zero. The assumption of identical, but spacially shifted electron density profiles in both dots allows one to establish a relation between the matrix elements $\alpha_{\mathbf{Q}}$ and $\beta_{\mathbf{Q}}$. That is, one has

$$\alpha_{\mathbf{Q}} = \lambda_{\mathbf{Q}} e^{i\mathbf{Q}\mathbf{r}_L} P_e(\mathbf{Q}), \quad \beta_{\mathbf{Q}} = \lambda_{\mathbf{Q}} e^{i\mathbf{Q}\mathbf{r}_R} P_e(\mathbf{Q})$$

$$P_e(\mathbf{Q}) := \int d^3\mathbf{x} e^{i\mathbf{Q}\mathbf{x}} \rho_e(\mathbf{x}) \tag{1.74}$$

whence

$$\beta_{\mathbf{Q}} = \alpha_{\mathbf{Q}} e^{i\mathbf{Q}\mathbf{d}}, \quad \mathbf{d} = \mathbf{r}_R - \mathbf{r}_L, \tag{1.75}$$

$$C(t - t') \equiv \langle X_t X_{t'}^{\dagger} \rangle_0 = e^{-\Phi(t-t')}$$

$$\Phi(t) := \int_0^{\infty} d\omega \rho(\omega) \left\{ (1 - \cos \omega t) \coth(\beta \omega / 2) + i \sin \omega t \right\}$$

$$\rho(\omega) = \sum_{\mathbf{Q}} \frac{|\alpha_{\mathbf{Q}} - \beta_{\mathbf{Q}}|^2}{\omega^2} \delta(\omega - \omega_{\mathbf{Q}}).$$
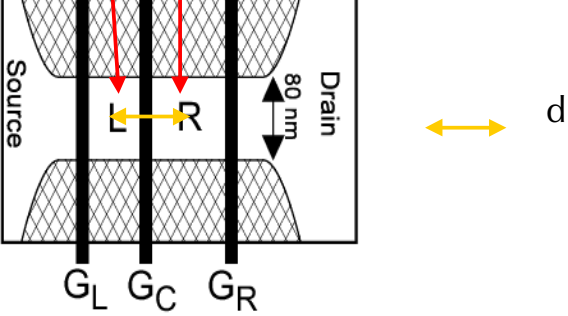
phaserelation

$$\beta_{\mathbf{Q}} = \alpha_{\mathbf{Q}} e^{i\mathbf{q}\mathbf{d}}, \quad \mathbf{d} = \mathbf{r}_R - \mathbf{r}_L,$$

Fig. 1.15: Phase relation between the electron phonon coupling matrix elements $\alpha_{\mathbf{Q}}$ ($\beta_{\mathbf{Q}}$) for coupling to left (right) dot for charge distributions centered sharply around the dot centers (distance d), cp. Eq.(1.75). The coupling constants enter the expression Eq.(1.66) for the function $\rho(\omega)$ which governs the effective electron–phonon coupling.

where $\mathbf{d}$ is the vector pointing from the center of the left to the center of the right dot.

One can check the validity of the above argumentation in the single particle case. In this case, the two states $|L\rangle$ and $|R\rangle$ correspond to single particle wave functions that can, at least in principle, be easily calculated for a given dot potential. Here, we write the wave functions as

$$\langle \mathbf{x} | R \rangle = \chi(z) \phi_R(|\mathbf{r} - \mathbf{r}_R|), \quad \langle \mathbf{x} | L \rangle = \chi(z) \phi_L(|\mathbf{r} - \mathbf{r}_L|), \quad (1.76)$$

where $\mathbf{x} = (\mathbf{r}, z)$, $\chi(z) = \chi(-z)$ is a quantum well wave function and ϕ_R and ϕ_L describe spherically symmetric wave functions for the additional electron in the right and the left dot which are centered around $\mathbf{r}_R$ and $\mathbf{r}_L$, respectively. Furthermore, $\mathbf{r}$ is a vector in the 2DEG x–y plane. Using the notation

$\mathbf{Q} = (\mathbf{q}, q_z)$ in Q-space, one has

$$
\begin{aligned}
\alpha_{\mathbf{Q}} &= \lambda_{\mathbf{Q}} \langle L | e^{i\mathbf{Q}\mathbf{x}} | L \rangle = \lambda_{\mathbf{Q}} \langle \chi | e^{i q_z z} | \chi \rangle \langle \phi_L | e^{i\mathbf{q}\mathbf{r}} | \phi_L \rangle \\
&= \lambda_{\mathbf{Q}} F(q_z) e^{i\mathbf{q}\mathbf{r_L}} P_L(\mathbf{q}),
\end{aligned}
$$

$$
F(q_z) := \langle \chi | e^{i q_z z} | \chi \rangle, \quad P_L(q) := \int d\mathbf{r}^2 |\phi_L(r)|^2 e^{i\mathbf{q}\mathbf{r}} \qquad (1.77)
$$

The real function $F(q_z)$ is a quantum well form factor that effectively cuts off phonon contributions with large q_z. Since $P_L(q)$ is the Fourier transform of a rotational symmetric function, it depends only on the modulus q, and $P_L(q) = P_L^*(q)$ is real. Using the same notation for $\beta_{\mathbf{Q}}$, we have

$$
\begin{aligned}
\alpha_{\mathbf{Q}} &= e^{i\mathbf{q}\mathbf{r}_L} \lambda_{\mathbf{Q}} F(q_z) P_L(\mathbf{q}) \\
\beta_{\mathbf{Q}} &= e^{i\mathbf{q}\mathbf{r}_R} \lambda_{\mathbf{Q}} F(q_z) P_R(\mathbf{q}).
\end{aligned} \qquad (1.78)
$$

For identical wave functions $\phi_R = \phi_L$, we again reckognize that the coupling constants $\alpha_{\mathbf{Q}}$ and $\beta_{\mathbf{Q}}$ just differ by a phase,

$$
\beta_{\mathbf{Q}} = \alpha_{\mathbf{Q}} e^{i\mathbf{q}\mathbf{d}}, \quad \mathbf{d} = \mathbf{r}_R - \mathbf{r}_L, \qquad (1.79)
$$

where $\mathbf{d}$ is the vector pointing from the center of the left to the center of the right dot. This agrees with Eq.(1.75) if the vector $\mathbf{d}$ is lying in the x–y plane, i.e. the centers of the electron density profiles in both dots are in the x–y plane.

1.6.2   The function $\rho(\omega)$

In order to explicitly calculate $\rho(\omega)$ (we re-insert the $\hbar$ into Eq. (1.66))

$$
\rho(\omega) = \sum_{\mathbf{Q}} \frac{|\alpha_{\mathbf{Q}} - \beta_{\mathbf{Q}}|^2}{\hbar^2 \omega^2} \delta(\omega - \omega_{\mathbf{Q}}), \qquad (1.80)
$$

we assume an identical charge density profile in the dot with Fourier transform $P_e(\mathbf{Q})$, Eq.(1.74). We write $\mathbf{Q} = (\mathbf{q}, q_z)$ and assume the vector $\mathbf{d}$ to lie in the x–y plane as well as $P_e(\mathbf{Q}) = P_e(q, q_z)$, i.e. a x–y rotational symmetric charge profile in the dot.

In the following, the phonons are assumed to be the three-dimensional modes of the bulk crystal. Since the material where the experiments are performed is Gallium–Arsenide which is piezoelectric, there are both deformation potential and piezoelectric modes in the low-energy dispersion (Debye-spectrum) of the phonons [105]. The optical branches of the phonon spectrum

can be savely neglected here. Their energies ($\sim 36 meV$) are orders of magnitudes larger than the energy transfers considered here, which are of the order of a few tenths or hundredth micro eV.

Piezoelectric interaction

We first consider the piezoelectric acoustical interaction with an interaction matrix element

$$|\lambda_Q|^2 = \frac{1}{V}\frac{\lambda^2}{cQ}, \quad \lambda^2 = \frac{\hbar P}{2\rho_M}, \tag{1.81}$$

where c is the longitudinal speed of sound, $\omega_Q = cQ \equiv c|\mathbf{Q}|$ the phonon dispersion, V the volume and ρ_M the mass density of the crystal, and P the piezoelectric coupling. Here, we followed [106] and used a simpifying angular average of the absolute square of the piezoelectric coupling function $\lambda_{\mathbf{Q}}$ with

$$P := (eh_{14})^2 \left(\frac{12}{35} + \frac{1}{x}\frac{16}{35}\right). \tag{1.82}$$

Here, for simplicity screening effects of the 2DEG have been absorbed into the value of P and dynamical screening has been neglected. Furthermore, the averages over the two transverse and the longitudinal mode are performed seperately and their contributions are added then. The only remaining velocity of sound in this approximation is the longitudinal one. We point out that this again is a simplifying approximation of the electron–phonon interaction. For quantitative agreement with experiments, the full directional dependence of the matrix elements has to be kept [107].

Within these approximations, one obtains

$$\begin{aligned}
\rho(\omega) &= \frac{\lambda^2}{\hbar^2\omega^3 V}\sum_{\mathbf{Q}}\delta(\omega - cQ)P_e^2(q, q_z)|1 - e^{i\mathbf{q}\mathbf{d}}|^2 = \\
&= \frac{g}{\omega}\int_0^1 dx P_e^2\left(\frac{\omega}{c}\sqrt{1-x^2}, \frac{\omega}{c}x\right)\left(1 - J_0\left(\frac{d}{c}\omega\sqrt{1-x^2}\right)\right) \\
g &:= \frac{\lambda^2}{\pi^2\hbar^2 c^3}.
\end{aligned} \tag{1.83}$$

Here, J_0 is the zeroth order Bessel function and g is a dimensionless electron phonon coupling constant. If the charge density profile is sharply peaked, the

form factor $P_e(\mathbf{Q})$ tends towards unity. We use this condition to evaluate the integral Eq.(1.83) analytically. In fact, in the single particle wave function model above one could assume dot wave functions with a Gaussian shape whence

$$
\begin{aligned}
P_L(q) &= P_R(q) = e^{-(lq)^2/2} \\
F(q_z) &= e^{-(aq_z)^2/2}
\end{aligned}
\tag{1.84}
$$

and

$$
\rho(\omega) = \frac{g}{\omega} \int_0^1 dx\, e^{-\frac{\omega^2}{c^2}\left(l^2(1-x^2)+a^2x^2\right)} \left(1 - J_0\left(\frac{d}{c}\omega\sqrt{1-x^2}\right)\right) \tag{1.85}
$$

The limit $a = l = 0$ (infinitely small wave function extension in all directions) corresponds to $P_e(\mathbf{Q}) = 1$ in Eq. (1.83) and one obtains

$$
\rho(\omega) \approx \frac{g}{\omega}\left(1 - \frac{\omega_d}{\omega}\sin\left(\frac{\omega}{\omega_d}\right)\right), \quad \omega_d := c/d, \quad P_e(\mathbf{Q}) \to 1. \tag{1.86}
$$

A finite extension of the wave functions leads to a cutoff of phonons with frequencies larger than $min(c/l, c/a)$ which sets the scale for the effective Debye (cutoff) frequency ω_c for the electron–phonon interaction. To take into account this cutoff, we use for the following calculations an approximated form of the function $\rho(\omega)$ with a smooth exponential cutoff $\propto \exp(-\omega/\omega_c)$,

$$
\boxed{\rho(\omega) \approx \frac{g}{\omega}\left(1 - \frac{\omega_d}{\omega}\sin\left(\frac{\omega}{\omega_d}\right)\right) e^{-\omega/\omega_c}.} \tag{1.87}
$$

We show a plot of $\rho(\omega)$ (without exponential cutoff), Eq.(1.86), in Fig. (1.16). The most striking feature is the appearance of the oscillations in ω, which occur on the scale $\omega_d = c/d$. In fact, these oscillations resemble the oscillations in the current profile on the emission side at low temperature in the experiment [30]. Using parameters $d = 200 \cdot 10^{-9} m$ and $c = 5000 m/s$, we obtain $\hbar\omega_d = 16.5 \mu eV$, which is in fact the scale on which the oscillations occur in [30]. In the following subsection, we will show by numerical evaluation of the stationary current I, that the oscillations of $\rho(\omega)$ will indeed show up in the current as a function of the energy difference ε. Using typical GaAs parameters, see Table (1.1), we obtain $g \approx 0.05$.

Parameter	Symbol	Value
Mass density	ρ	5300 kg m^{-3}
Longitudinal speed of sound	c_L	5200 m s^{-1}
Transversal speed of sound	c_T	3000 m s^{-1}
Deformation Potential	Ξ	2.2×10^{-18}J
Piezoelectric constant	eh_{14}	$1.38 \times 10^9 eV$ m^{-1}
Piezoelectric coupling	P	5.4×10^{-20} J^2 m^{-2}

Tab. 1.1: Electron-phonon parameters in GaAs. Parameters are taken from Ref. [106]

Deformation potential interaction

For the (unscreened) deformation potential , the matrix element is

$$|\lambda_{\mathbf{Q}}|^2 = \frac{1}{V} \frac{\hbar \Xi^2}{2 \rho_M c} Q, \tag{1.88}$$

i.e. one has a linear dependence on the frequency $\omega = Q/c$. The corresponding function $\rho(\omega)$ is calculate as above, the analogous expression to the approximation Eq. (1.86) without cutoff reads

$$\rho(\omega) \approx \frac{\omega}{\omega_\xi^2} \left(1 - \frac{\omega_d}{\omega} \sin\left(\frac{\omega}{\omega_d} \right) \right)$$

$$\frac{1}{\omega_\xi^2} := \frac{1}{\pi^2 c^3} \frac{\Xi^2}{2 \rho_M c^2 \hbar}. \tag{1.89}$$

Again using standard GaAs parameters (Table (1.1)), one has $1/\omega_\xi^2 \sim 10^{-25} s^2$. In order to compare to the piezoelectric case, we write

$$\rho(\omega)_{\text{piezo}} \approx \frac{1}{\omega_d} g \frac{\omega_d}{\omega} \left(1 - \frac{\omega_d}{\omega} \sin\left(\frac{\omega}{\omega_d} \right) \right)$$

$$\rho(\omega)_{\text{def}} \approx \frac{1}{\omega_d} \left(\frac{\omega_d}{\omega_\xi} \right)^2 \frac{\omega}{\omega_d} \left(1 - \frac{\omega_d}{\omega} \sin\left(\frac{\omega}{\omega_d} \right) \right). \tag{1.90}$$

With $\omega_d \sim 2.5 \times 10^{10} s^{-1}$, one typically has for the ratio $(\omega_d/\omega_\xi)^2 \sim 6 \times 10^{-5}$. This means that for frequencies ω which are on the scale of ω_d (which in fact is the relevant energy scale here), the contribution from the bulk deformation

potential phonons is relatively small. With $g = 0.05$, the relative weight of the latter with respect to the piezoelectric phonons is $(\omega_d/\omega_\xi)^2/g \sim 10^{-3}$. The sum of both contributions is shown in Fig. (1.16) for this ratio, where small deviations from the pure piezoelectric case become visible above $x = \omega/\omega_d \sim 10$.
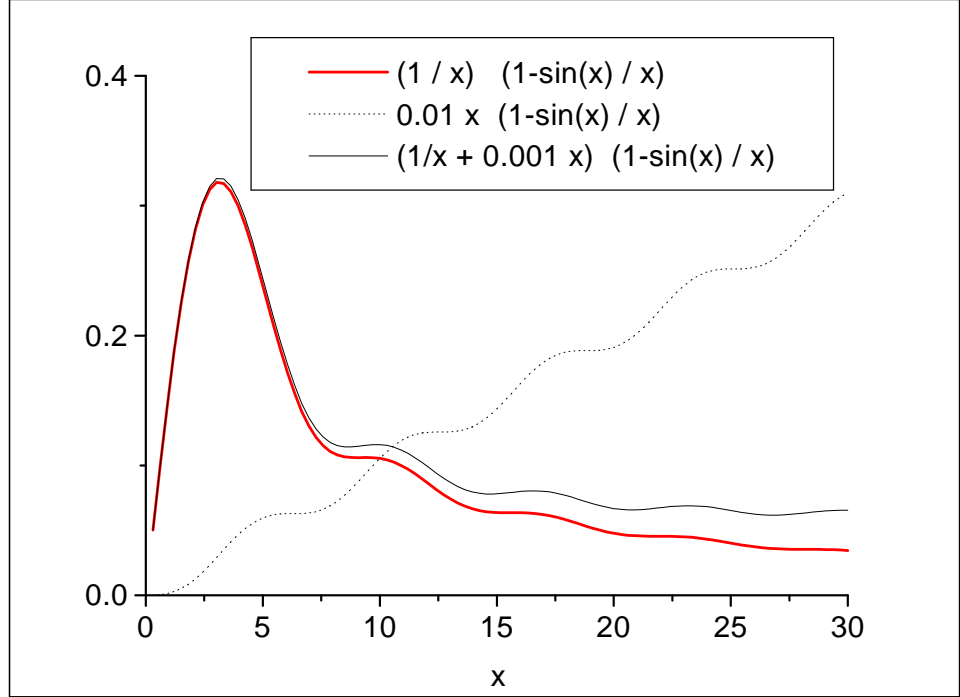
Fig. 1.16: Comparison of the two dimensionless functions $\rho(\omega)$, Eq. (1.90) (without prefactors), for bulk piezoelectrical coupling (thick red solid line) and for bulk deformation potential coupling (dashed). Note the factor 0.01 in the latter case. The sum of both contribution with a relative weight of the deformation potential phonons of 10^{-3} is shown as thin black solid line. The variable $x = \omega/\omega_d$.

1.6.3 Exactly solvable limit and physical meaning of the function C_ε

It is not possible to obtain an analytical form for the Laplace transform

$$C_\varepsilon := \lim_{\delta \to 0} \int_0^\infty dt e^{-\delta t} e^{i\varepsilon t} e^{-\Phi(t)} \tag{1.91}$$

of the correlation function $C(t) \equiv \exp\{-\Phi(t)\}$, Eq.(1.66), which is needed to evaluate the stationary current Eq.(1.62). Before we turn to its numerical evaluation, it is useful to consider the exactly solvable limit of pure piezo-electric interaction and vanishing frequency $\omega_d = c/d = 0$ in Eq.(1.87). This corresponds to the case where the distance between the two dots is much larger than a typical phonon wave length. In particular, this means that no interference effects are expected in this limit. In fact, the oscillatory term then vanishes in Eq.(1.87) and

$$\rho(\omega) = \frac{g}{\omega} e^{-\omega/\omega_c}. \tag{1.92}$$

At temperature $T = 0$, one can in fact evaluate exactly the function $\Phi(t)$ appearing in the exponent in Eq. (1.66),

$$\Phi(t) = \int_0^\infty d\omega \rho(\omega)(1 - e^{-i\omega t}). \tag{1.93}$$

That is, for a generic form of the function $\rho(\omega)$,

$$\rho(\omega) = \frac{g}{\omega_c}\left(\frac{\omega}{\omega_c}\right)^{s-2}\exp(-\omega/\omega_c), \tag{1.94}$$

one finds, using standard integrals [108],

$$
\begin{aligned}
\Phi(t) &= g\Gamma(s-1)\left\{1 - \left(\frac{1}{1+i\omega_c t}\right)^{s-1}\right\}, \quad s > 0, s \neq 1 \\
\Phi(t) &= g\log(1+i\omega_c t), \quad s = 1.
\end{aligned}
\tag{1.95}
$$

The case $s = 1$ in fact can be obtained from the case for general s as a limit $s \to 1$ of the first equality in Eq. (1.95). The spectral form Eq. (1.94) is known from the theory of quantum dissipation (Brownian motion of a free particle with dissipation) or tunneling [102]. There, it corresponds to the so–alled sub–ohmic ($s < 1$), ohmic ($s = 1$) and super–ohmic ($s > 1$) cases which each define different long–time behaviour of, e.g., the time evolution of the second moment of a wave packet.

The bulk, unscreened piezoelectric coupling surprisingly corresponds exactly to the ohmic case $s = 1$ in this classification. This gives us the chance to find an exact expression for C_ε. Explicitely, one finds

$$C_\varepsilon = -i\left(-(\varepsilon+i\delta)\right)^{g-1}\Gamma(1-g, -(\varepsilon+i\delta))e^{-\varepsilon} \tag{1.96}$$

in units where $\omega_c = 1$. For $\varepsilon \ll 1$ and $g < 1$, one has the *power-law* behaviour

$$C_\varepsilon \sim -i\Gamma(1-g)(-(\varepsilon + i\delta))^{g-1}, \tag{1.97}$$

with the *dimensionless coupling constant g appearing as the power in the exponent* of the variable ε. This indicates that we have derived a non–perturbative result.

One now can verify a relation between the real part of C_ε and the Fourier transform of $C(t)$,

$$\tag{1.98}$$

$$
\begin{aligned}
lim_{\delta \to 0} 2ReC_\varepsilon &= 2\pi P(\varepsilon) \\
P(\varepsilon) &:= \frac{1}{2\pi} \int_{-\infty}^{\infty} dt e^{i\varepsilon t} C(t),
\end{aligned}
\tag{1.99}
$$

The real quantity $P(\varepsilon)$ is proportional to the probability density for inelastic tunneling from the left dot to the right dot with energy transfer ε (see [72] and below). In the case of no phonon coupling,

$$P(\varepsilon) = \delta(\varepsilon), \quad \text{no phonons}, \tag{1.100}$$

i.e. only elastic tunneling is possible. On the other hand, for the model Eq.(1.96) above, we find

$$P(\varepsilon) = \frac{1}{\Gamma(g)} \varepsilon^{g-1} e^{-\varepsilon} \theta(\epsilon) \tag{1.101}$$

at zero temperature, which is a Gamma distribution with parameter g. In particular, the step function in Eq. (1.101) guarantees that only spontaneous emission of phonons, accompagnied with an energy loss $\varepsilon = \varepsilon_L - \varepsilon_R > 0$ is possible at zero temperature. We remark that the function Eq. (1.101) often appears in the context of inelastic tunneling, when the degrees of freedom of a bosonic environment are modeled by an oscillator distribution $\rho(\omega)$ according to Eq.(1.92). The use of the function $P(E)$, Eq. (1.98), in such models is refered to as $P(E)$–*theory*.

We thus have learned that the real part of the function C_ε has the direct physical meaning of a probability for energy transfer during tunneling. Note, however, that the current is determined by the *complex* function C_ε which contains all effects of energy renormalization due to the electron-phonon coupling.

1.6.4 Inelastic tunneling rate and inelastic current

A more general expression for the function $P(\varepsilon)$ can be derived at zero temperature $T = 0$, if one expands the function $C(t)$ in the electron–phonon coupling. This also clarifies why $P(\varepsilon)$ is proportional to an inelastic tunneling rate.

We expand $C(t)$ to second order in the coupling (first order in $\rho(\omega)$),

$$\begin{aligned} C(t) &= e^{-\Phi(t)} \approx 1 - \Phi(t) \\ &= 1 - \int_0^\infty \rho(\omega) \left[1 - e^{-i\omega t} \right]. \end{aligned} \tag{1.102}$$

The resulting expression for $P(\varepsilon)$ becomes

$$\begin{aligned} P(\varepsilon) &= \frac{1}{2\pi} \int_{-\infty}^\infty dt\, e^{i\varepsilon t} C(t) \approx \delta(\varepsilon) \left\{ 1 - \int_0^\infty d\omega \rho(\omega) \right\} \\ &\quad + \frac{1}{2\pi} \int_{-\infty}^\infty dt\, e^{i\varepsilon t} \int_0^\infty d\omega \rho(\omega) e^{-i\omega t} \\ &= \delta(\varepsilon) \left\{ 1 - \int_0^\infty d\omega \rho(\omega) \right\} + \rho(\epsilon), \end{aligned} \tag{1.103}$$

where $\rho(\epsilon)$ has been defined above in Eq.(1.66),

$$\rho(\varepsilon) = \sum_{\mathbf{Q}} \frac{|\alpha_{\mathbf{Q}} - \beta_{\mathbf{Q}}|^2}{\varepsilon^2} \delta(\varepsilon - \omega_{\mathbf{Q}}) \tag{1.104}$$

(note that we set $\hbar = 1$ and $\rho(\varepsilon < 0) = 0$ because the phonon frequencies $\omega_{\mathbf{Q}}$ are positive).

We can derive an expression for the inelastic part of the stationary current, Eq. (1.62), in the following limit:

$$\varepsilon \gg \Gamma_R, \Gamma_L, 1/P(\varepsilon). \tag{1.105}$$

In the expression Eq. (1.62), we then replace the denominator by 1 and neglect $2\Gamma_R |C_\varepsilon|^2$ in the numerator. Since $P(\varepsilon)$ can be replaced by $\rho(\varepsilon)$ for $\varepsilon \neq 0$, using Eq. (1.98) and Eq.(1.103) we find

$$I_{\text{in}} \approx 2\pi T_c^2 \rho(\varepsilon). \tag{1.106}$$
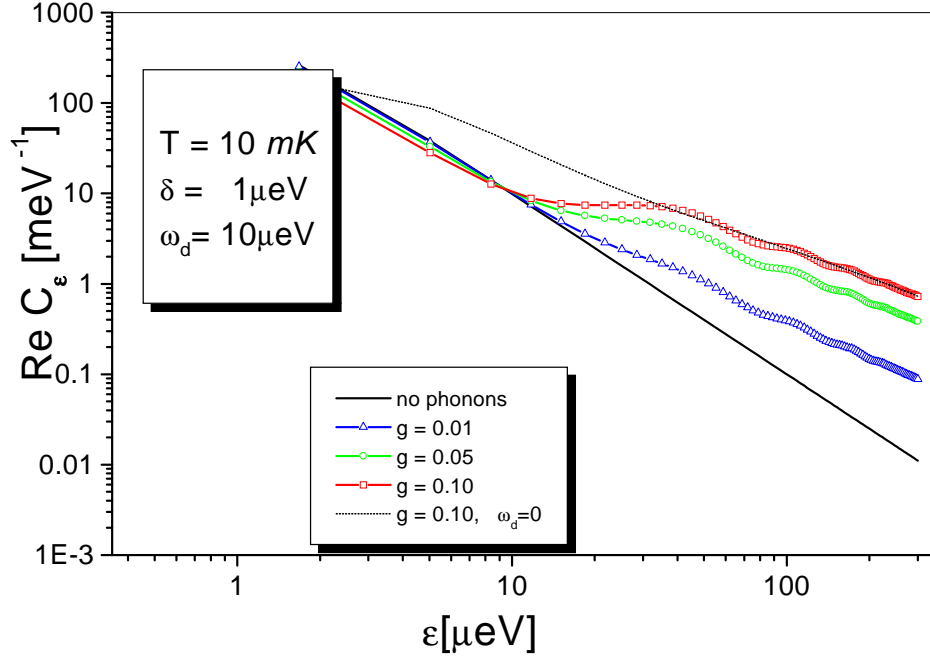
Fig. 1.17: Real part of C_ε, Eq.(1.91), as a function of the energy difference ε between left and right dot ground state energies. Energies $\hbar\omega_d = 10\mu$eV, $\hbar\delta = 1\mu$eV, cutoff $\hbar\omega_c = 1$meV.

This result is consistent with a previous model by Glazman and Matveev [2] for *inelastic tunneling through amorphous thin films* via pairs of impurities. There, perturbation theory in the electron–phonon deformation potential coupling was used to obtain the nonlinear current (without oscillations) for large area tunnel junctions after averaging over an ensemble of impurity pairs. In particular, if the tunneling through the two impurities is dominated by inelastic processes, the authors found $I_{in} = 2e\gamma$, where the *inelastic rate* γ

---

[2] L. I. Glazman and K. A. Matveev, Sov. Phys. JETP **67**, 1276 (88). Note that there, the expression for the spontaneous emission rate γ already contains the differences of phase factors ($\sim |1 - \exp\{i\mathbf{Q}\mathbf{d}\}|^2$ in our notation), which are averaged out in the cases they consider.

is defined as

$$\gamma(\varepsilon) := \pi T_c^2 \rho(\varepsilon) = \pi T_c^2 \sum_{\mathbf{Q}} \frac{|\alpha_{\mathbf{Q}} - \beta_{\mathbf{Q}}|^2}{\varepsilon^2} \delta(\varepsilon - \omega_{\mathbf{Q}}), \quad \varepsilon > 0, \tag{1.107}$$

cp. Eq.(1.103). We reckognize [109] that this rate is just the function $\rho(\varepsilon)$ multiplied with πT_c^2.

1.7 Results

1.7.1 Numerical evaluation

Explicit results for C_ε and the stationary current Eq.(1.62) have been obtained by numerical evaluation of Eq.(1.63), Eq.(1.66), with $\rho(\omega)$ given by Eq.(1.87). The integrand is split into zero–temperature and a finite temperature contributions as described in appendix A.1. The resulting double integral can be handled with standard numerical routines.

We kept the parameter δ, Eq.(1.63), at a small, but finite value to guarantee rapid convergence. In the strict limit $\delta \to 0$, there is a delta–peak like contribution to C_ε at $\varepsilon = 0$. This results from the fact the effective density of states $\rho(\omega)$ vanishes for $\omega = 0$ and the tunneling with energy transfer $\omega \to 0$ becomes elastic. This is the fact even in presence of the piezoelectric phonon coupling Eq.(1.81) that diverges for $\omega \to 0$. The reason is that for zero energy transfer the difference $\alpha_{\mathbf{Q}} - \beta_{\mathbf{Q}}$ vanishes and there is no boson shake–up effect. A small, but finite value of delta can be regarded as simulating the effect of the remaining off–diagonal electron–phonon interaction H_{ep}.

In Fig.(1.17) we show the real part of C_ε at a temperature of 10mK for different dimensionless electron–phonon coupling parameters g, Eq.(1.83). The curve for $g = 0$ is a sharply peaked Lorentzian whose width is determined by δ. On the absorption side $\varepsilon < 0$, there is practically no deviation for $g > 0$ compared with the $g = 0$–case. On the emission side $\varepsilon > 0$, the values are larger compared with $g = 0$ and increase with increasing g. Oscillations appear that become stronger for larger g. The dotted curve corresponds to the exactly solvable case Eq.(1.96), $\omega_d = 0$, which shows no oscillations but whose general shape coincides with the one for $\omega_d > 0$.
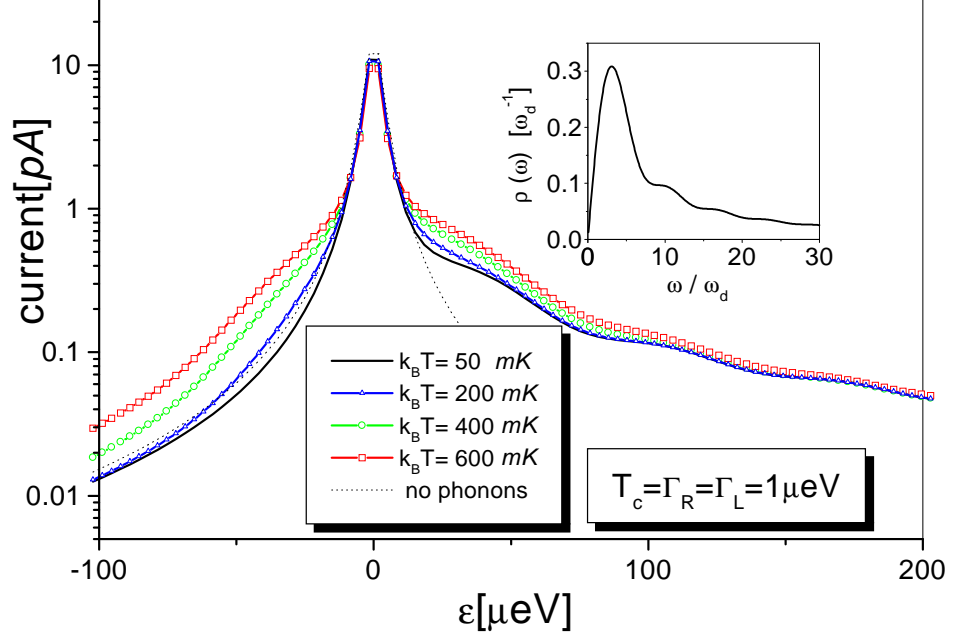
Fig. 1.18: Stationary tunnel current, Eq.(1.62), as a function of the energy difference ε between left and right dot ground state energies. Dimensionless electron–phonon coupling parameter: $g = 0.05$. Inset: effective density of states $\rho(\omega)$ of phonon modes, Eq.(1.86), for $g = 1$.

In Fig. 1.18 we show the stationary current Eq.(1.62) at different temperatures for parameters close to the ones of the experiment [30]. The inset shows the oscillatory structure of the effective density of states $\rho(\omega)$, Eq.(1.86), which is reflected in the oscillatory structure of the real part of C_ε. The cutoff energy in Eq.(1.86) and δ are chosen as $\hbar\omega_c = 1\text{meV}$ and $1\mu\text{eV}$, respectively. At low temperatures, there is a broad oscillatory shoulder on the emission side $\varepsilon > 0$ which reflects the structure of the real part of C_ε. At higher temperatures, on the absorption side the current increases to larger values faster than on the emission side where the oscillations start to be smeared out. The scaling of the current spectrum with energy and the relation between emission and absorption are discussed in section 1.8.2. Here we note that for $\varepsilon < 0$ and larger temperature, a new shoulder–like structure appears on the absorption side. A similar feature was also observed in the
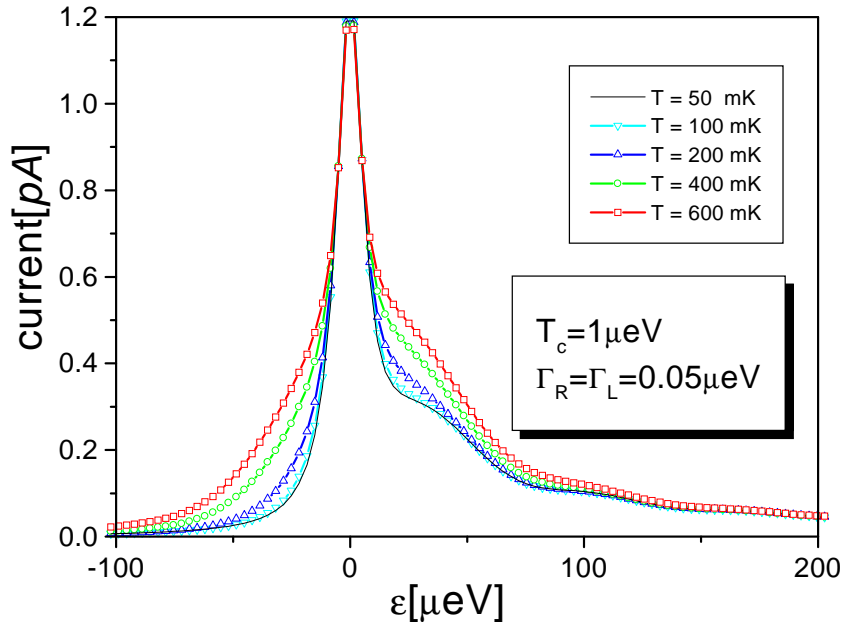
Fig. 1.19: Stationary tunnel current, Eq.(1.62), as a function of the energy difference ε between left and right dot ground state energies.

experiment [30].

1.7.2   Comparison with the experiment

Our theoretical results suggest that there is reason to assume that the microscopic mechanism for the spontaneous emission process in the experiment by Fujisawa et al. in fact is the coupling to acoustic phonons. Phonons in fact fit into the energy window $10 \sim 100$ μeV on the emission side tested in that experiment. One could argue that the generation of electron–hole pairs in the left and right reservoirs during the tunneling of electrons could be a competing mechanism. For this kind of processes we do not see, however, a microscopic explanation of the interference phenomenon on the emission side, i.e. the oscillations of the current $I(\varepsilon)$ as a function of ε. The coupling to phonons *within* the dot naturally leads to these oscillations due to the interference of matrix elements, i.e. the Dicke like effect as explained above. Still,
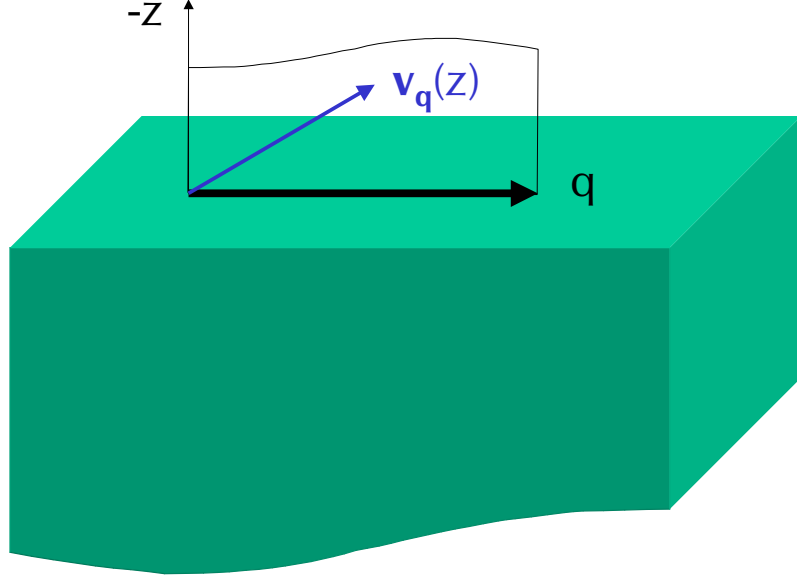
Fig. 1.20: Scheme of surface wave propagation. The vector $\mathbf{v_q}(z)$, eq.(1.108) is proportional to the displacement field induced by a wave running on the surface.

we have to point out that our numerical data indicate that for bulk piezo-electric phonons in GaAs, the resulting dimensionless coupling constant g appears to be too small to give quantitative agreement with the experimental magnitude of the inelastic current. In the experiment, the latter roughly reaches one fourth of the top value of the elastic current for $T_c \approx \Gamma_R \approx \Gamma_L$, curve (ii) in Fig.(1.12). On the other hand, our results indicate an inelastic current at least a factor two smaller than the experimental one. Our conclusion is that the assumption of *bulk* acoustic phonons is not realistic enough to give complete quantitative agreement. In fact, as the electron gas is situated only 100 nm below the sample surface, we propose surface acoustic phonons to give an additional (even larger then the bulk) contribution to the inelastic current. Surface acoustic phonons are therefore expected to have a large influence on the inelastic electron–phonon scattering properties. In the

simplest model of an elastic surface wave [110], a displacement field

$$\mathbf{u_q}(\mathbf{r}, t) = C_q e^{i(\mathbf{qr} - \omega_q t)} \mathbf{v_q}(z) + c.c. \tag{1.108}$$

for a mode with two-dimensional wave vector $\mathbf{q}$ is introduced, see Fig.(1.20). C_q is a normalization constant.

The determination of the form of the displacement field vector $\mathbf{v_q}(z)$ and in particular its coupling to the electronic degrees of freedom for small phonon wave lengths is a non–trivial problem and subject to present research [107, 111, 112]. Preliminary results [107, 112] show that the effect of surface acoustic waves with piezoelectric coupling can be comparable or even larger compared to the bulk phonon case, depending on the relative orientation of the double dot axis and the crystal axis. Still, the oscillations due to the interference effect for the matrix elements strongly appear in the function $\rho(\omega)$.

1.8 Discussion

1.8.1 X–ray singularity problem and orthogonality catastrophe

The appearance of a power-law singularity like the one in the inelastic tunneling probability $P(\epsilon)$, Eq. (1.101), is well-known from the so-called X-ray singularity problem. The latter belongs, together with the Kondo effect and the non Fermi–liquid effects in one dimensional interacting electron systems (Tomonaga–Luttinger liquid) [33,38,49,83,113], to a class of problems in theoretical solid state physics that are essentially non–perturbative [114]. That is, simple perturbation theory in interaction parameters leads to logarithmic singularities which transform into power laws for Greens functions or other correlation functions, when some higher kind of perturbation theory, renormalization group methods, or approximation by exactly solvable models is applied. In the following, we summarize the X–ray singularity physics in metals following Mahan [83] and thereafter discuss its relation to inelastic tunneling in double quantum dots. Further references to the X–ray problem can be found, e.g., in [83, 114].

X–ray transitions in metals are due to excitations of electrons from the metal ion core levels (e.g., the p–shells of sodium, magnesium, potassium) to the conduction band (absorption of photons), or the corresponding emission process with a transition of an electron from the conduction band to an empty
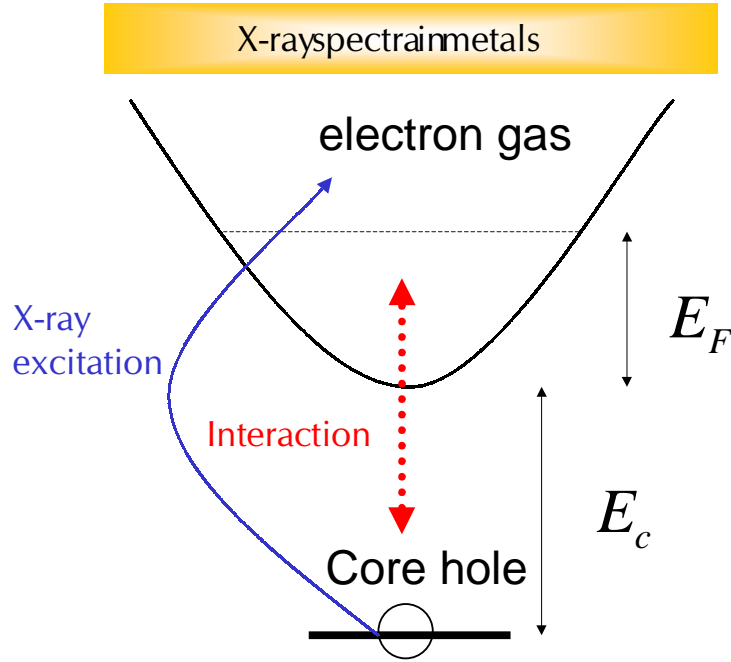
Fig. 1.21: Schematics for X–ray spectra in metals, after Mahan [83].

ion core level, i.e. a recombination with an *core hole*. Energy conservation in a simple one–electron picture requires that for absorption there is a *threshold* energy (edge) $\omega_T = E_F + |E_c|$ for such processes, where E_F is the Fermi energy and E_c the core level energy, counted from the conduction band edge (Fig.(1.21)).

Core hole spectral function

The core hole interacts with the conduction band electron gas, which is described in an effective Wannier exciton picture by a Hamiltonian [83]

$$H = E_c d^\dagger d + \sum_{\mathbf{k}\sigma} \varepsilon_{\mathbf{k}} c^\dagger_{\mathbf{k}\sigma} c_{\mathbf{k}\sigma} + \frac{1}{L^d} \sum_{\mathbf{k}\mathbf{k}'\sigma} V_{\mathbf{k}\mathbf{k}'} c^\dagger_{\mathbf{k}\sigma} c_{\mathbf{k}'\sigma} d^\dagger d. \qquad (1.109)$$

Here, $d^\dagger$ denotes the creation operator of the core hole and $c^\dagger_{\mathbf{k}}$ the creation operator of a conduction band electron with Bloch wave vector $\mathbf{k}$ and spin

σ. This Hamiltonian leads to the prediction of an *algebraic singularity* in the core hole spectral function

$$
\begin{aligned}
A_h(\omega) &= 2\Re e \int_0^\infty dt e^{i\omega t} \langle d(t) d^\dagger \rangle = \\
&= \theta(\Omega) \frac{2\pi}{\Gamma(g)} \frac{e^{-\Omega}}{\Omega^{1-g}}, \quad \Omega = (\omega - \bar{\omega}_T)/\xi_0,
\end{aligned}
\tag{1.110}
$$

where $\bar{\omega}_T$ is the (renormalized) photoemission threshold energy, and ξ_0 is a cutoff of the order of the Fermi energy. Here, the dimensionless parameter g for a three dimensional situation and for an interaction potential with $V_{\mathbf{k}\mathbf{k}'} = V(\mathbf{k} - \mathbf{k}')$ is defined as [83]

$$
g = \frac{m^2}{2\pi^2} \sum_{|\mathbf{q}| < 2k_F} \frac{V(q)^2}{q},
\tag{1.111}
$$

where m is the conduction band electron mass.

The core hole spectral function $A_h(\omega)$ is thus strongly modified by the interaction with the electron gas: the sharp delta peak for the case of no interactions becomes a power–law curve, see Fig. (1.22). The corresponding absorption step is obtained by integration of $A_h(\omega)$ [83], it vanishes for non–zero g when approaching from above $\Omega \to 0^+$. This vanishing of the absorption is called *orthogonality catastrophe*: the matrix elements for X–ray induced transitions in metals must depend on the overlap of two wave functions, i.e. the N–particle wave functions $|i\rangle$ and $|f\rangle$ before and after the appearance of the core hole, respectively. Here, N is the number of electrons in the conduction band. A partial wave scattering analysis shows that $|f\rangle$ (in the simplest case of s–wave scattering) can be considered as a Slater determinant composed of spherical waves $\propto \sin(kr + \delta)/kr$. The overlap of the two N–particle wave functions turns out to be

$$
\langle f|i \rangle = N^{-\frac{1}{2}\alpha}, \quad \alpha := 2\frac{\delta^2}{\pi^2}.
\tag{1.112}
$$

For large N, this overlap becomes very small though still finite for macroscopic numbers like $N \approx 10^{23}$ and $\alpha \approx 0.1$ [83]. The 'catastrophe' of this effect consists in the fact that although all overlaps of initial and final *single particle* scattering waves are finite, the resulting *many–body* wave function overlap becomes arbitrarily small for large N.
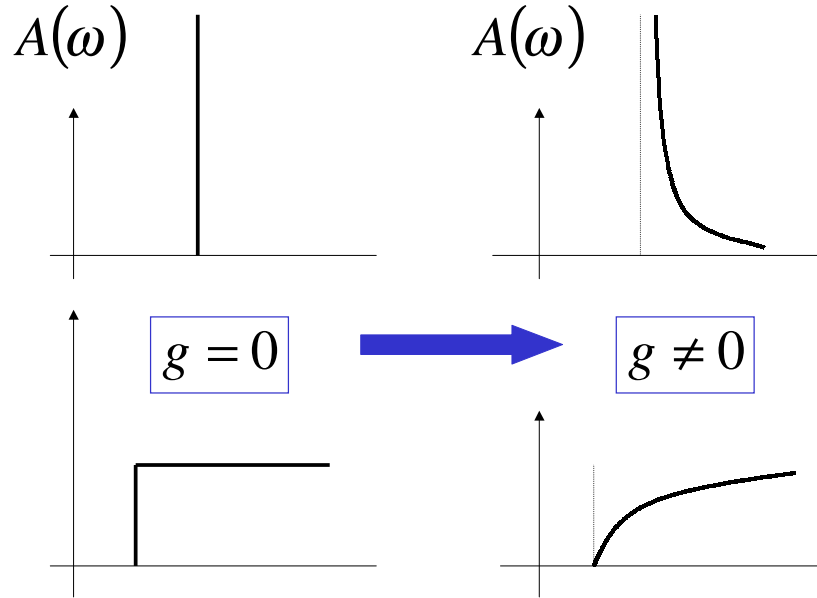
Fig. 1.22: X–ray spectra in metals: modification of core spectral function due to interactions, after Mahan [83].

The fully dynamical theory takes into account the dynamical process of the excitations in the Fermion system that are induced by the sudden appearance of the core hole after absorption of an X–ray photon. In fact, these excitations are particle–hole pairs in the conduction band which can be regarded as bosons. For a spherically symetric case, the X–ray problem can be solved exactly by a mapping to the Tomonaga model of interacting bosons in one dimension [83, 115].

Analogy with inelastic tunneling

This leads us to the relation of the X–ray photoemission problem to inelastic tunneling through double dots, where the analogy to the former is as follows: the core–hole of the metal corresponds to the (empty) dot states, and the bosonic excitations within the conduction band electron gas to the piezoelectric phonons.

We can clarify this analogy to the photoemission case by the following identification: consider the double dot, isolated from the leads, with only one electron initially in the left state $|L\rangle$. We recall that the operator $p^\dagger = |R\rangle\langle L|$ acts as a creation operator for an electron in the right dot. Trivially, because (as we always assume) there is only one electron in the double dot, $p^\dagger$ can be regarded as a creation operator for a *hole* in the left dot as well. We than may define the (retarded) hole Greens function

$$G_p(t) = -i\theta(t)\langle p(t)p^\dagger\rangle, \tag{1.113}$$

where the expectation value is with respect to the phonon equilibrium and the state with one electron in the left dot. The time evolution is with the Hamiltonian

$$
\begin{aligned}
H &= H_{LR} + H_p + H_{\alpha\beta} \\
H_{LR} &= \varepsilon_L n_L + \varepsilon_R n_R \\
H_{\alpha\beta} &= \sum_{\mathbf{Q}} (\alpha_{\mathbf{Q}} n_L + \beta_{\mathbf{Q}} n_R)\left(a_{-\mathbf{Q}} + a_{\mathbf{Q}}^\dagger\right) \\
H_p &= \sum_{\mathbf{Q}} \omega_{\mathbf{Q}} a_{\mathbf{Q}}^\dagger a_{\mathbf{Q}}.
\end{aligned} \tag{1.114}
$$

We assume that at time $t = 0$ the electron has tunneled from left to right, and we like to know the subsequent time–evolution of the hole in the left dot in presence of phonons. Note that the hole remains an empty state (no electron) throughout because we have not included the possibility for tunneling back into the Hamiltonian Eq.(1.114), see below. The time dependence of $G_p(t)$ is obtained by a canonical transformation of $H \to \bar{H}$ and $p \to \bar{p} = pX$ as worked out above. The electronic and phononic degrees of freedom decouple and

$$
\begin{aligned}
G_p(t) &= -i\theta(t)\langle pp^\dagger\rangle e^{i\varepsilon t}\langle X_t X^\dagger\rangle_0 \\
&= -i\theta(t)e^{i\varepsilon t}C(t),
\end{aligned} \tag{1.115}
$$

where we used $\langle pp^\dagger\rangle = \langle n_L\rangle = 1$ and the definition of the correlation function $C(t) = \langle X_t X^\dagger\rangle_0$ with the expectation value $\langle ..\rangle_0$ in the phonon equilibrium.

From the retarded Greens function $G_p(t)$, the correlations in time can be

translated into a frequency spectrum via the hole spectral function [83]

$$
\begin{aligned}
A_p(\omega) &= -2\Im m G_p(\omega) = 2i\Im m \int_0^\infty dt e^{i\omega t} e^{i\varepsilon t} C(t) \\
&= \int_0^\infty dt \left[e^{i(\omega+\varepsilon)t} C(t) + e^{-i(\omega+\varepsilon)t} C(-t) \right] \\
&= \int_{-\infty}^\infty dt e^{i(\omega+\varepsilon)t} C(t) = 2\pi P(\varepsilon + \omega), \qquad (1.116)
\end{aligned}
$$

where we used the detailed balance relation $C(t) = C^*(-t)$, Eq.(1.57), and the definition of the inelastic tunneling probability, Eq. (1.98), in the last line.

By comparing Eq.(1.101) and Eq.(1.116) to the spectral function $A_h(\omega)$ of the X–ray singularity problem, Eq.(1.110), we reckognize that the spectral functions have identical form if one identifies the cut–offs $\xi_0 = \omega_c$ (ω_c was set unity in Eq.(1.101)), and $\bar{\omega}_T$ with $-\varepsilon$. The only difference is the definition of the dimensionless coupling constant g.

Infrared divergence and power law

As pointed out by Mahan [83], the power law behavior of Eq.(1.116) and Eq.(1.101) is due to the logarithmic singular behavior of the function $\Phi(t)$ in $C(t) = \exp(-\Phi(t))$, Eq.(1.66), which in turn results from an *infrared divergence* of the coupling function $\rho(\omega)$ for small ω. This infrared divergence physically correspond to the generation of an infinite number of electron–hole pair excitations in the metal electron gas by the interaction with the core hole in the X–ray problem. In semiconductors, as shown above the bulk piezoelectric phonon coupling leads to the same kind of infrared divergence.

The analogy between the X–ray photoemission problem and the phonon–emission from quantum dots, however, is not complete for the following reasons:

1. In Eq.(1.116), the inelastic tunneling process between the dots is considered only as a caricature: it is contained only in the initial condition for the retarded Greens function $G_p(t)$, which has to be understood as the time–evolution of the remaining hole *after* the electron has tunneled to the other dot.

2. The influence of the leads in completely disregared. This is no serious restriction since our comparison was between X–ray photoemission and the inelastic *intra–dot* dynamics.

3. The form of the algebraic singularities Eq.(1.116) and Eq.(1.110) holds only for the 'ohmic' case $s = 1$, i.e. an effective boson density of states that has a $1/\omega$ pole for $\omega \to 0$.

This case is realized for the electron–hole pair excitations in three–dimensional metals in the X–ray photoemission problem, and for *bulk (three–dimensional) piezoelectric* phonons in the case when the oscillatory term in $\rho(\omega) = g/\omega(1 - (\omega_d/\omega)\sin(\omega_d/\omega))$ vanishes, i.e. for $\omega_d \equiv c/d = 0$ which means infinite distance between the dot centers. For any finite ω_d, $\rho(\omega)$ remains finite for small ω. The $1/\omega$ singularity in $\rho(\omega)$, on the other hand, is necessary for the appearance of an algebraic singularity, because only then the function $\Phi(t)$ is logarithmic in time and $C(t)$ becomes a pure power law, cp. Eq.(1.95). Therefore, we do not have the complete analogy to the original X–ray singularity problem.

The reason why we nevertheless discussed it at some length here is that we are in any case not so much interested in the region of the 'absorption edge' $\varepsilon = 0$ of the inelastic phonon spectrum, but in larger values of $\varepsilon > 0$. There, the results for the correlation function C_ε, obtained with the X–ray singularity ohmic form $\rho(\omega) = g/\omega$, can be regarded as a good approximation to the full problem. Furthermore, the derivation of the correlation function $C(t)$ from the X_t operators is completely general, only the final result depending on the effective phonon density of states.

Shaking up phonons

Finally, we again follow Mahan [116] and present an alternative physical picture for the inelastic tunneling described above. This time, we consider the tunneling process from the point of view of the phonon and not from the electron (hole) system [117]: The electrons and phonons are coupled by the Hamiltonian

$$H_{\alpha\beta} \;=\; \sum_{\mathbf{Q}} (\alpha_{\mathbf{Q}} n_L + \beta_{\mathbf{Q}} n_R)\left(a_{-\mathbf{Q}} + a_{\mathbf{Q}}^{\dagger}\right). \qquad (1.117)$$

It is therefore more appropriate to speak of a 'polaron', i.e. a quasiparticle composed of an electron that is surrounded of a cloud of phonons. If suddenly the electrons tunnels from the left to the right, from the point of view of the phonons it appears as if suddenly a potential

$$\delta H_{\alpha\beta} \;=\; \sum_{\mathbf{Q}} (\alpha_{\mathbf{Q}} - \beta_{\mathbf{Q}})\left(a_{-\mathbf{Q}} + a_{\mathbf{Q}}^{\dagger}\right) \qquad (1.118)$$

has been switched on which is the difference of the coupling energy before tunneling ($N_L = 1$, $N_r = 0$) and after tunneling ($N_L = 0$, $N_r = 1$). This sudden potential, which is linear in the phonon displacement $\left(a_{-\mathbf{Q}} + a_{\mathbf{Q}}^{\dagger} \right)$, 'shakes up' the phonon systems in form of a dynamical displacement (fluctuation) of the phonons. Exactly this displacement is expressed by the temporal correlation function $C(t) = \langle X_t X^{\dagger} \rangle$ of the X–operators

$$
\begin{aligned}
X &= \prod_{\mathbf{Q}} D_{\mathbf{Q}} \left(\frac{\alpha_{\mathbf{Q}} - \beta_{\mathbf{Q}}}{\omega_{\mathbf{Q}}} \right) \\
D_{\mathbf{Q}}(z) &:= e^{z a_{\mathbf{Q}}^{\dagger} - z^* a_{\mathbf{Q}}}
\end{aligned}
\tag{1.119}
$$

which themselves are expressed by the so-called *unitary displacement operators* $D(z) := \exp(z a^{\dagger} - z^* a)$. Note that the assumption of thermal equilibrium of the phonons is no contradiction to this dynamical 'shake–up' process: in thermal equilibrium, phonons are always fluctuating around, and the shake up due to the sudden electron tunneling just leads to the creation and fluctuation of additional phonons, like a harmonic oscillator that is suddenly kicked within a heat–bath.

1.8.2   Scaling with temperature and energy

Fujisawa *et al.* [30] used the Einstein relations between emission and absorption rates to demonstrate scaling of their data as a function of the ratio between temperature and energy $k_B T / |\varepsilon|$.

   We use our theoretical results to perform a scaling analysis by defining the spontaneous emission rate (we set the electron charge $e = 1$)

$$
A(\varepsilon > 0) = I(\varepsilon > 0, T_0) - I_{el}(\varepsilon > 0).
\tag{1.120}
$$

Here, $I_{el}(\varepsilon)$ is the elastic part of the current, i.e. the current for vanishing electron-phonon coupling $g = 0$. One furthermore defines the relative emission N and absorption N^+,

$$
\begin{aligned}
N(\varepsilon, T) &:= \left[I(\varepsilon, T) - I_{el}(\varepsilon) \right] / A(\varepsilon), \quad \varepsilon > 0 \\
N^+(\varepsilon, T) &:= \left[I(\varepsilon, T) - I(\varepsilon, T_0) \right] / A(|\varepsilon|), \quad \varepsilon < 0.
\end{aligned}
\tag{1.121}
$$

Here, T_0 is the reference temperature which we chose as $T_0 = 10$mK because with our parameters the currents practically do not change any longer for
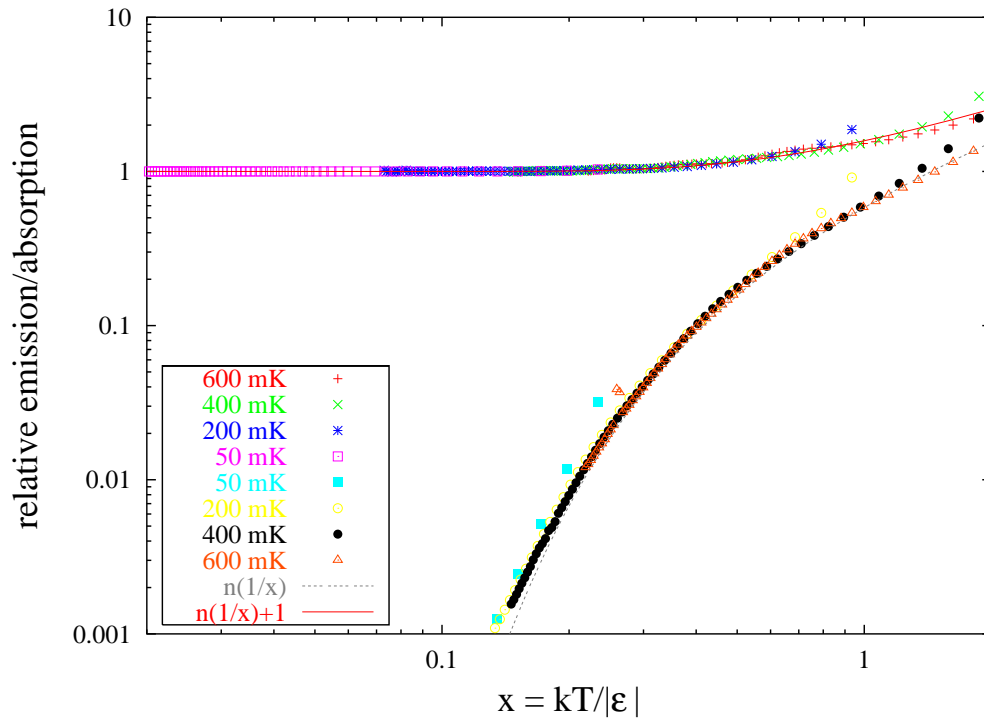
Fig. 1.23: Absorption (lower branch) and emission rates (upper branch), Eq.(1.121), from the data of Fig. (1.18).

lower temperatures. Also note that we use the full current $I(\varepsilon, T_0)$ and not $I_{el}(\varepsilon)$ as reference function on the absorption site $\varepsilon < 0$.

Figure (1.23) shows that the data can well be scaled to the bose distribution function $n(x) = 1/(e^x - 1)$, i.e. $N(\varepsilon, T) = n(|\varepsilon|/k_B T)$ for absorption $\varepsilon < 0$ and to $N^+(\varepsilon, T) = 1 + n(\varepsilon/k_B T)$ for emission $\varepsilon > 0$ over an energy window $220\mu eV > |\varepsilon| > 20\mu eV$. Here, we point out that the analysis in terms of Einstein coefficients works remarkably well, as was the case in the experiment [30], cp. Fig.(1.24).

1.8.3 Analogy between subradiance of a two–ion molecule and phonon emission from double dots

Let us come back to our introductory presentation of the spontaneous decay by emissions of *photons* from a laser–trapped two–ion system [68] in section 1.3. There, the appearance of two decay channels, that is the super– and
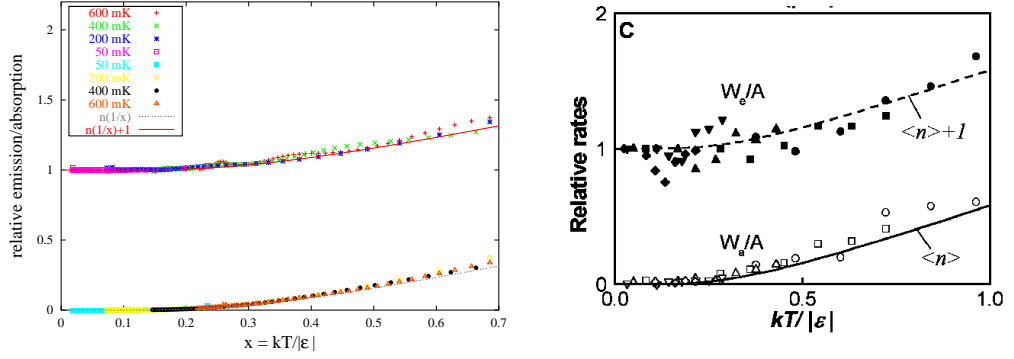
Fig. 1.24: Left: Absorption (lower branch) and emission rates (upper branch) as in Fig. (1.23) in linear scale. Right: Experimental results by Fujisawa *et al.* [30]. W_e and W_a are the emission and the absorption rate, normalized by the spontaneous emission rate A. These quantities correspond to $N(\varepsilon, T)$ and $N^+(\varepsilon, T)$ in our Eq.(1.121).

subradiant decay channels $\pm$ in the emission rate, was characteristic for the Dicke effect [52] which itself for only $N = 2$ ions is a precursor of the more general case of N radiators (*Dicke superradiance*).

The subradiant channel $(-)$ in the trapped–ion system is due to the decay of the singlet state that corresponds to the *difference* $\hat{\mathbf{d}}_1 \exp i\mathbf{Q}\mathbf{r}_1 - \hat{\mathbf{d}}_2 \exp i\mathbf{Q}\mathbf{r}_2$ of the dipole moments. To come back to the double dot system, the interaction with a *phonon* of mode $\mathbf{Q}$ in the double dot is $\propto n_L \exp i\mathbf{Q}\mathbf{r}_1 + n_R \exp i\mathbf{Q}\mathbf{r}_2$. Thus, it has the same 'interference form' as in the two-ion case, Eq.(1.1). The tunnel current through the double dot is modified by the phase *difference* of the electron before and after tunneling whence $\rho(\omega)$, Eq.(1.86), corresponds to the subradiant rate Γ_-.

Although the microscopic mechanism is not the same in both cases (for light the rates Γ_0 are $\propto \omega^3$, for piezoelectric phonons $\propto 1/\omega$), the interference term $\sin(Qd)/Qd$ in both cases is due to the 'interference of matrix elements'. The effect in both cases therefore can be regarded as a kind of *double slit interference* effect within two kinds of microscopic system, see Fig. (1.25).

In the atom–trap experiment, the Dicke effect, i.e. the existence of two different radiation channels $\Gamma_\pm$, has been verified by changing the ion distance. On the other hand, the experimental data of the double quantum dot [30] seem to indicate (see Fig.(1.13)) that for larger distance d of the dots, the oscillations $\propto \sin(\varepsilon/\hbar\omega_d)$ as a function of ε become faster which is
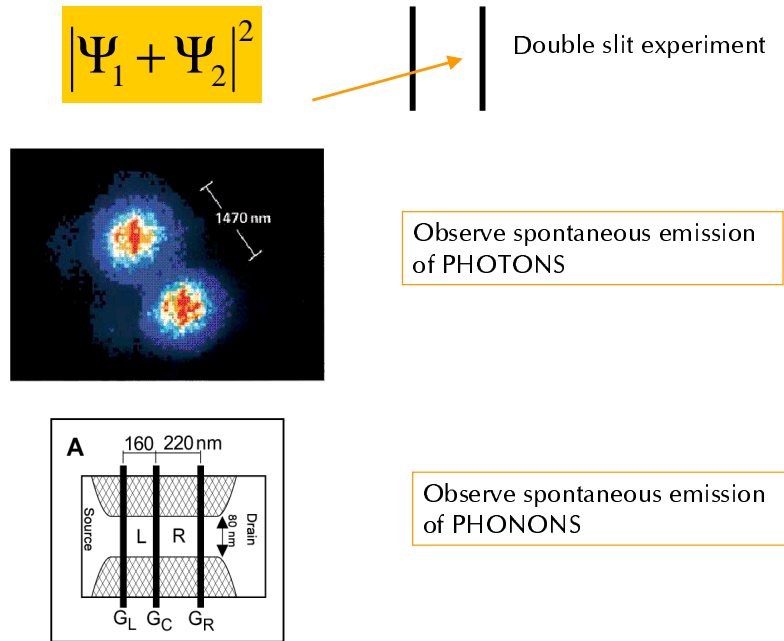
Fig. 1.25: Analogy between subradiance of a two–ion molecule and phonon emission from double dots: both effects are related to interference and can be regarded as a kind of 'double slit–experiment' in a microscopic system.

consistent with $\omega_d = c_s/d$ in Eq.(1.86).

1.8.4 Relation to dephasing in quantum dots

The form of the electron–phonon coupling we used in our model,

$$H_{\alpha\beta} = \sum_{\mathbf{Q}} \left(\alpha_{\mathbf{Q}} n_L + \beta_{\mathbf{Q}} n_R\right) \left(a_{-\mathbf{Q}} + a_{\mathbf{Q}}^{\dagger}\right), \qquad (1.122)$$

implies a special coupling of the bosonic environment to the charge: the energy levels ε_L and ε_R in the left and the right dot can be interpreted to become *fluctuating* quantities with the fluctuations depending on the bosonic (phonon) environment. This form of coupling to the electron number operators n_L and n_R is closely related to *dephasing*. The reason is, roughly speaking, that the number operator is canonically conjugate to the phase

(note, however, that a proper definition of a 'phase operator' is a non–trivial problem [118]).

The form Eq.(1.122) of coupling to an environment has been used recently by Levinson [119] in a discussion of dephasing in (single) quantum dots with a single energy level ε_0 coupled capacitively to a nanostructure. Interference effects like the Aharonov–Bohm effect in ring–structures [120, 121] are sensitive to the effect of phase–destroying processes [43, 122]. An effective description of the resulting loss of interference is obtained by assuming that on one of the ring arms the electron interacts dissipatively with some inelastic degrees of freedom that can be modeled by, e.g., a Caldeira–Leggett type of coupling.

For resonant transmission $t(\varepsilon)$ through a dot level ε_0, the Breit–Wigner form is smeared out according to

$$
\begin{aligned}
t(\varepsilon) &\propto \int_0^\infty dt \exp\left[-\Gamma t - \Phi(t) + i(\varepsilon - \varepsilon_0)t\right] \\
\Phi(t) &= \frac{1}{2} \int_0^t \int_0^{t'} dt'' \langle \delta\varepsilon_0(t') \delta\varepsilon_0(t'') \rangle
\end{aligned}
\tag{1.123}
$$

by the appearance of a term $\Phi(t)$ in the exponential that is governed by the fluctuations of the energy levels [119]. Here, Γ is the elastic tunnel rate.

The determination of the microscopic origin of the function $\Phi(t)$ is the main task to understand the origin of dephasing. Levinson could express this quantity by the scattering properties of the 'environment' that in the case he considered was a multi-terminal ballistic nanostructure. The dephasing turned out to be caused by *non–equilibrium fluctuations* of the electron density in the nanostructure.

The appearance of the exponential $e^{-\Phi(t)}$ in Eq.(1.123) is in complete analogy with the function $C(t) = e^{-\Phi(t)}$ whose Fourier transform enters our expression for the stationary current through the double quantum dot, Eq. (1.62). In our case, however, the environment is in thermal equilibrium (phonon bath), although our theoretical description in terms of the function $C(t)$ allows a generalization to arbitrary environments.

1.8.5   High–frequency detector

The tunability and sensitivity of the double dot system to its environment makes it very attractive as a detector for energies in the micro eV regime.

Aguado and Kouwenhoven in fact have proposed a circuit where double quantum dots are used as detectors for high–frequency quantum noise in mesoscopic conductors such as quantum point contacts [123]. In their scheme, the double dot is capacitively coupled to a second mesoscopic device that can be, e.g., a quantum point contact. Fluctuations generated by the current noise spectrum $S_I(\omega)$ of a nearby mesoscopic device can be shown to produce an inelastic current

$$I_{in}(\varepsilon) \propto S_I(\varepsilon/\hbar)/\varepsilon^2, \qquad (1.124)$$

i.e. the inelastic current in such a set–up would be a direct measure of the noise spectrum.

1.8.6   Dephasing of a Qubit

The double dot and its coupling to phonon degrees of freedom in fact serves as a simple model for the dephasing mechanism in quantum bits (*qubits*). Basically, any two-level system can serve as a physical realization of the qubit, i.e. a system that allows a coherent superposition of the two basis states in the Hilbert space $\mathcal{H} = C^2$. Qubits are considered as the elementary parts of quantum computers [124], the latter generalizing the (classical) mathematical concept of a computer to the quantum case. Since any quantum computational step relies on *unitary* operations, phase destroying processes are undesired. Still, every physical system is connected to the 'outer world' whose degrees of freedom can not be disregarded but in general are a source of dissipation. On the microscopic level, the investigation of such processes has a long tradition, of which the spin-boson problem is perhaps the most prominent model system where dissipation has been studied well in the past [102].

Single qubit

For the case of a single qubit, dephasing can be studied in a simple, exactly soluble model which still demonstrates the basic principle very nicely. The discussion below follows previous work [99,100] on the decay of an initial polarization within a qubit. The model considered there is a special case of the previously discussed double dot problem in the case of vanishing tunneling T_c between two dots, which in addition are only coupled to phonon degrees of freedom and not to external electron reservoirs. Still, this model contains enough physics to study the decay of off-diagonal matrix elements of the

reduced density operator of the dot. This decay, which in nuclear magnetic resonance or quantum optics is associated with the relaxation time T_2, shows in fact some non-trivial temporal behavior depending on the precise form of the coupling constants of the phonon degrees of freedom.

We begin with the Hamiltonian

$$H = H_0 + V, \quad H_0 = \varepsilon J_z + \sum_{\mathbf{Q}} \omega_{\mathbf{Q}} a_{\mathbf{Q}}^{\dagger} a_{\mathbf{Q}},$$

$$V = J_z \sum_{\mathbf{Q}} (\alpha_{\mathbf{Q}} - \beta_{\mathbf{Q}}) \left(a_{-\mathbf{Q}} + a_{\mathbf{Q}}^{\dagger} \right) \tag{1.125}$$

and use the interaction picture for the density operator $\rho(t)$ of the system (dot+phonons),

$$\tilde{\rho}(t) := e^{iH_0 t} e^{-iHt} \rho(t=0) e^{iHt} e^{-iH_0 t}$$

$$e^{-iHt} = e^{-iH_0 t} S(t), \quad S(t) = T \exp\left[-i \int_0^t dt' \tilde{V}(t') \right]$$

$$\tilde{V}(t) = e^{iH_0 t} V e^{-iH_0 t}, \tag{1.126}$$

so that

$$\tilde{\rho}(t) := S(t)\rho(t=0)S^{\dagger}(t). \tag{1.127}$$

The operator $S(t)$ can be calculated explicitely,

$$S(t) = \exp\left[J_z \sum_{\mathbf{Q}} \left(a_{\mathbf{Q}}^{\dagger} z_{\mathbf{Q}}(t) - a_{\mathbf{Q}} z_{\mathbf{Q}}^*(t) \right) \right]$$

$$= \Pi_{\mathbf{Q}} D_{\mathbf{Q}} \left(J_z z_{\mathbf{Q}}(t) \right)$$

$$z_{\mathbf{Q}}(t) := (\alpha_{\mathbf{Q}} - \beta_{\mathbf{Q}}) \frac{1 - e^{i\omega_{\mathbf{Q}} t}}{\omega_{\mathbf{Q}}}, \tag{1.128}$$

where again we introduced the unitary displacement operator $D_{\mathbf{Q}}(z) = \exp(z a_{\mathbf{Q}}^+ - z^* a_{\mathbf{Q}})$.

Using $\tilde{J}_z(t) = J_z$ and $\tilde{J}_{\pm}(t) = e^{\pm i\varepsilon t} J_{\pm}$, we find

$$\langle J_z \rangle_t := \mathrm{Tr}\left(\rho(t) J_z \right) = \mathrm{Tr}\left(\tilde{\rho}(t) \tilde{J}_z \right)$$

$$= \mathrm{Tr}\left(\rho(t=0) J_z \right) = \langle J_z \rangle_{t=0}, \tag{1.129}$$

since J_z commutes with the operators $S(t)$. This means that the population of the dot levels remains unchanged by the interaction V. On the other hand,

$$
\begin{aligned}
\langle J_+ \rangle_t &:= \operatorname{Tr}\left[\rho(t) J_+\right] = \operatorname{Tr}\left[\tilde{\rho}(t) \tilde{J}_+\right] \\
&= \operatorname{Tr}\left[\rho(t=0) S^\dagger(t) J_+ S(t)\right] e^{i\varepsilon t} \\
&= \operatorname{Tr}\left[\rho(t=0) J_+ \Pi_{\mathbf{Q}} D_{\mathbf{Q}}(z_{\mathbf{Q}}(t))\right] e^{i\varepsilon t}.
\end{aligned} \tag{1.130}
$$

For factorizing initial conditions $\rho(t=0) = \rho_{dot}(t=0)\rho_{ph}(t=0)$ and a phonon system in thermal equilibrium at temperature $1/\beta$, we can again use the phonon expectation value

$$
\langle \Pi_{\mathbf{Q}} D_{\mathbf{Q}}(z_{\mathbf{Q}})\rangle_{ph} = \Pi_{\mathbf{Q}} \exp\left\{-\frac{1}{2}|z_{\mathbf{Q}}|^2 \coth(\beta\omega_{\mathbf{Q}}/2)\right\} \tag{1.131}
$$

to obtain

$$
\begin{aligned}
\langle J_+ \rangle_t &= \langle J_+ \rangle_{t=0} e^{-\Phi_1(t)+i\varepsilon t} \\
\Phi_1(t) &:= \int_0^\infty d\omega \rho(\omega)\left\{(1-\cos\omega t)\coth(\beta\omega/2)\right\} \\
\rho(\omega) &= \sum_{\mathbf{Q}} \frac{|\alpha_{\mathbf{Q}} - \beta_{\mathbf{Q}}|^2}{\omega^2}\delta(\omega - \omega_{\mathbf{Q}}).
\end{aligned} \tag{1.132}
$$

We reckognize that the function $\Phi_1(t)$ is exactly the real part of $\Phi(t)$, Eq.(1.66) in section 1.6.4, where we calculated the phase-phase correlation function $C(t)$ for electrons tunneling from the left to the right dot. There, the initial polarization of the dot was assumed to be zero, i.e. $\langle J_\pm \rangle_{t=0} = 0$, and the decay described by the factor $\exp(-\Phi(t))$ was the decay of a polarization that builds up in the course of electron tunneling between the dots. In our qubit model here, we have a somewhat complementary situation because we assumed no tunneling between the dots but an *initial nonvanishing polarization* $\langle J_\pm \rangle_{t=0} \neq 0$.

We note that this initial condition corresponds to an initial non-equilibrium state $\rho_{t=0}$ that does not commute with the total Hamiltonian H of the coupled system (dot+phonons). If we had assumed an equilibrium state $\rho_{t=0} \propto \exp(-\beta H)$ as initial condition, there would be no dephasing at all: using the canonical transformation technique used in our former calculation, we would find that $\exp(-\beta H)$ factorizes into an equilibrium dot and phonon part whence $\langle J_\pm \rangle_{t=0} = 0$ from the beginning. In other words, in order to

correctly describe the non-equilibrium initial condition (non-vanishing po-larization), we had to use the interaction picture method explained here and not the canonical transformation.

Quantum registers

The extension of the above dephasing model from the case of one two-level system (single qubit) to a *quantum register*, i.e. a finite number of two-level systems, is quite obvious: The simplest way is to assume identical two–level systems and a coupling to the environment that does not depend on the index i labeling the individual qubits. The operators J_z, $J_\pm$ then operate in the space of Dicke states $|JM\rangle$ of total pseudo spin J and spin projection M as in the superradiance problem, see chapter 2. Palma, Suominen and Ekert [100] discussed the general case for dissipation in quantum registers of $N = 2$ and $N > 2$ qubits. For the case $N = 2$, the collective decay rate again contains an *interference term* $\propto [1 \pm \cos(\mathbf{kR})]$, where $\mathbf{k}$ is the wave vector of a bosonic excitation of the environment and $\mathbf{R}$ is the distance between the qubits. For larger N, the collective entanglement between the qubits and the environment (as defined by a Dicke–like Hamiltonian) leads to the possibility of *super–decoherence* and *sub–decoherence*. This is in analogy with the splitting of an inelastic spontaneous decay channel into a sub– and a superradiant channel, cp. section 1.2.3.

1.9   Other Phonon geometries

1.9.1   Quantization of the phonon spectrum

indexphonon spectrum In the following, we shortly discuss the influence of re-stricted phonon geometries on the inelastic current through double quantum dots. In confined geometries, the phonon system experiences a quantization similar to electrons in two– or one–dimensional structures. The spontaneous emission properties of such *phonon cavities* therefore are qualitatively differ-ent from the case of phonon emission from bulk material, similar to *photon* cavities that change the spontaneous emission of light from atoms.

The quantization of the phonon spectrum is expected to show up in the inelastic current through double quantum dots. The possibility to detect phonon quantization by transport spectroscopy is an attractive way to inves-tigate how inelastic processes can be controlled and manipulated by geometry
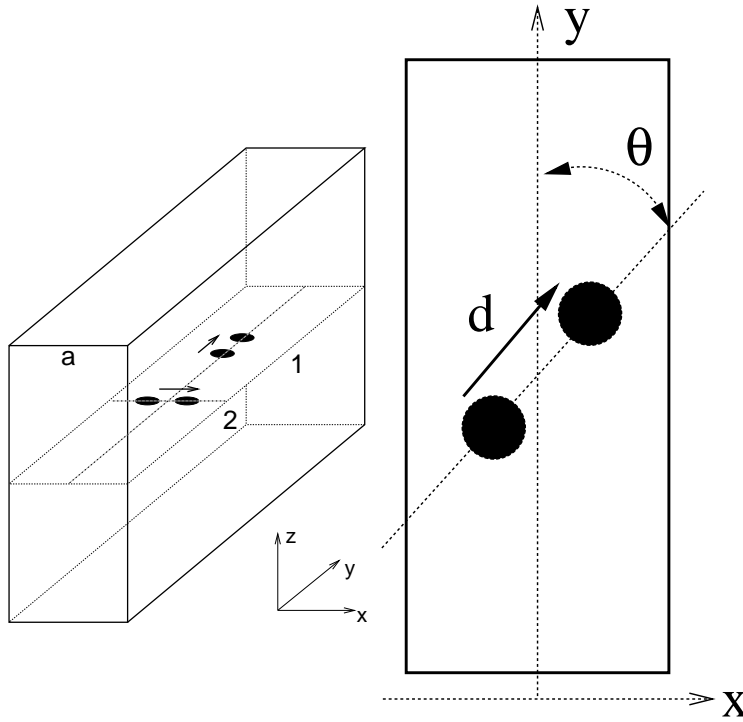
(confinement).

For the inelastic current I_{in}, we use the (perturbative in T_c) form, expressing the it by the inelastic rate $\gamma(\varepsilon)$ (we again set $\hbar = e = 1$),

$$I_{\text{in}}(\varepsilon) \approx 2\pi T_c^2 \rho(\varepsilon) = 2\gamma(\varepsilon)$$

$$\gamma(\varepsilon) := \pi T_c^2 \sum_{\mathbf{Q}} |\lambda_{\mathbf{Q}}|^2 \frac{\left|1 - e^{i\mathbf{d}\mathbf{q}}\right|^2}{\varepsilon^2} \delta(\varepsilon - \omega_{\mathbf{Q}}), \qquad (1.133)$$

where we used $\beta_{\mathbf{Q}} = \alpha_{\mathbf{Q}} e^{i\mathbf{q}\mathbf{d}}$, and $\mathbf{d} = \mathbf{r}_R - \mathbf{r}_L$ is the vector pointing from the center of the left to the center of the right dot, both of which are lying in the x–y plane. The three-dimensional phonon momentum is $\mathbf{Q} = (\mathbf{q}, q_z)$ with the component in the x–y plane $\mathbf{q}$, the component q_z in z- direction. Here, $\lambda_{\mathbf{Q}}$ is the electron-phonon interaction matrix element.

Fig. 1.26: Left: Scheme of phonon cavity with double dot inside. Right: Orientation of double dot inside the cavity. Both figures courtesy of S. Debald [125].

We consider a confinement of phonon modes into the x– directions within

the x–y-plane, i.e. the phonons correspond to standing waves in x–direction and running waves in y–z direction. This kind of confinement ideally would be achieved for a 'plate' of finite thickness $x = x_0$ with infinite extension into the y and the z direction, see Fig. (1.26). Even for such simplified geometries, the determination of phonon modes and electron-phonon interaction coupling constants is a highly nontrivial task [125–128].

Three types of confined phonon modes can be distinguished. They appear in the classification of the vibrational eigenmodes in the plate with proper boundary conditions at each of the sides [129] and are called *shear waves, dilatational waves*, and *flexural waves* depending on their spatial symmetry. Since the confinement cuts off small phonon momenta which determine piezoelectric electron–phonon coupling, it is argued [127] that deformation potential coupling is dominant over piezoelectric coupling in confined electron–phonon geometries. For deformation potential scattering, there is no coupling to shear waves and one is left with a Hamiltonian

$$
\begin{aligned}
H_{def} &= \sum_{\boldsymbol{q}_\parallel, n} \lambda_n(\boldsymbol{q}_\parallel) e^{i \boldsymbol{q}_\parallel \boldsymbol{r}_\parallel} \left\{ \begin{array}{c} \cos q_{x,n} x \\ \sin q_{x,n} x \end{array} \right\} \left[a_n(\boldsymbol{q}_\parallel) + a_n^\dagger(-\boldsymbol{q}_\parallel) \right] \\
&\quad \text{for} \left\{ \begin{array}{c} \text{dilatational} \\ \text{flexural} \end{array} \right\} \quad \text{waves.} \tag{1.134}
\end{aligned}
$$

The angular dependence of the matrix elements entering into the expression for $\gamma(\varepsilon)$, Eq.(1.133), are

$$
|\alpha_n(\boldsymbol{q}_\parallel) - \beta_n(\boldsymbol{q}_\parallel)|^2 = |\lambda_n(\boldsymbol{q}_\parallel)|^2 \begin{cases} \cos^2(\frac{q_{x,n} d}{2} \sin \Theta)|1 - e^{i\boldsymbol{q}_\parallel \boldsymbol{d}}|^2 \\ \sin^2(\frac{q_{x,n} d}{2} \sin \Theta)|1 + e^{i\boldsymbol{q}_\parallel \boldsymbol{d}}|^2. \end{cases} \tag{1.135}
$$

1.9.2   Inelastic scattering rate in restricted geometries

From the general form of these expression, one can already draw a number of conclusions concerning the inelastic current spectrum $I_{\text{in}}(\varepsilon)$ through double quantum dots. First of all, the appearance or non–appearance of the Dicke effect, i.e. oscillations of $\gamma(\varepsilon)$, Eq.(1.133), depends on the scalar product $\boldsymbol{q}_\parallel \boldsymbol{d}$ and therefore on the orientation of the double dot axis with respect to the confinement direction, see Fig.(1.26).

One can distinguish the following cases:
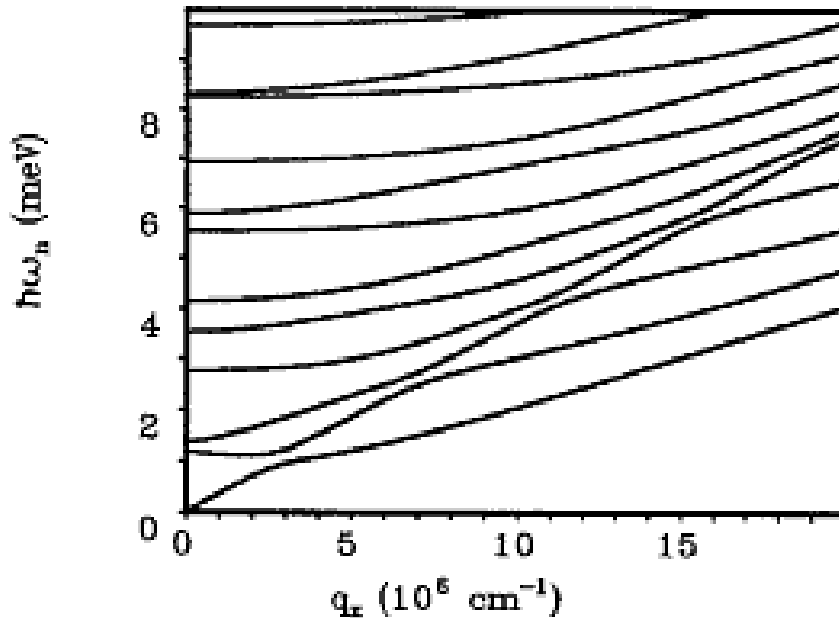
Fig. 1.27: Numerical results by Bannov et al. [127] for the phonon dispersion $\hbar\omega_n(q_\parallel)$ for several dilatational modes n in a free–standing plate.

- For $\Theta = \pi/2$, the scalar product $\boldsymbol{q}_\parallel \boldsymbol{d}$ vanishes and $|1 - e^{i\boldsymbol{q}_\parallel \boldsymbol{d}}|^2 = 0$ (dilatational waves), while $|1 + e^{i\boldsymbol{q}_\parallel \boldsymbol{d}}|^2 = 4$ (flexural waves). In both cases, there is are no oscillations due to interference of matrix elements. The coupling to dilatational waves vanishes. The double-slit like interference pattern in the inelastic current occurs only if there are acoustic waves (phonons) that have a running (not standing) component in transport direction.

- For $\Theta = 0$, the coupling to the (antisymmetric) flexural waves vanishes. Numerical calculations by Bannov *et al.* show a quantization of the phonon spectrum in a free-standing plate geometry, see Fig. (1.27).

The quantization of the phonon spectrum should show up in the form of a staircase [125, 128] in the inelastic current $I_{in}(\varepsilon)$ as a function of the left and right dot energy difference ε, Eq. (1.133). Thus, it is in principle possible to

access the phonon spectra of a confined phonon system (phonon cavity) by inelastic current spectroscopy in coupled quantum dots.

Finally, we mention that recently interest has grown in so–called *phononic crystals* [130], where a periodic modulation of the elastic medium leads to a number of novel effects, in analogy with photonic crystals (which are associated with the modulation of the dielectric constant). Inelastic current spectroscopy with double dots would be an interesting tool to investigate the elastic properties of such systems.

2. OSCILLATORY DICKE SUPERRADIANCE

Abstract

We investigate a superradiating system coupled to external reservoirs. Under conditions where electrons tunneling at a rate T act like an electron pump, we predict a novel phenomenon in the form of oscillations with a frequency $\omega \simeq \sqrt{2\Gamma T}$ that appear in the (photon) emission intensity, where Γ is the spontaneous decay rate of a single two–level system. The effect, together with a strong enhancement of the superradiant peak, should be observable in semiconductor quantum wells in strong magnetic fields, or in quantum dot arrays.

2.1   Introduction

Spontaneous emission as one of the most basic concepts of quantum physics is mostly discussed in the context of an atom coupled to a radiation field: it is one of the paradigms of quantum optics. Another paradigm is stimulated emission, which leads for the case of a large number of atoms to the concept of a laser. The corresponding concept in the case of spontaneous emission of an ensemble with a large number of atoms is the *superradiator*.

Superradiance occurs in the spontaneous coherent decay of an initially excited ensemble of N two–level systems which are interacting with a common photon field. The corresponding emission rate of photons is proportional to N^2 which is abnormally large when compared to the incoherent decay of N independent systems [52, 73, 131, 132]. Furthermore, the emission is not exponentially in time but has the form of a very sudden peak on a short time scale $\sim 1/N$. This problem has been first discussed by Dicke in 1954 [52] who introduced the term 'superradiant':

"For the want of a better term, a gas which is radiating strongly because of coherence will be called 'superradiant' " [52].

Surprisingly, it took nearly 20 years for the first experimental verification to be carried out by Skribanowitz et al. [133], which was shortly after a renewed interest in the effect had begun in the early 70ies of the last century [134]. The observation in [133] of the predicted superradiant emission peak was in an optically pumped hydrogen fluoride gas where the intensity of the emitted light was proportional to the *square* of the number of atoms (molecules) of the emitting gas. In the visible light range, the first observation of superfluorescence [1] was made later by Cahuzac, Sontag and Toschek in atomic Europium [135]. A lot of theoretical and experimental investigations of the effect followed until today. Still, it has never become as popular as the laser, not to speak of its use in the form of a device [136].

Nevertheless, many investigations of superradiance [73, 131, 137, 138] concentrated on modifications through geometry effects and dephasing processes such as dipole–dipole interactions which had been neglected in the original Dicke paper. Since superradiance intrinsically is a many–body problem, this also gave and gives the possibility to study the concept of coherence and dephasing in a many–body context [139, 140].

The physics of superradiance is in our opinion one of the most interesting in the field of quantum physics, because it comprises a number of fundamental concepts such as coherence, symmetry, interaction between particles, the non–equilibrium physics of transient processes, and the notion of a quasiclassical limit [73, 131]:

1. *coherence*: the radiation is due to a collective decay of (ideally) a many–body wave function that is formed as a coherent superposition of the wave functions of the single radiators.

2. this coherence can get lost through *interaction processes* (van der Waals dephasing). At the same time, it is just the interaction via the common electromagnetic field that leads to the effect.

3. in the time domain, the whole process is a transient, i.e. *non–equilibrium* process. In the frequency domain, it appears as a sharpening or narrowing of spectral line shapes, see chapter 5

---

[1] Some authors distinguish between the terms superradiance and *superfluorescence*. In this terminology, superradiance is refered to as the decay of an initially fully excited correlated state, whereas superfluorescence refers to an initially uncorrelated state. A coherent initial state can be generated, e.g., by coherent pulse pumping. In this thesis, however, we prefer the use of the term superradiance throughout in the broader sence to denote a collective decay due to spontaneous emission, cp. the discussion in the introduction of the textbook by Benedict *et al.* [73].
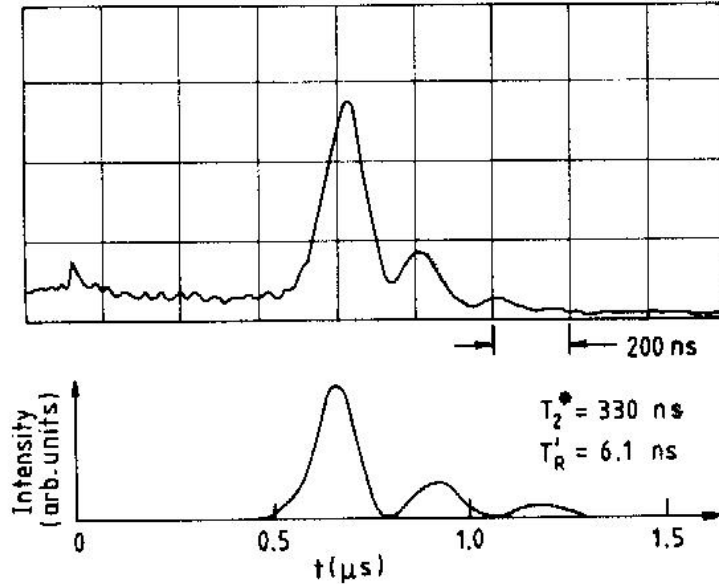
Fig. 2.1: Oscilloscope trace of the first observation of a superradiant pulse (Dicke–peak) in HF gas by Skribanowitz et al. [133]. Below: theoretical fit with dephasing time T_2^* and characteristic superradiant time scale T_R' [73].

4. there is a *quasiclassical limit*: after an initial phase that is governed by quantum fluctuations, the systems evolves according to classical equations [73, 141].

This wealth of physical concepts related to superradiance may in part have contributed to the quite recent revival of a considerable interest in the effect. First of all, coherent effects in semiconductors optics [51, 142] have become accessible experimentally, e.g., by ultrafast spectroscopy. There, the superradiance effect has been found in radiatively coupled quantum–well excitons [143–147].

Second, in the field of electronic transport, the effect has been rediscovered by Shahbazyan and Raikh in the resonant tunneling through two impurities [148] and by Shahbazyan and Ulloa in the resonant scattering in a strong magnetic field [149]. Very recent studies address mesoscopic cooperative emission from disordered systems [150].
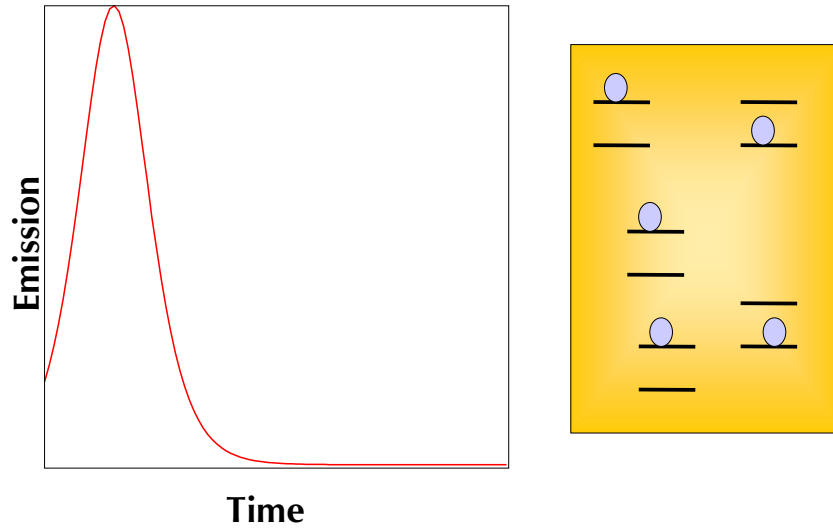
Fig. 2.2: Dicke peak: Emission of a superradiating ensemble of two–level systems (left) as a function of time, cp. Eq.(2.16).

Furthermore, the quasiclassical limit of superradiance describes, in the simplest case, the radiative decay in analogy to a non–linear pendulum that falls down from an initially 'inverted' position, see Fig. (2.3). The study of this limit has attracted some interest recently [151–153] in the context of macroscopic superposition of quantum states, i.e. so–called Schrödinger cat–states [67]. In more complicated cases, the classical equations (which are in fact the equations of motions of Heisenberg operators in a certain approximation) become coupled, nonlinear equations which in principle always can show a *chaotic* behavior [154].

Superradiance is an effect that involves transitions between many–particle wave functions $|JM\rangle$. Here, the *correspondence with the two–level system*, i.e. the physics of an (abstract) spin 1/2 particle, gives rise to a 'pseudo' spin 1/2 picture, where the combination of many such spins leads to the quantum numbers J (the total pseudo spin) and M (total spin projection). In the simplest case, 'spin–up' means an electron in the upper level and

'spin–down' an electron in the lower level of a two–level transition in, e.g., radiating atoms.
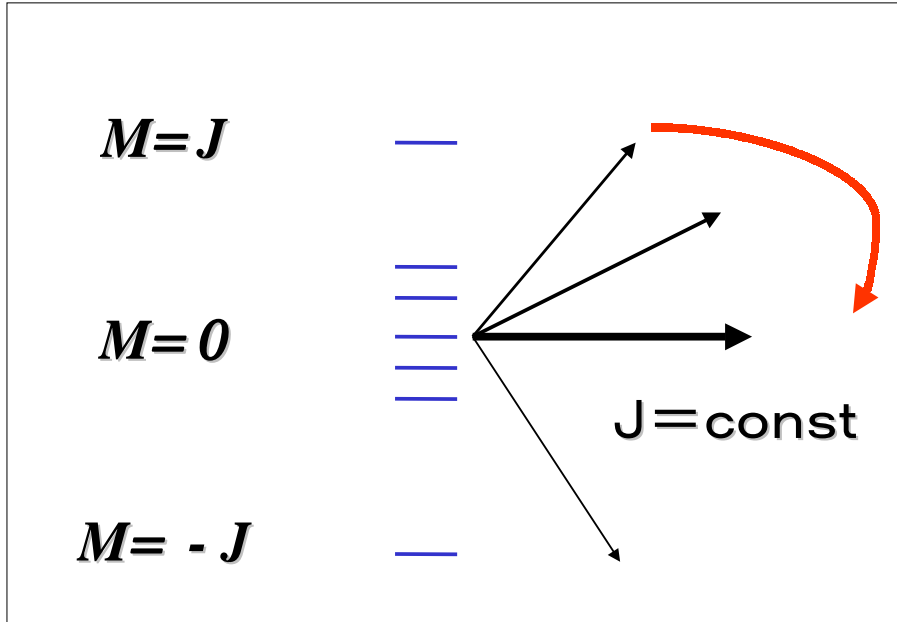
Fig. 2.3: Decay of a large pseudo spin due to spontaneous emission.

As a transient process, superradiance (in its pure form of a single light pulse due to coherent emission, cp. Fig.(2.2)) occurs only if the observation time scale t is shorter than a *dephasing time scale* T_2 of processes that destroy phase coherence, and longer than the time τ which photons need to escape from the optical active region where the effect occurs, such that recombination processes are unimportant [131]. The condition

$$\tau \ll t \ll T_2, \Gamma^{-1}, \tag{2.1}$$

determines the superradiant regime, together with the last inequality which involves Γ^{-1}, the time scale for the decay of an *individual* atom.

The restriction Eq. (2.1) of the *time–scale* for the superradiant process can be seen in analogy to the restriction

$$l \ll L \ll L_\phi \tag{2.2}$$

defining the *length scale L* of a mesoscopic system where physics occurs between a microscopic (e.g. atomar) length scale l and a dephasing length L_ϕ [8]. A superradiant system thus can be regarded as mesoscopic in time–scale. This comparison, together with the fact that the superradiant problem intrinsically is a many–body problem, indicates the possibility to study the concept of coherence and dephasing processes in a many–body context.

In fact, in his original paper, Dicke neglected such processes; in particular the total pseudo spin $J = N/2$ is constant for the emission cascade from the totally up–inverted to the totally down–inverted ensemble of N radiators. A lot of works have appeared since which concentrated on the effect of the dipole-dipole interactions between neighboring atoms [73,131,141]. Such processes no longer leave J constant and are regarded as dephasing mechanism, leading to states with smaller J [73]. Precise predictions [139,140] have been made for, e.g., the resulting modifications of the emission peak. Another feature of the original Dicke model is that the number of electrons remains constant in the course of the transitions from 'upper' to 'lower' atomic levels. On the other hand, this restriction is not necessary for superradiance to occur; we will even show below that giving up the restriction of a constant electron number will lead to a novel phenomenon that we call 'driven' superradiance oscillations.

In this chapter, we investigate an extension of the original Dicke problem by allowing electrons to tunnel to and from reservoirs in an optical active, superradiating region. We exploit an analogy with a similar situation in a mesoscopic system by considering the two–level ensemble in the radiation field as a quantum dot, coupled to external leads. In contrast to the original Dicke problem, the total pseudo spin J is no longer conserved due to the tunneling processes. We specify to a configuration where the tunneling of electrons acts like optically pumping the system. The particular coupling between the total pseudo spin J and its projection M through *Clebsch–Gordan coefficients* leads to a time evolution which is governed by an oscillating decrease and increase of J and M and subsequent oscillations of the emitted intensity with a frequency

$$\omega \approx \sqrt{2\Gamma T}. \qquad (2.3)$$

Here, the spontaneous decay time of a single level Γ^{-1} acts like an internal effective inertia ('mass') of the system that is driven by an external 'force' with 'force constant' proportional to the tunnel rate T. Numerical evaluation

of the master equation confirms the qualitative picture that can be justified in a semiclassical approximation. We furthermore present a concrete experimental realization for the observation of the effect. The main idea is to realize the superradiant 'active region' in a semiconductor and to couple it to external electron reservoirs through tunnel barriers, thus allowing for a varying electron number. We predict that for reservoir conditions which work like an electron pump, an initial coherent superradiant peak can be strongly enhanced if the tunnel rate T is high enough. The photon emission from the recombination between electrons and holes is predicted to show oscillations Eq. (2.3) if a tunnel current of electrons and holes 'pumps' the system. The oscillations should also show up in the tunnel current itself.

Furthermore, we predict a novel phenomenon in the form of strong oscillations of the emitted light with a frequency ω that in good approximation is given by Eq. (2.3) for large $T > 2\Gamma$, where Γ is the spontaneous decay rate of a single two-level system. For smaller tunnel rates T, there is a smooth crossover to the conventional Dicke peak [52] in the limit $T \to 0$. In contrast to oscillatory superradiance in atomic systems (section 2.6.3, [131]), these oscillations are not due to reabsorption of photons, but due to tunneling of electrons into an active region which is described by many–body wave functions.

2.2 Model

2.2.1 Pseudo spin picture

We consider our model as an extension of the original Dicke model in presence of electron reservoirs. The Dicke Hamiltonian originally describes an ensemble of N_s two–level atoms coupled to a radiation field that allows for transitions 'up–down' and 'down–up' within each atom. In our model, a bosonic field with creation operator $a_{\mathbf{Q}}^{\dagger}$ for a mode $\mathbf{Q}$ gives rise to transitions between the inner degrees of freedom σ of one–particle electronic states

labeled (j, σ).

$$
\begin{aligned}
H_D &= H_0 + H_{ep} + H_p \\
H_0 &= \sum_{j,\sigma} \varepsilon_{j,\sigma} c_{j,\sigma}^\dagger c_{j,\sigma} \\
H_{ep} &= \sum_{\mathbf{Q}} g_{\mathbf{Q}} \left(a_{\mathbf{Q}}^\dagger + a_{\mathbf{Q}} \right) \sum_j \left(c_{j,\uparrow}^\dagger c_{j,\downarrow} + c_{j,\downarrow}^\dagger c_{j,\uparrow} \right) \\
H_p &= \sum_{\mathbf{Q}} \Omega_{\mathbf{Q}} a_{\mathbf{Q}}^\dagger a_{\mathbf{Q}}.
\end{aligned} \tag{2.4}
$$

Note that in a transition, only σ is changed, but not j. The index σ can, e.g., be the real electron spin for Zeeman–split levels j in a magnetic field, or a pseudo–spin denoting 'up' and 'down' position within a specific level j. In the experimental configuration described below, σ is related to electrons occupying the conduction band or holes occupying the valence band of a semiconductor quantum well. In the following, we will always use the term 'spin'. Furthermore, we do not explicitly refer to the geometry of the system, assuming only that we are in the 'small sample superradiance regime' [141] where propagation and diffractions effects of the electromagnetic field do play no role. We neither refer to the explicit form of the states (j, σ) that could describe levels in artificial quantum dots as well as, e.g, in quantum wells. It will turn out that it is rather a few quantum numbers, namely the number of occupied levels N, the total spin J and the total spin projection M which determines the basic physics in our semiclassical approach. In the same sense, it is not necessary to assume from the beginning that the boson modes in H_p are photons. Consequently, the Hamiltonian Eq. (2.4) represents a whole class of physical systems rather than one specific experimental situation. The important aspect is that the different levels are coupled by the common bosonic field. It is this aspect which makes the problem essentially a many–particle problem.

One key assumption (which we retain here) of the original Dicke model is the independence of the coupling matrix element $g_{\mathbf{Q}}$ from the electronic quantum numbers (j, σ). If the coupling is to a photon field vector potential in the form

$$
H_{ep} = (-e/m^*) \int d^d\mathbf{x} \Psi^\dagger(\mathbf{x}) \mathbf{A}(\mathbf{x}) \mathbf{p} \Psi(\mathbf{x}), \tag{2.5}
$$

this assumption is justified if the matrix element

$$
\begin{aligned}
\langle j\sigma|\mathbf{p}|j'\sigma'\rangle &= im^*(\varepsilon_{j\sigma} - \varepsilon_{j'\sigma'})\langle j\sigma|\mathbf{x}|j'\sigma'\rangle \\
\sigma &\neq \sigma'
\end{aligned}
\tag{2.6}
$$

can be considered as a constant, and the spatial geometry allows to neglect the $\mathbf{x}$–dependence of the photon field, i.e. to consider the latter in the long wavelength limit. In the standard literature, this most simplest situation of superradiance corresponds to the 'small sample superradiance case' where in particular reabsorption of photons and/or sample specific effects are completely neglected.

2.2.2 Extension of the Dicke model

The situation described so far by the Hamiltonian Eq.(2.4) corresponds to a *closed* system with respect to the electron number that remains constant throughout the time–evolution.

We now include processes by which the number of electron within the optical active region may change. The simplest way to do so is to include a term H_T that allows the number of electrons N to vary, that is by tunneling to and from electron reservoirs α. For simplicity, we denote the possible values for α as 'left(L)'and 'right(R)'; a generalization to 'multiterminal' situations with more than two different α's is straightforward. We thus have

$$
\begin{aligned}
H_\alpha &= \sum_k \varepsilon_{k,\alpha} c^\dagger_{k,\alpha} c_{k,\alpha}, \quad \alpha = L/R \\
H_T &= \sum_{k,j,\sigma,\alpha=L/R} \left(t^\alpha_{k,j,\sigma} c^\dagger_{k,\alpha} c_{j,\sigma} + c.c. \right)
\end{aligned}
\tag{2.7}
$$

The analogy to the double quantum dot problem is obvious; indeed this analogy will be important in the theoretical description in terms of a master equation below. Within this description, our 'dot' will be *a priori* regarded as a many–body system even in absence of electron–electron interactions.

In the following, we first discuss the modifications of the Dicke superradiance through the effects which result from the tunneling processes only and neglect any other interaction processes like Coulomb or Hubbard correlations. The total Hamiltonian therefore becomes

$$
H = H_D + H_L + H_R + H_T.
\tag{2.8}
$$
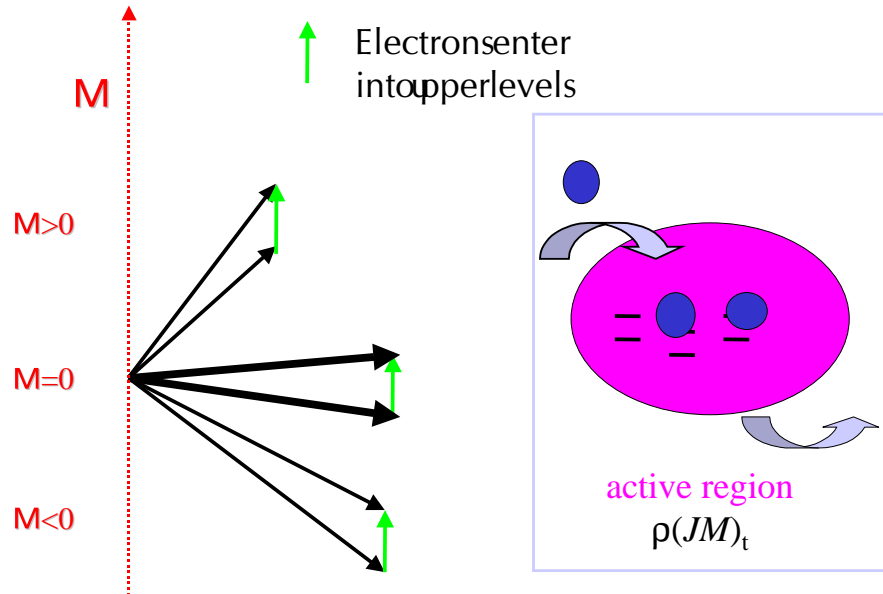
Fig. 2.4: Extended Dicke model. Right: electrons can tunnel out of and into an optical active region. Left: the tunneling leads to a change of the total (pseudo) spin J and its z–component M. These are the two variables that enter into the effective density matrix $\rho(JM)_t$ describing the state of the optical active region at time t.

In the nect section, we shortly review the concept of the Dicke states and the time evolution of the superradiant process, before discussing its modifications through the tunneling processes Eq. (2.7).

2.3   Superradiance in the original Dicke model

2.3.1   Dicke states

Superradiance in its original form as proposed by Dicke is due to the fact that the coupling of the radiation field in Eq. (2.4) is not to the individual

atoms j but to the sum of the (pseudo) spin operators

$$J_+ := \sum_j c_{j,\uparrow}^\dagger c_{j,\downarrow}, \quad J_- := \sum_j c_{j,\downarrow}^\dagger c_{j,\uparrow}. \tag{2.9}$$

Together with the z–component

$$J_z := \frac{1}{2} \sum_j \left(c_{j,\uparrow}^\dagger c_{j,\uparrow} - c_{j,\downarrow}^\dagger c_{j,\downarrow} \right), \tag{2.10}$$

these operators form an angular momentum algebra with eigenstates ('Dicke states') $|JM; \lambda\rangle$ defined via

$$\begin{aligned} J^2|JM; \lambda\rangle &= J(J+1)|JM; \lambda\rangle \\ J_z|JM; \lambda\rangle &= M|JM; \lambda\rangle, \end{aligned} \tag{2.11}$$

where J is the total spin. Here, λ denotes all additional quantum numbers apart from J and M that are necessary to characterize the eigenstates of $H_0 + H_I$. The classification of the eigenstates of H_0, Eq. (2.4), in terms of the permutation group P_N of N numbers has been given by Arecchi, Courtens, Gilmore, and Thomas [155]. It is a formidable task to write down these eigenstates explicitely, say in the basis of product states of the individual levels. Fortunately, it is possible to get a clear understanding of the physics without this explicit form.

Radiative transitions are not within individual atoms j but between eigenstates Eq. (2.11) that belong to the total entity of levels. These transitions obey the selection rule $M \to M \pm 1$, that is, the only non–vanishing matrix elements of the operator $J_+ + J_-$ are

$$\langle JM|J_+ + J_-|JM \pm 1\rangle = \sqrt{J(J+1) - M(M \pm 1)}. \tag{2.12}$$

Dicke considered a situation where each of the N two–level systems (atoms) is initially occupied by one electron in the upper level. Spontaneous emission of one photon from this totally inverted, initial state $|JJ\rangle$ with $J = N/2$ leads to a state $|JJ - 1\rangle$. In the course of the emission, the quantum number M decreases by one step by step (see Fig. (2.5)); the spontaneous emission intensity from a state $|JM\rangle$ is

$$I_{JM} = \hbar\omega_0 \Gamma \nu_{JM}, \quad \nu_{JM} := (J+M)(J-M+1), \tag{2.13}$$
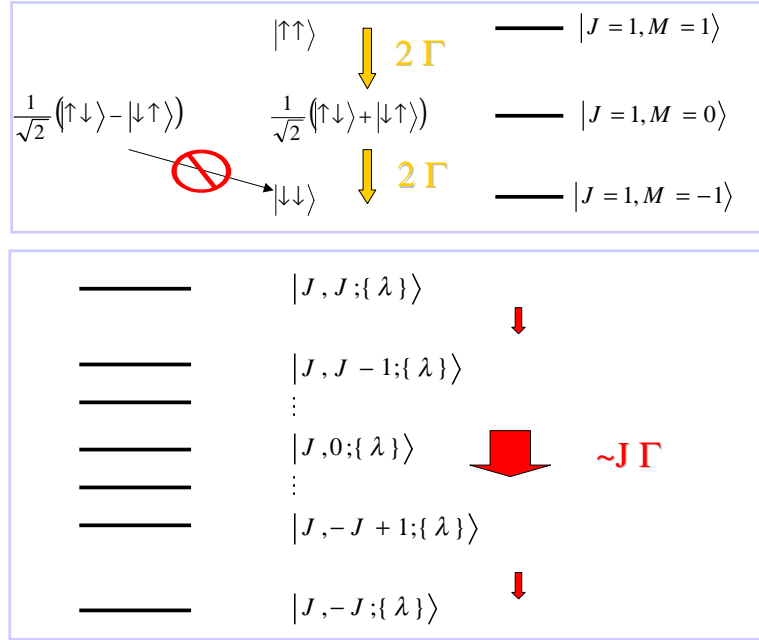
Fig. 2.5: Down–cascades for the spontaneous decay of a system of two (above) and N atoms. The Dicke states $|JM; \{\lambda\}\rangle$ in the N–atom system are the generalization of the triplet state in the two–atom system (there is no transition involving the singlet state in this case).

where Γ is a microscopic parameter given by the spontaneous emission rate of one *single* atom from its excited state. Since $-J \leq M \leq J$, the expression Eq. (2.13) reveals that in the course of the spontaneous decay starting from the initial state, the intensity ν_{JM} reaches a maximum at $M = 0$. The value of this so–called 'Dicke peak' is proportional to N^2, i.e. abnormally large in comparison with the intensity $N\nu_0$ of the radiation of N independently decaying atoms. The superradiant state $|JM = 0\rangle$ is generated by subsequent application of the ladder operator J_- in the course of the spontaneous decay. In the basis of the individual atoms $j = 1, ..., N$, this state is a complicated coherent superposition of a large number of product states.

2.3.2   Time evolution in the original Dicke problem

The time dependence of the emission peak can be obtained from a simple quasi–classical argument, that regards the quantum number M as a time–dependent, classical quantity. For an ensemble of identical atoms, one has

$$H_0 = \omega_0 J_z, \tag{2.14}$$

i.e. $\varepsilon_{j\uparrow} = -\varepsilon_{j\downarrow} = \omega_0/2$ in Eq. (2.4). Equating the average energy loss, $-\omega_0(d/dt)M(t)$, with the radiated intensity, Eq. (2.13), one obtains an equation of motion for $M(t)$,

$$-\frac{d}{dt}M(t) \;=\; \Gamma\left(J + M(t)\right)\left(J - M(t) + 1\right) \tag{2.15}$$

The solution of this equation gives the hyperbolic secant solution to the superradiance problem, that is a time–dependent intensity (see Fig.(2.2))

$$\nu(t) = \nu_0 \frac{N^2}{2\cosh^2\left(N\Gamma[t - t_d]/2\right)}, \tag{2.16}$$

where the delay time t_d depends on the initial condition at time $t = 0$. As has been discussed by Gross and Haroche [141], the quasi–classical description of the decay process becomes good if the system is prepared initially in a state $|JM_0\rangle$ with a large number s_0, $1 \ll s_0 \ll N$, of photons already emitted. If one starts from the totally inverted state $|JJ\rangle$, the initial time evolution is dominated by strong quantum fluctuations (the phases of the single atoms are completely uncorrelated). In the following, we will continue the qualitative description in the quasi–classical picture before numerically solving the master equations that contain the full quantum dynamics.

2.4   Tunneling and Clebsch–Gordan coefficients

2.4.1   Total pseudo spin

The original Dicke problem assumed a fixed total number of electrons: one electron per atom or, in the spin language, exactly one spin (up or down) σ on each site j. We now discuss what happens if this restriction is lifted, i.e. if electrons can enter or leave the superradiant region. Since the electron number is no longer conserved, there is no longer an exact 'half–filling':

sites with double occupancy (spin up and spin down) and empty sites become possible. One immediate consequence is that a tunneling electron will change the quantum numbers J and M. The pseudo–spin projection M will increase by $1/2$ when an electron enters and occupies an upper level; it will decrease by $1/2$ when the electron occupies a lower level. This process leads to a corresponding change of the total spin J, $J \to J \pm 1/2$ as dictated by the Clebsch–Gordan coefficients (see below). The total spin J is thus no longer conserved in the course of the dynamical evolution. In fact, in the original Dicke model there are no transitions between integer and half–integer quantum numbers J; for an even number of atoms the possible J are integer (e.g. $5, 4, 3, ...$), for an odd number of atoms they are half–integer (e.g. $5.5, 4.5, 3.5, ...$). Note that apart from λ, Eq. (2.11), additional quantum numbers are required to fully characterize all states $|JM; \lambda\rangle$ in the total Hilbert space. In a fully microscopic calculation, these should include, e.g., the number of empty sites and the number of double occupied sites.

2.4.2 Clebsch Gordan coefficients

Apart from the emission rate ν_{JM}, it is the tunneling rate that governs the time evolution in presence of reservoirs. In the pseudo–spin language, a tunneling electron means adding (or removing) a spin ($j = 1/2, m = \pm 1/2$) to a Dicke state $|JM\rangle$, cp. Fig. (2.4). The tunnel rate is determined by the overlap matrix element of the new state $|JMjm\rangle$ with the Dicke states $|J'M'\rangle$, i.e. the Clebsch–Gordan coefficients [156]

$$\langle J'M'|JMjm \;=\; \pm 1/2\rangle = \sqrt{\frac{J \pm M + 1}{2J + 1}}\delta_{M',M+m}, \quad J' = J + 1/2$$

$$\langle J'M'|JMjm \;=\; \pm 1/2\rangle = \mp\sqrt{\frac{J \mp M}{2J + 1}}\delta_{M',M+m}, \quad J' = J - 1/2. \text{(2.17)}$$

The matrix element for tunneling also depends on the coefficients $t^{\alpha}_{k,j,\sigma}$, Eq. (2.7), and (more important) on the specific form of the many body wave functions of the optical active region. In the derivation of the tunneling rates below we will make the approximation that these effects can be absorbed into a simple renormalization of the tunneling amplitude, and that the tunneling is governed by the quantum numbers J and M via the Clebsch-Gordan coefficients Eq. (2.17). This approach, together with the subsequent derivation of the 'tunneling' part of the master equation, is very similar to a recent cal-

culation of the tunnel current through an interacting few–electron quantum dot by Weinmann *et al.* [157, 158].

2.4.3 Time evolution: phenomenological model

Equations of motion for J and M

Let us consider the specific case where spin–up electrons enter the optical active region, i.e. electrons occupy upper levels on entering, and spin–down electrons leave it, i.e. electrons in lower levels tunnel to the outside. Consider the 'tunnel in' case first: if the optical active region is in the initial phase of superradiance, adding an up spin to the state $|JM = J\rangle$ leads to the state $|J+1/2, M+1/2\rangle$ with amplitude 1, the amplitude to obtain $|J-1/2, M+1/2\rangle$ is zero. In the superradiant phase , $M = 0$, states with $J + 1/2$ and $J - 1/2$ are obtained with nearly equal absolute amplitudes $\sqrt{(J+1)/(2J+1)}$ and $-\sqrt{J/(2J+1)}$, respectively. In the 'final phase' of superradiance, i.e. $M = -J$, adding an up spin leads to $J + 1/2$ with nearly zero amplitude (we consider large $J \gg 1$), but to $J - 1/2$ with amplitude ≈ 1. For tunneling of an up spin into the , M is increased by $1/2$ as is the case for tunneling of a down spin out of the optical active region: M increases by 1 with the tunnel rate T. At the same time, the change of J is $+1/2$ for $M = J$, nearly zero for $M = 0$, and $-1/2$ for $M = -J$. The more accurate estimate below gives $d/dt J(t) = T M(t)/J(t)$, i.e. the change of J is indeed proportional to M itself. This leads us to the coupled equations

$$
\boxed{
\begin{aligned}
\dot{M}(t) &= -\Gamma \nu_{J(t)M(t)} + T \\
\dot{J}(t) &= T \cdot M(t)/J(t) \\
\nu_{JM} &:= (J + M)(J - M + 1)
\end{aligned}
}
\tag{2.18}
$$

which are governed by the two parameters Γ and T, the emission rate and the tunnel rate.

What is particular with these equations is the fact that they possess *oscillatory* solutions: this can be seen best by deriving from Eq. (2.18) a second order differential equation,

$$
\frac{d^2}{dt^2} M(t) - 2\Gamma M(t) \frac{d}{dt} M(t) + 2\Gamma T M(t) = 0,
\tag{2.19}
$$

where we approximated in the emission rate $J - M + 1 \approx J - M$. Eq. (2.19) describes a harmonic oscillator with amplitude dependent damping and frequency

$$\omega = \sqrt{2\Gamma T}. \tag{2.20}$$

Driven oscillator picture

The harmonic oscillator picture and the form Eq. (2.20) of the frequency becomes more evident by considering the time scales of the problem: the decay *time* Γ^{-1} of a single two level system gives rise to the time-scale of the 'undriven' ($T = 0$) system. That is, large decay times correspond to a slow motion of the latter or a large 'mass' m (inertia) whence $\Gamma^{-1} \sim m$. On the other hand, the system is driven by a 'force' (tunneling electrons) with force constant k proportional to the tunneling rate T, thus giving rise to oscillations with a frequency $\sim \sqrt{k/m} \sim \sqrt{\Gamma T}$. In the mechanical analogon, an external force $F(q)$ couples the phase space coordinates p and q via Newton's equation $\dot{p} = F(q)$. Here, it is the tunneling of single electrons that induces a coupling between the total spin J and the total spin projection M via the Clebsch–Gordan coefficients.

Integrating the equation for $J(t)$, one reckognizes that the oscillations also show up in the intensity ν_{JM} itself which is confirmed below by the exact numerical solution of the master equation. The addition of the source term T which describes the change of the total spin projection by the tunneling electrons (spin up tunnels in, spin down tunnels out) thus leads to a drastically modification of the simple pulse–shaped 'Dicke peak' of superradiation. We point out that the oscillatory behavior as predicted by Eq. (2.18) - Eq. (2.20) is totally different from the 'oscillatory superradiance' which is known from the original Dicke problem and has its origin in a reabsorption of a photon that had been emitted before (for a discussion of this phenomenon, see e.g. [131]).

2.5   Master equation

We now proceed from the qualitative discussion of the preceding chapter to a more detailed analysis. The coupling to the reservoirs brings about the combination of two physical problems: the dynamics of a two–level ensemble coupled to a boson field, i.e. a many spin–boson problem on the one hand,

and the electronic transport through a region of electrons interacting with each other and with bosons. Both individual problems are not exactly solvable. The master equation method is usually applied in both cases in order to calculate approximately expectation values like the intensity of emitted light, or the electric current. In the following, our strategy therefore is to set up the master equation for our problem. We will furthermore consider only diagonal elements of the density operator; this level of theoretical description is still sufficient to obtain the time–dependent intensity of the emitted radiation, in particular the characteristic Dicke–peak and its modifications. Furthermore, the basic physics of the electron transport through the 'dot' optical active region is still accessible within this picture, e.g. if one were interested in describing Coulomb blockade effects.

The master equation

$$\frac{d}{dt}\rho = L_{e-p}[\rho] + L_{e-l}[\rho] \tag{2.21}$$

is an operator equation for the density matrix ρ of the system, reduced to a small number of degrees of freedom, i.e. in our case the electronic degrees of freedom of the optical active region. The splitting of the operator L in Eq. (2.21) requires that one works in lowest order of the perturbation theory with no interference between the electron–boson coupling H_{ep}, Eq. (2.4), and the coupling to the leads H_T, Eq. (2.8). We furthermore work in the basis of the Dicke states Eq. (2.11), but disregard the index λ that represents all quantum numbers apart from J, M, and the electron number N. In particular, we will neglect electron–electron interactions and describe the whole dynamics in terms of the probabilities $\rho(JMN)$, i.e. the diagonal elements of the density operator at a given electron number N. The expression for L_{e-p} then coincides with the one for the original Dicke problem and has been derived by many authors, see e.g. [74]. On the other hand, the expression for L_{e-l} is known from the master equation for tunneling through quantum dots [63, 157] and is determined by microscopic rates $\Gamma_{JMN \to J'M'N'}$ by which the state of the optical active region changes through tunneling events (these rates will be derived below). Thus, the master equation describing the combined effects of the coupling to the boson field and the electron leads is given

by

$$\frac{d}{dt}\rho(JMN) = -\Gamma\left(\nu_{JM}\rho(JMN) - \nu_{JM+1}\rho(JM+1N)\right)$$
$$+ \sum_{J'M'N'}\left(\Gamma_{J'M'N'\to JMN}\rho(J'M'N') - \Gamma_{JMN\to J'M'N'}\rho(JMN)\right).(2.22)$$

2.5.1 Transition Rates

The transition rates $\Gamma_{JMN\to J'M'N'}$ have the explicit expressions for tunneling from/to reservoir α

$$\Gamma^{\alpha}_{JMN\to J'M'N'} = T^{\alpha}\,|\sum_{j\sigma}\langle J'M'N'|c^{\dagger}_{j\sigma}|JMN\rangle|^2\,f_{\alpha}(E_{J'M'N'} - E_{JMN})\,(2.23)$$
$$+ \;T^{\alpha}|\sum_{j\sigma}\langle J'M'N'|c_{j\sigma}|JMN\rangle|^2\,\left[1 - f_{\alpha}(E_{JMN} - E_{J'M'N'})\right],$$

where

$$T^{\alpha} := 2\pi\sum_{k}t^{\alpha}_{kj\sigma}(t^{\alpha}_{kj'\sigma'})^*\delta(E - \varepsilon^{\alpha}_k)\qquad(2.24)$$

is the tunnel rate for lead α. The latter in fact is a tensor in both the site and the spin indices (j,σ) and depends on the energy difference E of initial and final state of the optical region after a tunnel event. We neglect the energy and site dependence, furthermore the spin dependence is absorbed into the index α through the boundary conditions : we enforce a condition that makes the tunneling work as a 'spin–up' pump where only 'spin–up' electrons can tunnel in (from the left) and 'spin–out' electrons out (to the right) of the optical active region. For the case of two reservoirs 'left' and 'right', the situation is very similar to the double dot problem, with 'up' corresponding to the left dot and 'down' to the right dot. Effectively, one ends up with only two parameters T^R and T^L then.

The leads are assumed to be in an equilibrium described by the Fermi distribution f_{α}. The energy argument of the latter equals the energy transfer to or from the optical active region with many–particle state energies E_{JMN}. The state $c^{\dagger}_{j\sigma}|JMN\rangle$ is a $N+1$ electron state which is generated by placing one electron into an upper level and therewith adding a (pseudo–)spin $1/2$ to a many–particle state with total spin J and projection M. As mentioned above, the main approximation in calculating the matrix elements in

Eq. (2.24) consists in neglecting the specific form of the many–particle wave function, i.e. approximating the matrix element by the Clebsch–Gordan coefficient sum

$$\sum_{j\sigma} \langle J'M'N'|c_{j\sigma}^\dagger|JMN\rangle|^2 \quad \approx \quad \delta_{N+1,N'}\gamma_{JM\to J'M'} \tag{2.25}$$

$$\gamma_{JM\to J'M'} \quad := \quad |\sum_{\sigma=\pm 1/2} \langle J'M'|JM,j=1/2m=\sigma\rangle|^2,$$

where the proportionality factor is absorbed into the constant T^α, Eq. (2.24). The calculation of the quantity γ, Eq. (2.25), is straightforward and yields

$$
\begin{aligned}
\gamma_{JM\to J'M'} \quad := \quad & \frac{1}{2J+1}\big(\delta_{J',J+1/2} \\
\times \quad & \big[\delta_{M',M+1/2}(J+M+1) \\
+ \quad & \delta_{M',M-1/2}(J-M+1)\big] \\
+ \quad & \delta_{J',J-1/2}\big[\delta_{M',M+1/2}(J-M) \\
+ \quad & \delta_{M',M-1/2}(J+M)\big]\big).
\end{aligned}
\tag{2.26}
$$

To enforce the 'spin–up–pump' boundary condition, the chemical potential left is assumed to be situated above all possible energy differences of many–body states with M differing by plus $1/2$. In addition, tunneling from left to the 'down' levels is excluded by assuming the corresponding matrix elements to be negligibly small. On the other hand, the chemical potential right is chosen such that 'down' electrons can tunnel out to the right, but not tunnel in. The tunnel matrix elements are T^α, $\alpha = I$ (in), O (out), allow for tunneling to/from the right/left only, respectively. In equations, this means

$$
\begin{aligned}
\sum_{\alpha=R/L} t^\alpha f_\alpha(E_{J\pm 1/2,M+1/2,N+1} - E_{JMN}) &= T^I > 0 \\
\sum_{\alpha=R/L} t^\alpha \bar{f}_\alpha(E_{JMN} - E_{J\pm 1/2,M+1/2,N-1}) &= T^O > 0 \\
\sum_{\alpha=R/L} t^\alpha f_\alpha(E_{J\pm 1/2,M-1/2,N+1} - E_{JMN}) &= 0 \\
\sum_{\alpha=R/L} t^\alpha \bar{f}_\alpha(E_{JMN} - E_{J\pm 1/2,M-1/2,N}) &= 0,
\end{aligned}
\tag{2.27}
$$

where we abbreviated $\bar{f} := 1 - f$.

We show below that a possible experimental setup with the corresponding boundary conditions in principle can be realized in an electron–hole semiconductor quantum well, or an array of coupled double quantum dots.

2.6   Results

### 2.6.1   Numerical evaluation of the master equation

The time dependence of the expectation value of the emission rate, Eq. (2.13), was obtained from the time evolution of $\rho(JM)_t$ by numerical solution of Eq. (2.21). The result is shown in Fig. (2.6) for an initially excited state with $J = 6$, $M = 5$. The initial emission maximum is the original 'Dicke peak', followed by oscillations that die out at an intensity proportional to the tunnel rate T that was chosen symmetric, $T = T^I = T^O$. The frequency of the oscillations increases with $\sqrt{T}$ and follows in good approximation the law Eq. (2.20). In particular, the initial peak is strongly enhanced with increasing tunnel rate. This behavior is related to an initial increase of the total pseudo spin as can be seen from the 'phase–space' plot (inset of Fig. (2.6)) of the expectation values of J and M which both oscillate in time.

2.6.2   Quasi–classical probability packets

From the master equation Eq. (2.21), equations for the expectation values $M(t) := \langle M \rangle_t$, $\langle J \rangle_t$, and $\langle N \rangle_t$ can be derived in a quasiclassical approximation [141] that neglects fluctuations and writes the (time dependent) probability distribution

$$\rho(JMN)_t = \delta_{M,M(t)}\delta_{J,J(t)}\delta_{N,N(t)}. \qquad (2.28)$$

The detailed form of the intensity peak and the intensity oscillations obtained in this way deviate from the exact solution of Eq. (2.21). The qualitative features, however, coincide and it is in particular possible to derive the expression Eq. (2.20) for the oscillation frequency.
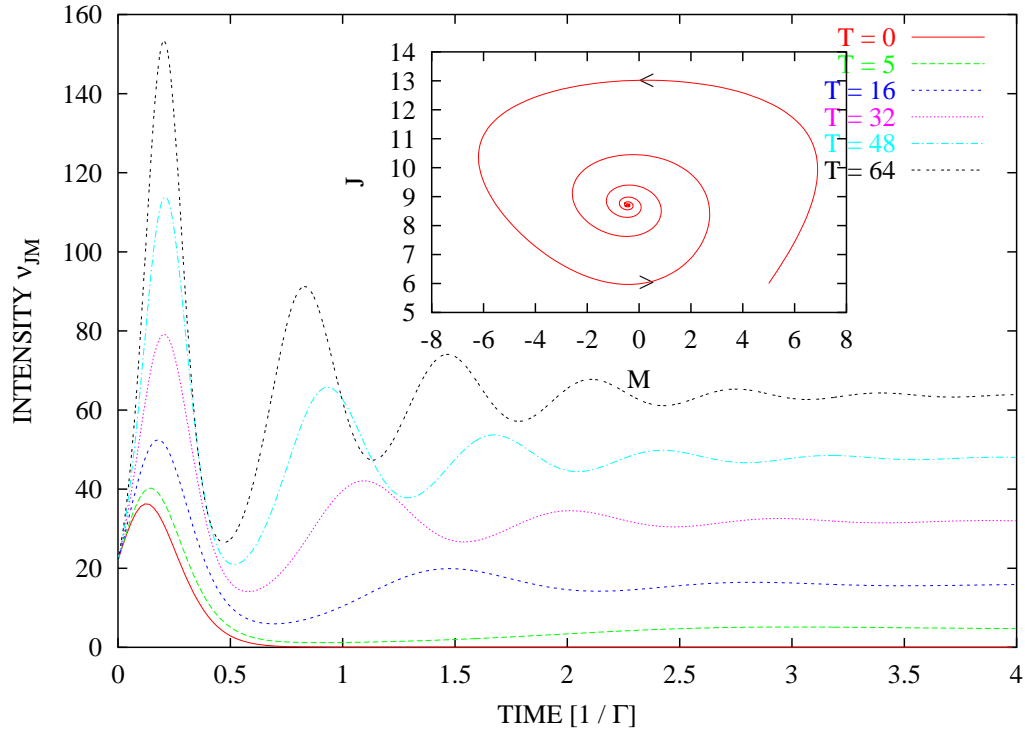
Fig. 2.6: Time evolution of the emission intensity $\nu_{JM} = I_{JM}/\Gamma\hbar\omega_0$ for different transmission rates T. Inset: $\langle J \rangle_t$ vs. $\langle M \rangle_t$ for $T = 64$.

Combining Eq. (2.28) and Eq. (2.21), one obtains

$$\frac{d}{dt}\begin{pmatrix} M(t) \\ J(t) \\ N(t) \end{pmatrix} = -\Gamma\begin{pmatrix} \nu_{J(t)M(t)} \\ 0 \\ 0 \end{pmatrix} \tag{2.29}$$

$$- \sum_{J'M'N'\alpha} \Gamma^{\alpha}_{J(t)M(t)N(t)\to J'M'N'}\begin{pmatrix} M(t) - M' \\ J(t) - J' \\ N(t) - N' \end{pmatrix}.$$

Combining Eq. (2.27) and Eq. (2.29) leads to three coupled equations

$$
\frac{d}{dt}\begin{pmatrix} M(t) \\ J(t) \\ N(t) \end{pmatrix} = -\Gamma \begin{pmatrix} \nu_{J(t)M(t)} \\ 0 \\ 0 \end{pmatrix}
$$
$$
+\; T^I \begin{pmatrix} \frac{1}{2} \\ \frac{1}{2}\frac{2M+1}{2J+1} \\ 1 \end{pmatrix} - T^O \begin{pmatrix} -\frac{1}{2} + \frac{M}{4J(J+1)} \\ -\frac{M}{4}\frac{2J+1}{J(J+1)} \\ 1 - \frac{M}{2J(J+1)}, \end{pmatrix} \tag{2.30}
$$

which can be further simplified for large J where one can neglect terms $1/J$ (but not M/J) whence the N–equation decouples. For equal tunnel matrix elements $T^I = T^O =: T$, one obtains

$$
\begin{aligned}
\dot{M} &= -\Gamma \nu_{JM} + T \\
\dot{J} &= TM/J \\
\dot{N} &= 0, \qquad T^R = T^I =: T \\
\nu_{JM} &:= (J+M)(J-M+1)
\end{aligned} \tag{2.31}
$$

which agrees with the previous phenomenological derivation.

In the original Dicke problem, a fixed total number N of electrons with exactly one pseudo spin σ on each site i is assumed. Here, we work in a grand–canonical ensemble where N varies through single electron tunneling: doubly occupied or empty single particle levels i become possible, i.e. there is no longer an exact 'half–filling'. One immediate consequence is that a tunneling electron changes the quantum numbers J and M. The change $\dot{J}$ of J is proportional to M itself, $\dot{J}(t) = TM(t)/J(t)$, which follows considering the Clebsch–Gordan coefficients for adding a pseudo up spin. At the same time, M is increased by $1/2$ as is the case for out–tunneling of a pseudo down spin: M increases by 1 at the tunnel rate T and decreases by spontaneous emission at a rate $\Gamma\nu_{JM}$. Therefore, J and M obey roughly the Eq.(2.31).

2.6.3 Oscillations (ringing) in conventional superradiance versus pumped superradiance oscillations

Oscillations in superradiating systems have been well known since the first experimental confirmation of the effect [133]. In fact, the emission intensity from a superradiating ensemble is subject to a 'ringing' effect. In particular, photons that have been emitted by one atom can be reabsorbed elsewhere,

an effect which is not contained in the simplifying description of the original Dicke superradiance model. This flow of energy between the atoms and the field modes leads to a revival of the inversion due to reabsorption of photons. In general, the physics of this mechanism and the related light propagation effects are a complicated time– and space dependent process. A quite complete analysis of this kind of oscillation has been given by Bonifacio and Preparata [159] in a one–mode model with generalized Rabi–oscillations in a Jaynes–Cummings like model. In fact, the mean field theory of the Maxwell–Bloch equations in a one–dimensional model [73] leads to an oscillation frequency

$$\omega \approx \Omega / 2 \ln N, \quad \Omega := (2\pi N d^2 \omega_0 / \hbar)^{1/2}, \tag{2.32}$$

where ω_0 is the transition frequency, d the dipole moment, and N the number of two–level systems.

We point out that in contrast to these oscillations between atom and field mode energy, the oscillations with frequency

$$\omega \approx \sqrt{2\Gamma T} \tag{2.33}$$

in our model are due to the combination of two mechanisms, i.e. spontaneous decay and pumping, as discussed above. In particular, backflow of energy from the electric field is neglected in our model since we assume that a photon, once emitted, can escape from the system.

2.6.4 Pumped superradiance in an atomic system

We mention that an oscillation effect similar to the one predicted by us has been found by Steudel and Leonhardt [160]. They discussed the Maxwell–Bloch equations (see chapter 3) for an atomic system with a level scheme shown in Fig. (2.7). Continous optical pumping from 0 to 3 and fast relaxation to 2 provide a pumping mechanism for the superflourescent transition from $2 \rightarrow 1$. This pumping is the optical analog to our tunneling mechanism as described by the parameter T. Interestingly, in [160], self–similar solutions of the Maxwell–Bloch equations [73] were found that had also an oscillatory character. These solutions should describe experiments of superfluorescence in two–level systems where pumping is continous and not (as in usual atomic superfluorescence experiments) just used to generate an approximately complete inversion of the system.
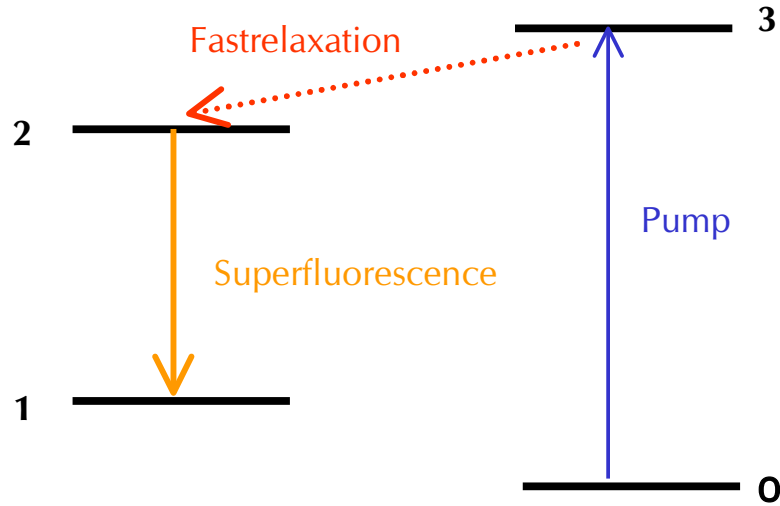
Fig. 2.7: Level scheme for pumped atomic superflourescence, after Steudel and Leonhardt [160].

2.7   Discussion

We now turn to the question in what physical systems the effects described above can be observed experimentally.

2.7.1   Experimental realization

We note that the tunneling processes can be replaced with classical injection processes over potential barriers, because we have assumed that quantum correlation is absent between subsequent tunneling processes. We thus propose the system of electrons and holes in semiconductor quantum wells in strong magnetic fields. Vertical injection of conduction band electrons and valence band holes into an active region acts like the pumping mechanism described above. In fact, this mechanism is exactly what is used in lasers or light emitting diodes with forward biased pn junctions. In our case, mirrors

as in a laser are not necessary, in particular stimulated emission processes must play no role. The strong magnetic field is necessary to have dispersionless single electron levels $i = X$, corresponding to the lowest Landau bands ($n = 0$) and guiding center X [161] in the conduction and the valence bands. In this case, the interband optical matrix elements are diagonal in i. The correspondence with our model can be seen by mapping its four basic single particle states to the states of the electron–hole system (Fig. (2.8)): the empty state becomes the hole (h), the pseudo–spin down electron becomes the empty state, the doubly occupied state becomes the electron (e), and the pseudo–spin up electron becomes the state with one electron and one hole. The number of total electrons N in our model has its correspondence via

$$N = N_e + N_s - N_h, \tag{2.34}$$

where $N_s = \Phi/\Phi_0$ is the degeneracy for a given magnetic flux Φ ($\Phi_0 = hc/e$ is the flux quantum), N_e the number of electrons in the conduction band, and N_h the number of holes in the valence band.

We predict that an initial optical or current excitation of the system leads to a superradiant peak of emitted light that becomes strongly enhanced if the tunneling rate becomes higher. Furthermore, subsequent oscillations of the emitted light should be visible at an approximate frequency Eq. (2.20). We also expect similar oscillations to be visible as weak corrections to the injection current. In chapter 3, we present detailed calculations of the superradiance effect in the emission of light from a magnetoplasma.

As a second experimental setup, we propose an array of identical quantum dots, coupled to electron reservoirs as above. The array must have the capability to coherently radiate, where each dot has a pair of well-defined internal levels that allow for transitions under emission of photons. Alternatively the coherent emission of *phonons* from an array of *double quantum dots* could be a candidate for oscillatory superradiance. This system will be discussed in chapter 4.

Another possible realization could be a geometry as in the quantum cascade laser which has been proposed recently [162, 163] as an alternative to conventional semiconductor diode lasers. In this case, transitions between different electronic subbands lead to photon emission. Note that in all three cases, the photon escape time $\tau = L/c$ (L is the linear dimension of the active region and c the speed of light) has to be much smaller than all other time scales of the problem, because in our model we assumed the 'small sample superradiance case' where reabsorption effects play no role.

model

electron-hole system
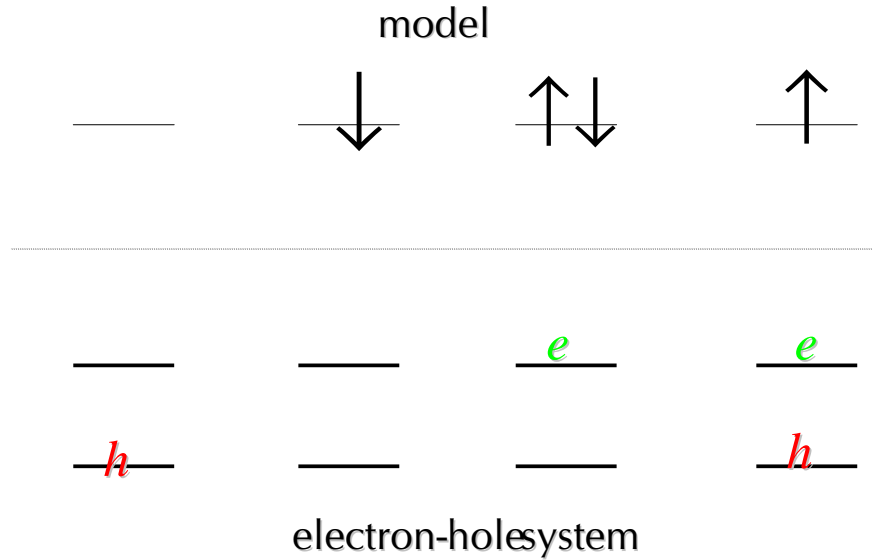
Fig. 2.8: Correspondence of our model (superradiance with reservoir) with an electron–hole system. 'e' denotes an electron in the conduction band, 'h' a hole in the valence band.

We mention that all the effects described above should in principle be observable not only for photons, but also for other bosonic fields such as phonons, or magnons.

2.7.2   Phase coherence

We point out that so far we have not addressed the question of phase coherence. In fact, the conventional superradiance is a transient process that occurs only on a 'mesocopic' time scale with an upper boundary given by a phase coherence time τ_ϕ (The lower boundary is given by the photon escape time τ). Inelastic processes such as dipole–dipole interactions [139, 140] in general destroy the phase coherence between single particle states and the description using the Dicke states with well–defined J and M becomes void. On the other hand, coherence between states with different J and different

M is not required in our formalism, on the contrary this would require consideration of coherent tunneling which is beyond the scope of our approach. We assume that dephasing processes are weak such that the time to observe the initial Dicke peak and some cycles of the subsequent oscillations is still shorter than τ_ϕ. An ideal case would be a strong initial excitation to a high initial pseudo spin J, and a high tunnel rate T that yields fast oscillations. Furthermore, strong magnetic fields in general suppress scattering rates although at the present state we can give no quantitative estimates for τ_ϕ.

The following two chapters are devoted to a more detailed discussion of a possible experimental realization of the oscillatory superradiance effect.

3. SUPERRADIANCE IN A MAGNETOPLASMA

We present theoretical results for superradiance, i.e. the collective coherent decay of a radiating system, in a semiconductor heterostructure under a strong quantizing magnetic field. Pumping of electrons and holes into an optical active region at a rate T leads to a novel kind of oscillations with frequency $\sim \sqrt{T}$ in the limit of the lowest Landau level. If more Landau levels are involved, the emitted intensity shows a chaotic–like behavior as a function of time.

3.1 Introduction

In this chapter, we discuss the superradiance effect in the electron–hole gas of a two–dimensional semiconductor quantum well under a strong, quantizing magnetic field. For such a system, in the calculation of chapter 2 we predicted a novel form of superradiance in case that an optical active region is pumped externally by electron (hole) reservoirs. In the limit of only the lowest Landau level occupied, the coherent decay of electron–hole pairs leads to a peak of the emitted light with a strong intensity that, as a function of time, shows oscillations with a frequency

$$\omega \simeq \sqrt{2\Gamma T}, \tag{3.1}$$

where Γ is the spontaneous decay rate of a single electron–hole pair and T the rate at which electrons are pumped in the conduction and holes into the valence band. Our previous calculation was based on a master equation description of the optical active region that was described in a simplifying manner in the space of the so–called Dicke states by only two quantum numbers J and M, the total pseudo spin and its projection. Here, we extend these calculations in the following way:

1. We start from the microscopic wave functions of the heterostructure under the magnetic field.

2. We take into account Coulomb interactions between electron and holes on the Hartree–Fock level.

3. We set up the microscopic Maxwell–semiconductor Bloch equations (MBE) for the expectation values of the inversion and polarization. These equations are solved for a simplified model of a two–band semiconductor magnetoplasma, neglecting intraband scattering processes.

We note that Belyanin et al. [164] also found the possibility of superradiance in *bulk* (3d) semiconductors in magnetic fields, but without interactions among the electrons and without pumping.

Our results are the following:

1. In the strong magnetic field limit of only the lowest Landau level occupied in both conductance and valence band, the equations describe superradiance in exact correspondence to atomic systems: each two–level atom corresponds, roughly speaking, to an electron–hole pair with quantum numbers $n = 0$ (Landau level) and k, the momentum in one direction perpendicular to the magnetic field. The density of atoms corresponds to the number of flux quanta per optical active volume. Excitations with an incoherent light pulse shorter than 1 ps shall provide a total inversion at initial time $t = 0$. Thereafter, the emitted light has the form of the *characteristic Dicke peak with a maximum that is proportional to the square of the magnetic field* for constant filling factors $\nu = 1$.

2. We consider only Coulomb effects in s–wave approximation. Then, Coulomb effects only show up if more than one Landau level is involved, i.e. at larger filling factors. In this case, there are additional oscillations after the initial Dicke peak even without external pumping. The oscillations are smeared out by the Coulomb interactions.

3. In case of pumping of electrons and holes into the system (as in laser diodes), the solutions of the MBE have a much richer structure: a) for only the lowest Landau level occupied, we basically recover our former result, i.e. 'pumped superradiance'. The emission peak periodically disappears and reappears as a function of time, it is (in contrast to our previous model) nearly undamped, but with the same period; b) for a larger number of occupied Landau levels, i.e. in the limit of smaller magnetic fields, the total emission shows a completely irregular, chaotic bebavior as a function of time.

3.2 Model

3.2.1 Electrons in a magnetic field

We start from non–interacting electrons in a semiconductor heterostructure under a strong magnetic field ($\hbar = c = 1$),

$$H_0 = \frac{(\mathbf{p} - e\mathbf{A}_B(\mathbf{x}))^2}{2m} + U(\mathbf{x}) + V(z), \qquad (3.2)$$

where $\mathbf{A}_B$ is the vector potential of the homogeneous magnetic field in z–direction, $U(\mathbf{x})$ the periodic lattic potential and $V(z)$ the potential that confines the electron motion to a two–dimensional plane. Here, m is the bare electron mass and e the charge of the electron in vacuum. The eigenstates of H_0 in absence of confinement potential and magnetic field are

$$\chi_{l\mathbf{k}}(\mathbf{x}) = \frac{1}{L^{3/2}} e^{i\mathbf{k}\mathbf{x}} u_{l\mathbf{k}}(\mathbf{x}), \qquad (3.3)$$

where the Bloch function $u_{l\mathbf{k}}$ is periodic in the Bravais lattice of the crystal (with volume L^3) and has dimension one. We assume spin–polarization throughout the rest of the calculation. The eigenvalues $\varepsilon_l(\mathbf{k})$ determine the bandstructure of the ideal crystal (no interactions, no magnetic fields and no potentials other than U), where l is the band index. The determination of the eigenstates and eigenvalues of H_0 is in general non–trivial even for non–interacting electrons. Here, we use the approximation of Luttinger and Kohn [165]: the eigenstates of H_0 have the form

$$\psi_{l\alpha}(\mathbf{x}) = \phi_{l\alpha}(\mathbf{x}) u_l(\mathbf{x}); \quad u_l(\mathbf{x}) = u_{l\mathbf{k}=\mathbf{0}}(\mathbf{x}), \qquad (3.4)$$

where $\phi_{l\alpha}(\mathbf{x})$ is the solution of

$$[\varepsilon_l(\mathbf{p} - e\mathbf{A}_B(\mathbf{x})) + V(\mathbf{x})] \phi_{l\alpha}(\mathbf{x}) = \varepsilon_{l\alpha} \phi_{l\alpha}(\mathbf{x}). \qquad (3.5)$$

For a more detailed discussion of this approximation, see [166, 167]. The wave functions ϕ are given by

$$\phi_{l\alpha}(\mathbf{x}) = \frac{e^{iky}}{\sqrt{L}} \phi_n(x + k/eB) \chi_l(z), \quad \alpha = (n, k), \qquad (3.6)$$

where k is the momentum in y–direction, B the magnetic field in z–direction, ϕ_n the n–th harmonic oscillator wave function, and χ_l a standing wave for the lowest subband of the quantum well as determined by the potential $V(z)$. Note that the harmonic oscillator wave functions ϕ_n do not depend on the effective electron mass in band l.
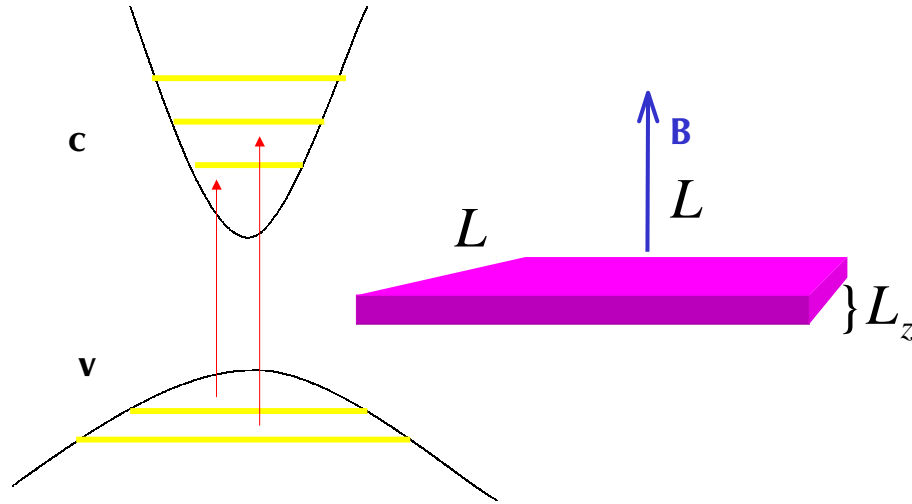
Fig. 3.1: Valence (v) and conductance band (c) of a two–band semiconductor model (left) under a quantizing field B perpendicular to the two–dimensional magnetoplasma (right).

3.2.2 Electric field

The theoretical description of superradiance can be done in two alternative schemes [141]:

a) *Schrödinger picture*: a master equation for the reduced density operator of the electronic system is derived. The degrees of freedom of the electromagnetic field are integrated out. In the Markov approximation (no retardation effects), the coupling to the electromagnetic field basically enters as one single parameter (the decay rate of a single radiator).

b) *Heisenberg picture*: the equations of motion for the field operators of the polarization, occupation numbers, and the polarization are derived. This approach is useful to discuss propagation effects of the polarization (soliton solutions etc.). At the same time, it is sufficient to treat the electromagnetic field classically as described by Maxwells equations, as long as one is not

interested in the initial stage of the superradiant process that is governed by quantum fluctuations. For a more detailed discussion of the relation between the two approaches, see [141].

Here, we adopt the description b) and treat the electric field classically. This has two advantages: 1. The description becomes close to the usual semiconductor Maxwell–Bloch equations [51] and 2. These equations have a superradiant solution even for spatially homogeneous electric fields, if an additional damping of the field (escape of photons) is introduced [73]. Since we are interested in interaction and multilevel effects (more than one Landau level), this simplified description is of great advantage.

The vector potential of the electric field $\mathcal{E}(t)$ is denoted by $\mathbf{A}^e(t)$ and gives rise to an additional Hamiltonian $H^e(t)$ whence the total Hamiltonian $H(t) = H_0 + H^e(t)$ becomes time–dependent. The matrix elements of $H^e(t)$ become

$$
\begin{aligned}
\langle lnk|H^e(t)|l'n'k'\rangle &= \delta_{kk'} h_{nn'}^{ll'}(t) \\
h_{nn'}^{ll'}(t) &= -\left[e\mathbf{v}_{nn'}^l \mathbf{A}^e(t) + \frac{e^2}{2m^l}\mathbf{A}^e(t)^2 \delta_{nn'} \right] \delta_{ll'} \\
&\quad - \frac{e}{m}\mathbf{p}_{ll'}\mathbf{A}^e(t)F_{ll'}\delta_{nn'},
\end{aligned}
\tag{3.7}
$$

where $\mathbf{v}_{nn'}^l = \mathbf{v}_n^l \delta_{n,n'+1} + \mathbf{v}_{n'}^{l*}\delta_{n,n'-1}$, $\mathbf{v}_n = il_B\omega_B^l\sqrt{n/2}(\mathbf{e}_x - i\mathrm{sgn}(e)\mathbf{e}_y)$, and

$$
l_B = \sqrt{\frac{1}{|e|B}}, \quad \omega_B^l = \frac{|e|B}{m^l},
\tag{3.8}
$$

and

$$
\mathbf{p}_{ll'} = \frac{1}{\nu_0}\int_{\nu_0} d^3\mathbf{x}\, u_l^*(\mathbf{x})\mathbf{p}u_{l'}(\mathbf{x}),
\tag{3.9}
$$

where ν_0 is the volume of the primitive cell of the lattice. Furthermore,

$$
F_{ll'} = \int dz\chi_l^*(z)\chi_{l'}(z).
\tag{3.10}
$$

In Eq.(3.7), one reckognizes intraband ($l = l'$) and interband ($l \neq l'$, note that $\mathbf{p}_{ll} = 0$) terms. When intraband terms are not neglected, the Luttinger–Kohn approximation , in which only the $\mathbf{k} = \mathbf{0}$ Bloch wave functions u are retained, becomes problematic. In general, intraband processes involve Bloch

functions with all $\mathbf{k}$ vectors [167]. Physically, to describe processes within one and the same band, an effective Hamiltonian as given by the bandstructure $\varepsilon_l(\mathbf{k})$ has to be used which means that the masses m in the terms $\sim \delta_{ll'}$ in Eq.(3.7) become renormalized $m \to m_l$ to the effective mass in band l.

3.2.3 Coulomb interaction

We consider the Coulomb interaction in the form of an additional Hamiltonian H_c,

$$H_c = \frac{1}{2} \sum_{n_1,\dots,n_4,k,k',\mathbf{q}\neq\mathbf{0};ll'} V_{kk'}^{ll';n_1,\dots,n_4}(\mathbf{q}) c_{n_1 kl}^\dagger c_{n_2 k'l'}^\dagger c_{n_3 k'+q_y l'} c_{n_4 k-q_y l}. \tag{3.11}$$

In principle, there are additional terms in H_c which do not conserve the number of electrons in each band. Such processes would be energetically unfavourable and are therefore neglected. The matrix elements V can be calculated from the eigenfunctions $\phi_{l;nk}$, Eq.(3.6),

$$\begin{aligned}
V_{kk'}^{ll';n_1,\dots,n_4}(\mathbf{q}) &= \frac{1}{L^2} \tilde{U}_{ll'}(\mathbf{q}) M_{kk-q_y}^{n_1 n_4}(q_x) M_{k'k'+q_y}^{n_2 n_3}(-q_x) \\
M_{kk'}^{nn'}(q) &= \int dx e^{iqx} \phi_n(x + k/eB) \phi_{n'}(x + k'/eB) \tag{3.12} \\
\tilde{U}_{ll'}(\mathbf{q}) &= \int dx\,dy\,dz\,dz' |\chi_l(z)|^2 |\chi_{l'}(z')|^2 U_c(x, y, z - z') e^{-i(xq_x + yq_y)},
\end{aligned}$$

where $U_c(\mathbf{x}) = e^2/(\varepsilon_r |\mathbf{x}|)$ is the three–dimensional Coulomb potential screened by the static dielectric constant ε_r of the bulk semiconductor. In the following, for the calculation of these matrix elements we neglect the finite thickness of the quantum well, i.e. we set $|\chi_l(z)|^2 = \delta(z)$. The matrix elements that are required for the Hartree–Fock calculation below then become

$$\begin{aligned}
V_{q_y,0}^{nn'nn'}(\mathbf{q}) &= \frac{2\pi e^2}{\varepsilon_r q} \frac{min(n!,n'!)^2}{n! n'!} |z|^{2|n-n'|} \left[L_{min(n,n')}^{|n-n'|}(|z|^2) \right]^2 \\
|z|^2 &= \frac{l_B^2}{2} q^2, \quad q = |\mathbf{q}|, \tag{3.13}
\end{aligned}$$

where $\mathbf{q}$ is a two-dimensional vector and L a Laguerre polynomial.

3.3 Equations of motion

We now set up the equations of motion for the one–particle quantities

$$p^{ll'}_{nn'kk'}(t) := \langle c^\dagger_{nkl} c_{n'k'l'} \rangle_t. \tag{3.14}$$

With the expectation value of any operator A defined by

$$\langle A \rangle_t = Tr(\rho(t)A), \quad i\frac{d}{dt}\langle A \rangle_t = \langle [A, H(t) + H_c] \rangle_t, \tag{3.15}$$

one soon reckognizes that due to the interaction term H_c no closed system of equations can be obtained. We use the Hartree–Fock approximation to factorize higher order correlation functions, furthermore we consider only terms in Eq.(3.14) diagonal in the momentum k, i.e.

$$p^{ll'}_{nn'kk'}(t) =: \delta_{kk'} p^{ll'}_{nn';k}(t). \tag{3.16}$$

The result is

$$
\left(i\frac{\partial}{\partial t} + \varepsilon_{ln} - \varepsilon_{l'n'} \right) p^{ll'}_{nn';k} =
$$

$$
- \; eA^e(t) \sum_{n''} \left(\mathbf{v}_{n'n''} p^{ll'}_{nn'';k} - \mathbf{v}_{n''n} p^{ll'}_{n''n';k} \right)
$$

$$
- \; eA^e(t) \sum_{n''} \left(\mathbf{w}_{l'l''} p^{ll''}_{nn';k} - \mathbf{w}_{l''l} p^{l''l}_{nn';k} \right)
$$

$$
- \; \frac{1}{2} \sum_{n_1 n_3 n_4 \mathbf{q} l''} V^{n_1 n' n_3 n_4}_{k+q_y k}(\mathbf{q}) p^{l''l'}_{n_1 n_3;k+q_y} p^{ll''}_{nn_4;k}
$$

$$
+ \; \frac{1}{2} \sum_{n_1 n_2 n_3 \mathbf{q} l''} V^{n_1 n_2 n_3 n}_{k+q_y k}(\mathbf{q}) p^{ll''}_{n_1 n_3;k+q_y} p^{l''l'}_{n_2 n';k}
$$

$$
- \; \frac{1}{2} \sum_{n_2 n_3 n_4 \mathbf{q} l''} V^{n' n_2 n_3 n_4}_{k k-q_y}(\mathbf{q}) p^{ll''}_{nn_3;k} p^{l''l'}_{n_2 n_4;k-q_y}
$$

$$
+ \; \frac{1}{2} \sum_{n_1 n_2 n_4 \mathbf{q} l''} V^{n_1 n_2 n n_4}_{k k-q_y}(\mathbf{q}) p^{l''l'}_{n_1 n';k} p^{ll''}_{n_2 n_4;k-q_y}. \tag{3.17}
$$

Here, we introduced

$$\mathbf{w}_{ll'} = \frac{F_{ll'}}{m} \mathbf{p}_{ll'}, \tag{3.18}$$

and ε_{ln} is the sum of the band energy $\varepsilon_l(\mathbf{k} = 0)$ and the energy of Landau level n in band l with effective electron mass m_l,

$$\varepsilon_{ln} = \varepsilon_l + \frac{|e|B}{cm_l}(n + \frac{1}{2}). \tag{3.19}$$

3.3.1 The equations in the case of no intraband processes

The above equations can be greatly simplified with, when

1. intraband scattering processes are neglected: such processes are due to terms in Eq.(3.17) $\sim \mathbf{v}_n$. These terms correspond to scattering from one Landau level n to $n \pm 1$ within the same band. The r.h.s. of Eq.(3.17) suggests that such terms can be neglected if $|\mathbf{v}_n| \ll |\mathbf{w}|$. A rough estimate leads to $|\mathbf{v}_n|/|\mathbf{w}| \approx 0.01\sqrt{nB[Tesla]}$ for typical bandgaps of 1 eV. However, this ratio becomes larger if not the bare but the band masses of the electron in GaAs are used; thus intraband processes in principle are important.

2. only s–wave scattering is considered in the Coulomb terms in Eq.(3.17), which means that the momentum change q_y in y–direction is neglected. In this case one finds that the Hartree–Fock terms coincide with the HF terms from an analogous calculation for the magneto–electron–hole plasma in the angular momentum base, where only s–wave scattering as the most relevant contribution for optical processes is considered [51].

The quantities p, Eq.(3.14), now effectively become independent of the momentum k,

$$p^{ll'}_{nn'kk'}(t) =: \delta_{kk'}\delta_{nn'}p^{ll'}_n(t). \tag{3.20}$$

3.3.2 Two–band semiconductor

We furthermore specify to the case of only one conductance band c and one valence band v in the semiconductor and neglect the contributions from all other bands. We introduce the *energy difference*

$$\Delta_n := \varepsilon_{cn} - \varepsilon_{vn} \tag{3.21}$$

and the *inversion*

$$z_n(t) := p^{cc}_n - p^{vv}_n(t) \tag{3.22}$$

and find

$$i\frac{\partial}{\partial t}z_n = -2e\mathbf{A}^e(t)[\mathbf{w}_{cv}p_n^{cv} - \mathbf{w}_{vc}p_n^{vc}] + 2\sum_{n'}\gamma_{nn'}[p_{n'}^{cv}p_n^{vc} - p_{n'}^{vc}p_n^{cv}]$$

$$i\frac{\partial}{\partial t}p_n^{cv} = -\Delta_n p_n^{cv} - e\mathbf{A}^e(t)\mathbf{w}_{vc}z_n + \sum_{n'}\gamma_{nn'}[p_n^{cv}z_{n'} - p_{n'}^{cv}z_n], \qquad (3.23)$$

where

$$\gamma_{nn'} = \frac{1}{L^2}\sum_{\mathbf{q}}\tilde{U}(\mathbf{q})|M_{q_y 0}^{nn'}(q_x)|^2. \qquad (3.24)$$

3.3.3 Polarization

Neglecting intraband terms, the polarization at point $\mathbf{x}$ is given by

$$\mathbf{P}(\mathbf{x}) = \sum_{ll'\alpha}\phi_{l\alpha}^*(\mathbf{x})\phi_{l'\alpha}(\mathbf{x})\mathbf{d}_{ll'}c_{l\alpha}^\dagger c_{l'\alpha}, \quad \alpha = (n, k)$$

$$\mathbf{d}_{ll'} = \frac{1}{\nu_0}\int_{\nu_0}d^3\mathbf{x}\,u_l^*(\mathbf{x})\mathbf{x}u_{l'}(\mathbf{x}). \qquad (3.25)$$

The macroscopic Maxwell equations for the electric field are

$$\nabla\times\nabla\times\mathcal{E}(\mathbf{r}, t) + \frac{\partial^2}{\partial t^2}\mathcal{E}(\mathbf{r}, t) = -4\pi\frac{\partial^2}{\partial t^2}\mathbf{P}(\mathbf{r}, t) \qquad (3.26)$$

Here, we already have neglected current densities, charge densities and a term $\sim\nabla\mathbf{P}$, since we are interested in the spatially homogeneous case. We define an averaged polarization $\mathbf{P}(t)$,

$$\mathbf{P}(t) = \frac{1}{V}\int d^3\mathbf{x}\langle\mathbf{P}(\mathbf{x})\rangle_t, \qquad (3.27)$$

where

$$V = L^2 L_z \qquad (3.28)$$

is the optical active volume of the system. Here, L_z is an estimate for the thickness of the quantum well. At the same time, the electric field is assumed to be polarized in the x–y plane and to be extended homogeneously over the volume V. We note that this is only an approximate description neglecting,

e.g., boundary conditions for the fields. Performing the k–sum in Eq.(3.25), one has

$$\mathbf{P}(t) = \mathbf{d}_{cv} \sum_n \beta_n [p_n^{cv}(t) + p_n^{vc}(t)], \tag{3.29}$$

where we used $\mathbf{d}_{cv} = \mathbf{d}_{vc}$ and set the form factor F_{cv}, Eq.(3.10, to unity. Here, $\Phi = BL^2$ is the magnetic flux, $\Phi_0 = hc/e$ the flux quantum, and

$$\beta_n := \begin{cases} \frac{\Phi}{\Phi_0 V}, & n = 0, ..., n_{\max} - 1 \geq 0 \\ \left(\frac{N_e}{V} - \frac{\Phi}{\Phi_0 V} n_{\max} \right), & n = n_{\max} \geq 1 \\ \frac{N_e}{V}, & n = n_{\max} = 0, \end{cases} \tag{3.30}$$

The last condition in Eq.(3.30) comes from the fact that the number of possible radiating electron–hole pairs for filling factor $\nu \leq 1$ is given by the number of electrons in the lowest Landau level. The filling factor at flux Φ and electron number N_e is defined as

$$\nu = N_e \frac{\Phi_0}{\Phi}. \tag{3.31}$$

3.3.4   Maxwell–Bloch equations

The derivation of the combined Maxwell–semiconductor Bloch equations is done in analogy to the case of atomic systems [73]. One introduces

$$\begin{aligned} \mathcal{E}(\mathbf{r}, t) &= \Re \left[\mathbf{E}(\mathbf{r}, t) e^{-i(\omega t - kx)} \right] \\ R_n(t) &= 2 p_n^{vc}(t) e^{i\omega t}, \end{aligned} \tag{3.32}$$

where the frequency $\omega = \Delta_{n=0}$ is in resonance with the transition frequency between the lowest Landau levels in the valence and conduction band. One starts from a one–dimensional version of Eq.(3.26). In the rotating wave approximation and neglecting time and space derivatives $|\partial_t \mathbf{E}| \ll \omega |\mathbf{E}|$, $|\partial_x \mathbf{E}| \ll (\omega/c)|\mathbf{E}|$ (c speed of light), $|\partial_t \mathbf{R}| \ll \omega |\mathbf{R}|$, $|\partial_x \mathbf{R}| \ll (\omega/c)|\mathbf{R}|$, one obtains

$$\begin{aligned} (\partial_x + \partial_t) E(x, t) &= i2\pi\omega d \sum_n \beta_n R_n(t) \\ &\quad - \kappa E(x, t), \quad \kappa := c/\varepsilon_r l_e. \end{aligned} \tag{3.33}$$

Here, κ is a phenomenological escape rate for photons that simulates the decay of the electromagnetic field modes [73] due to escape of photons on a length scale l_e. This term is not necessary to find superradiant solutions of the MBE, if either

1. the full x–dependence of all quantities is kept. Then, one finds so–called automodelling solutions as a function of a dimensionless variable that contains both time and space coordinate, or

2. the x–dependence is neglected and one finds (without the damping term $\sim \kappa$) a flow of energy oscillating between the field and the electronic system. Here, we chose the third possibility and introduce the damping term, at the cost of having one additional phenomenological parameter. As a gain, this allows to eliminate the electric field from the equations if $|\partial_t E(t)| \ll \kappa E(t)$. A second term is introduced in the equation for the inversion of Landau level n, z_n, in order to simulate the pumping of electrons and holes into the optical active region. This term has been derived microscopically in chapter 2, cp. Eq.(2.31) for $\dot{M}$ there. In the classical limit of the superradiance equations, it leads to a term $\partial_t z_n \sim T_n$, i.e. a population increase at a rate T_n. The final form of the equations then becomes

$$
\frac{\partial}{\partial t} z_n = -\Re\mathrm{e}\left[R_n^* \sum_{n'} \Gamma_{n'} R_{n'} \right] - \Im\mathrm{m}\left[\sum_{n'} \gamma_{nn'} R_{n'} R_n^* \right] + T_n \quad (3.34)
$$

$$
\frac{\partial}{\partial t} R_n = -i\overline{\omega}_n R_n z_n \sum_{n'} \Gamma_{n'} R_{n'} + \sum_{n'} \frac{\gamma_{nn'}}{2i} \left[R_{n'} z_n - R_n z_{n'} \right].
$$

Here, we introduced the definitions

$$
\overline{\omega}_n = n\frac{eB}{cm_r}, \quad \frac{1}{m_r} = \frac{1}{m_c} + \frac{1}{|m_v|}
$$

$$
\Gamma_n := \frac{\Omega_n^2}{\kappa}, \quad \Omega_n = \left(2\pi\Delta d^2\beta_n\right)^{1/2}. \quad (3.35)
$$

3.4 Discussion

For the following discussion and the numerical evaluation of Eq.(3.34), we have assumed integer filling factors

$$
\nu = n_{\max} + 1 \quad (3.36)
$$

for simplicity. In this case, $N_e = (n_{\max} + 1)\Phi/\Phi_0$ and $\beta_n = \Phi/\Phi_0 V$ for all n independent of n. In particular, the *Rabi frequency*

$$\Omega_\Delta := \left(2\pi\Delta d^2 \frac{\Phi}{\Phi_0 V}\right)^{1/2} \tag{3.37}$$

becomes independent of n then.

3.4.1 Transitions between the lowest Landau levels

We first discuss the case where only the lowest Landau level $n = 0$ is involved. Then, Eq. (3.34) simplify to two coupled equations for $Z = z_{n=0}$ and $R = R_{n=0}$, where R can be chosen real. There is a constant of motion

$$J^2 := R^2(t) + Z^2(t) \tag{3.38}$$

in the case without pumping $T = T_{n=0} = 0$. For non–vanishing T, one has

$$\begin{aligned} \dot{Z} &= -\frac{\Omega_\Delta^2}{\kappa}\left(J^2 - Z^2\right) + T \\ \dot{J} &= TZ/J. \end{aligned} \tag{3.39}$$

These equation have been derived and discussed previously in the context of pumped superradiance [168]. In the case $T = 0$, they describe Dicke superradiance, i.e. a strong peak in the emission

$$|E(t)|^2 = \left(\frac{\Omega_\Delta R(t)}{d\kappa}\right)^2, \tag{3.40}$$

where the emission peak is reached for $Z(t) = 0$ with the emission maximum $\sim (\Omega_\Delta^2/d\kappa)^2$. Thus, the maximal emission is proportional to the square of the number of flux quanta per optical active volume. In fact, the frequency Ω_Δ is identical with the generalized Rabi frequency for the case of one–dimensional atomic superradiance, if the density of atoms is identified with $\Phi/(\Phi_0 L^2 L_z)$, and the band gap energy Δ with the energy difference between the higher and the lower energy level of the atom [73].

  For $T = 0$, Eq. (3.39) is the equation of an unharmonic, overdamped pendulum that falls down from an initially inverted position ($Z(0) > 0$, $R(0) \neq 0$) with J being the total length of the pendulum and Z its projection to a quantization axis [52, 73]. For $T > 0$, this pendulum starts to

Parameter	Symbol	Value
electron mass	m_c	$0.07 m_0$
electron mass	$|m_v|$	$0.7 m_0$
dielectric constant	ε_r	13.4
band gap	Δ	$1.4 eV$
dipole moment/e	d/e	$1.7 \cdot 10^{-10} m$
escape rate	κ	$2.2 \cdot 10^{13} s^{-1} (l_e [\mu m])^{-1}$
escape length	$l_e = c/\varepsilon_r \kappa$	10-100 μm
Rabi frequency	Ω_Δ	$2.2 \cdot 10^{12} s^{-1} B[T]^{1/2}$
well thickness	L_z	$10^{-8} m$
Larmor frequency	$\hbar \overline{\omega}_n$	$n \times 1.7 meV B[T]$
Coulomb energy	$E_c = e^2/(\sqrt{2}\varepsilon_r l_B)$	$2.9 meV B[T]^{1/2}$

Tab. 3.1: Parameters for numerical calculation.

oscillate because it is periodically driven upwards again, the period of these oscillations given by Eq.(3.1). If damping of the electric field is not considered, $\kappa = 0$, the time–scale of the superradiant process is given by Ω_Δ. In this case, even without pumping ($T = 0$) there are oscillations of the energy between the field and the electronic system with frequency $\sim \Omega_\Delta$, see the discussion in section 2.6.3. In the overdamped limit $|\partial_t E(t)| \ll \kappa E(t)$ that we consider here, these oscillation do not appear because all photons that have been emitted once escape within a time $\sim 1/\kappa$, which now sets the relevant time scale.

The Coulomb interaction terms drop out in the case of only the lowest Landau level occupied: Hartee– and Fock–term cancel exactly. This cancellation is, however, only due to our s–wave approximation. Without this approximation, Hartree–Fock yields the magneto–exciton eigenstates in the equilibrium case [51]; our approximation therefore cannot fully describe magneto–exciton effects, but only the frequency renormalization and carrier redistribution effects in an interacting 'electron–hole plasma' [51]. Neither did we include the effect of incoherent Coulomb scattering terms, i.e. the incoherent collision terms in the carrier Boltzmann equation. This is a serious limitation of the present model because it does not allow the inclusion of dephasing effects in the magnetoplasma [169]. The following predictions therefore have to be understood as addressing to a completely coherent dynamics with time–scales such that dephasing is of minor importance.
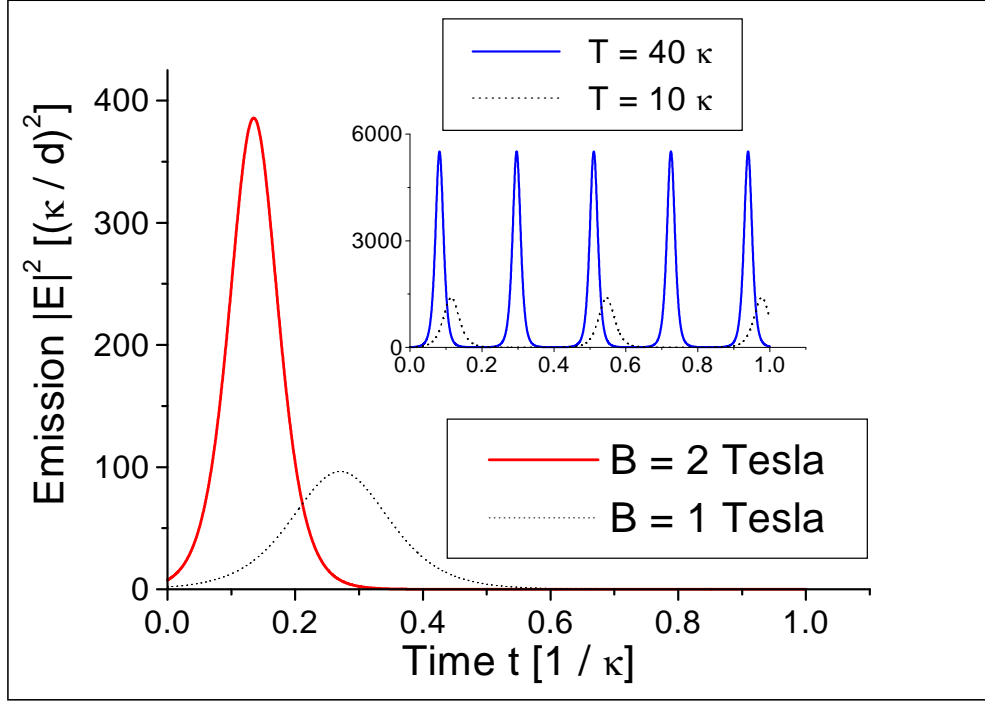
Fig. 3.2: Time evolution (time in units $1/\kappa$, horizontal axis) of the emission intensity $|E(T)|^2$ (units $(\kappa/d)^2$, vertical axis) for lowest Landau level, $l_e = 100\mu m$, and magnetic field 1 and 2 Tesla. Inset: same with pumping $T = 10\kappa$, $T = 40\kappa$ at 2 Tesla.

3.4.2   Time scales

For the numerical evaluation of Eq.(3.34), we estimate the parameters for a GaAs/AlGaAs heterostructure. The dipole moment is approximated as $d/e \approx \sqrt{\hbar^2/2\Delta m}$, the quantum well form factor is set $F_{cv} = 1$.

Results for the lowest Landau level are shown in Fig.(3.2). The system starts from an initially completely inverted state $Z(t = 0)$ with a finite polarization $\Re R(t = 0) = \Im R(t = 0) = 0.1$. The time evolution of the emitted light is in the form of a peak with a maximum $\sim B^2$. This is the so-called Dicke peak: the radiation is due to transitions of electrons in the conduction band to empty states in the valence band. The strong magnetic field quenches the kinetic energy so that all radiators have the same energy difference $\omega = \Delta_{n=0}$. They decay not individually, but in a collective way coupled by the common radiation field. If electrons are pumped into the
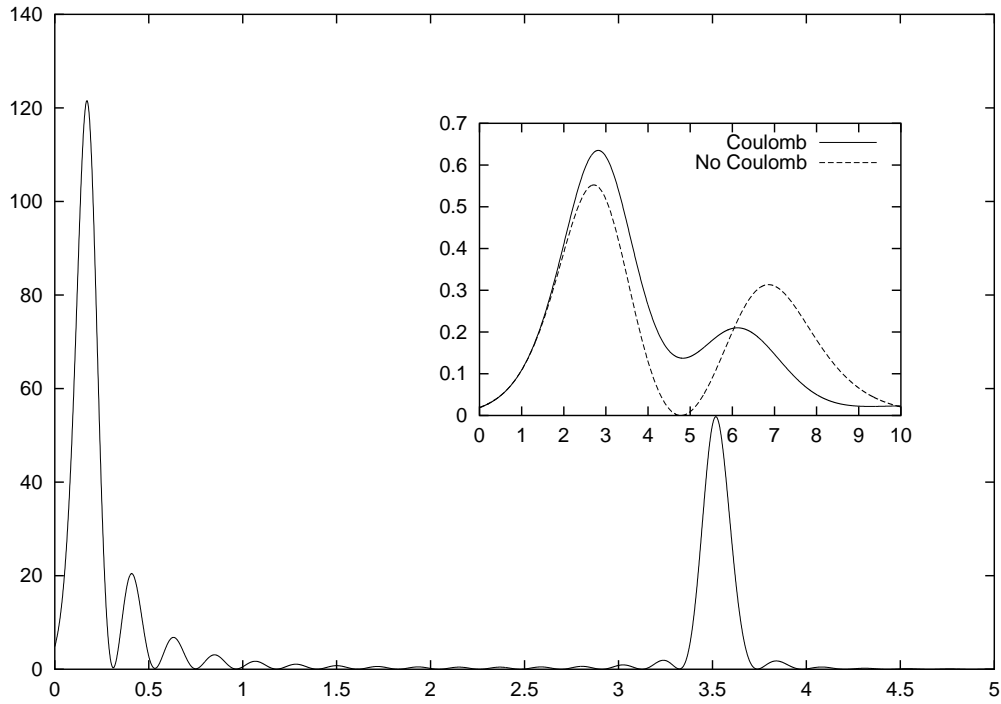
Fig. 3.3: Time evolution of the emission intensity. Number of highest Landau level $n = 15$, no pumping, $l_e = 100\mu m$, $B = 1$ Tesla, and initial inversion $z_n(0) = 0.1$. Inset: two lowest Landau levels $n = 0, 1$ with $B = 5$ Tesla with and without Coulomb interaction at $l_e = 10\mu m$. Scales as in Fig. (3.2).

conduction band and holes into the valence band, the emission begins to oscillate because after each collective decay the system is 'reloaded' again. Note that for the parameters used here, typical time scales are very short $\lesssim 1ps$.

3.4.3 Higher Landau levels

For higher Landau levels, the Coulomb terms do not cancel any longer. In addition, coherent oscillations appear. These oscillations are not due to pumping ($T_n = 0$ in each case), but due to the appearance of the new energy scale, the Larmor frequency $\overline{\omega}_n$. The Dicke peak repeats itself after a number of n_{max} oscillations at a lower intensity. The Coulomb interactions (see inset Fig. (3.3)) smear out these oscillations, but also lead to a small shift of the
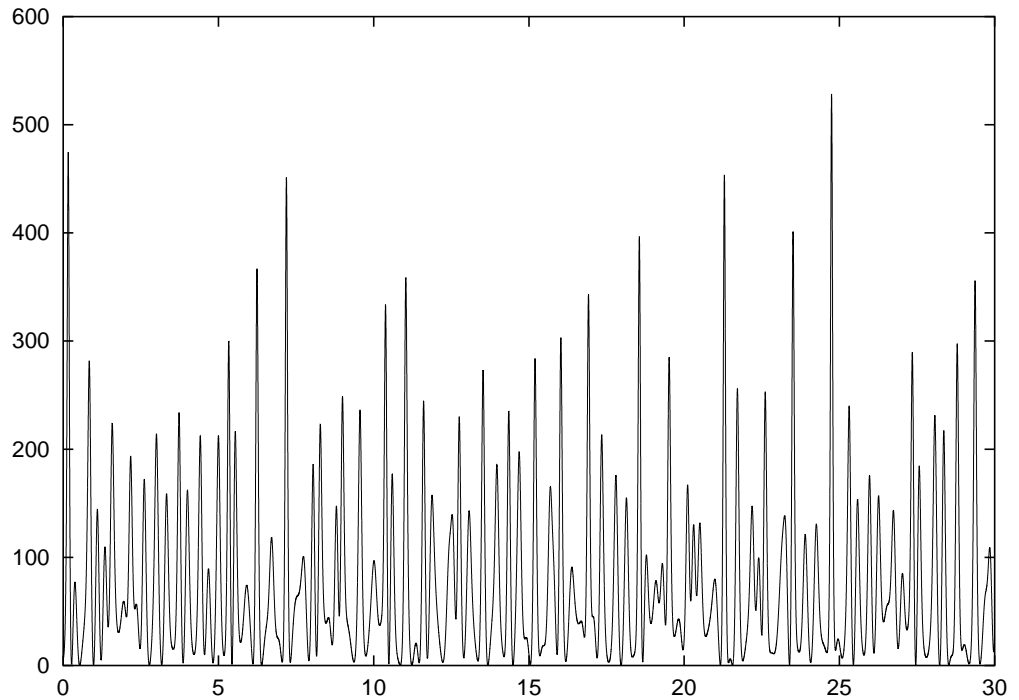
Fig. 3.4: Time evolution of the total emission intensity $|E(T)|^2$. Number of highest Landau level $n = 15$, pumping $T = 0.5\kappa$, $l_e = 100\mu m$, $B = 1$ Tesla. Scales as in Fig. (3.2).

peak height and position.

The situation changes drastically, if one turns from vanishing pumping to a non-vanishing pump rate $T = T_n$ at higher Landau levels. The numerical solution Fig.(3.4) indeed implies that even for moderate pumping $T = 0.5\kappa$, the behavior of the total emitted intensity $|E(t)|^2$ becomes completely irregular. This fact is underlined by the behavior of the polarization $R_0(t)$ as a function of time in the lowest Landau level, Fig.(3.5).

3.4.4 Conclusion

It seems plausible that the nonlinear coupled equations (3.34) can have chaotic solutions. Our numerical results imply that the pumping rate T in this case has the function of a control parameter. Further investigations are required for the detailed understanding of the crossover to the chaotic
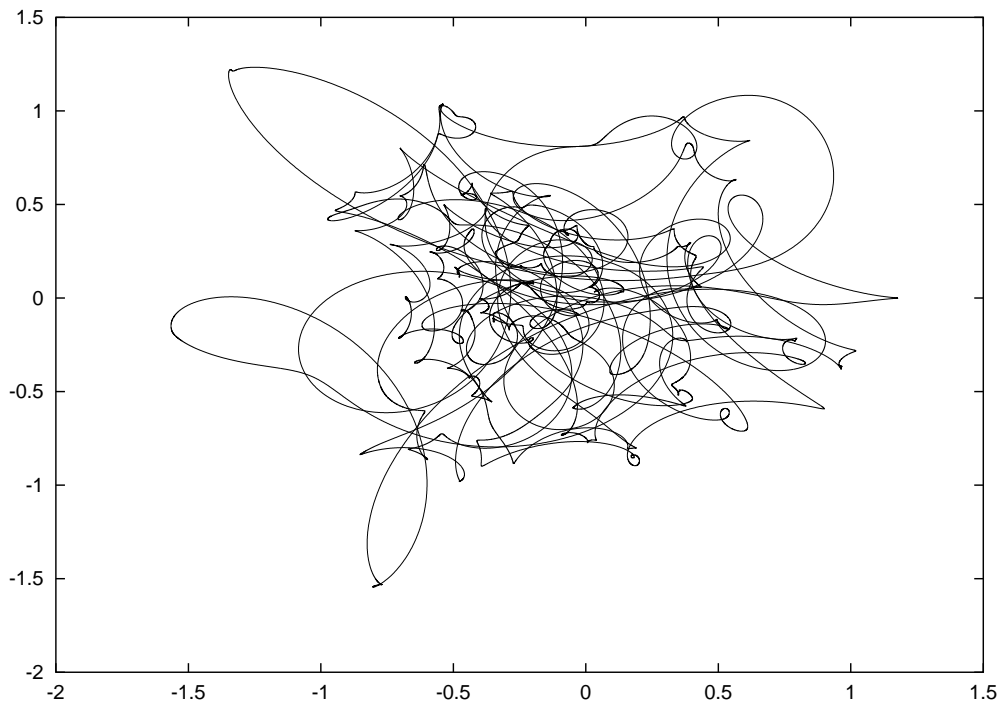
Fig. 3.5: Real (x-axis) and imaginary part (y-axis) of the polarization $R_{n=0}(t) \times \Omega_\Delta/\kappa$. Parameters as in Fig. (3.4)

regime.

Furthermore, the microscopic derivation above shows that Dicke super-radiance is possible at least in the quantum limit of only the lowest Landau levels occupied (strong magnetic fields). Still, we have not included the full magneto-exciton effect into our calculation, but rather considered a magneto plasma, where excitonic and dephasing effects are assumed to be less important. At least in this case, the complete analogy with conventional superradiance in atomic systems could be proven. It will remain an interesting task to investigate the interaction effects beyond the s-wave approximation. This would provide a system where interaction effects in combination with a chaotic dynamic can be studied from a microscopic model.

4. SUPERRADIANCE IN COUPLED DOTS

Abstract

The model of superradiance in open systems is applied to arrays of double quantum dots. For geometries that allow a collective interaction of the double dots with phonons, oscillations in the tunnel current are predicted in agreement with the general scheme developed in chapter 2.

4.1   Introduction

In this chapter, we return back to coupled quantum dots as discussed in chapter (1). Our aim is to investigate coherence in the transport and radiation properties of an *array* of N double quantum dots. The bosonic field through which the double dots are coupled is assumed to be due to phonons since this is the situation which is the closest to the experiments like the ones by Fujisawa et al. [30] on lateral dots.

The individual double dots are labeled by an index i and coupled to electron reservoirs left L and R by tunnel barriers. The i–th dot is described in just the same way as we did in chapter (1), where we discussed the emission of phonons from an individual double dot. In the following, we use the spin–boson form of the dot–phonon Hamiltonian Eq.(A.11). Generalizing to the case of N dots, this Hamiltonian becomes

$$
\begin{aligned}
H_{dp} \quad := \quad & \sum_{i=1}^{N} \{\varepsilon^i J_z^i + 2T_c^i J_x^i\} + \sum_{\mathbf{Q},i=1}^{N} J_z^i \left(\alpha_{\mathbf{Q}}^i - \beta_{\mathbf{Q}}^i\right) \left(a_{-\mathbf{Q}} + a_{\mathbf{Q}}^\dagger\right) \\
& + \sum_{\mathbf{Q}} \omega_{\mathbf{Q}} a_{\mathbf{Q}}^\dagger a_{\mathbf{Q}}.
\end{aligned}
\tag{4.1}
$$

The energy difference ε^i and the tunnel matrix elements T^i now depend

on the individual dot i, as does the coupling matrix elements $\alpha_{\mathbf{Q}}^{i}$ and $\beta_{\mathbf{Q}}^{i}$. Recalling the electron–phonon interaction potential,

$$V_{ep}(\mathbf{x}) = \sum_{\mathbf{Q}} \lambda_{\mathbf{Q}} e^{i\mathbf{Q}\mathbf{x}} \left(a_{-\mathbf{Q}} + a_{-\mathbf{Q}}^{\dagger} \right), \quad \lambda_{\mathbf{Q}} = \lambda_{-\mathbf{Q}}^{*}, \tag{4.2}$$

the coupling matrix elements become

$$\begin{aligned} \alpha_{\mathbf{Q}}^{i} &= \lambda_{\mathbf{Q}} e^{i\mathbf{Q}\mathbf{r}_{L}^{i}} \\ \beta_{\mathbf{Q}}^{i} &= \lambda_{\mathbf{Q}} e^{i\mathbf{Q}\mathbf{r}_{R}^{i}}, \end{aligned} \tag{4.3}$$

where we already neglected the formfactors P and F, cp. Eq. (1.78) and the discussion following there.

Can a system as described by Eq.(4.1) exhibit superradiant properties? As we have learned above, superradiance is closely related to a collective time-evolution of the whole system. Collective operators can be introduced in the superradiant limit

$$\begin{aligned} \varepsilon^{i} &= \varepsilon, \quad T_{c}^{i} = T_{c} \\ \alpha_{\mathbf{Q}}^{i} = \alpha_{\mathbf{Q}}, &\quad \beta_{\mathbf{Q}}^{i} = \beta_{\mathbf{Q}}, \end{aligned} \tag{4.4}$$

i.e. if the matrix elements do not depend on the index i labeling the individual double dot.

If the double dot array is fabricated within a semiconductor structure, the restriction of identical energies ε and tunnel matrix element T_{c} can, at least in principle, be reached by a careful adjustment of gate-voltages. The condition of identical coupling constants $\alpha_{\mathbf{Q}}^{i}$ and $\beta_{\mathbf{Q}}^{i}$, however, at first glance seems to be difficult to realize. That is, these constants depend on the positions of the individual dots, $\mathbf{r}_{L}^{i}$ and $\mathbf{r}_{R}^{i}$ and therefore on the index i. On the other hand, the limit of *small sample superradiance* we discuss here is defined as the case where this dependence can be neglected [52, 73, 131], with the argument that the phase factors $e^{i\mathbf{q}\mathbf{r}_{L/R}^{i}}$ play no role as long as a typical wavelength of the emitted radiation is much larger than the maximal distance $\mathbf{r}_{L}^{i} - \mathbf{r}_{L}^{i'}$ ($\mathbf{r}_{R}^{i} - \mathbf{r}_{R}^{i'}$) between pairs of left (right) dots i and i'. It seems to be difficult to fulfill this condition together with the requirement $\mathbf{Q}(\mathbf{r}_{L}^{i} - \mathbf{r}_{R}^{i}) \gg 0$, which comes from the fact that only wavelengths which give a finite phase difference $|1 - e^{i\mathbf{Q}(\mathbf{r}_{L}^{i} - \mathbf{r}_{R}^{i})}|$ between the left and the right dots contribute to the spontaneous emission from the individual double dots i.
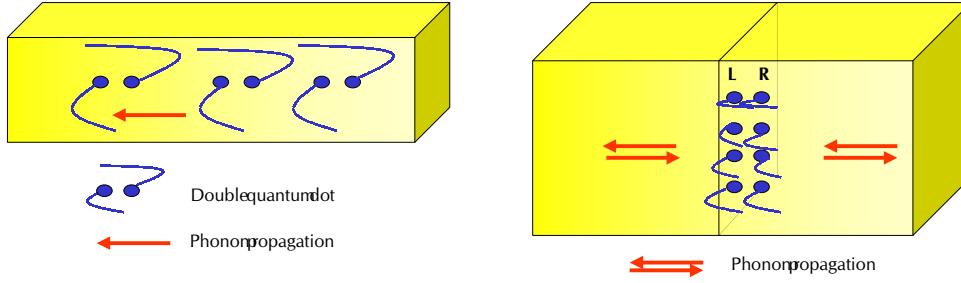
Fig. 4.1: Scheme for quasi one–dimensional superradiance in a slab (phonon–cavity) with several double quantum dots. The left case is a geometry suitable for one–mode superradiance with only one phonon wave vector $\mathbf{Q}$ supported by the structure. In this case, the double dots do not need to be on top of each other as in the right geometry.

Fortunately, in the superradiance literature a number of investigations exists for superradiance in pencil–shaped active volumes, i.e. quasi–one dimensional geometries that favor a certain direction of the bosonic modes $\mathbf{Q}$ [73, 137, 138]. In fact, we suggest a geometry where all double quantum dots are centered symmetrically around a plane $(y\text{–}z)$ that is perpendicular to a direction of phonon propagation in a phonon cavity, cp. section 1.9.2. If the phonon wave vector direction is along the x–axis, the phase factors become (we neglect the formfactors F and P in Eq.(4.3))

$$\alpha_{\mathbf{Q}}^i \propto e^{iq_x x_L^i} = e^{iq_x x_L}, \quad \beta_{\mathbf{Q}}^i \propto e^{iq_x x_R^i} = e^{iq_x x_R}, \tag{4.5}$$

where $x_{R/L} = x_{R/L}^i$ is the x–coordinate of the right/left dots, such that the matrix elements in fact become independent of i. This situation could be realized experimentally in phonon cavities that strongly favor one certain direction of phonon propagation, cp. the right configuration in Fig. (4.1). A second possibility could be a geometry where only one phonon wave vector $\mathbf{Q}$ is allowed. This corresponds to the one–mode case of superradiance where there is no longer a sum over the different phonon modes. This could be interesting for experiments where the phonon waves are generated externally (e.g. by a transducer generating surface acoustic waves) in the form of a pulse running through the slab.

In the following, we only consider the first case (right configuration in Fig. (4.1), for which the corresponding geometry might be difficult to fabricate,

but which is close to the 'pure' Dicke superradiance case. The Hamiltonian becomes (cp. Eq.(4.5))

$$
\begin{aligned}
H_{dp} \; &:= \; \varepsilon J_z + T_c(J_+ + J_-) \\
&+ \; \sum_{\mathbf{Q}} J_z\,(\alpha_{\mathbf{Q}} - \beta_{\mathbf{Q}})\left(a_{-\mathbf{Q}} + a_{\mathbf{Q}}^\dagger\right) + \sum_{\mathbf{Q}} \omega_{\mathbf{Q}} a_{\mathbf{Q}}^\dagger a_{\mathbf{Q}} \\
J_z \; &:= \; \sum_{i=1}^{N} J_z^i, \quad J_\pm := \sum_{i=1}^{N} J_\pm^i
\end{aligned}
\tag{4.6}
$$

Here, we introduced the collective operators J_z and $J_\pm$, which form the angular momentum algebra with the Dicke eigenstates, Eq. (2.11).

4.2   Canonical transformation, equations of motion

We have seen above how to describe the time evolution of a superradiating system in terms of a master equation that could be derived from the equation of motion of the density matrix (statistical operator). Here, we will follow the steps that we used in the derivation of the equations of motion for the double dot in part 1. In particular, the use of the polaron–transformation technique allows one to go beyond a simple perturbation expansion in terms of the coupling to the bosonic field.

We introduce the unitary transformation for operators O,

$$
\begin{aligned}
\bar{O} \; &:= \; e^{\sigma J_z} O e^{-\sigma J_z} \\
\sigma \; &:= \; \sum_{\mathbf{Q}} \left(\frac{\alpha_{\mathbf{Q}} - \beta_{\mathbf{Q}}}{\omega_{\mathbf{Q}}}\right)\left(a_{-\mathbf{Q}} + a_{\mathbf{Q}}^\dagger\right)
\end{aligned}
\tag{4.7}
$$

and use the commutation relations

$$
[J_+, J_-] = 2J_z, \quad [J_z, J_\pm] = \pm J_\pm
\tag{4.8}
$$

to obtain

$$
\bar{J}_z \; = \; J_z, \quad \bar{J}_+ = X J_+, \quad \bar{J}_- = X^\dagger J_-, \quad X := e^\sigma,
\tag{4.9}
$$

whence the Hamiltonian H_{dp} is transformed into

$$
\begin{aligned}
\bar{H}_{dp} \; &:= \; H_1 + \bar{H}_T, \quad \bar{H}_T := T_c(J_+ X + J_- X^\dagger) \\
H_1 \; &:= \; \varepsilon J_z - \alpha J_z^2 + \sum_{\mathbf{Q}} \omega_{\mathbf{Q}} a_{\mathbf{Q}}^\dagger a_{\mathbf{Q}}, \quad \alpha := \sum_{\mathbf{Q}} \frac{|\alpha_{\mathbf{Q}} - \beta_{\mathbf{Q}}|^2}{\omega_{\mathbf{Q}}}
\end{aligned}
\tag{4.10}
$$

4.3 Equation of motion for a closed system

Let us first discuss the dynamics of the system without coupling to electron reservoirs. We calculate the time-evolution of the current operator that is defined by

$$I := iT_c(J_+ - J_-) = -2T_c J_y \tag{4.11}$$

The density matrix $\tilde{\rho}(t)$ obeys the equation

$$\begin{aligned} \tilde{\rho}(t) &:= e^{iH_1 t} \bar{\rho}(t) e^{-iH_1 t} \\ &= \bar{\rho}_0 - i \int_0^t dt' [\tilde{H}_T(t'), \tilde{\rho}(t')], \end{aligned} \tag{4.12}$$

where we again defined an interaction picture for arbitrary operators O in the unitary transformed frame and the X operators according to

$$\tilde{O}(t') := e^{iH_1 t} \bar{O} e^{-iH_1 t}, \quad X_t := e^{iH_1 t} X e^{-iH_1 t}. \tag{4.13}$$

By this we can write

$$\begin{aligned} \langle I \rangle_t &:= \mathrm{Tr}(\tilde{\rho}(t)\tilde{I}(t)) = \tag{4.14} \\ &= \langle I \rangle_t^0 - i \int_0^t dt' \mathrm{Tr}(\tilde{\rho}(t')[\tilde{I}(t), \tilde{H}_T(t')]). \end{aligned}$$

Here, $\langle I \rangle_t^0$ describes the decay of an initial current I at $t = 0$. This equation, still being exact, is not of great value unless one can find a reasonable approximation to evaluate the trace. Again, we use a decoupling of the density matrix according to

$$\tilde{\rho}(t') \approx \rho_{ph}^0 \mathrm{Tr}_{ph} \tilde{\rho}(t'). \tag{4.15}$$

Still, for the case of more than one double dot $N > 1$, one needs an additional approximation. That is, the time evolution of operators according to Eq.(4.13) in general can not be performed analytically because of the non-linear term $-\alpha J_z^2$ in the Hamiltonian H_1. For the case $N = 1$, we had $J_z = (1/2)\sigma_z$, and because $\sigma_z^2 = 1$ this term is just an additive constant. This is no longer the case for the algebra of (pseudo)–spin operators for $N > 1$.

We note that the existence of the non–linear term $-\alpha J_z^2$ in the canonically transformed Hamiltonian $\bar{H}_{dp}$, Eq.(4.10), is closely related to the occuring of

an equilibrium phase transition for strong coupling to the bosonic field, as discussed by Hepp and Lieb for the one–mode superradiance model [170,171].

In the following, we assume that for small electron–phonon coupling we can omit this term and set $\alpha = 0$. Then,

$$
\begin{aligned}
\tilde{I}(t) &= iT_c(J_+ e^{i\varepsilon t} X_t - J_- e^{-i\varepsilon t} X_t^\dagger) \\
\tilde{H}_T(t') &= T_c(J_+ e^{i\varepsilon t'} X_{t'} + J_- e^{-i\varepsilon t'} X_{t'}^\dagger)
\end{aligned}
\tag{4.16}
$$

Performing the commutator and the phonon trace in Eq.(4.14), one obtains

$$
\begin{aligned}
\langle I \rangle_t &= \tag{4.17} \\
&= T_c^2 \int_0^t dt' e^{i\varepsilon(t-t')} \left\{ \langle J_+ J_- \rangle_{t'} C(t-t') - \langle J_- J_+ \rangle_{t'} C(t'-t) \right\} \\
&- T_c^2 \int_0^t dt' e^{-i\varepsilon(t-t')} \left\{ \langle J_- J_+ \rangle_{t'} C(t-t') - \langle J_+ J_- \rangle_{t'} C(t'-t) \right\} \\
&= T_c^2 2\Re \int_0^t dt' e^{i\varepsilon(t-t')} \left\{ \langle J_+ J_- \rangle_{t'} C(t-t') - \langle J_- J_+ \rangle_{t'} C^*(t-t') \right\},
\end{aligned}
$$

where we set the initial current to zero and we again used Eq. (1.57) for an equilibrium phonon system

$$
\begin{aligned}
\langle X_t X_{t'}^\dagger \rangle_0 &=: C(t-t') \\
C(t-t') &= C^*(t'-t).
\end{aligned}
\tag{4.18}
$$

4.4 Superradiant inelastic current

We perfom a Laplace transformation of Eq.(4.17),

$$
\begin{aligned}
\langle I \rangle_z &= T_c^2 \langle J_+ J_- \rangle_z \left[C_\varepsilon(z) + C_\varepsilon^*(z) \right] - T_c^2 \langle J_- J_+ \rangle_z \left[C_{-\varepsilon}(z) + C_{-\varepsilon}^*(z) \right] \\
C_\varepsilon(z) &:= \int_0^\infty dt e^{-zt} e^{i\varepsilon t} C(t); \quad z > 0.
\end{aligned}
\tag{4.19}
$$

To extract the long-time behaviour of the time-evolution, we replace $C_\varepsilon(z) \rightarrow C_\varepsilon(z=0) =: C_\varepsilon$ in Eq.(4.19), which then can be rewritten with the help of the tunneling probability $P(\varepsilon)$, Eq.(1.98),

$$
\Re C_\varepsilon = \pi P(\varepsilon)
\tag{4.20}
$$

as

$$\langle I \rangle_z \quad \approx \quad 2\pi T_c^2 P(\varepsilon)\langle J_+ J_- \rangle_z - 2\pi T_c^2 P(-\varepsilon)\langle J_- J_+ \rangle_z. \qquad (4.21)$$

We consider the case $\varepsilon > 0$, where at zero temperature $T = 0$ only spontaneous emission is possible, i.e. $P(-\varepsilon) = 0$. Noting that the *current I in the closed system* is related to J_z by

$$\frac{d}{dt} J_z = i[H_{dp}, J_z] = -I, \qquad (4.22)$$

and transforming back eq.(4.21) from $z-$ into $t-$space, we obtain the differential equation

$$-\frac{d}{dt}\langle J_z \rangle(t) = 2\pi T_c^2 P(\varepsilon)\langle J_+ J_- \rangle(t). \qquad (4.23)$$

We can identify the spontaneous emission rate

$$\gamma(\varepsilon) := T_c^2 \Re C_\varepsilon \equiv \pi T_c^2 P(\varepsilon), \qquad (4.24)$$

cp. Eq. (1.107). We use the *quasiclassical approximation* [141] that neglects quantum fluctuations in the operator product $J_+ J_-$ and should work well for large N,

$$\langle J_+ J_- \rangle(t) \quad = \quad [J(t) + J_z(t)]\,[J(t) - J_z(t) + 1]\,, \qquad (4.25)$$

where $J(t) = J = const$ because the system is closed. Eq.(4.23) then becomes

$$-\frac{d}{dt}\langle J_z \rangle(t) \quad = \quad 2\gamma(\varepsilon)\,[J + J_z(t)]\,[J - J_z(t) + 1]\,, \qquad (4.26)$$

which coincides with the superradiance equation of motion, Eq.(2.15). Note that $\langle J_z \rangle(t) \equiv M(t)$ and the identification $2\gamma(\varepsilon) = \Gamma$ has to be made.

4.5 Pumped superradiance for double dot arrays

In the following, we consider a system of N coupled double dots which are connected to electron reservoirs. As in the case of the single double dot, we assume that electrons can tunnel from the left reservoir into the i–th left dot at a rate Γ_L^i, and out of the i–th right dot into the right reservoir at a rate Γ_R^i.

For simplicity, we assume identical rates $\Gamma_L^i = \Gamma_R^i = \Gamma$. The coherent part of the equations of motions for the expectation values of the operators $\langle J_z \rangle$ and $\langle J_\pm \rangle$ is derived as above. The coupling to the electron reservoirs introduces incoherent terms in the equations of motion, which are proportional to Γ: we remember that for the case of $N = 1$ double dot, the corresponding equation Eq.(1.51) for the occupation number difference and identical tunneling rates is

$$\frac{d}{dt} \left(\langle n_L \rangle - \langle n_R \rangle \right) = -iT_c 2 \langle p - p^+ \rangle + 2\Gamma (N - \langle n_L \rangle), \qquad (4.27)$$

where $N = 1$. For $N > 1$, a simple counting argument shows that the electron tunneling changes $\langle J_z \rangle$ by

$$\left. \frac{d}{dt} \right|_{\text{res}} \langle J_z \rangle = \Gamma(N - \langle N_L \rangle) = \Gamma(N/2 - \langle J_z \rangle - \langle N_0 \rangle), \qquad (4.28)$$

where $\langle N_L \rangle$ is the expectation value of the total electron number in all left dots, and $\langle N_0 \rangle$ is the expectation value of the *number of empty double dots.* Furthermore, we introduced the notation $|_{\text{res}}$ to denote the contribution from the interaction with the electron reservoirs to the time derivative. Furthermore, in Eq.(4.28) have excluded the possibility of double occupancy (two electrons per double dot), i.e. we address the strong Coulomb blockade regime where only one additional electron can enter (and leave) the dot. It is understood that this description again assumes weak coupling to the reservoirs, i.e. we are outside the Kondo transport regime where higher order tunneling processes become important, cp. section 1.5.2.

4.5.1 Equations of motion for the open system

For the following evaluation, we make the simplifying assumption that the number of *empty dots* $\langle N_0 \rangle_t$ remains small compared to the total number of double dots during the time evolution of the system, i.e. we assume $\langle N_0 \rangle_t \ll N$ for all times t. Physically this means that the tunneling rate Γ for electrons to tunnel into empty dots should be much larger than the spontaneous emission rate. In this case, the dots are filled up at a fast rate due to electrons tunneling in, but the out–tunneling is slow due to a slow inelastic rate. In order to be consistent, we will check below that this assumption does not contradict the choice of the parameters and the results of our numerical calculation.

In this case, the equations of motion become

$$
\frac{d}{dt}\langle J_z\rangle_t = -iT_c\left[\langle J_+\rangle_t - \langle J_-\rangle_t\right] + \Gamma\left[\frac{N}{2} - \langle J_z\rangle_t\right]
$$

$$
\langle J_+\rangle_t = -\Gamma\int_0^t dt' e^{i\varepsilon(t-t')}\langle J_+\rangle_{t'}
$$

$$
- iT_c\int_0^t dt' e^{i\varepsilon(t-t')}\left\{\langle J_+J_-\rangle_{t'}C(t-t') - \langle J_-J_+\rangle_{t'}C(t'-t)\right\}
$$

$$
\langle J_-\rangle_t = -\Gamma\int_0^t dt' e^{-i\varepsilon(t-t')}\langle J_-\rangle_{t'}
$$

$$
+ iT_c\int_0^t dt' e^{-i\varepsilon(t-t')}\left\{\langle J_+J_-\rangle_{t'}C^*(t-t')\ \langle J_-J_+\rangle_{t'}C^*(t'-t)\right\}.
$$

Here, we neglected the terms $\langle J_\pm\rangle_t^0$ corresponding to the decay of initial coherences $\langle J_\pm\rangle$ at time $t=0$.

We use the identity

$$
J^2 = \frac{1}{2}\left[J_+J_- + J_-J_+\right] + J_z^2. \tag{4.29}
$$

to calculate

$$
\left.\frac{d}{dt}\right|_{\text{res}}\langle J_+J_- + J_-J_+\rangle_t = \langle \dot{J}_+J_- + J_+\dot{J}_- + \dot{J}_-J_+ + J_-\dot{J}_+\rangle_t
$$

$$
= -4\Gamma\langle J^2 - J_z^2\rangle_t
$$

$$
\left.\frac{d}{dt}\right|_{\text{res}}\langle J_z^2\rangle_t = 2\Gamma\left\langle J_z\left[\frac{N}{2} - J_z\right]\right\rangle_t, \tag{4.30}
$$

and one obtains

$$
\frac{d}{dt}\langle J^2\rangle_t = \left.\frac{d}{dt}\right|_{\text{res}}\langle J^2\rangle_t = \Gamma\left[NJ_z - 2J^2\right]. \tag{4.31}
$$

To find an (approximate) solution of these equations, we first Laplace transform them into z–space according to

$$
\langle J_+\rangle_z = \int_0^\infty dt e^{-zt}\langle J_+\rangle_t \quad \text{etc}, \tag{4.32}
$$
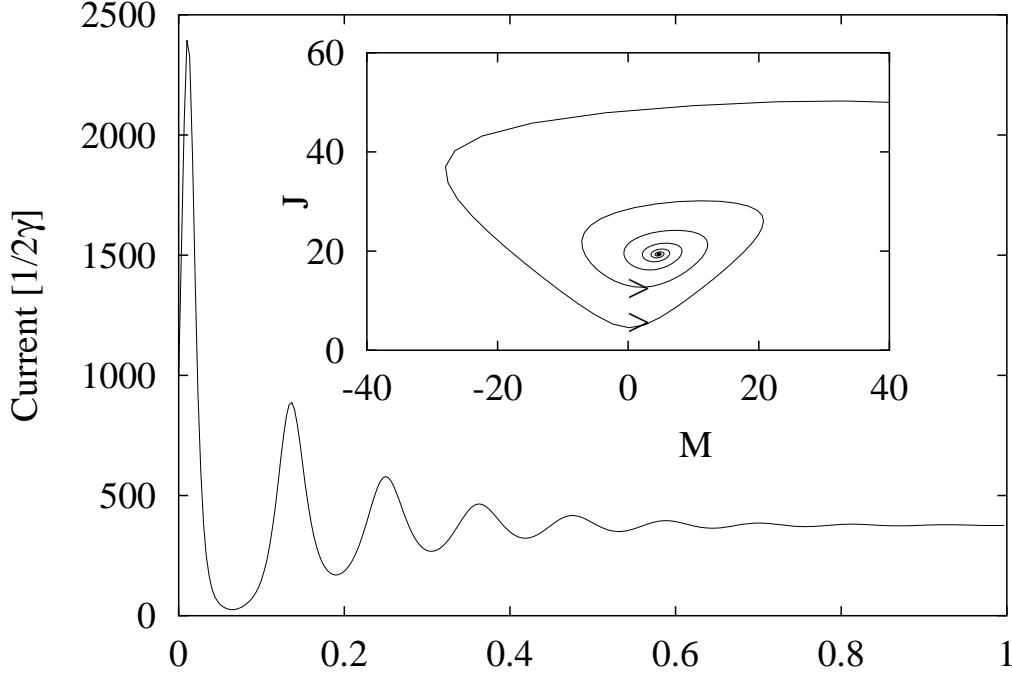
Fig. 4.2: Solution of Eq. (4.36) superradiance of phonons from a system of double quantum dots. Number of double dots $N = 160$. Inset: 'phase–space' plot.

obtaining

$$
\begin{aligned}
\langle J_+ \rangle_z &= \frac{-iT_c}{1 + \frac{\Gamma}{z-i\varepsilon}} \left\{ \langle J_+ J_- \rangle_z C_\varepsilon(z) - \langle J_- J_+ \rangle_z C^*_{-\varepsilon}(z) \right\} \\
z\langle J_z \rangle_z &= -iT_c \left[\langle J_+ \rangle_z - \langle J_- \rangle_z \right] + \Gamma \left[\frac{N}{2} - \langle J_z \rangle_z \right] \\
&= -2T_c^2 \left\{ \langle J_+ J_- \rangle_z \Re e \left(\frac{C_\varepsilon(z)}{1 + \frac{\Gamma}{z-i\varepsilon}} \right) + \langle J_- J_+ \rangle_z \Re e \left(\frac{C^*_{-\varepsilon}(z)}{1 + \frac{\Gamma}{z-i\varepsilon}} \right) \right\} \\
&+ \Gamma \left[\frac{N}{2} - \langle J_z \rangle_z \right].
\end{aligned}
\tag{4.33}
$$

We now assume

$$\left| \frac{\Gamma}{z - i\varepsilon} \right| \ll 1, \tag{4.34}$$

and approximate $C_\varepsilon(z) \to C_\varepsilon(z = 0) \equiv C_\varepsilon$. In particular, we require the energy differences ε between the left and right dots to be much larger than the energy $\hbar\Gamma$. Then, Eq. (4.33) simplifies in the zero–temperature limit, where $\Re C_{-\varepsilon} = 0$:

$$z\langle J_z \rangle_z = -2\gamma(\varepsilon)\langle J_+ J_- \rangle_z + \Gamma\left[\frac{N}{2} - \langle J_z \rangle_z \right], \tag{4.35}$$

where we again introduced the inelastic rate $\gamma(\varepsilon)$ Eq. (4.24).
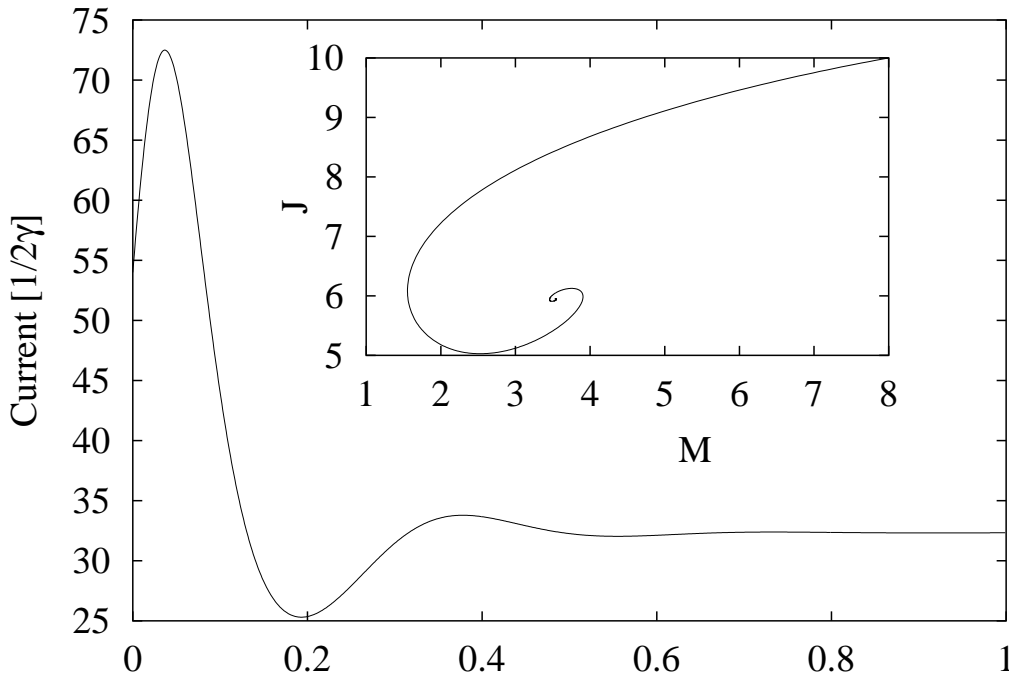
Fig. 4.3: Solution of Eq. (4.36): superradiance of phonons from a system of double quantum dots. Number of double dots $N = 20$.

We transform Eq.(4.35) back into the time-domain and use the *classical approximation* Eq.(4.25). Combining with the equation for $J(t)$, Eq.(4.31),

we end up with a closed system of two equations for J_z and J,

$$
\begin{aligned}
\frac{d}{dt}M &= -2\gamma(\varepsilon)(J+M)(J-M+1) + \Gamma\left(\frac{N}{2} - M\right) \\
\frac{d}{dt}J^2 &= \Gamma\left(NM - 2J^2\right).
\end{aligned}
\tag{4.36}
$$

4.5.2   Discussion

In Figs. (4.2) and (4.3) we show solutions of these equations for a fixed value of the inelastic rate $\gamma(\varepsilon) \equiv \gamma$. The total electric current is the expectation value

$$
\langle I \rangle_t = iT_c\left[\langle J_+ \rangle_t - \langle J_- \rangle_t\right] = -\left(\frac{d}{dt}\langle J_z \rangle_t - \Gamma\left[\frac{N}{2} - \langle J_z \rangle_t\right]\right),
\tag{4.37}
$$

cp. Eqs. (4.11) and (4.29). We observe that the current exhibits the typical features of the oscillatory superradiance as discussed above in chapter 2. Note that the explicit form of the Eqs. (4.36) differs from the ones in our abstract model in chapter 2, i.e. Eqs.(2.18). The reason is our special assumption of no double occupancy and no empty double dots that we made above. Nevertheless, one reckognizes the obvious qualitative agreement with the results for the oscillatory type of superradiance in chapter 2, cp. Fig.(2.6).

We also note that our choice $\Gamma/\gamma = 10$ in the solution Fig. (4.2) is consistent with the requirement that the elastic tunnel rate Γ should be much larger than the rate for spontaneous emission γ, which was required to neglect the contribution from empty double dots in our calculation.

5. SPECTRAL LINESHAPES AND THE DICKE EFFECT

Abstract

Line shapes of absorption spectra of atoms in a gas can become very sharp by velocity changing collisions (Dicke effect). We show that the appearance of this Dicke effect is a general feature due to the pole structure of correlation functions for coupled systems. It therefore can appear in spectral functions for resonant tunneling through two impurity levels (Shahbazyan, Raikh 1994), or in the (Drude) ac conductivity for quantum wires in a strong magnetic field (chapter 6).

5.1 Introduction

The original Dicke effect as predicted by Dicke in 1953 [53] is a phenomenon that occurs in the line shapes of absorption spectra of atoms in a gas. Line shapes for the absorption of light with wave vector $\mathbf{k}$ are subject to Doppler broadening due to frequency shifts $\mathbf{kv}$, where $\mathbf{v}$ is the velocity of an individual atom. Dicke showed that velocity–changing collisions of the radiating atoms with the atoms of a (non–radiating) buffer gas can lead to a substantial *narrowing* of the spectral line shape in the form of a very sharp peak on top of a broad line shape, centered around the transition frequency of the atom.

Spectral lineshapes are determined by poles of correlation functions in the complex frequency plane. The poles are eigenvalues of a collision matrix which, for the simplest case of only two poles, belong to symmetric and antisymmetric eigenmodes. As a function of an external parameter (e.g. the pressure of an atomic gas or the magnetic field applied to wires, see below), these poles can move through the lower frequency half–plane, whereby the spectral lineshape becomes a superposition of a strongly broadened and a strongly sharpened peak. This phenomenon is in analogy with the formation of a bonding and an anti–bonding state by a coherent coupling of two (real)

energy levels (level repulsion), with the difference that the Dicke effect is the splitting of decay rates, i.e. imaginary energies, into a fast (superradiant) and a slow (subradiant) mode. In fact, the case of a splitting into two modes can be considered as a precursor of the phenomenon of superradiance [52], where a symmetric mode of N radiators gives rise to an abnormally large decay on a time scale $1/N$.
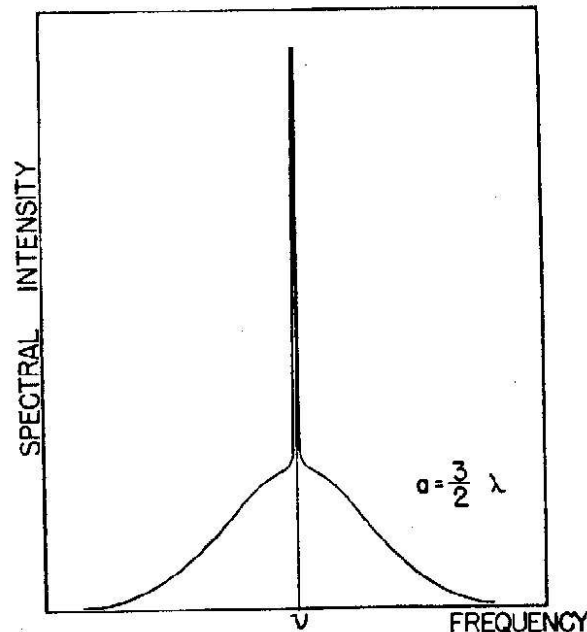
Fig. 5.1: Line narrowing due to collisions of a Doppler–broadened spectral line in the original 1953 Dicke paper [53]. The radiating gas is modeled within a one–dimensional box of width a; λ is the light wavelength.

From an abstract point of view, this effect thus is of quite general origin and can be expected to appear in a number of physical situations. Although the Dicke effect has been known and experimentally verified for a long time in atomic systems [73, 131, 172], only recently predictions were made for it to occur in transport and scattering properties of mesoscopic systems. The Dicke effect was predicted to appear in the conductance for resonant tunneling via two impurities [148], the resonant scattering in a strong magnetic

field [149], and the emission from disordered mesoscopic systems [150]. It was shown to appear in the intensity of emitted light [168] from quantum dot arrays, two–dimensional magnetoplasmas [173], and the inelastic current through double quantum dots [174].

In this and the following chapter, we will extend these analogies and give a direct comparison between the collision–induced narrowing of the polarizability $\chi(\omega)$ of an atomic gas, as was considered in Dicke's 1953 paper, and the ac conductivity $\sigma(\omega)$ of quantum wires in a magnetic field. When only the two lowest subbands of the wire are occupied, the absorptive part of $\sigma(\omega)$ shows (as a function of ω) a crossover from a broad Lorentzian to a very sharp and high peak on top of a broad Lorentzian, when the backscattering becomes more and more suppressed by an increasing magnetic field. This behavior is due to inter–subband scattering by which the transport rates for the two subbands become coupled and split into one fast and one slow mode. The absorptive behavior of this system can be simulated by a classical circuit consisting of two impedances in parallel. The effect should be observable in the frequency dependent microwave absorption properties of wires under magnetic fields.

5.2 Atomic line shapes and collision effects

The Dicke effect (line narrowing due to collisions), its experimental consequences and the conditions under which it can been observed have been reviewed excellently in the past [172]. Here, we will review the theoretical approach in terms of a Boltzmann equation.

5.2.1 Boltzmann equation

A gas of two–level atoms of mass M can be described by a one–particle density matrix, defined as a trace of the statistical operator ρ,

$$\rho_{\sigma\sigma'}(\mathbf{r}_1, \mathbf{r}_2; t) := Tr\left(\rho \Psi_{\sigma'}^+(\mathbf{r}_2 t)\Psi_\sigma(\mathbf{r}_1 t)\right), \tag{5.1}$$

where the field operator $\Psi_\sigma^+(\mathbf{r}_2)$ creates an atom at position $\mathbf{r}_2$ with the upper level ($\sigma = \uparrow$) or the lower level ($\sigma = \downarrow$) occupied. The 'spin'–index σ thus denotes the internal degree of freedom of the atom.

An electric field $\mathbf{E}(\mathbf{x}, t)$ now gives rise to dipole transitions within an atom at position $\mathbf{x}$. If the corresponding matrix element is denoted as $\mathbf{d}$ (for

simplicity we set $\mathbf{d} \equiv \mathbf{d}_{\uparrow\downarrow} \equiv \mathbf{d}_{\downarrow\uparrow}$), and the transition frequency is ω_0, the Hamiltonian of the system in second quantization is

$$
\begin{aligned}
H &= \sum_{\sigma=\pm} \int d^3\mathbf{x} \Psi_\sigma^+(\mathbf{x}) \left[\sigma \frac{\omega_0}{2} - \frac{\Delta}{2M} \right] \Psi_\sigma(\mathbf{x}) \\
&+ \int d^3\mathbf{x}(-\mathbf{d}\mathbf{E}(\mathbf{x},t)) \left[\Psi_\uparrow^+(\mathbf{x})\Psi_\downarrow(\mathbf{x}) + \Psi_\downarrow^+(\mathbf{x})\Psi_\uparrow(\mathbf{x}) \right],
\end{aligned} \quad (5.2)
$$

where Δ is the Laplacian and we have set $\hbar = 1$. The quantum-mechanical distribution function

$$
f(\mathbf{p},\mathbf{r},t) = \frac{1}{(2\pi)^3} \int d^3\mathbf{r}' e^{-i\mathbf{p}\mathbf{r}'} \rho(\mathbf{r},\mathbf{r}';t) \quad (5.3)
$$

with $\mathbf{r} = (\mathbf{r}_1 + \mathbf{r}_2)/2$ and $\mathbf{r}' = \mathbf{r}_1 - \mathbf{r}_2$ is introduced, for which one derives an equation of motion from the Heisenberg equations of the field operators $\Psi_\sigma(\mathbf{x})$, as

$$
\begin{aligned}
\left(\frac{\partial}{\partial t} - i\omega_0 + \mathbf{v_p}\nabla_\mathbf{r} \right) f_{\downarrow\uparrow}(\mathbf{p},\mathbf{r},t) &= i\mathbf{d}\mathbf{E}(\mathbf{r},t) \left[f_{\uparrow\uparrow}(\mathbf{p},\mathbf{r},t) - f_{\downarrow\downarrow}(\mathbf{p},\mathbf{r},t) \right], \\
\left(\frac{\partial}{\partial t} + i\omega_0 + \mathbf{v_p}\nabla_\mathbf{r} \right) f_{\uparrow\downarrow}(\mathbf{p},\mathbf{r},t) &= -i\mathbf{d}\mathbf{E}(\mathbf{r},t) \left[f_{\uparrow\uparrow}(\mathbf{p},\mathbf{r},t) - f_{\downarrow\downarrow}(\mathbf{p},\mathbf{r},t) \right] \\
\mathbf{v_p} &= \mathbf{p}/M,
\end{aligned} \quad (5.4)
$$

and corresponding equations for $f_{\uparrow\uparrow}$ and $f_{\downarrow\downarrow}$. The electric field $\mathbf{E}(\mathbf{x},t)$ has been assumed to vary spatially on a length scale which is much larger than the de-Broglie wave length of the atoms; apart from this Eq.(5.4) is exact.

The Dicke effect has its origin in collisions of the atoms with a buffer gas. These collisions are assumed to change only the momentum $\mathbf{p}$ of the atoms and no their internal degree of freedom σ. Furthermore, the buffer gas is optically inactive. This situation corresponds to elastic scattering of electrons at impurities in electronic systems like metals or semiconductors. In the theoretical description of these scattering events, one introduces a *collision term*

$$
\mathcal{L}[f_{\sigma,\sigma'}](\mathbf{p},\mathbf{r},t) := - \int d\mathbf{p}' W(\mathbf{p},\mathbf{p}') \left[f_{\sigma,\sigma'}(\mathbf{p},\mathbf{r},t) - f_{\sigma,\sigma'}(\mathbf{p}',\mathbf{r},t) \right] \quad (5.5)
$$

on the r.h.s. of the kinetic equation Eq.(5.4). Here, $W(\mathbf{p},\mathbf{p}')$ is the probability for scattering from $\mathbf{p}$ to $\mathbf{p}'$, which can be calculated in second order

perturbation theory (Fermi's Golden rule) from a scattering potential. Furthermore, the spontaneous decay due to spontaneous emission of light from the upper level of the atoms leads to a decay of the polarization at a rate γ. This dissipative process is introduced as an additional collision term for $f_{\uparrow\downarrow}$ and $f_{\downarrow\uparrow}$

$$\mathcal{L}'[f_{\downarrow\uparrow}] = -\gamma f_{\downarrow\uparrow}, \quad \mathcal{L}'[f_{\uparrow\downarrow}] = -\gamma f_{\uparrow\downarrow}. \tag{5.6}$$

The *polarization* of the atom gas

$$\mathbf{P}(\mathbf{r}, t) = \mathbf{d} \int d\mathbf{p} \left[f_{\uparrow\downarrow}(\mathbf{p}, \mathbf{r}, t) + f_{\downarrow\uparrow}(\mathbf{p}, \mathbf{r}, t) \right] \tag{5.7}$$

can be obtained in *linear response* to the electric field: the occupation probabilities of the upper and lower level are assumed to be constant in time and space, $f_{\uparrow\uparrow}(\mathbf{p}, \mathbf{r}, t) - f_{\downarrow\downarrow}(\mathbf{p}, \mathbf{r}, t) = N(\mathbf{p})$. The resulting equation of motion for $f_{\uparrow\downarrow}$ then becomes

$$\left(\frac{\partial}{\partial t} + i\omega_0 + \gamma + \mathbf{v_p}\nabla_{\mathbf{r}} \right) f_{\uparrow\downarrow}(\mathbf{p}, \mathbf{r}, t) \quad = \tag{5.8}$$

$$= -i\mathbf{d}\mathbf{E}(\mathbf{r}, t)N(\mathbf{p}) + \mathcal{L}[f_{\uparrow\downarrow}](\mathbf{p}, \mathbf{r}, t).$$

Eq. (5.8) is a linearized *Boltzmann equation* for the distribution function $f_{\uparrow\downarrow}$.

5.2.2 One–dimensional model

Dicke originally considered the scattering processes in a one–dimensional model: atoms bouncing back and forth within a one–dimensional container [53]. In fact, a one-dimensional version of the Boltzmann equation is very suitable to understand the line narrowing from Eq.(5.8). Due to energy conservation, $W(p, p') \propto \delta(p^2 - p'^2)$, which we can write as

$$W(p, p') = \Gamma(p)[\delta(p - p') + \delta(p + p')], \tag{5.9}$$

where $\Gamma(p) = \Gamma(-p)$ is a scattering rate with dimension 1/time.
In the collision integral, only the backscattering term remains, i.e.

$$\mathcal{L}[f_{\sigma,\sigma'}](p, r, t) := -\int dp' \Gamma(p)\delta(p + p') \left[f_{\sigma,\sigma'}(p, r, t) - f_{\sigma,\sigma'}(-p, r, t) \right]$$

$$= -\Gamma(p) \left[f_{\sigma,\sigma'}(p, r, t) - f_{\sigma,\sigma'}(-p, r, t) \right]. \tag{5.10}$$

The solution of Eq.(5.8) is easily obtained in Fourier-space where $\partial_t \to -i\omega$ and $\partial_r \to ik$;

$$(-i\omega + i\omega_0 + \gamma + \Gamma(p) + iv_p k) \, f_{\uparrow\downarrow}(p, k, \omega)$$
$$- \; \Gamma(p) f_{\uparrow\downarrow}(-p, k, \omega) = -idE(q, \omega)N(p). \tag{5.11}$$

This can be solved by writing a second equation for $f_{\uparrow\downarrow}(-p, k, \omega)$ by simply changing $p \to -p$. The result is a two-by-two system of equations for $f_{\uparrow\downarrow}(p)$ and $f_{\uparrow\downarrow}(-p)$ (we can omit all other variables for the moment),

$$\begin{pmatrix} -i\Omega_p + \Gamma(p) & -\Gamma(p) \\ -\Gamma(p) & -i\Omega_{-p} + \Gamma(p) \end{pmatrix} \begin{pmatrix} f_{\uparrow\downarrow}(p) \\ f_{\uparrow\downarrow}(-p) \end{pmatrix} = \begin{pmatrix} g(p) \\ g(-p) \end{pmatrix}, \tag{5.12}$$

where we introduced the abbreviations

$$\begin{aligned} g(p) &:= -idE(k, \omega)N(p) \\ \Omega_p &:= \omega - \omega_0 - v_p k + i\gamma. \end{aligned} \tag{5.13}$$

Note that the velocity v_p is an odd function of p,

$$v_p \equiv p/M = -v_{-p}. \tag{5.14}$$

The solution can be found by inverting the two–by–two matrix as

$$\begin{aligned} f_{\uparrow\downarrow}(p, k, \omega) &= idE(k, \omega)N(p) \times \tag{5.15} \\ &\times \; \frac{-i(\omega - \omega_0 + v_p k + i\gamma) + 2\Gamma(p)}{[\omega - \omega_+(p, k)][\omega - \omega_-(p, k)]}. \end{aligned}$$
$$\tag{5.16}$$

Here, the two poles $\omega_\pm(p, k)$ in the denominator of Eq.(5.15) are given by

$$\boxed{\omega_\pm(p, k) := \omega_0 - i\gamma - i\left(\Gamma(p) \pm \sqrt{\Gamma(p)^2 - v_p^2 k^2}\right),} \tag{5.17}$$

and the result for $f_{\downarrow\uparrow}(p, k, \omega)$ is obtained from Eq.(5.15) by changing $\omega_0 \to -\omega_0$ and $N(p) \to -N(p)$.

5.2.3   Pole–structure

Using these results, one can now express a linear relation between the Fourier transform of the polarization, Eq.(5.7), and the electric field $E(k, \omega)$,

$$
\begin{aligned}
P(k, \omega) &= \chi(k, \omega) E(k, \omega) \\
\chi(k, \omega) &= d^2 \int dp N(p) \frac{\omega - \omega_0 + v_p k + i\gamma + 2i\Gamma(p)}{[\omega - \omega_+(p, k)][\omega - \omega_-(p, k)]} \\
&\quad - (\omega_0 \rightarrow -\omega_0).
\end{aligned} \tag{5.18}
$$

The spectral line shape is determined by the *polarizability* $\chi(k, \omega)$, the form of which in turn depends on the poles $\omega_\pm(p, k)$. The position of the poles in the complex plane is a central point for the (abstract) understanding of the Dicke effect, and we discuss it in some detail here and in Fig.(5.2). We can distinguish two limiting cases:

1. collisionless limit $\Gamma^2(p) \ll v_p^2 k^2$, cp. Fig.(5.2) : in this case, $\omega_\pm(p, k) = \omega_0 \pm v_p k - i\gamma$. The linewidth is determined by the broadening through spontaneous emission γ and is shifted from the central position ω_0 by the *Doppler–shifts* $\pm v_p k$. Note that the final result for the polarizability still involves an integration over the distribution function $N(p)$ and therefore depends on the occupations of the upper and lower levels. This leads to the final *Doppler broadening* due to the Doppler–shifts $\pm v_p k$.

2. *Dicke–limit* $\Gamma^2(p) \gg v_p^2 k^2$, cp. Fig.(5.2): this is the most interesting case, where in the square–root in the two poles the Doppler–broadening can be neglected and

$$
\begin{aligned}
\omega_+ &= \omega_0 - i\gamma - 2i\Gamma(p) \\
\omega_- &= \omega_0 - i\gamma.
\end{aligned} \tag{5.19}
$$

The first pole ω_+ corresponds to a broad resonance of width $\gamma + 2\Gamma(p)$, the second pole ω_- corresponds to a resonance whose width is solely determined by the 'natural' line-width γ, i.e. a resonance which is no longer Doppler–broadened.

The splitting into two qualitatively different decay channels is the key feature of the Dicke effect. We have already encountered it in the emission of light from a two–ion system, where the spontaneous decay splitted into one fast
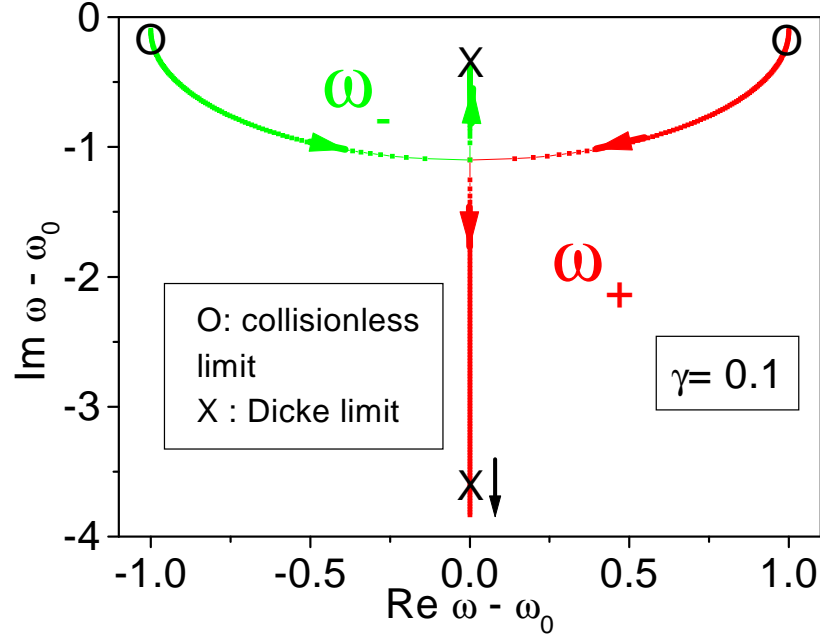
Fig. 5.2: Zeros $\omega_\pm - \omega_0$ according to Eq.(5.17) appearing in the distribution function Eq.(5.15) and the polarizability Eq.(5.18). The real and imaginary part of the frequencies are in units of the Doppler shift $v_p k$ which is fixed here. The two curves are plots parametric in the elastic collision rate $\Gamma(p)$; the arrows indicate the direction of increasing $\Gamma(p)$. For $\Gamma(p) \gg |v_p k|$, both curves approach the *Dicke limit* Eq.(5.19), where the imaginary part of $\omega_- - \omega_0$ becomes the negative of γ, and the imaginary part of $\omega_+ - \omega_0$ flows to minus infinity.

(superradiant) and one slow (subradiant) channel, cp. chapter 1. In fact, in the Dicke limit the polarizability is given by a sum of the two resonances $\omega_\pm$: from Eq.(5.18), one obtains

$$
\begin{aligned}
\chi(k,\omega) &= d^2 \int dp N(p) \frac{\omega - \omega_0 + v_p k + i\gamma + 2i\Gamma(p)}{\omega_+ - \omega_-} \times \\
&\quad \times \left[\frac{1}{\omega - \omega_+} - \frac{1}{\omega - \omega_-} \right] - (\omega_0 \to -\omega_0)
\end{aligned}
\tag{5.20}
$$

In the Dicke limit, this becomes

$$
\begin{aligned}
\chi(k,\omega) \;\approx\; & d^2 \int dp \frac{N(p)}{-2i\Gamma(p)} \times \\
& \times \left[\frac{v_p k}{\omega - \omega_+} - \frac{2i\Gamma(p)}{\omega - \omega_-} \right] - (\omega_0 \to -\omega_0).
\end{aligned}
\tag{5.21}
$$

The two resonances thus correspond to an *antisymmetric term* $v_p k/(\omega - \omega_+)$ (odd function of p) and a *symmetric term* $2i\Gamma(p)/(\omega - \omega_-)$ (even function of p). Note that the antisymmetric term gives no contribution to $\chi(k,\omega)$ for even distribution $N(p) = N(-p)$. Still, the appearance of a definite type of symmetry together with each type of resonance is typical for the Dicke effect and has its origin in the coupling of the two components $f(p)$ and $f(-p)$ in the matrix equation Eq.(5.12). We can re-write this equation in a suggestive way, that is (we again consider only the component $f_{\uparrow\downarrow}$)

$$
(A - \lambda 1) \begin{pmatrix} f_{\uparrow\downarrow}(p) \\ f_{\uparrow\downarrow}(-p) \end{pmatrix} = -ig(p) \begin{pmatrix} 1 \\ 1 \end{pmatrix},
\tag{5.22}
$$

where we already used $N(p) = N(-p)$ and defined

$$
\begin{aligned}
A \;&:=\; \begin{pmatrix} v_p k - i\Gamma(p) & i\Gamma(p) \\ i\Gamma(p) & -v_p k - i\Gamma(p) \end{pmatrix} \\
\lambda \;&:=\; \omega - \omega_0 + i\gamma.
\end{aligned}
\tag{5.23}
$$

In the limit $\Gamma(p) \gg |v_p k|$, the matrix A has the eigenvectors $(1,1)$ and $(1,-1)$,

$$
\begin{aligned}
-i\Gamma(p) \begin{pmatrix} 1 & -1 \\ -1 & 1 \end{pmatrix} \begin{pmatrix} 1 \\ 1 \end{pmatrix} \;&=\; 0 \\
-i\Gamma(p) \begin{pmatrix} 1 & -1 \\ -1 & 1 \end{pmatrix} \begin{pmatrix} 1 \\ -1 \end{pmatrix} \;&=\; -2i\Gamma(p) \begin{pmatrix} 1 \\ -1 \end{pmatrix}.
\end{aligned}
\tag{5.24}
$$

For the symmetric eigenvector, the effect of the collisions therefore is annihilated to zero, and this eigenvector solves Eq.(5.22) with

$$
-\lambda f_{\uparrow\downarrow}(p) = -ig(p),
\tag{5.25}
$$

which means

$$
f_{\uparrow\downarrow}(p) = \frac{dE(k,\omega)N(p)}{\omega - \omega_0 + i\gamma}.
\tag{5.26}
$$

This agrees with our previous result Eq.(5.15) in the Dicke limit $\Gamma(p) \gg |v_p k|$: the collision broadening has disappeared and the line is determined by the remaining natural line width γ.
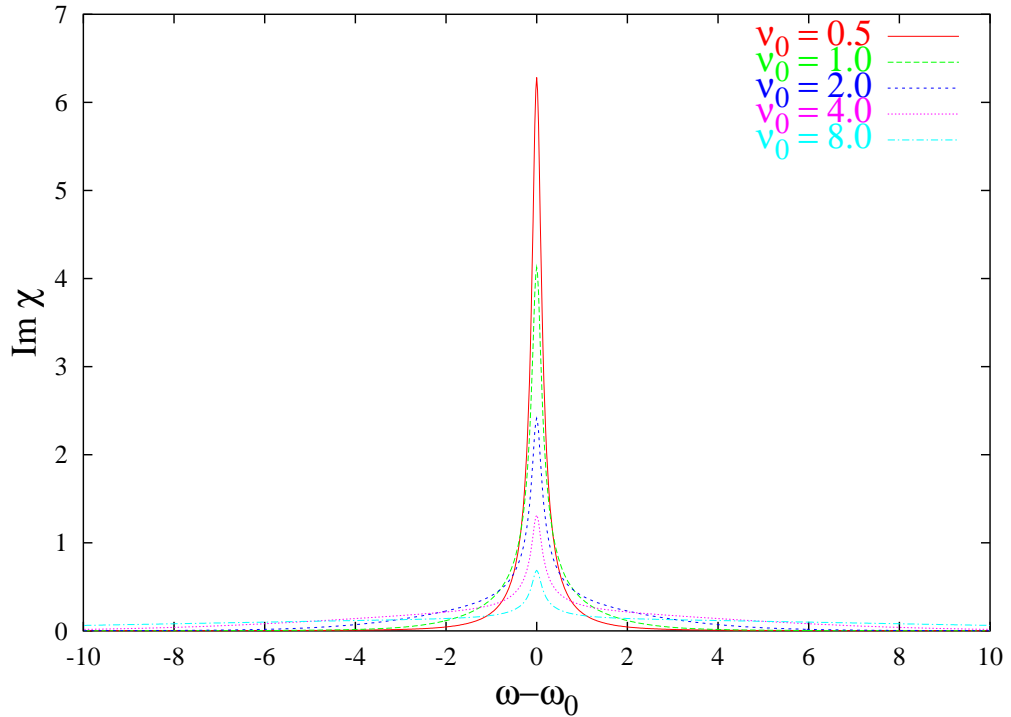
Fig. 5.3: Imaginary part of the polarizability $\chi(k,\omega)$ in units of d^2/Γ (d: dipole moment) around $\omega = \omega_0$ for a one–dimensional model. All frequencies are in units of the collision rate Γ of the radiating atoms with the atoms of the buffer gas. The spontaneous emission rate $\gamma = 0.1$; the atom mass M and the light wave vector k enter into the frequency $\nu_0 = kp_0/M$ which determines the width of the momentum distribution Eq.(5.27).

5.2.4 Numerical example

To conclude this discussion, we give a quantitative numerical example. The distribution function $N(p) = f_{\uparrow\uparrow} - f_{\downarrow\downarrow}$ is assumed to be a 1d Gaussian

$$-N(p) = \frac{1}{\sqrt{2\pi}p_0}e^{-\frac{p^2}{2p_0^2}}, \tag{5.27}$$
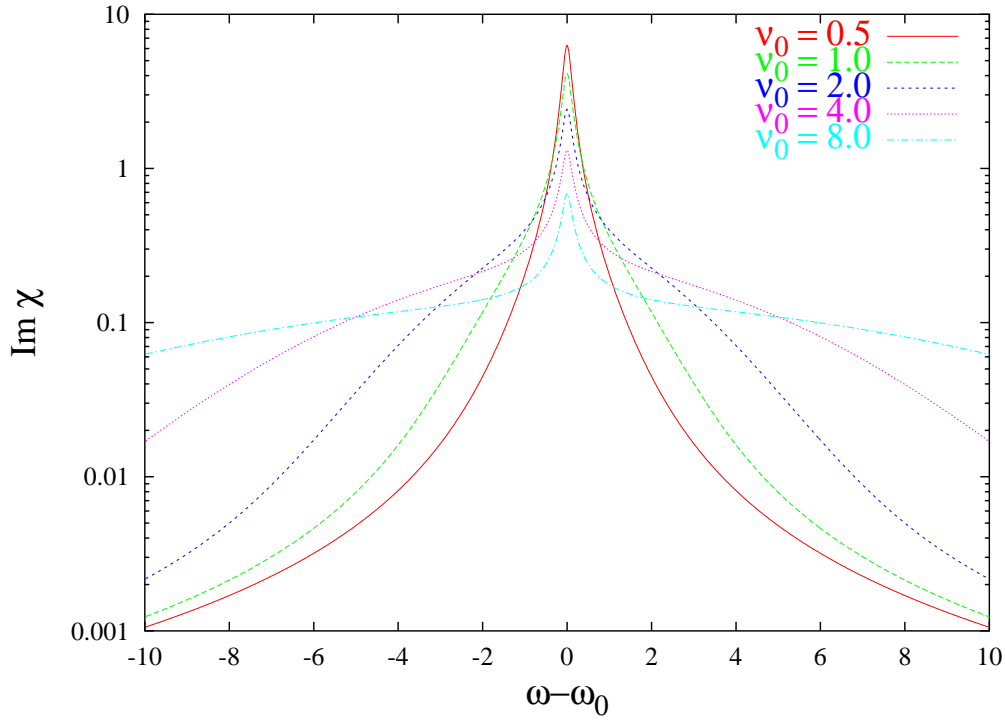
Fig. 5.4: Same as Fig.(5.3) in logarithmic scale. For broad distributions (larger ν_0), the sharp 'Dicke–peak' appears on top of the Doppler–broadened lineshape.

i.e. a symmetric momentum distribution of width p_0. We plot the imaginary part $\chi_1''(k, \omega)$ of the first term in the polarizability Eq.(5.18),

$$\chi_1''(k, \omega) := d^2 \Im\text{m} \int dp N(p) \frac{\omega - \omega_0 + v_p k + i\gamma + 2i\Gamma(p)}{[\omega - \omega_+(p, k)][\omega - \omega_-(p, k)]}, \qquad (5.28)$$

i.e. the resonance around $\omega \approx \omega_0$. We assume a constant $\Gamma(p) = \Gamma$ and introduce the frequency $\nu_0 := p_0 k / M$ for a fixed k. The result (which requires one numerical integration) is shown in Fig.(5.3) for different widths ν_0 of the distribution $N(p)$. For a sharp momentum distribution (small ν_0), the line-width is determined by the spontaneous emission rate γ and there is basically no Doppler–broadening (Dicke–limit). In the opposite case of a broad momentum distribution, the form of the line is determined by a sharp peak of width $\sim \gamma$ on top of a broad curve of width $\sim v_0$. This last case is

best visible in the logarithmic plot Fig.(5.4) and reflects the appearance of
the *two poles* ω_+ and ω_- in $\chi(k,\omega)$.

5.3   Spectral function for two impurity levels (Shahbazyan, Raikh)

The appearance of the Dicke effect in a spectral function for electronic states
has been found first by Shahbazyan and Raikh [148]. They considered the
two–channel resonant tunneling of electrons through a systems of two res-
onant impurities (localized states) of energy ε_1 and ε_2, see Fig.(5.5). The
conductance of such a system can be expressed by its scattering properties,
if Coulomb interactions among the electrons are neglected [15, 16, 175]. Here,
we follow the discussion of Shahbazyan and Ulloa who later generalized this
problem to the case of scattering properties in a strong magnetic field [149].
  The spectral function of an electronic system can be related to the imag-
inary part of its retarded Green's function [83, 114]. For the case of two
energy levels ε_1 and ε_2 that are assumed to belong to two spatially separated
localized impurity states, one can define the spectral function in the Hilbert
space of the two localized states where it becomes a two–by–two matrix,

$$S(\omega) = -\frac{1}{\pi}\Im\mathrm{m}\frac{1}{2}\mathrm{Tr}\frac{1}{\omega - \hat{\varepsilon} + i\hat{W}}. \tag{5.29}$$

It is assumed that transitions between the localized states $i \rightarrow |\mathbf{k}\rangle \rightarrow j$ are
possible via virtual transitions to extended states (plane waves $|\mathbf{k}\rangle$). Such
a situation is realized, e.g., for a coupling of two resonant impurity levels
which are both coupled via a tunnel barrier to a continuum. The two levels
then become coupled indirectly by virtual transitions of electrons from the
impurities to the continuum and back again. Then, ε is diagonal in the ε_i,
and $\hat{W}$ is a self–energy operator that describes the possibility of transitions
between localized levels i and j via extended states with wave vector $\mathbf{k}$. In
second order perturbation theory, the self–energy operator $\hat{W}$ is given by

$$W_{ij} = \pi \sum_{\mathbf{k}} t_{i\mathbf{k}} t_{\mathbf{k}j} \delta(\omega - E_{\mathbf{k}}), \tag{5.30}$$

where $\hbar = 1$ and the dependence on ω of $\hat{W}$ is no longer indicated. The
quantities $t_{i\mathbf{k}}$ are overlaps between the localized states i and the plane waves
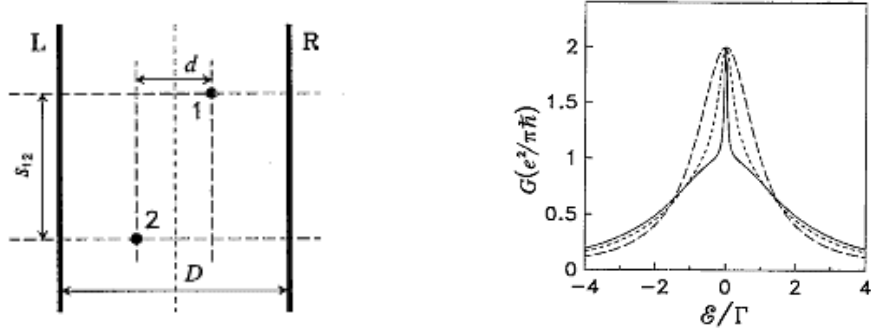
Fig. 5.5: Resonant tunneling through two impurity levels, from Shahbazyan and Raikh [148]. Left: Tunnel junction with two resonant impurities 1 and 2 in a distance d in horizontal and distance s_{12} in vertical direction. Left: linear conductance for identical impurity levels E as a function of $\mathcal{E} = E_F - E$, where E_F is the Fermi energy of the tunneling electron. The characteristic shape of the spectral function Eq.(5.32), as known from the Dicke effect, appears here in the conductance with increasing parameter $q = 0$, $q = 0.75$, $q = 0.95$, cp. Eq.(5.31). Γ is the tunneling rate through the left and the right barrier.

$|\mathbf{k}\rangle$, their dependence on the impurity position $\mathbf{r}_i$ is given by the phase factor from the plane wave at the position of the impurity, i.e. $t_{i\mathbf{k}} \propto \exp(i\mathbf{k}\mathbf{r}_i)$.

We reckognize that this spatial dependence of the matrix element $t_{i\mathbf{k}}$ is analogous to the relation $\alpha_{\mathbf{Q}} \propto \exp(i\mathbf{Q}\mathbf{r}_L)$, $\beta_{\mathbf{Q}} \propto \exp(i\mathbf{Q}\mathbf{r}_R)$ of the electron–phonon coupling in the left (L) and (R) dot in the double dots discussed in chapter 1, cp. Eq. (1.78) there. Furthermore, the product $\alpha_{\mathbf{Q}}\beta_{\mathbf{Q}}^* \propto \exp i\mathbf{Q}\mathbf{d}$ there ($\mathbf{d}$ was the distance between the two dots) appears in a completely analogous way here, i.e. $t_{i\mathbf{k}}t_{j\mathbf{k}}^* \propto \exp i\mathbf{Q}\mathbf{r}_{ij}$, where r_{ij} is the distance between the two impurities. The non–diagonal elements W_{12} can then be shown to become an oscillating function of the distance r_{ij},

$$W_{12} = q\sqrt{W_1 W_2}, \quad q = J_0(r_{12}k_F), \qquad (5.31)$$

where k_F is the Fermi wave vector and J_0 the Bessel function, resulting from an angular integral in the plane of the two impurities. If the diagonal elements W_{11} and W_{22} and both energies are assumed to be identical for

simplicity, $\varepsilon_1 = \varepsilon_2 = \varepsilon$ and $W_{11} = W_{22} = W$, inversion of Eq.(5.29) yields

$$
\begin{aligned}
S(\omega) &= \frac{1}{2\pi}\left[\frac{W_-}{(\omega - \varepsilon)^2 + W_-^2} + \frac{W_+}{(\omega - \varepsilon)^2 + W_+^2}\right] \\
W_\pm &= (1 \pm q)W.
\end{aligned}
\tag{5.32}
$$

This spectral function represents a superposition of two Lorentzians: one narrow line with width W_-, corresponding to a subradiant channel, and one broad line with width W_+, corresponding to a superradiant channel. This splitting is fact is analogous to the spitting of a radiating decay channel of two coupled radiators as discussed in chapter 1. If the parameter q is small, $q \ll 1$, one has $W_+ \approx W_- \approx W$ and the spectral function is a simple Lorentzian if width W. The crossover to the Dicke regime with the splitting into a sharp and a broad part of $S(\omega)$ is thus governed by $q = J_0(r_{12}k_F)$ and therefore by the ratio of the distance of the impurities to the Fermi wavelength of the electron. This again shows that the effect is due to interference.

The two localized impurity states are therefore coupled by the continuum of plane waves. As for their scattering properties, they have to be considered as *one quantum mechanical entity* as long as their distance is of the same order or smaller than the wavelength of scattering electrons. In this case, the (linear) conductance $G(E_F)$ for resonant tunneling shows the typical feature of the Dicke effect as a function of the energy E_F of a tunneling electron: as it is determined by the spectral function $S(\omega)$ [175], the Dicke peak becomes directly visible in the conductance, see Fig. (5.5). If the energies ε_1 and ε_2 of the two impurity levels become different, the resonant peak even shows a more complex behavior; as a function of the parameter q there is a crossover to a sharp transmission minimum [148].

6. THE DICKE EFFECT IN THE AC DRUDE CONDUCTIVITY

Abstract

We show that in quantum wires in a strong magnetic field, impurity interband scattering leads to a (Drude) ac conductivity which shows (as a function of frequency) a sharp peak on top of a broad Lorentzian. This is a realization of the Dicke effect (as discussed in the previous chapter) in an electronic system.

6.1 Introduction

We now turn from the collision–induced narrowing of the polarizability $\chi(\omega)$ of an atomic gas, as was considered first in Dicke's 1953 paper, to a completely different quantity, that is the ac conductivity $\sigma(\omega)$ of quantum wires in a magnetic field. Quantum wires are electronic systems where the motion of electrons is confined in two perpendicular direction of space and free in the third. The large amount of literature about the transport and optical properties of such systems indicates the fascinating physics contained in them. We will not try to give a review here and refer to some recent textbook presentations [5–8, 50, 51]. We will neither touch the many novel aspects [49] concerning localization and interaction effects in transport and optical properties of quantum wires here. Rather, in the following our strategy will be to concentrate on basically one aspect, that is the quasi–one dimensional band structure of wires.

In the presence of impurity scattering and when only the two lowest subbands of the wire are occupied, the absorptive part of $\sigma(\omega)$ shows (as a function of ω) the Dicke effect in analogy to the spectral line narrowing discussed above. The parameter that drives the effect is the magnetic field B. Impurity backscattering becomes more and more suppressed with increasing B, which leads to a crossover in $\sigma(\omega)$ from a broad Lorentzian to a very sharp

and high peak on top of a broad Lorentzian. This is due to inter–subband
scattering by which the transport rates for the two subbands become coupled
and split into one fast and one slow mode, corresponding to the superradiant
and the subradiant channel in the superradiance problem.

As mentioned in the introduction, this splitting of decay rates ('imaginary
energies') is similar to level repulsion of real energy levels, its origin being
the particular pole structure of a response function (the conductivity) of a
coupled system. The 'wandering' of poles in the complex frequency plane as
a function of an external parameter (here the magnetic field B) has already
been discussed in detail in the foregoing section. In the following, we concen-
trate on the details of this mechanism in the context of frequency dependent
transport in a quantum wire under a magnetic field.

6.2   Model

We consider a quantum wire in x–direction within a quantum well in the
x–y–plane under a magnetic field in z direction , see Fig.(6.1).

The wire is defined by a harmonic confinement potential of frequency ω_0.
The single electron eigenstates $|nk\rangle$ with eigenenergies ε_{nk} of the clean system
(no impurities, Landau gauge) have two quantum numbers n (Landau band)
and k (momentum in direction of the wire) [14]. In the Drude conductivity,
quantum interference effects and localization of electrons are disregarded,
and the electronic transport is determined by the average electron scattering
rate at the impurities [176–179].

We use the memory function formalism [180, 181] to calculate the fre-
quency dependent conductivity $\sigma(\omega)$. An alternative way to calculate this
quantity is to solve the Boltzmann equation [176], which has been done for the
DC conductivity of quantum wires by, e.g., Bruus, Flensberg and Smith [106]
or Akera and Ando [182]. The basic advantage of the memory function for-
malism is that non–trivial interaction effects can in principle be incorporated
in the form of interaction dependent correlation functions. It is in particular
useful to combine exact results, e.g. for correlation functions of interacting
one–dimensional systems, with a perturbative description of impurity scat-
tering [34,183]. Although such effects are neglected here (and the final result
can be shown to coincide with the one obtained from the Boltzmann equation
in the limit of zero temperature and small frequencies ω we are interested
here), we chose the memory function formalism for its generality.
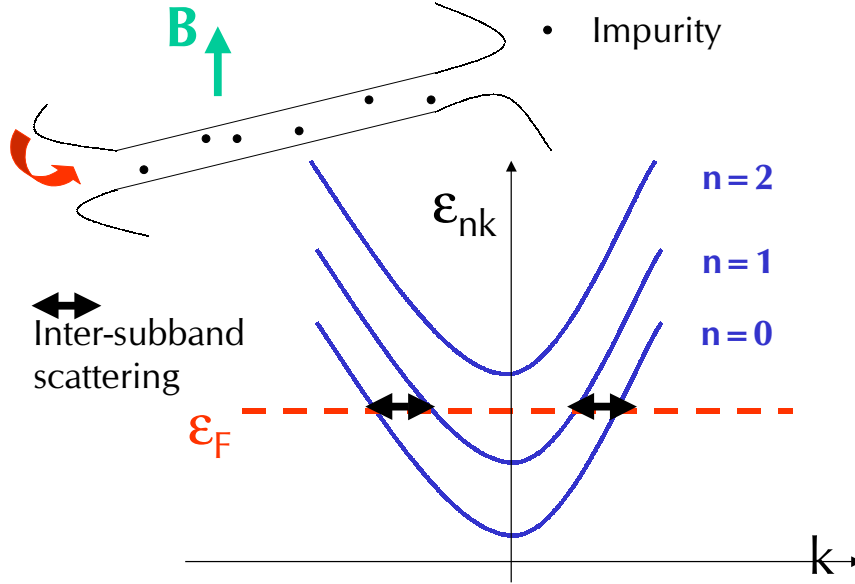
Fig. 6.1: Subband dispersion ε_{nk} of a wire (upper left) in a magnetic field B.

In our model, the Hamiltonian of the wire is given by

$$H = \sum_{nk} \varepsilon_{nk} c_{nk}^{+} c_{nk} + \frac{1}{L_s} \sum_{nmkq} V_{nm}(q) c_{nk}^{+} c_{mk+q}, \qquad (6.1)$$

where L_s is the length of the wire, c_{nk} the electron creation operator for band n, and $V_{nm}(q)$ the matrix element for impurity scattering with momentum transfer q from a state with quantum number nk to a state $mk+q$. To simplify the notation, the spin index σ in the operators $c_{nk\sigma}^{(+)}$ has not been written out explicitly. The scattering potential is assumed to be spin–independent, so that we implicitly include the summation over the spin in all k, k'–sums.

6.3   The conductivity and the memory function formalism

The linear response of an electronic system to a monochromatic electric field $\mathbf{E}(\mathbf{x}) \cos(\omega t)$ in general is governed by a non–local conductivity tensor

$\sigma(\mathbf{x}, \mathbf{x}', \omega)$. Many electronic transport properties of quantum wires (many–subband quasi one–dimensional systems) have to be discussed in terms of the *conductance* Γ (the inverse resistance) [15, 16, 99, 184–186] rather than the conductivity, although the former is related to the latter in special cases [187–191]. The conductance is regarded as the proper transport property to explain, e.g., phenomena like step–like features in the electronic transport properties, i.e. a quantization of Γ in multiples of $2e^2/h$ [49]. This and other phenomena like localization due to disorder [12] in general are believed to exist due to phase coherence [121, 122, 192].

In presence of phase breaking processes, a crossover to a regime that can be described by a Drude–like theory is expected even for one–dimensional systems when their length L_s becomes larger than the distance L_ϕ over which phase coherence is maintained. In this case, the conductivity $\sigma(\omega)$ becomes a meaningful quantity (we mention that the problems of phase coherence, localization, and interactions in quantum wires are the subject of intensive ongoing research). Furthermore, the conductivity as physical quantity in quantum wires is also used to describe *deviations* from ideal, unperturbed situations, e.g. deviations from conductance plateaus due to scattering processes where a low order (sometimes renormalized) perturbation theory [193] is possible. It is these two regimes that we have in mind when considering the (homogeneous, impurity averaged) conductivity of a quantum wire in the following.

The starting point is the expression of the homogeneous conductivity as a function of complex frequency z in terms of the current–current correlation function [180, 181],

$$\sigma(z) = -i\frac{e^2}{z}\left(\chi(z) - \frac{n_e}{m^*}\right), \tag{6.2}$$

where

$$-\chi(z) = \langle\langle \hat{j}; \hat{j} \rangle\rangle_z =: -iL_s \int_0^\infty dt\, e^{izt} \langle [\hat{j}(t), \hat{j}(0)] \rangle_0 \tag{6.3}$$

is the (Zubarev) correlation function of the $q = 0$ component of the mass current density operator $\hat{j} = \hat{j}(q = 0)$. Furthermore, n_e is the electron density, $-e < 0$ the electron charge and m^* its conduction band mass. The multichannel wire is described as a set of quasi one-dimensional subbands (channels) $n = 1, ..., N_c$ of dispersion ε_{nk} and corresponding electron velocities $v_{nk} = \partial\varepsilon_{nk}/\partial k$ (we set $\hbar = 1$). The current in the total system is the

sum of the currents of all channels,

$$\hat{j} = \frac{1}{L_s} \sum_{n,k} v_{nk} c_{nk}^+ c_{nk}, \qquad (6.4)$$

which allows for writing the conductivity as

$$\sigma(z) = -i \frac{e^2}{z} \left(\sum_{n,m} \chi_{nm}(z) - \frac{n_e}{m^*} \right), \qquad (6.5)$$

where

$$\chi_{nm}(z) := -\langle\langle j_n, j_m \rangle\rangle_z, \qquad j_n := \frac{1}{L_s} \sum_{k} v_{nk} c_{nk}^+ c_{nk} \qquad (6.6)$$

is the matrix of the current–current correlation functions. The total number of electrons N_e is given by $N_e = \sum_{n,|k|<k_n}$. Here, the Fermi momentum k_n in subband n is related to the Fermi energy ε_F as $\varepsilon nk = \varepsilon_F, k = k_n$, which in turn is determined by the total number of electrons via $N_e = \sum_{n,|k|<k_n}$ and the magnetic field dependent band structure ε_{nk}. One has

$$\frac{n_e}{m^*} =: \sum_{nm} \chi_{nm}^0, \quad \chi_{nm}^0 := \delta_{nm} \frac{s}{\pi} v_n, \quad s \text{ spin degeneracy}, \qquad (6.7)$$

where

$$v_n = v_{nk=k_n} = k_n/m^* \qquad (6.8)$$

is the Fermi velocity in subband n and the sum in Eq. (6.7) runs over all occupied subbands.

In Appendix (B.1), a multichannel version of the memory function formalism [180] is used to find the expression for the frequency dependent conductivity $\sigma(\omega)$ at zero temperature $T = 0$ and small excitations $\hbar\omega$ around the Fermi surface, i.e. frequencies $\omega \ll |\varepsilon_F - \varepsilon_{n=0,k=0}|/\hbar$. In this paper, we restrict ourselves to excitations much smaller than the inter–subband distance $\hbar\omega_B = \hbar\sqrt{\omega_0^2 + \omega_c^2}$, where $\omega_c = |e|B/m^*c$ is the cyclotron frequency for magnetic field B. To get an estimate for the relevant frequency range, we consider $B = 0$ and $\hbar\omega_0 = 1$ meV, i.e. $\omega_0 = 1500$ GHz. Frequencies ω from $0 - 100$ GHz $\ll \omega_0$ thus are in the microwave spectroscopy regime.

The general expression for $\sigma(\omega)$ is given in Appendix (B.1), Eqs. (B.15), (B.7), together with (6.7). In the following, we discuss the case where the two lowest subbands $n = 0$ and $n = 1$ are occupied. The expression for the conductivity is

$$\sigma(z) = ie^2 \frac{z\frac{s}{\pi}(v_0 + v_1) + i\left[\frac{v_0}{v_1}L_{11} + \frac{v_1}{v_0}L_{00} - 2L_{01}\right]}{\left(z + i\frac{\pi L_{00}}{sv_0}\right)\left(z + i\frac{\pi L_{11}}{sv_1}\right) + \frac{\pi^2 L_{01}^2}{s^2 v_0 v_1}} \tag{6.9}$$

with

$$
\begin{aligned}
L_{00} &= \frac{s}{\pi}L_s\frac{v_0}{v_1}\left(|V_{01}(k_0 - k_1)|^2 + |V_{01}(k_0 + k_1)|^2 + \frac{2s}{\pi}V_{00}(2k_0)^2\right) \\
L_{11} &= \frac{s}{\pi}L_s\frac{v_1}{v_0}\left(|V_{01}(k_0 - k_1)|^2 + |V_{01}(k_0 + k_1)|^2 + \frac{2s}{\pi}V_{11}(2k_1)^2\right) \\
L_{01} &= \frac{s}{\pi}L_s\left(|V_{01}(k_0 + k_1)|^2 - |V_{01}(k_0 - k_1)|^2\right). \tag{6.10}
\end{aligned}
$$

Here, $s = 2$ if the electrons are taken as spin degenerate, and $s = 1$ if the electrons are assumed to be spin-polarized.

6.4 Conductivity for impurity scattering

We consider scattering of electrons at random impurities. In lowest order perturbation theory (Born approximation) in the impurity scattering, it is sufficient to know the impurity averaged square of the matrix element

$$\overline{|V_{nn'}(k - k')|^2} = n_i^{2D}\sum_{\mathbf{q}}|u(\mathbf{q})|^2|\langle nk|e^{-i\mathbf{q}\mathbf{x}}|n'k'\rangle|^2, \tag{6.11}$$

that enters into the expressions L_{ij} in Eq.(6.10). Here, $u(\mathbf{q})$ is the two-dimensional Fourier transform of the static potential of a single impurity potential $u(x, y)$. All impurities are assumed to be identical scatterers and distributed with a concentration n_i^{2D} per area L^2. Finite quantum well thickness corrections (form factors) are neglected here for simplicity. The averaged matrix elements are calculated in Appendix (B.2) for Delta-scatterers, where the Fourier component $|u(\mathbf{q})|^2 =: V_0^2$ is a constant. The dependence on the magnetic field is only through the ratio $\beta := (\omega_c/\omega_0)^2$.
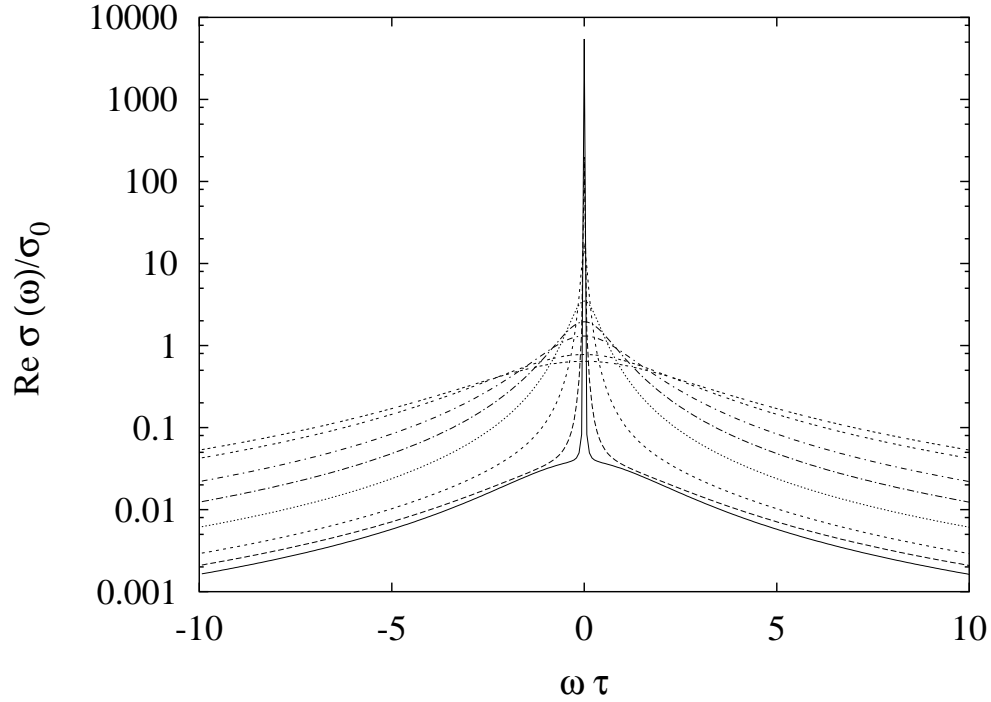
Fig. 6.2: Real part of the frequency-dependent Drude conductivity of a two–channel quantum wire in a magnetic field, Eq. (B.26), in units of $\sigma_0 :=e^2 s v_{F_0} \tau/\pi$ (s=1 for spin–polarized electrons). Different curves are for ω_c/ω_0 = $0, 0.4, 0.8, 1.2, 1.6, 2.0, 2.4, 2.8$, where ω_0 is the frequency of the harmonic confinement potential, and $\omega_c = eB/m$ the cyclotron frequency for magnetic field B.

We express the scattering matrix elements by the scattering rate τ^{-1} without magnetic field,

$$\tau^{-1} \quad := n_i^{2D} V_0^2 m^*/\sqrt{4\pi}\hbar^3 \tag{6.12}$$

(in comparison with [106], we defined τ^{-1} with an additional factor of $1/\sqrt{4\pi}$ for convenience). In the following, we discuss the conductivity $\sigma(\omega)$ as a function of frequency ω and magnetic field B for the Fermi energy fixed between the bands $n = 1$ and $n = 2$, i.e. $\varepsilon_F = 2\hbar\omega_B$, cp. Fig.(6.1).
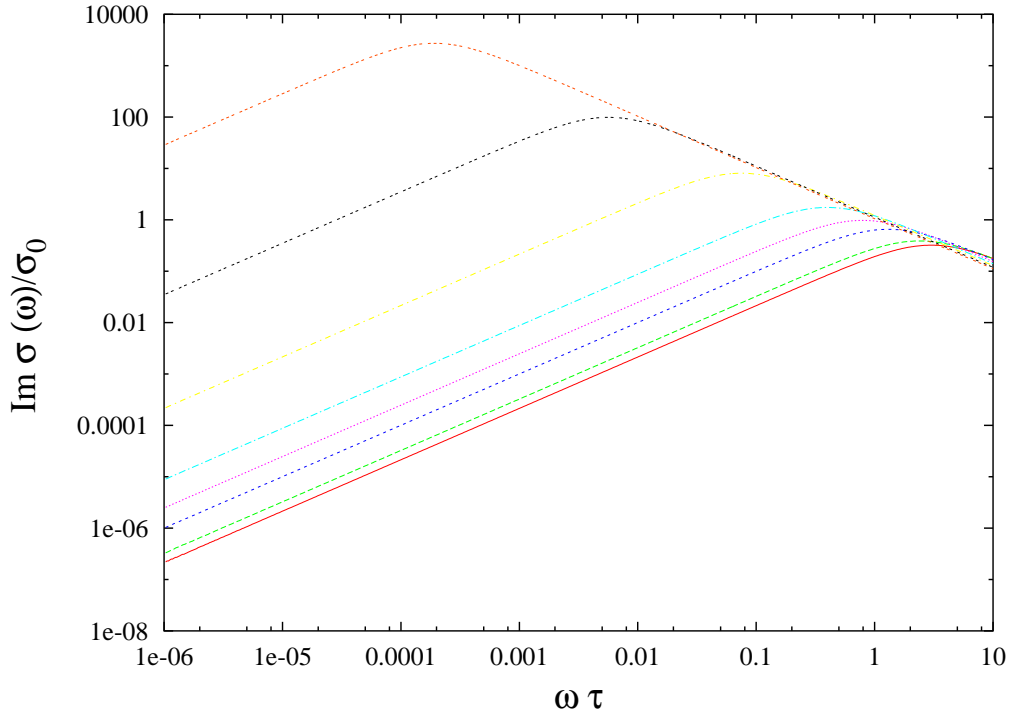
Fig. 6.3: Imaginary part of the frequency–dependent Drude conductivity of a two–channel quantum wire in a magnetic field, Eq. (B.26). Different curves are for $\omega_c/\omega_0 = 0, 0.4, 0.8, 1.2, 1.6, 2.0, 2.4, 2.8$ (from below, note the double–logarithmic scale).

6.5   Discussion

The frequency dependence of the conductivity Eq.(B.26) is shown in Fig. (6.2) and (6.3). The real part $\Re e \sigma(\omega)$ has a Lorentzian shape for small magnetic fields. For increasing magnetic field, i.e. larger ω_c/ω_0, this shape develops into a very sharp Lorentzian on top of a broad Lorentzian . This indicates that one of the two poles $z_\pm$ in $\sigma(z)$ approaches zero: this is the *Dicke effect* as discussed in the previous chapter. Here, in the Dicke limit the subradiant pole is zero and has no small finite imaginary part, since we have not included scattering processes other than impurity scattering in contrast to Eq.(5.19), where spontaneous emission at a rate γ lead to a finite imaginary part $-i\gamma$ in both zeros.
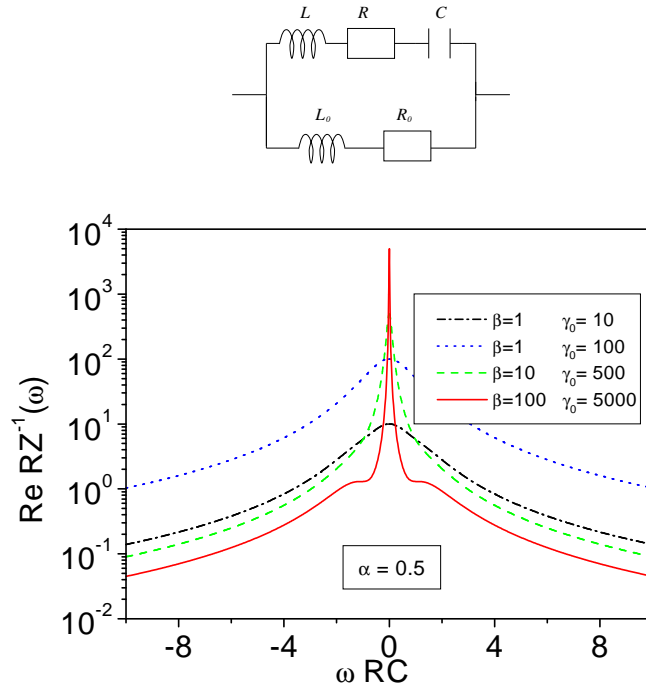
Fig. 6.4: Real part of the inverse impedance $Z^{-1}(\omega)$ (conductance in units of R) for a classical circuit, Fig.(6.4), that simulates the Dicke effect in a two–subband quantum wire, Fig.(6.2). Above: Classical circuit to simulate the Dicke effect in a two–subband quantum wire.

The two poles of $\sigma(z)$ determine the width of $\Re e\sigma(\omega)$. In fact, for large magnetic fields B, in $\tilde{L}_{00}$, $\tilde{L}_{11}$, $\tilde{L}_{01}$ one can neglect the terms which are not due to intersubband *forward* scattering, and

$$\tilde{L}_{01} \approx \frac{-s}{L_s\pi}|V_{01}(k_0 - k_1)|^2, \quad \tilde{L}_{00} = \frac{v_0}{v_1}\tilde{L}_{01}, \quad \tilde{L}_{11} = \frac{v_1}{v_0}\tilde{L}_{01}. \quad (6.13)$$

The quadratic equation that determines the poles of $\sigma(z)$ then has the solutions

$$z_- = 0, \quad z_+ = \frac{-i|V_{01}(k_0 - k_1)|^2}{L_s}\left(\frac{1}{v_0} + \frac{1}{v_1}\right), \quad (6.14)$$

i.e. in this limit one of the poles becomes zero, corresponding to the very sharp peak in $\Re e\sigma(\omega)$.

This analysis shows that the coupling of the two subbands by the intersubband impurity scattering is essential for the appearance of the Dicke effect here. Furthermore, for large magnetic fields, backscattering with momentum transfer $2k_0$, $2k_1$, and $k_0 + k_1$ from one side to the other side of the wire becomes largely suppressed due to the exponential dependence of the matrix elements on the square of the momentum transfer, cp. Eq.(B.24), (B.20). With increasing magnetic fields, such scattering processes become much weaker than intersubband forward scattering, i.e. scattering between the bands $n = 0$ and $n = 1$. This absence of backward scattering, of course, leads to a more and more increasing DC conductivity.

In the Dicke–limit Eq.(6.13), simple algebraic manipulations lead to an expression for $\sigma(z)$ with the Fermi velocities v_0 and v_1 in subband $n = 0$ and $n = 1$,

$$\sigma(z) \quad \approx \quad ie^2 \frac{s}{\pi} \left(\frac{v_+}{z - z_+} + \frac{v_-}{z - z_-} \right)$$

$$v_+ \quad := \quad (v_0 - v_1) \frac{v_0/v_1 - 1}{v_0/v_1 + 1}, \quad v_- := \frac{4v_0 v_1}{v_0 + v_1}. \tag{6.15}$$

The conductivity then becomes a sum of two contributions from the 'super-radiant' mode corresponding to z_+ and the 'subradiant' mode corresponding to z_-. Note that these modes are superpositions of contributions from both subbands $n = 0$ and $n = 1$.

We note that it is possible to simulate the behavior at least of $\Re e\sigma(\omega)$ as a function of ω by a classical circuit composed of two impedances in parallel: This circuit consists of one huge inductance L_0 which is in series with a small resistance R_0, the whole being in parallel with a small inductance L, a large resistance R, and a capacitance C in series. Such classical circuits are sometimes useful to simulate the ac transport properties of other, more complicated systems [186, 194]. The complex impedance

$$Z^{-1}(\omega) = \frac{i\omega C}{1 + i\omega RC - \omega^2 LC} + \frac{1}{R_0 + i\omega L_0} \tag{6.16}$$

contains the time scale RC and the three parameters

$$\alpha := L/R^2 C, \quad \beta := L_0/RR_0 C, \quad \gamma_0 := R/R_0 \tag{6.17}$$

by which a fit that qualitatively compares well with $\Re e\sigma(\omega)$ can be achieved. Note that the case $\beta/\alpha \equiv L_0 R_0/LR \gg 1$ together with $\gamma_0 \equiv R/R_0 \gg 1$ sets

very drastic conditions for the possible ratios L_0/L and R_0/R, if one tried to simulate $\Re e\sigma(\omega)$ by a classical circuit in real experiment.

Finally, we check if the range of frequencies where the effect could be observed experimentally is accessible. From Figs. (6.2) and (6.3), one should be able to vary ω such that $0.1 \lesssim \omega\tau \lesssim 5$ in order to scan the characteristic shape of the Dicke peak. Impurity scattering times for AlGaAs/GaAs heterostructures are between $3.8 \cdot 10^{-12}$ s and $3.8 \cdot 10^{-10}$ s for mobilities between $10^5 - 10^7$ cm^2/Vs, cp. [6]. A scattering time of 10^{-11} s requires frequencies of $\omega \approx 100$ GHz for $\omega\tau \approx 1$, which is consistent with the requirement of ω being much smaller than the effective confinement frequency ($\omega_0 = 1500$ Ghz for $\hbar\omega_0 = 1$ meV). For an experimental check of the Dicke effect in quantum wires under magnetic fields, we therefore suggest microwave absorption experiments, i.e. determination of $\Re e\sigma(\omega)$ in relatively long wires. Our calculation applies for the case where the two lowest subbands are occupied. Temperatures T should be much lower than the subband–distance energy $\hbar\omega_B$, because thermal excitation of carriers would smear the effect. For $\hbar\omega_B$ of the order of a few meV, T should be of the order of a few Kelvin or less. The Dicke peak appears for magnetic fields such that ω_c/ω_0 becomes of the order and larger than unity. For convenience, we note that the cyclotron energy in GaAs is $\hbar\omega_c[\text{meV}] = 1.728B[\text{T}]$.

We have neglected electron interaction effects throughout our calculations. Recent experiments seem to indicate that such effects (Tomonaga–Luttinger liquid behavior) become weaker in longer $> 10\mu$m cleaved–edge–overgrowth wires [195], which might be due to loss of phase coherence in long wires. The transport regime where interaction effects are of minor importance and the (incoherent) Drude–like theory can be applied is, on the other hand, just the regime where we expect the effects discussed above to appear.

7. SUMMARY, ACKNOWLEDGEMENTS

This thesis has been devoted to the study of a class of interference phenomena in electronic transport that are related to the Dicke–effect.

Our first chapter introduced the simplest case of this effect, that is the splitting of a decay channel for two coupled radiators into a sub– and a super-radiant channel. We discussed how interference of matrix elements leads to oscillations in the inelastic current through coupled semiconductor quantum dots, and compared our results to recent experiments in such systems. In the second chapter, we generalized the Dicke superradiance model to allow for a varying electron number. This lead to an 'oscillatory' superradiance, the realization of which we discussed in chapter 3 for light emission from a magnetoplasma and in chapter 4 for superradiance of phonons in double dot arrays. The Dicke spectral line narrowing effect was reviewed in chapter 5, where we worked out its mathematical origin, i.e. a certain behavior of correlation function poles in the complex plane. We discussed the appearance of the electronic analogon of this effect in resonant tunneling and finally predicted the effect to appear also in the ac conductivity of disordered wires under a magnetic field. [1]

As mentioned in the introduction, one of our motivations throughout this work has been the transfer of ideas from quantum optics to electronic transport. We are aware of the fact that many questions remain open and that this new area of coherent, collective effects in the transport properties of

---

[1] Part of the present material has been published in the form of short letters and conference contributions: [174], [196], [197] (chapter 1); [168], [198] (chapter 2); [173] (chapter 3). The material in chapter 6 is based partly on work on ac transport in electronic systems [179, 199–202] and quantum wires [193]. Section 1.9.2 is work which is partly still in progress in collaboration with cand–phys. S. Debald [125] and Dipl.–Phys. T. Vorrath [107], University of Hamburg. This thesis is an original work of the author.

Effect	Quantity	Reference
Dicke superradiance	Spontaneous *light emission* from N radiators	Dicke 1954 [52]; [chapter 2]
Oscillatory superradiance	*Light emission* from a magnetoplasma	[chapter 3]
Pumped atomic superradiance	Spontaneous *light emission* from atomic gases	Steudel, Leonhardt 1994 [160] [section 2.6.4]
Oscillatory superradiance	*Time–dependent current* through quantum dot arrays	[chapter 4]
Sub– and superradiance	Spontaneous *light emission* from trapped ions	DeVoe, Brewer [68] [section 1.2.2, 1.8.3]
Spontaneous emission of phonons	*Stationary current* through double dots	[chapter 1]
Spectral line narrowing	Collision induced narrowing of atomic *polarizability*	Dicke 1953 [53] [chapter 5]
Dicke effect in resonant tunneling	Narrowing of *spectral function* for two impurity levels	Shahbazyan, Raikh 1994 [148] [section 5.3]
Dicke effect in quantum wires	*Drude AC conductivity* for two–subband wire in magnetic field	[chapter 6]

The Dicke effect as discussed in this thesis.

mesoscopic systems is still a very new and developing field. We therefore have tried to achieve a style of presentation that allows an advanced student or newcomer to use it as a sort of textbook, where further study might be facilitated by the references.

is a pleasure to thank Prof. A. Kawabata for my postdoc time in his lab in Tokyo where I could study many interesting aspects of mesoscopic transport.

Finally, I have profited a lot from discussions with many collegues, co–workers and friends, all of whom I would like to thank here.

Hamburg, January 2000   *Tobias Brandes*

APPENDIX

A. DOUBLE QUANTUM DOTS

A.1   The function C_ε

Here, we describe the splitting into a zero–temperature and a finite temperature contributions to the function $\Phi(t)$ in the calculation of the correlation function C_ε. This function was defined as

$$C_\varepsilon \;:=\; \lim_{\delta\to 0}\int_0^\infty dt\, e^{-\delta t}e^{i\varepsilon t}e^{-\Phi(t)} \tag{A.1}$$

$$\Phi(t) \;:=\; \int_0^\infty d\omega\,\rho(\omega)\left\{(1-\cos\omega t)\coth(\beta\omega/2)+i\sin\omega t\right\}$$

$$\rho(\omega)) \;:=\; \rho_0(\omega)-\rho_1(\omega)$$

$$\rho_0(\omega) \;:=\; \frac{g}{\omega}e^{-\omega/\omega_c}$$

$$\rho_1(\omega) \;:=\; \frac{g\omega_d}{\omega^2}\sin\left(\frac{\omega}{\omega_d}\right)e^{-\omega/\omega_c},$$

where ω_c is the cutoff frequency for the smooth exponential cutoff of the effective phonon density of states $\rho(\omega)$, and $\omega_d := c/d$ (c is the speed of sound and d the distance between the two wave function centers in the right and the left dot). Throughout the numerical calculations, the approximate form of the function $\rho(\omega)$, Eq.(1.87), is used.

Numerically, it is of advantage to separate the $T=0$ contribution of $\Phi(t)$, which can be calculated analytically, from the $T>0$ contribution: We write

$$\Phi(t) \;=\; \Phi_0(t)+\Phi_1(t)+\Phi_{T0}(t)+\Phi_{T1}(t)$$

$$\Phi_{0/1}(t) \;=\; \int_0^\infty d\omega\,\rho_{0/1}(\omega)\left\{1-\cos\omega t+i\sin\omega t\right\}$$

$$\Phi_{T0/T1}(t) \;=\; \int_0^\infty d\omega\,\rho_{0/1}(\omega)\left\{(1-\cos\omega t)\right.$$

$$\times \;\; \left.[\coth(\beta\omega/2)-1]\right\}. \tag{A.2}$$

For the function $\Phi_0(t)$, we find

$$e^{-\Phi_0(t)} = (1 + (\omega_c t)^2)^{-g/2} e^{-ig \arctan(\omega_c t)}. \tag{A.3}$$

For the function $\Phi_1(t)$, we find

$$
\begin{aligned}
\Phi_1(t) &= g\frac{\omega_d}{\omega_c}\left[2f\left(\omega_c t, \frac{\omega_c}{\omega_d}\right) + ig\left(\omega_c t, \frac{\omega_c}{\omega_d}\right)\right] \\
f(x,y) &:= \frac{1}{8}\left\{y\ln\left[\frac{(1+(x+y)^2)(1+(x-y)^2)}{(1+y^2)^2}\right]\right. \\
&\quad + x\ln\left[\frac{1+(x+y)^2}{1+(x-y)^2}\right] \\
&\quad + 2\arctan(x+y) + 2\arctan(y-x) \\
&\quad \left.- 4\arctan(y)\ \right\} \\
g(x,y) &:= \frac{1}{2}\left\{\frac{1}{2}\ln\left[\frac{1+(x+y)^2}{1+(x-y)^2}\right]\right. \\
&\quad + (x+y)\arctan(x+y) \\
&\quad \left.- (y-x)\arctan(y-x)\ \right\}. \tag{A.4}
\end{aligned}
$$

For $\Phi_{T0}(t)$, we find

$$\Phi_{T0}(t) = -2g\ln\left|\frac{\Gamma\left(1 + \frac{1}{\beta\omega_c} + i\frac{t}{\beta}\right)}{\Gamma\left(1 + \frac{1}{\beta\omega_c}\right)}\right|. \tag{A.5}$$

Summarizing, we have

$$
\begin{aligned}
C_\varepsilon &:= \lim_{\delta\to 0}\int_0^\infty dt\,\exp\left\{i[(\varepsilon + i\delta)t - g\arctan(\omega_c t)]\right\} \\
&\times\ \exp\left\{\Phi_1(t)\right\}(1 + (\omega_c t)^2)^{-g/2} \\
&\times\ \left|\frac{\Gamma\left(1 + \frac{1}{\beta\omega_c} + i\frac{t}{\beta}\right)}{\Gamma\left(1 + \frac{1}{\beta\omega_c}\right)}\right|^{2g}\exp\left\{-\Phi_{T1}(t)\right\}. \tag{A.6}
\end{aligned}
$$

This form is convenient for the final numerical evaluation of the function C_ε. It is useful to take advantage of special routines for integrals over the semi-infinite, positive real axis with weight functions sin and cos. Eq. (A.6) is already in a form so that one can directly apply these routines.

A.2 Relation to the spin–boson model

The spin–boson model is a generic model for the description of dissipation in two–level systems [101, 102]. Without coupling to the electron reservoirs, the double dot in presence of phonons can be described by the generic spin–boson Hamiltonian: We introduce the operators

$$
\begin{aligned}
J_z &:= \frac{1}{2}(n_L - n_R) = \frac{1}{2}\begin{pmatrix} 1 & 0 \\ 0 & -1 \end{pmatrix} \\
J_- &:= |R\rangle\langle L| = \begin{pmatrix} 0 & 0 \\ 1 & 0 \end{pmatrix} \\
J_+ &:= |L\rangle\langle R| = \begin{pmatrix} 0 & 1 \\ 0 & 0 \end{pmatrix} \\
J_x &:= \frac{1}{2}(J_+ + J_-), \quad J_y := \frac{1}{2i}(J_+ - J_-),
\end{aligned}
\tag{A.7}
$$

where we used the representation of the two states as

$$
|R\rangle = \begin{pmatrix} 0 \\ 1 \end{pmatrix}, |L\rangle = \begin{pmatrix} 1 \\ 0 \end{pmatrix}.
\tag{A.8}
$$

Note the factor $1/2$ in the definition of J_z which we used to be consistent with the definition of the higher angular momentum operators used in the superradiance literature and in chapter 2. In particular, the relation of the spin $1/2$ matrices J_z, J_x, and J_y to the Pauli matrices is

$$
J_i = \frac{1}{2}\sigma_i, \quad i = x, y, z
\tag{A.9}
$$

Using these definitions, we can re–write the Hamiltonian Eq.(1.17),(1.18) as

$$
\begin{aligned}
H_d \equiv &= \varepsilon_L n_L + \varepsilon_R n_R + T_c(p + p^\dagger) \\
&= \frac{1}{2}(\varepsilon_L + \varepsilon_R) + (\varepsilon_L - \varepsilon_R)J_z + 2T_c J_x \\
H_{\alpha\beta} &= \sum_{\mathbf{Q}} (\alpha_{\mathbf{Q}} n_L + \beta_{\mathbf{Q}} n_R)\left(a_{-\mathbf{Q}} + a_{\mathbf{Q}}^\dagger\right) \\
&= J_z \sum_{\mathbf{Q}} (\alpha_{\mathbf{Q}} - \beta_{\mathbf{Q}})\left(a_{-\mathbf{Q}} + a_{\mathbf{Q}}^\dagger\right) \\
&+ \frac{1}{2}\sum_{\mathbf{Q}} (\alpha_{\mathbf{Q}} + \beta_{\mathbf{Q}})\left(a_{-\mathbf{Q}} + a_{\mathbf{Q}}^\dagger\right).
\end{aligned}
\tag{A.10}
$$

The term $(1/2)(\varepsilon_L + \varepsilon_R)$ is a constant and can be omitted. The last term of $H_{\alpha\beta}$ can be eliminated by shifting the phonon operators according to $a_{\mathbf{Q}} \to b_{\mathbf{Q}} := a_{\mathbf{Q}} - (\alpha_{\mathbf{Q}} + \beta_{\mathbf{Q}})/\omega_{\mathbf{Q}}$. This leads to a phonon Hamiltonian $H_p = \sum_{\mathbf{Q}} \omega_{\mathbf{Q}} b_{\mathbf{Q}}^{\dagger} b_{\mathbf{Q}} - \sum_{\mathbf{Q}} |(\alpha_{\mathbf{Q}} + \beta_{\mathbf{Q}})/\omega_{\mathbf{Q}}|^2$, and an additional energy $-J_z \sum_{\mathbf{Q}} (\alpha_{\mathbf{Q}} - \beta_{\mathbf{Q}})(\alpha_{\mathbf{Q}}^* + \beta_{\mathbf{Q}}^*)/\omega_{\mathbf{Q}}$. The latter is a mere renormalization of the energy variable $\varepsilon = \varepsilon_L - \varepsilon_R$. Therefore, the Hamiltonian for the coupling of the double dot to the phonons, Eq.(A.10), can be written as

$$
\begin{aligned}
H & := & \varepsilon J_z + 2 T_c J_x + J_z \sum_{\mathbf{Q}} (\alpha_{\mathbf{Q}} - \beta_{\mathbf{Q}}) \left(a_{-\mathbf{Q}} + a_{\mathbf{Q}}^{\dagger} \right) \\
& + & \sum_{\mathbf{Q}} \omega_{\mathbf{Q}} a_{\mathbf{Q}}^{\dagger} a_{\mathbf{Q}},
\end{aligned} \tag{A.11}
$$

where for simplicity we used the same symbols for the renormalized energy ε and the shifted phonon operators, and omitted the constant energy shifts.

This can be compared to the spin–boson Hamiltonian [101]

$$
\begin{aligned}
H_{SB} & = & -\frac{1}{2} \Delta \sigma_x + \frac{1}{2} \varepsilon \sigma_z + \sum_{\alpha} \left(\frac{1}{2} m_{\alpha} \omega_{\alpha}^2 x_{\alpha}^2 + p_{\alpha}^2 / 2 m_{\alpha}^2 \right) \\
& + & \frac{1}{2} q_0 \sigma_z \sum_{\alpha} C_{\alpha} x_{\alpha},
\end{aligned} \tag{A.12}
$$

where $x_{\alpha}, p_{\alpha}, m_{\alpha}$, and ω_{α} are, respectively, the coordinate, momentum, mass, and frequency of the α's harmonic oscillator coupled to the two–level system via the last term in Eq.(A.12).

The bias ε in the spin–boson model is the difference ε between left and right dot energies. Furthermore, the bare tunneling matrix element $\Delta = -2 T_c$ with T_c the coupling between the two dots. The spectral function of the spin–boson model

$$
J(\omega) = \frac{\pi}{2} \sum_{\alpha} \frac{C_{\alpha}^2}{m_{\alpha} \omega} \delta(\omega - \omega_{\alpha}) \tag{A.13}
$$

is proportional to our effective electron–phonon coupling function $\rho(\omega)$,

$$
\rho(\omega) = \sum_{\mathbf{Q}} \frac{|\alpha_{\mathbf{Q}} - \beta_{\mathbf{Q}}|^2}{\hbar^2 \omega^2} \delta(\omega - \omega_{\mathbf{Q}}), \tag{A.14}
$$

the latter being defined with one additional factor ω in the denominator.

B. THE DICKE EFFECT IN THE AC DRUDE CONDUCTIVITY

B.1 Memory function

The memory function formalism starts from the observation that it is better to perform an expansion of the inverse conductivity σ^{-1} rather than of σ itself. The reason is that $\sigma \sim \tau$, the transport time which (to lowest order) in turn is *inversely* proportional to the potential. Therefore, one introduces a memory function [180], which in the multichannel case becomes a matrix,

$$M(z) := z\chi(z)[\chi^0 - \chi(z)]^{-1}. \tag{B.1}$$

Solving for the matrix

$$\chi(z) = [z + M(z)]^{-1}M\chi^0 \tag{B.2}$$

and inserting into Eq. (6.5), with Eq. (6.7) one obtains

$$\sigma(z) = ie^2 \sum_{nm} \left([z + M]^{-1}\chi^0\right)_{nm}. \tag{B.3}$$

Note that M and χ^0 are matrices so that in the multichannel case a matrix inversion is required. The calculation is started by expanding Eq. (B.2) in terms of the memory matrix, $z\chi = M\chi^0 + \ldots$. Since M is calculated here only to second order in the scattering potential V_{nm}, the resulting expression for σ is only an approximation and, e.g., localization effects can not be described correctly. However, by calculating M rather then χ, a partial summation in the scattering potential (ladder diagrams) is already performed.

The equation of motion

$$z\langle\langle j_n; j_m\rangle\rangle_z = L_s\langle[j_n, j_m]\rangle + \langle\langle A_n; j_m\rangle\rangle_z, \quad A_n := [j_n, H], \tag{B.4}$$

together with $[j_n, j_m] = 0$ is used twice [180] to obtain an expression for M,

$$z(M\chi^0)_{nm} = \phi_{nm}(z) - \phi_{nm}(0), \quad \phi_{nm}(z) := \langle\langle A_n; A_m \rangle\rangle_z. \tag{B.5}$$

The matrix $M(z)$ has a spectral representation and can be decomposed into real and imaginary part, $M(\omega+i0) = M'(\omega)+iM''(\omega)$ with real matrices $M'(\omega) = -M'(\omega)$ and $M''(\omega) = M''(-\omega)$. For $\omega \to 0$, the real part $M'(0) = 0$. Consequently, in the DC limit $z = \omega + i0 \to 0 + i0$,

$$M(z)\chi^0 = \frac{\phi(z) - \phi(0)}{z} \to i\mathrm{Im} \left. \frac{\partial}{\partial\omega}\phi(\omega)\right|_{\omega=0} =: iL. \tag{B.6}$$

An expression for the ac conductivity can be obtained in the limit of frequencies z so small that the dependence of $M(z)$ on z can be neglected. In the limit of $\hbar\omega \ll \varepsilon$, the energy dependence of the scattering rates around the Fermi energy ε_F is assumed to be negligeable. In terms of the L–matrix, $\sigma(z)$ then can be written as

$$\sigma(z) = ie^2 \sum_{nm} \left(\chi^0[z\chi^0 + iL]^{-1}\chi^0\right)_{nm}. \tag{B.7}$$

The commutator A_n is easily obtained as

$$A_n = \frac{1}{L_s^2} \sum_{k,q,n'} \left[V_{nn'}(k,q)v_{nk}c_{nk}^+ c_{n'k+q} - V_{n'n}(k,q)v_{nk+q}c_{n'k}^+ c_{nk+q}\right]. \tag{B.8}$$

Calculation of the matrix elements $z(M(z)\chi^0)_{nm}$, Eq. (B.5), requires the correlation function matrix elements which we denote by

$$< n, n'; m, m' > := \langle\langle c_{nk}^+ c_{n'k+q}; c_{mk'}^+ c_{m'k'+q'}\rangle\rangle_z, \tag{B.9}$$

suppressing the indices k, k', q, q' which remain the same. This leads to

$$\begin{aligned}
\phi_{nm}(z) \quad = \quad & \frac{1}{L_s^4} \sum_{n'm'kk'qq'} [V_{nn'}(k,q)V_{mm'}(k'q')v_{nk}v_{mk'} < n, n'; m, m' > \\
- \quad & V_{nn'}(k,q) \quad V_{m'm}(k'q')v_{nk} \quad v_{mk'+q'} < n, n'; m', m > \\
- \quad & V_{n'n}(k,q) \quad V_{mm'}(k'q')v_{nk+q}v_{mk'} \quad\quad < n', n; m, m' > \\
+ \quad & V_{n'n}(k,q) \quad V_{m'm}(k'q')v_{nk+q}v_{mk'+q'} < n', n; m', m >].
\end{aligned} \tag{B.10}$$

The above equations constitute the general framework for the calculation of the conductivity in a multichannel system. To second order in the potential scattering, they are still completely general.

For non–interacting electrons, one has

$$
\begin{aligned}
< n, n'; m, m' > \;\; &= \;\; \delta_{q,-q'}\delta_{k',k+q}\delta_{nm'}\delta_{n'm}L_s\varphi_{nm}(z) \\
\varphi_{nm}(z) \;\; &:= \;\; \frac{f(\varepsilon_{nk}) - f(\varepsilon_{mk+q})}{z + \varepsilon_{nk} - \varepsilon_{mk+q}},
\end{aligned}
\tag{B.11}
$$

where we again suppressed the indices k and $k + q$. One obtains from Eq. (B.11) and Eq. (B.10)

$$
\begin{aligned}
\phi_{nm}(z) \;\; = \;\; & \frac{1}{L_s^3}\sum_{kq}|V_{nm}(q)|^2 \left[v_{nk}v_{mk+q}\varphi_{nm}(z) + v_{nk+q}v_{mk}\varphi_{mn}(z)\right] \quad \text{(B.12)} \\
& -\; \delta_{nm}\frac{1}{L_s^3}\sum_{kqn'}|V_{nn'}(q)|^2 \left[v_{nk}v_{mk}\varphi_{nn'}(z) + v_{nk+q}v_{mk+q}\varphi_{n'n}(z)\right].
\end{aligned}
$$

In the limit of temperatures $k_B T, \hbar\omega \ll \varepsilon_F$, one has

$$
\begin{aligned}
-\mathrm{Im}\,\varphi_{nm}(\omega) \;\; = \;\; & \frac{\pi\omega}{v_n v_m}\left[\; \delta(k - k_n)\left\{\delta(q + k_n - k_m) + \delta(q + k_n + k_m)\right\} \right. \\
& \left. +\; \delta(k + k_n)\left\{\delta(q - k_n - k_m) + \delta(q - k_n + k_m)\right\}\right]. \quad \text{(B.13)}
\end{aligned}
$$

This leads to

$$
\begin{aligned}
-\mathrm{Im}\,\phi_{nm}(\omega) \;\; = \;\; & s\frac{4\pi\omega}{(2\pi)^2 L_s}\left(|V_{nm}(k_n - k_m)|^2 - |V_{nm}(k_n + k_m)|^2\right) \quad \text{(B.14)} \\
& -\; \delta_{nm}\sum_{n'}s\frac{4\pi\omega}{(2\pi)^2 L_s}\frac{v_n}{v_{n'}}\left(|V_{nn'}(k_n - k_{n'})|^2 + |V_{nn'}(k_n + k_{n'})|^2\right),
\end{aligned}
$$

where $s = 1$ or $s = 2$ is the spin degeneracy. Using Eq. (6.7) and Eq. (B.6), the matrix L thus is

$$
L_{nm} \;\; = \;\; \frac{s}{\pi L_s}\left(|V_{nm}(k_n + k_m)|^2 - |V_{nm}(k_n - k_m)|^2\right), \quad n \neq m \tag{B.15}
$$

$$
L_{nn} \;\; = \;\; \frac{s}{\pi L_s}\left[\sum_{n'\neq n}\frac{v_n}{v_{n'}}\left(|V_{nn'}(k_n - k_{n'})|^2 + |V_{nn'}(k_n + k_{n'})|^2\right) + 2|V_{nn}(2k_n)|^2\right].
$$

B.2 Potential scattering matrix elements

The momentum matrix element

$$
\langle nk|e^{-i\mathbf{qx}}|n'k'\rangle = \delta_{k,k'+q_x}M_{nn'}^{q_x}(q_y) \tag{B.16}
$$

reflects momentum conservation in x–direction. The matrix elements M can be calculated exactly, their explicit expressions for $n = 0, 1$ are

$$
\begin{aligned}
|M_{00}^{q_x}(q_y)|^2 &= e^{-\frac{1}{2}(\xi^2+\eta^2)} \\
|M_{10}^{q_x}(q_y)|^2 &= e^{-\frac{1}{2}(\xi^2+\eta^2)}\frac{1}{2}\left[\xi^2 + \eta^2\right] \\
|M_{11}^{q_x}(q_y)|^2 &= e^{-\frac{1}{2}(\xi^2+\eta^2)}\left[1 - \frac{1}{2}(\xi^2 + \eta^2)\right]^2 \\
\xi &= l_B\alpha q_x, \quad \eta = l_B q_y,
\end{aligned}
\tag{B.17}
$$

where we introduced the effective magnetic length l_B, the cyclotron frequency ω_B, and the parameter α according to

$$
\alpha := \frac{\omega_c}{\omega_B}, \quad \omega_c := \frac{eB}{m^*c}, \quad \omega_B := \sqrt{\omega_0^2 + \omega_c^2}, \quad l_B := \sqrt{\frac{\hbar}{m^*\omega_B}}.
\tag{B.18}
$$

B.2.1 Delta scatterers

The matrix elements Eq. (6.11) can be evaluated explicitely for Delta–scatterers with $u(\mathbf{q})$ independent of $\mathbf{q}$. In this case,

$$
|u\left(\mathbf{q} = (k - k', q_y)\right)|^2 =: V_0^2,
\tag{B.19}
$$

The remaining sum $(1/L_s)\sum_{q_y}|M_{nn'}^{q_x}(q_y)|^2$ can be transformed into an integral and yields the result

$$
\begin{aligned}
\overline{|V_{00}(q)|^2} &= \frac{n_i V_0^2 L_s}{\sqrt{2\pi l_B^2}}e^{-\frac{1}{2}(l_B\alpha q)^2} \\
\overline{|V_{10}(q)|^2} &= \overline{|V_{00}(q)|^2}\frac{1}{2}\left[1 + (l_B\alpha q)^2\right] \\
\overline{|V_{11}(q)|^2} &= \overline{|V_{00}(q)|^2}\left[\frac{3}{4} - \frac{1}{2}(l_B\alpha q)^2 + \frac{1}{4}(l_B\alpha q)^4\right]
\end{aligned}
\tag{B.20}
$$

B.2.2 Explicit expression for $\sigma(z)$

The energy bandstructure of a quantum wire with parabolic confinement potential of strength $\hbar\omega_0$ in a perpendicular magnetic field B is

$$
\varepsilon_{nk} = \left(n + \frac{1}{2}\right)\hbar\omega_B + \gamma_B\frac{\hbar^2}{2m^*}k^2, \quad \gamma_B = \left(\frac{\omega_0}{\omega_B}\right)^2 = \frac{1}{1 + \left(\frac{\omega_c}{\omega_0}\right)^2},
\tag{B.21}
$$

i.e. a set of equidistant parabolas, labeled by the Landau band index n.

We fix the Fermi energy between the subbands $n = 1$ and $n = 2$, i.e. $\varepsilon_F = 2\hbar\omega_B$. The two subband Fermi wave vectors then become

$$
\begin{aligned}
k_0 &= \sqrt{\frac{2m^*}{\gamma_B\hbar^2}\left(\varepsilon_F - \frac{1}{2}\hbar\omega_B\right)} = \sqrt{\frac{3}{2}}\left(\frac{\omega_B}{\omega_0}\right)^{3/2} k_{F0} \\
k_1 &= \sqrt{\frac{2m^*}{\gamma_B\hbar^2}\left(\varepsilon_F - \frac{3}{2}\hbar\omega_B\right)} = \sqrt{\frac{1}{2}}\left(\frac{\omega_B}{\omega_0}\right)^{3/2} k_{F0} \\
k_{F0} &:= \sqrt{\frac{2m^*\omega_0}{\hbar}}.
\end{aligned}
\tag{B.22}
$$

Reckognizing that

$$
(l_B\alpha)^2 \left(\frac{\omega_B}{\omega_0}\right)^3 k_{F0}^2 = 2\left(\frac{\omega_c}{\omega_0}\right)^2,
\tag{B.23}
$$

the arguments $l_B\alpha q$ in the matrix elements become

$$
\begin{aligned}
(l_B\alpha q)^2 &=
\begin{cases}
\beta[\sqrt{3} + 1]^2, & q = k_0 + k_1 \\
\beta[\sqrt{3} - 1]^2, & q = k_0 - k_1 \\
\beta[2]^2, & q = 2k_0 \\
\beta[2\sqrt{3}]^2, & q = 2k_1
\end{cases} \\
\beta &:= \left(\frac{\omega_c}{\omega_0}\right)^2
\end{aligned}
\tag{B.24}
$$

for the four cases of intraband backscattering $q = 2k_0, 2k_1$, interband backward ($q = k_0 - k_1$) and interband forward scattering ($q = k_0 + k_1$).

The dependence on the magnetic field can be completely absorbed into the parameter β. We express the scattering matrix elements by the scattering rate τ^{-1} without magnetic field,

$$
\tau^{-1} := \frac{n_i^{2D}V_0^2}{\sqrt{2\pi l_0^2}v_{F_0}\hbar^2} = \frac{n_i V_0^2 m^*}{\sqrt{4\pi}\hbar^3}
\tag{B.25}
$$

with $v_{F_0} := \hbar k_{F0}/m^*$ and $l_0 = \sqrt{\hbar/m^*\omega_0}$. Then, one has $l_B = l_0(1 + \beta)^{-1/4}$,

and the conductivity can be written as

$$
\begin{aligned}
\sigma(z) \;=\; & ie^2 \frac{s}{\pi} v_{F0}\tau(1+\beta)^{-1/4} \\[4pt]
& \times \; \frac{z\tau\left(\sqrt{\tfrac{3}{2}}+\sqrt{\tfrac{1}{2}}\right)+i\left[\sqrt{3}\tilde{L}_{11}+\frac{1}{\sqrt{3}}\tilde{L}_{00}-2\tilde{L}_{01}\right]}{\left[z\tau+i\sqrt{\tfrac{2}{3}}\tilde{L}_{00}\right]\left[z\tau+i\sqrt{\tfrac{1}{2}}\tilde{L}_{11}\right]+\frac{2}{\sqrt{3}}\tilde{L}_{01}^2}
\end{aligned}
$$

$$
\tilde{L}_{00} \;:=\; \sqrt{1+\beta}\left\{\frac{\sqrt{3}}{2}\sum_{\sigma=\pm1}\left\{\left(1+\left[1+\sigma\sqrt{3}\right]^2\beta\right)e^{-\frac{1}{2}\beta[1+\sigma\sqrt{3}]^2}\right\}+2e^{-6\beta}\right\}
$$

$$
\tilde{L}_{11} \;:=\; \sqrt{1+\beta}\left\{\frac{1}{2\sqrt{3}}\sum_{\sigma=\pm1}\left\{\left(1+\left[1+\sigma\sqrt{3}\right]^2\beta\right)e^{-\frac{1}{2}\beta[1+\sigma\sqrt{3}]^2}\right\}\right\}
$$

$$
\qquad+\; 2\sqrt{1+\beta}\left(\frac{3}{4}-2\beta+4\beta^2\right)e^{-2\beta}
$$

$$
\tilde{L}_{01} \;:=\; \sqrt{1+\beta}\,\frac{1}{2}\sum_{\sigma=\pm1}\left\{\sigma\left(1+\left[1+\sigma\sqrt{3}\right]^2\beta\right)e^{-\frac{1}{2}\beta[1+\sigma\sqrt{3}]^2}\right\}, \qquad \text{(B.26)}
$$

where we used Eq.(6.10),(B.24),

$$
\frac{n_i V_0^2}{\sqrt{2\pi l_B^2}} = v_{F_0}\tau^{-1}\frac{l_0}{l_B} = v_{F_0}\tau^{-1}(1+\beta)^{\frac{1}{4}}, \qquad \text{(B.27)}
$$

and dimensionless functions $\tilde{L}_{00}=\pi L_{00}/(sv_{F_0}\tau^{-1})$ etc.

The Fermi velocities v_0 and v_1 can be expressed by the Fermi velocity v_{F_0} as

$$
v_0 = v_{F_0}\sqrt{\frac{3}{2}}(1+\beta)^{-\frac{1}{4}}, \quad v_1 = v_{F_0}\sqrt{\frac{1}{2}}(1+\beta)^{-\frac{1}{4}}. \qquad \text{(B.28)}
$$

BIBLIOGRAPHY

[1] K. von Klitzing, G. Dorda, and M. Pepper, Phys. Rev. Lett. **45**, 494 (1980).

[2] (Ed.) B. Kramer, *Quantum Coherence in Mesoscopic Systems*, Vol. 254 of *NATO ASI Series B* (Plenum Press, New York, 1991).

[3] (Ed.) H. Cerdeira, B. Kramer, and G. Schön, *Quantum Dynamics of Submicron Structures*, Vol. 291 of *NATO ASI Ser. E* (Kluwer Academic Publishers, Dordrecht, 1994).

[4] (Ed.) B. Kramer, *Quantum Transport in Semiconductor Submicron Structures*, Vol. 326 of *NATO ASI Ser. E* (Kluwer Academic Publishers, Dordrecht, 1996).

[5] T. Dittrich, P. Hänggi, G.L. Ingold, B. Kramer, G. Schön, W. Zwerger, *Quantum Transport and Dissipation* (Wiley-VCH, Weinheim, 1997).

[6] D. Ferry and S. Goodnik, *Transport in Nanostructures* (Cambridge University Press, Cambridge, UK, 1997).

[7] S. Datta, *Electronic Transport in Mesoscopic Systems* (Cambridge University Press, Cambridge, 1997).

[8] Y. Imry, *Introduction to Mesoscopic Physics* (Oxford University Press, Oxford, 1997).

[9] G. Bastard, *Wave Mechanics applied to semiconductor heterostructures* (Les Editions de Physique, Les Ulis Cedex, France, 1988).

[10] (Ed.) H. Fukuyama and T. Ando, *Transport Phenomena in Mesoscopic Systems*, Vol. 109 of *Springer Series in Solid State Sciences* (Springer-Verlag, Berlin, 1991), p. 53.

[11] (Ed.) B. Kramer and G. Bergmann and Y. Bruynseraede, *Localization, Interaction, and Transport Phenomena*, Vol. 61 of *Springer Series in Solid State Sciences* (Springer-Verlag, Berlin, 1985).

[12] For a review, see, e.g. : B. Kramer and A. MacKinnon, Rep. Prog. Phys. **56**, 1469 (1994).

[13] T. Chakraborty and P. Pietiläinen, *The Fractional Quantum Hall Effect*, 2 ed. (Springer, Berlin, 1995).

[14] M. Janssen, O. Viehweger, and U. Fastenrath and J. Hajdu, *Introduction to the Theory of the Integer Quantum Hall Effect* (VCH, Weinheim, 1995).

[15] R. Landauer, Philos. Mag. **21**, 863 (1970).

[16] M. Büttiker, Phys. Rev. Lett. **57**, 1761 (1986).

[17] B. J. van Wees, H. Van Houten, C. W. J. Beenacker, J. G. Williamson, L. P. Kouwenhoven, D. van der Marel, and C. T. Foxon, Phys. Rev. Lett. **60**, 848 (1988).

[18] D. Wharam, T. J. Thornton, R. Newbury, M. Pepper, H. Ahmed, J. E. F. Frost, D. G. Husko, D. C. Peacock, D. A. Ritchie, and G. A. C. Jones, J. Phys. **C 21**, 209 (1988).

[19] D. Y. Sharvin and Y. V. Sharvin, JETP Letters **34**, 272 (1981).

[20] M. A. Kastner, Rev. Mod. Phys. **64**, 849 (1992).

[21] R. C. Ashoori, Nature **379**, 413 (1996).

[22] M. Devoret and C. Glattli, Phys. World **September**, 29 (1998).

[23] L. P. Kouwenhoven, T. H. Oosterkamp, M. W. S. Danoesastro, M. Eto, D. G. Austing, T. Honda, and S. Tarucha, Science **278**, 1788 (1997).

[24] L. Kouwenhoven and C. Marcus, Phys. World **June**, 35 (1998).

[25] T. Heinzel, S. Manus, D. A. Wharam , J. P. Kotthaus, G. Böhm, W. Klein, G. Tränkle, and G. Weimann, Europhys. Lett. **26**, 689 (1994).

[26] T. Heinzel, D. A. Wharam, J. P. Kotthaus, G. Böhm, W. Klein, G. Tränkle, and G. Weimann, Phys. Rev. B **50**, 15113 (1994).

[27] R. H. Blick, D. W. van der Weide, R. J. haug, and K. Eberl, Phys. Rev. Lett. **81**, 689 (1998).

[28] R. H. Blick, D. Pfannkuche, R. J. Haug, K. v. Klitzing, and K. Eberl, Phys. Rev. Lett. **80**, 4032 (1998).

[29] T. Fujisawa and S. Tarucha, Superlatt. Microstr. **21**, 247 (1997).

[30] T. Fujisawa, T. H. Oosterkamp, W. G. van der Wiel, B. W. Broer, R. Aguado, S. Tarucha, and L. P. Kouwenhoven, Science **282**, 932 (1998).

[31] K. A. Matveev, L. I. Glazman, and H. U. Baranger, Surf. Scie. **361**, 623 (1996).

[32] (Ed.) H. Grabert and M. H. Devoret, *Single Charge Tunneling*, Vol. 294 of *NATO ASI Series B* (Plenum Press, New York, 1991).

[33] S. Tomonaga, Prog. Theor. Phys. **5**, 544 (1950).

[34] J. Sólyom, Adv. Phys. **28**, 201 (1979).

[35] V. M. Agranovich and A. A. M. (editors), *Electron–electron interactions in disordered systems* (North Holland, Amsterdam, 1985).

[36] C. L. Kane and M. P. A. Fisher, Phys. Rev. Lett. **68**, 1220 (1992).

[37] A. Furusaki and N. Nagaosa, Phys. Rev. B **47**, 4631 (1993).

[38] J. Voit, Rep. Progr. Phys. **58**, 977 (1995).

[39] B. Altshuler, A. Aronov, and D. Khmel'nitskii, Solid State Comm. **39**, 619 (1981).

[40] B. Altshuler, A. Aronov, and D. Khmel'nitskii, J. Phys. C **15**, 7367 (1982).

[41] H. Fukuyama and E. Abrahams, Phys. Rev. B **27**, 5976 (1983).

[42] W. Eiler, Journal of Low Temperature Physics **56**, 481 (1984).

[43] W. H. Zurek, Physics Today **October**, 36 (1991).

[44] P. Mohanty, E. Jariwala, and R. A. Webb, Phys. Rev. Lett. **78**, 3366 (1997).

[45] B. L. Altshuler, M. E. Gershenson, and I. L. Aleiner, Physica E **3**, 58 (1998).

[46] D. S. Golubev, A. D. Zaikin, Phys. Rev. B **59**, 91995 (1999).

[47] A. B. Gougam, F. Pierre, H. Potier, D. Esteve, and N. O. Birge, preprint, cond-mat/9912137 (1999).

[48] A. Zawadowski, J. von Delft, and D. C. Ralph, Phys. Rev. Lett. **83**, 2632 (1999).

[49] *Interactions and Transport in lower dimensional systems*, *Lecture notes in physics*, edited by T. Brandes (Springer, Heidelberg, to appear 2000).

[50] H. Haug and A.-P. Jauho, *Quantum Kinetics in Transport and Optics of Semiconductors*, Vol. 123 of *Solid-State Sciences* (Springer, Berlin, 1996).

[51] H. Haug and S. Koch, *Quantum Theory of the optical and electronic properties of semiconductors* (World Scientific, Singapore, 1990).

[52] R. H. Dicke, Phys. Rev. **93**, 99 (1954).

[53] R. H. Dicke, Phys. Rev. **89**, 472 (1953).

[54] A. Einstein, Annalen der Physik **17**, 145 (1905).

[55] A. Einstein, Phys. Z. **18**, 121 (1917).

[56] L. de Broglie, Ann. d. Phys. sér. 10 **2** (1925); "Licht und Materie" (Goverts, Hamburg 1944) .

[57] D. R. Stewart, D. Sprinzak, C. M. Marcus, C. I. Duruöz, and J. S. Harris Jr., Science **278**, 1784 (1997).

[58] W. Becken, P. Schmelcher, and F. Diakonos, J. Phys. **B 32**, 1557 (1999); S. Jordan, P. Schmelcher, W. Becken, and W. Schweizer, Astron. u. Astrophys. **336**, L33 8 (1998); see also *Physikalische Blätter* **55,11**, 59 (1999) (in German).

[59] U. Merkt, J. Huser, and M. Wagner, Phys. Rev. B **43**, 7320 (1991).

[60] D. Pfannkuche and R. R. Gerhardts, Phys. Rev. B **44**, 13132 (1991).

[61] U. Meirav, M. A. Kastner, and S. J. Wind, Phys. Rev. Lett. **65**, 771 (1990).

[62] Y. Meir, N. S. Wingreen, and P. A. Lee, Phys. Rev. Lett. **66**, 3048 (1991).

[63] D. Weinmann, Ph.D. thesis, Univ. Hamburg, Germany, 1994.

[64] P. A. M. Dirac, Proc. Roy. Soc. A **114**, 243 (1927).

[65] V. Weisskopf and E. Wigner, Z. Phys. **63**, 54 (1930).

[66] V. Weisskopf and E. Wigner, Z. Phys. **65**, 18 (1930).

[67] D. F. Walls and G. J. Milburn, *Quantum Optics* (Springer, Berlin, 1994).

[68] R. G. DeVoe and R. G. Brewer, Phys. Rev. Lett. **76**, 2049 (1996).

[69] C. A. Stafford, R. Kotlyar, and S. Das Sarma, Phys. Rev. B **58**, 7091 (1998).

[70] Ph. Brune, C. Bruder, and H. Schoeller, Phys. Rev. B **56**, 4730 (1997).

[71] S. M. Girvin, L. I. Glazman, M. Jonson, D. R. Penn, and M. D. Stiles, Phys. Rev. Lett. **64**, 3183 (1990).

[72] G.-L. Ingold and Y. V. Nazarov, in *Single Charge Tunneling*, Vol. 294 of *NATO ASI Series B*, edited by H. Grabert and M. H. Devoret (Plenum Press, New York, 1991), p. 21.

[73] M. G. Benedict, A. M. Ermolaev, V. A. Malyshev, I. V. Sokolov, and E. D. Trifonov, *Super–Radiance*, *Optics and Optoelectronics Series* (Institute of Physics, Bristol, 1996).

[74] G. S. Argawal, *Quantum Statistical Theories of Spontaneous Emission* (Springer, Berlin, 1974), Vol. 70.

[75] M. Gross, S. Haroche, Phys. Rep. **93**, 301, Chapter 2.6 (1982).

[76] M. G. Benedict, A. M. Ermolaev, V. A. Malyshev, I. V. Sokolov, and E. D. Trifonov, in *Super–Radiance, Optics and Optoelectronics Series* (Institute of Physics, Bristol, 1996), Chap. 11.5.

[77] T. H. Stoof and Yu. V. Nazarov, Phys. Rev. B **53**, 1050 (1996).

[78] See M. Raikh, A. Asenov, Superlatt. Microstr. **11**, 325 (92), where the crossover to $V_{SD} > U_c$ shows up as a step in the I-V curve.

[79] R. E. Prange, Phys. Rev. **131**, 1083 (1964).

[80] J. Fransson, *'Tunneling and non–orthogonality'*, Licentiate Thesis, Uppsala University (1999).

[81] J. Fransson, O. Eriksson, B. Johansson, I. Sandalov, Physica B **272**, 28 (1999).

[82] L. I. Glazman and K. A. Matveev, Sov. Phys. JETP **67**, 1276 (1988).

[83] G. D. Mahan, *Many–Particle Physics* (Plenum Press, New York, 1990).

[84] L. I. Glazman and R. I. Shekter, Sov. Phys. JETP **67**, 163 (1988).

[85] N. S. Wingreen, K. W. Jacobsen, and J. W. Wilkins, Phys. Rev. Lett. **61**, 1396 (1988).

[86] D. V. Averin, Yu. V. Nazarov, in *Single Charge Tunneling*, Vol. 294 of *NATO ASI Series B*, edited by H. Grabert and M. H. Devoret (Plenum Press, New York, 1991), Chap. 6, p. 217.

[87] J. König, J. Schmid, H. Schoeller, and G. Schön, Phys. Rev. B **54**, 16820 (1996).

[88] J. König and H. Schoeller, Phys. Rev. Lett. **81**, 3511 (1998).

[89] T. Ivanov, Phys. Rev. B **59**, 169 (1999).

[90] P. Nordlander, M. Pustilnik, Y. Meir, N. S. Wingreen, D. C. Langreth, Phys. Rev. Lett. **83**, 808 (1999).

[91] T. Ivanov, Europhys. Lett. **40**, 183 (1997).

[92] R. Kotlyar and S. Das Sarma, Phys. Rev. B **56**, 13235 (1997).

[93] A. Georges and Y. Meir, Phys. Rev. Lett. **82**, 3508 (1999).

[94] H. Schoeller, in *Interactions and Transport in lower dimensional systems*, *Lecture notes in physics*, edited by T. Brandes (Springer, Heidelberg, to appear 2000).

[95] T. Ivanov, Phys. Rev. B **56**, 12339 (1997).

[96] R. López, R. Aguado, G. Platero, and C. Tejedor, Phys. Rev. Lett. **81**, 4688 (1998).

[97] A. Kaminski, Yu. V. Nazarov, and L. I. Glazman, Phys. Rev. Lett. **83**, 384 (1999).

[98] J. M. Elzerman, S. De Franceschi, D. Goldhaber–Gordon, W. G. van der Wiel, and L. P. Kouwenhoven, preprint, cond-mat/9912126 (1999).

[99] T. Brandes, Ph.D. thesis, University of Hamburg, Germany, PTB-Bericht 1994, ISBN 3-89429-556-2.

[100] G. M. Palma, K.-A. Suominen, A. K. Ekert, Proc. Roy. Soc. Lond. A **452**, 567 (1996).

[101] A. J. Leggett, S. Chakravarty, A. T. Dorsey and M. P. A. Fisher, A. Garg and W. Zwerger, Review of Modern Physics **59**, 1 (1987).

[102] U. Weiss, *Quantum Dissipative Systems*, Vol. 2 of *Series of Modern Condensed Matter Physics* (World Scientific, Singapore, 1993).

[103] J. Fricke, Annals of Physics **252**, 479 (1996).

[104] G. Doetsch, *Anleitung zum praktischen Gebrauch der Laplace-Transformation und der Z-Transformation* (Oldenbourg, München, 1989).

[105] V. F. Gantmakher and Y. B. Levinson, *Carrier Scattering in Metals and Semiconductors*, Vol. 19 of *Modern Problems in Condensed Matter Sciences* (North–Holland, Amsterdam, 1987).

[106] H. Bruus, K. Flensberg, and H. Smith, Phys. Rev. B **48**, 11144 (1993).

[107] T. Vorrath, PhD thesis (in preparation, University of Hamburg, Germany), unpublished.

[108] I. S. Gradshteyn and I. M. Ryzhik, *Table of Integrals, Series, and Products* (Academic Press, New York, 1980).

[109] Note that in [82], the expression (2.8) for the stationary current I reduces to $I = 4e\chi/2R = 2e\gamma$ ($\chi = 1$), if $R = 1/\Gamma_1 + 1/\Gamma_2 + 1/\gamma$ is replaced by $1/\gamma$, i.e. in the case where the inelastic tunneling rate γ is much smaller than the elastic rates $\Gamma_{1,2}$ for tunneling to/from the reservoirs.

[110] A. Knäbchen, Y. B. Levinson, and O. Entin-Wohlmann, Phys. Rev. B **54**, 10696 (1996).

[111] S. Simon, Phys. Rev. B **54**, 13878 (1996).

[112] T. Vorrath and T. Brandes, unpublished .

[113] F. D. M. Haldane, J. Phys. **C14**, 2585 (1981).

[114] S. Doniach and E. H. Sondheimer, *Green's Functions for Solid State Physicists, Frontiers in Physics* (W. A. Benjamin, Reading, Massachusetts, 1974).

[115] K. D. Schotte and U. Schotte, Phys. Rev. **182**, 479 (1969).

[116] See the book of Mahan [83], chapter 4.3.

[117] This duality between 'system' (here the hole) and the 'bath' (here the phonon system) has been extensively discussed in the context of dephasing and loss of interference in A. Stern, Y. Aharonov, and Y. Imry, Phys. Rev. **A 41**, 3436 (1990).

[118] D. F. Walls and G. J. Milburn, in *Quantum Optics* (Springer, Berlin, 1994), Chap. 2.8.

[119] Y. Levinson, preprint, cond-mat/9907055 (1999).

[120] Y. Levinson, Europhys. Lett. **39**, 299 (1997).

[121] A. Stern, Y. Aharonov, and Y. Imry, Phys. Rev. A **41**, 3436 (1990).

[122] W. Zwerger and T. Brandes, Z. Phys. B **87**, 89 (1992).

[123] R. Aguado and L. Kouwenhoven, preprint cond-mat/9905283.

[124] For a good introduction, see J. Preskill, Lecture Notes for Physics (California Institute of Technology, 1998), available at http://www.theory.caltech.edu/people/preskill/. See also the introductory material under http://www.qubit.org/.

[125] S. Debald, Master thesis (in preparation, University of Hamburg, Germany), unpublished.

[126] N. Bannov, V. Mitin, and M. .A .Stroscio, phys. stat. sol. (b) **183**, 131 (1994).

[127] N. Bannov, V. Aristov, V. Mitin, and M. A .Stroscio, Phys. Rev. B **51**, 9930 (1995).

[128] S. Debald and T. Brandes, unpublished .

[129] L. D. Landau and E. M. Lifshitz, *Theory of Elasticity*, Vol. 7 of *Landau and Lifshitz, Course of Theoretical Physics* (Pergamon Press, Oxford, 1970).

[130] Y. Lu, Y. Zhu, Y. Chen, S. Zhu, N. Ming, and Y. Feng, Science **284**, 1822 (1999).

[131] A. Andreev, V. Emel'yanov, and Y. A. Il'inski, *Cooperative Effects in Optics, Malvern Physics Series* (Institute of Physics, Bristol, 1993).

[132] J. H. Eberly, Am. J. Physics **40**, 1374 (1972).

[133] N. Skribanowitz, I. Herman, J. MacGillivray, and M. Feld, Phys. Rev. Lett. **30**, 309 (1973).

[134] See ref. [73] for references for the superradiance literature. .

[135] Ph. Cahuzac, H. Sontag, and P. E. Toschek, Opt. Comm. **31**, 37 (1979).

[136] There is, however, a recent interest in random lasing material and suggestions for cooperative emission (superradiance) in such systems, see [150].

[137] R. Bonifacio, P. Schwendimann, and F. Haake, Phys. Rev. A **4**, 302 (1971).

[138] R. Bonifacio, P. Schwendimann, and F. Haake, Phys. Rev. A **4**, 854 (1971).

[139] T. Tokihiro, Y. Manabe, and E. Hanamura, Phys. Rev. B **47**, 2019 (1993).

[140] T. Tokihiro, Y. Manabe, and E. Hanamura, Phys. Rev. B **51**, 7655 (1995).

[141] M. Gross, S. Haroche, Phys. Rep. **93**, 301 (1982).

[142] For a short recent review see, e.g., F. Rossi, Semicond. Sci. Technol. **13**, 147 (1998).

[143] T. Stroucken, A. Knorr, P. Thomas, and S. W. Koch, Phys. Rev. B **53**, 2026 (1996).

[144] S. Haas, T. Stroucken, M. Hübner, J. Kuhl, B. Grote, A. Knorr, F. Jahnke, S. W. Koch, R. Hey, K. Ploog, Phys. Rev. B **57**, 14860 (1998).

[145] T. Stroucken, S. Haas, B. Grote, S. W. Koch, M. Hübner, D. Ammerlahn, J. Kuhl, in *Festkörperprobleme–Advances in Solid State Physics*, edited by B. Kramer (Vieweg, Braunschweig, 1998), Vol. 38, p. 265.

[146] J. Kuhl, M. Hübner, D. Ammerlahn, T. Stroucken, B. Grote, S. Haas, S. W. Koch, G. Kitrova, H. M. Gibbs, R. Hey, and K. Ploog, in *Festkörperprobleme–Advances in Solid State Physics*, edited by B. Kramer (Vieweg, Braunschweig, 1998), Vol. 38, p. 281.

[147] H. Giessen, A. Knorr, S. Haas, S. W. Koch, S. Linden, J. Kuhl, M. Hetterich, M. Grün, C. Klingshirn, Phys. Rev. Lett. **81**, 4260 (1998).

[148] T. V. Shahbazyan and M. E. Raikh, Phys. Rev. B **49**, 17123 (1994).

[149] T. V. Shahbazyan and S. E. Ulloa, Phys. Rev. B **57**, 6642 (1998).

[150] T. V. Shahbazyan, M. E. Raikh, and Z. V. Vardeny, preprint, cond-mat/9903255 (1999).

[151] D. Braun, P. A. Braun and F. Haake, Physica D **131**, 265 (1999).

[152] P. A. Braun, D. Braun, F. Haake, and J. Weber, Europ.Phys.Journ. **D 2**, 165 (1998).

[153] P. A. Braun, D. Braun, and F. Haake, Europ.Phys.Journ. **D 3**, 1 (1998).

[154] F. Haake, *Quantum Signatures of Chaos* (Springer, New York, 1991).

[155] F. T. Arecchi, E. Courtens, R. Gilmore, and H. Thomas, Phys. Rev. A **6**, 2211 (1972).

[156] M. Abramowitz and A. Stegun, *Handbook of mathematical functions* (Dover Publications, New York, 1972).

[157] D. Weinmann, W. Häusler, and B. Kramer, Phys. Rev. Lett. **74**, 984 (1995).

[158] K. Jauregui, W. Häusler, D. Weinmann, B. Kramer, Phys. Rev. B **53**, R1713 (1996).

[159] R. Bonifacio and G. Preparata, Phys. Rev. A **2**, 336 (1970).

[160] H. Steudel and I. Leonhardt, Opt. Comm. **107**, 88 (1994).

[161] L. D. Landau and E. M. Lifshitz, *Quantum Mechanics*, Vol. 3 of *Landau and Lifshitz, Course of Theoretical Physics* (Pergamon Press, Oxford, 1965).

[162] J. Faist, F. Capasso, D. .L. Sivco, C. Sirtori, A. L. Hutchinson, and A. Y. Cho, Science **264**, 553 (1994).

[163] J. Faist, F. Capasso, C. Sirtori, D. .L. Sivco, A. L. Hutchinson, and A. Y. Cho, Appl. Phys. Lett. **66**, 538 (1995).

[164] A. A. Belyanin, V. V. Kocharovsky, and Vl. V. Kocharovsky, Solid State Comm. **80**, 243 (1991); Laser Physics **2**, 952 (1992).

[165] J. M. Luttinger, W. Kohn, Phys. Rev. **97**, 869 (1955); L. Roth, B. Lax, and S. Zwerdling, Phys. Rev. **114**, 90 (1959).

[166] C. Kittel, *Quantum Theory of Solids* (John Wiley, New York, 1963).

[167] A. Shimizu in: *Mesoscopic Physics and Electronics*, Ed. T. Ando, H. Nakashima, and S. Komiyama (Springer, Berlin 1998). .

[168] T. Brandes, J. Inoue, and A. Shimizu, Phys. Rev. Lett. **80**, 3952 (1998).

[169] M. W. Wu and H. Haug, Phys. Rev. B **58**, 13060 (1998).

[170] K. Hepp and E. Lieb, Ann. Phys. **76**, 360 (1971).

[171] A. Andreev, V. Emel'yanov, and Y. A. Il'inski, in *Cooperative Effects in Optics*, *Malvern Physics Series* (Institute of Physics, Bristol, 1993), Chap. 5.8.

[172] P. R. Berman, Appl. Phys. **6**, 283 (1975).

[173] T. Brandes, J. Inoue, and A. Shimizu, Physica B **272**, 341 (1999).

[174] T. Brandes and B. Kramer, Phys. Rev. Lett. **83**, 3021 (1999).

[175] H. Haug and A.-P. Jauho, in *Quantum Kinetics in Transport and Optics of Semiconductors*, Vol. 123 of *Solid-State Sciences* (Springer, Berlin, 1996), Chap. 12.

[176] J. Jaeckle, *Einführung in die Transporttheorie* (Vieweg, Braunschweig, 1978).

[177] H. Haug and A.-P. Jauho, in *Quantum Kinetics in Transport and Optics of Semiconductors*, Vol. 123 of *Solid-State Sciences* (Springer, Berlin, 1996), Chap. 1.

[178] D. L. Maslov, Y. B. Levinson, and S. M. Badalian, Phys. Rev. B **46**, 7002 (1992).

[179] T. Brandes, in *NATO Advanced Study Institute, Bad Lauterberg*, Vol. 326 of *Nato ASI Series E*, edited by B. Kramer (Kluwer Academic Publishers, Dordrecht, 1996), p. 353.

[180] W. Götze and P. Wölfle, Phys. Rev. B **6**, 1226 (1972).

[181] W. Brenig, *Statistical Theory of Heat* (Springer, Berlin, Heidelberg, 1989), Vol. 2.

[182] H. Akera and T. Ando, Phys. Rev. B **41**, 11967 (1990).

[183] W. Apel and T. M. Rice, Phys. Rev. B **26**, 7063 (1982).

[184] Y. Fu and S. C. Dudley, Phys. Rev. Lett. **70**, 65 (1993).

[185] M. Büttiker, A. Prêtre, and H. Thomas, Phys. Rev. Lett. **70**, 4114 (1993).

[186] T. Brandes, D. Weinmann, and B. Kramer, Europhys. Lett. **22**, 51 (1993).

[187] D. S. Fisher and P. A. Lee, Phys. Rev. B **23**, 6851 (1981).

[188] A. D. Stone and A. Szafer, IBM J. Res. Dev. **32**, 384 (1988).

[189] J. Mašek and B. Kramer, Z. Phys. B **75**, 37 (1989).

[190] B. Kramer and J. Mašek, Z. Phys. B **76**, 457 (1989).

[191] B. Velický, J. Mašek, and B. Kramer, Phys. Lett. A **140**, 447 (1989).

[192] S. Chakravarty and A. Schmid, Phys. Rep. **140**, 193 (1986).

[193] A. Kawabata and T. Brandes, J. Phys. Soc. Japan **65**, 3712 (1996).

[194] G. Cuniberti, M. Sassetti, and B. Kramer, Phys. Rev. B **57**, 1515 (1998).

[195] M. Rother, private communication.

[196] T. Brandes, Physica B **28x**, xxx (April 2000).

[197] T. Brandes and B. Kramer, Physica B **272**, 42 (1999).

[198] T. Brandes, J. Inoue, and A. Shimizu, in *The physics of Semiconductors-24th ICPS*, edited by D. Gershoni (World Scientific, Singapore, 1999).

[199] T. Brandes, Europhys. Lett. **33**, 629 (1996).

[200] T. Brandes, Phys. Rev. B **56**, 1213 (1997).

[201] T. Brandes, Annalen der Physik **7**, 120 (1998).

[202] T. Brandes, M. Sassetti, and B. Kramer, in *The physics of Semiconductors-24th ICPS*, edited by D. Gershoni (World Scientific, Singapore, 1999).

INDEX